TEACHING RESEARCH & INNOVATION SYMPOSIUM 2023

PROCEEDINGS OF THE BIUST TEACHING, RESEARCH & INNOVATION SYMPOSIUM 2023 (TRDAIS 2023)

PALAPYE, BOTSWANA
18-19 SEPTEMBER 2023

Powered by:

DEBSWANA
Mining diamonds, enriching the nation

LUCARA DIAMOND

bhc

absa

CARERRA HOLDINGS

standard chartered

Stanbic Bank
A member of Standard Bank Group

BIUST
BOTSWANA INTERNATIONAL UNIVERSITY OF SCIENCE & TECHNOLOGY

EDITED BY:
RODRIGO S. JAMISOLA JR

ISSN: 2521-2293

BIUST Teaching, Research, & Innovation Symposium 2023 (TRDAIS 2023)
Botswana International University of Science and Technology
Palapye, Botswana, 18 - 19 September 2023
ISSN: 2521-2293

ISSN: 2521-2293

BIUST Contact Information:
Phone: +267-493-1395
Email: mozilaw@biust.ac.bw

BIUST Teaching, Research, & Innovation Symposium 2023 (TRDAIS 2023)
Botswana International University of Science and Technology
Palapye, Botswana, 18 - 19 September 2023
ISSN: 2521-2293

Preface

This year, the BIUST Teaching, Research, and Innovation Symposium 2023 (TRDAIS 2023) is held as part of the 10th-anniversary celebration of Botswana International University of Science and Technology. This is the third BIUST Symposium, with an added new topic on "Teaching." It aims to attract multi-disciplinary research to showcase the latest work of teachers, researchers, and innovators in the country and abroad. It accepted three types of abstract submissions, namely, Full Paper, Poster, and Exhibit. The submission types are further subdivided into five tracks, namely, Life Sciences and Environment, Pure and Applied Sciences, Infrastructures and Mining, Computing and Industries, and Teaching.

There were 99 abstracts submitted at an acceptance rate of 98%. Each submitted abstract was reviewed with a minimum of three to a maximum of five reviews. This review record has been maintained for all three BIUST symposia. Through this symposium, BIUST students and researchers are provided with a platform to enhance their research and presentation skills by interacting and collaborating with other researchers in their areas of interest.

Firstly, I would like to thank all authors who participated by submitting their abstracts, despite the short period allocated to respond to the Call for Participation. Secondly, I would also wholeheartedly thank the BIUST academics who have been the strongest support in the review process. Special mention to the reviewers who have the highest number of reviewed abstracts: Venecio Ultra, Abid Yahya, Albert Ude, Phillip Oladijo, Norman Gwangwava, Vivekanandhan Chinnasamy, Ravi Samikannu, and Gafar Oniyide.

Thirdly, I would like to thank the Program Committee who tirelessly and unceasingly worked through the submissions, review process, and proceedings for the symposium. Particularly, the Program Committee Co-Chair Dr. Chamunorwa Kureba and the members who were in-charge on the review process for the five tracks, namely, Refilwe Setso, Mello Tumisang, Sebinanyane Babedi, Thabang Matabana, and Dineo Sebuso. In addition, I thank the new members who joined to help in the symposium preparations, namely, Kediemetse Kgakole, and Hendrick Ontlafetse. Lastly, I would like to acknowledge the online conference management software sciencesconf.org that provided the free software in the submission and review processes.

September 18, 2023
Palapye, Botswana

Professor Rodrigo S. Jamisola Jr.
TRDAIS 2023
Overall and Program Chair

ISSN: 2521-2293

Welcome Message

It is my great honour and privilege to be able to witness and welcome the holding of the third BIUST Symposium. This time, it is called Teaching, Research, and Innovation Symposium 2023 (TRDAIS 2023) and is conducted as one of the major highlights of the BIUST 10th Anniversary Celebration. Welcome all participants!

Our collective pursuit of understanding has brought together brilliant minds from within Botswana and outside, each contributing a unique perspective to the tapestry of human progress. As we engage in lively discussions, thought-provoking presentations, and spirited debates, let us remember the purpose that unites us: the pursuit of truth through science and technology. I extend my deepest gratitude to the researchers, scholars, sponsors, and organizers who have dedicated their time, effort, and expertise to make this symposium possible. Your contributions have ignited the spark that fuels our intellectual exploration. Let us foster an atmosphere of curiosity, respect, and open-mindedness by embracing the rich perspectives from different areas of expertise.

Let us look forward to depart from this event with renewed enthusiasm in continuing to pursue our excellent research and innovation activities, with the affirmation that we are the real drivers of change for the country and the world. Let the symposium begin!

September 18, 2023
Palapye, Botswana

Professor Otlogetswe Totolo
BIUST Vice Chancellor

ISSN: 2521-2293

Welcome Message

It is with great pleasure that I welcome all participants of the 3rd BIUST Symposium entitled BIUST Teaching, Research and Innovation Symposium 2023 (TRDAIS 2023). This symposium forms a major part of our University's 10 th Anniversary Celebrations. Your participation in this very important activity shows your shared commitment to the pursuit of knowledge and the advancement of ground-breaking research with global impact.

The symposium provides a unique platform to celebrate the tireless efforts of researchers, scholars, and experts who dedicate their work towards advancing research and innovation in Botswana and the world at large. This symposium has attracted participation beyond our university, and I hope that we keep this momentum going in the coming years. I would like to express my deep gratitude to all the speakers, panelists, and contributors who will graciously share their expertise and knowledge with us during the symposium. Your dedication to knowledge dissemination is truly inspiring and will undoubtedly leave a lasting impact on humanity. Let us make the most of this unique opportunity to engage, connect, and learn from one another.

Lastly, I would like to express my gratitude to the organizers of this symposium who dedicated time and energy to make this event a success, I anticipate an engaging two-day symposium.

Thank you very much.

September 18, 2023
Palapye, Botswana

Professor Elisha M. Shemang
BIUST Deputy Vice-Chancellor
Academic Affairs

ISSN: 2521-2293

Welcome Message

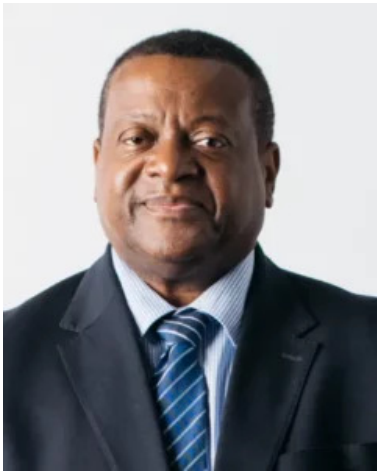

The BIUST Teaching, Research and Innovation Symposium (TRDAIS 2023) is now on for the third time. I am delighted to extend my warm greetings to all participants in this event, in commemoration of the BIUST 10th Anniversary Celebrations. The holding of the symposium is a manifestation of BIUST's commitment to lead research and innovation for Botswana. Our university is fully dedicated to being the driver of change for the country.

Truly, your participation is a testament to your commitment to advance knowledge and explore the frontiers of research. Over the next two days, we will come together to engage in thoughtful discussions, share ground-breaking insights, and forge valuable connections with fellow researchers and experts in various fields. This symposium is a celebration of intellectual curiosity and collaboration, a platform where ideas flourish and innovative solutions emerge. As we delve into the exciting line-up of oral and poster presentations, exhibitions, and networking opportunities, I encourage you to actively participate, ask questions, and engage in fruitful discussions.

I extend my appreciation to our distinguished speakers, presenters, sponsors, and the organizing committee, without which this symposium would not be possible.

I thank you.

September 18, 2023
Palapye, Botswana

Professor Abraham Atta Ogwu
BIUST Deputy Vice-Chancellor
Research, Development, and Innovation

BIUST Teaching, Research, & Innovation Symposium 2023 (TRDAIS 2023)
Botswana International University of Science and Technology
Palapye, Botswana, 18 - 19 September 2023
ISSN: 2521-2293

Table of Contents

ISSN: 2521-2293

ISSN: 2521-2293

ISSN: 2521-2293

ISSN: 2521-2293

ISSN: 2521-2293

BIUST Teaching, Research, & Innovation Symposium 2023 (TRDAIS 2023)
Botswana International University of Science and Technology
Palapye, Botswana, 18 - 19 September 2023
ISSN: 2521-2293

Full Papers

BIUST Teaching, Research, & Innovation Symposium 2023 (TRDAIS 2023)
Botswana International University of Science and Technology
Palapye, Botswana, 18 - 19 September 2023
ISSN: 2521-2293

HOCHSCHILD COHOMOLOGY OF SULLIVAN ALGEBRAS AND MAPPING SPACES BETWEEN MANIFOLDS

J.-B. GATSINZI

Abstract. Let $e : N^n \to M^m$ be an embedding of closed, oriented manifolds of dimension n and m respectively. We study the relationship between the homology of the free loop space LM on M and of the space $L_N M$ of loops of M based in N and define a shriek map $H_*(e)_! : H_*(LM, \mathbb{Q}) \to H_*(L_N M, \mathbb{Q})$ using Hochschild cohomology and study its properties. In particular we extend a result of Félix on the injectivity of the map induced by $\mathrm{aut}_1 M \to \mathrm{map}(N, M; f)$ on rational homotopy groups when M and N have the same dimension and $f : N \to M$ is a map of non zero degree.

1. Introduction

All spaces are assumed to be simply connected and (co)homology coefficients are taken in the field $\mathbb{Q}$ of rationals. If M is a compact oriented manifold of dimension m and $LM = \mathrm{map}(S^1, M)$ the space of free loops in M, then there is an intersection product

$$\mu : H_{p+m}(LM) \otimes H_{q+m}(LM) \to H_{p+q+m}(LM)$$

which induces a graded multiplication on $\mathbb{H}_*(LM) = H_{*+m}(LM)$, turning it into a commutative graded algebra [3]. Consider the embedding $e : N \to M$ of a closed, oriented submanifold of degree n. Construct the pullback

(1)
$$\begin{array}{ccc} L_N M & \xrightarrow{\tilde{e}} & LM \\ {\scriptstyle \tilde{p}}\downarrow & & \downarrow{\scriptstyle p} \\ N & \xrightarrow[e]{} & M, \end{array}$$

2010 *Mathematics Subject Classification.* Primary 55P62; Secondary 54C35.
Key words and phrases. Loop space homology, Poincaré duality, Hochschild cohomology.
A partial support from the IMU-Simons Africa Fellowship is acknowledged.

ISSN: 2521-2293

where p is the evaluation of a loop at $1 \in S^1$. There is also an intersection product on $\mathbb{H}_*(L_N M) = H_{*+n}(L_N M)$, turning it into commutative graded algebra [15].

We consider a morphism $f : (A, d) \to (B, d)$ which models the embedding e, where (A, d) and (B, d) are Poincaré duality commutative differential graded algebras (cdga for short) [5]. We show that there is an A-linear shriek map $f_! : (B, d) \to (A, d)$ of degree $m-n$. We consider induced maps $HH^*(f) : HH^*(A, A) \to HH^*(A, B)$ and $HH^*(f_!) : HH^*(A, B) \to HH^*(A, A)$ in Hochschild cohomology. Moreover we obtain the following.

Theorem 1. *The composition map*

$$HH^*(f_!) \circ HH^*(f) : HH^*(A, A) \to HH^*(A, A)$$

is the multiplication by the Poincaré dual of the fundamental class of N in M.

Theorem 2. *Let $g : N^m \to M^m$ be a map between manifolds of same dimension m such* $\deg f \neq 0$ *and $f : (A, d) \to (B, d)$ a cdga model of g. Then*

$$HH^*(A, A) \to HH^*(A, B)$$

is injective.

The above result suggests that $\mathbb{H}(\tilde{g}) : \mathbb{H}_*(L_N M) \to \mathbb{H}_*(LM)$ is an injective algebra morphism, where $\tilde{g} : L_N M \to LM$ is the pullback of $g : N \to M$ along the fibration $p : LM \to M$ defined by $p(\gamma) = \gamma(0)$.

The paper is organized as follows: In Section 2 we define a shriek map $f_! : (B, d) \to (A, d)$ and prove Theorem 1. In Section 3, we recall a resolution to compute $HH^*(C^*(M), C^*(N))$ and in Section 4 we prove Theorem 2.

2. A shriek map

We first recall some facts in Rational Homotopy Theory. We make use of Sullivan models for which the standard reference is [6]. All vector spaces are over the ground field $\mathbb{Q}$. A differential graded algebra (A, d) is a direct sum of vector spaces A^p, that is, $A = \oplus_{p \geq 0} A^p$ together with a graded multiplication $\mu : A^p \otimes A^q \to A^{p+q}$ which is associative. An element $a \in A^p$ is called homogeneous of degree $|a| = p$. Moreover there is a differential $d : A^p \to A^{p+1}$ which an algebra derivation, that is, $d(ab) = (da)b + (-1)^{|a|}a(db)$ and satisfies $d^2 = 0$.

BIUST Teaching, Research, & Innovation Symposium 2023 (TRDAIS 2023)
Botswana International University of Science and Technology
Palapye, Botswana, 18 - 19 September 2023
ISSN: 2521-2293

A graded algebra A is called commutative if $ab = (-1)^{|a||b|}ba$ for $a, b \in A$. If (A, d) is a commutative differential graded algebra, then $H^*(A, d)$ is graded commutative. A morphism $f : (A, d) \to (B, d)$ of cdga's is called a quasi-isomorphism if $H^*(f)$ is an isomorphism. A cdga (A, d) is called simply connected if $H^0(A) = \mathbb{Q}$ and $H^1(A) = 0$.

A commutative graded algebra A is free if it is of the form $\wedge V = S(V^{even}) \otimes E(V^{odd})$, where $V^{even} = \oplus_{i\geq 1} V^{2i}$ and $V^{odd} = \oplus_{i\geq 0} V^{2i+1}$. A Sullivan algebra is a cdga $(\wedge V, d)$, where $V = \oplus_{i\geq 1} V^i$ admits a homogeneous basis $\{x_i\}_{i\in I}$ indexed by a well ordered set I such $dx_i \in \wedge(\{x_i\})_{i<j}$. A Sullivan algebra is called minimal if $dV \subset \wedge^{\geq 2} V$ [6]. If there is a quasi-isomorphism $f : (\wedge V, d) \to (A, d)$, where $(\wedge V, d)$ is a (minimal) Sullivan algebra, then we say that $(\wedge V, d)$ is a (minimal) Sullivan model of (A, d). Any connected cdga (A, d) admits a Sullivan model [6].

To a simply connected topological space X of finite type, Sullivan associates in a functorial way a cdga $A_{PL}(X)$ of piecewise linear forms on X such $H^*(A_{PL}(X)) \cong H^*(X, \mathbb{Q})$ [16]. A Sullivan model of X is a Sullivan model of $A_{PL}(X)$. Moreover any cdga (A, d) is called a model of X if there is a sequence of quasi-isomorphisms

$$(A, d) \to (A_1, d) \leftarrow \ldots \to (A_{n-1}, d) \leftarrow A_{PL}(X).$$

We state here the fundamental result of Sullivan algebras.

Proposition 3. *If (A, d) is a simply connected cdga then there is a minimal Sullivan algebra $(\wedge V, d)$ together with a quasi-isomorphism $(\wedge V, d) \to (A, d)$. Moreover $(\wedge V, d)$ is unique up to isomorphism. It is called the minimal Sullivan model of (A, d)* [6, § 12].

Definition 4. A simply connected space X is called formal if there is a quasi-isomorphism $(\wedge V, d) \to H^*(\wedge V, d)$, where $(\wedge V, d)$ is a Sullivan model of X. Formal spaces include spheres, compact Lie groups and complex projective spaces.

Definition 5.
(1) A connected graded commutative algebra A is called an oriented Poincaré duality algebra of dimension n if there is a linear map $\epsilon : A^n \to \mathbb{Q}$ such that the induced bilinear forms, $\beta : A^k \otimes A^{n-k}$ defined by $\beta(x \otimes y) = \epsilon(ab)$, are non degenerate.
(2) A commutative differential graded algebra (A, d) is a Poincaré algebra of formal dimension n if A is an oriented Poincaré duality algebra such that $\epsilon(dA^{n-1}) = 0$.

ISSN: 2521-2293

Remark 6. It comes from the definition that there is a cocycle $\omega_A \in A^n$ such that $\epsilon(\omega_A) = 1$. We call $[\omega_A]$ the fundamental class of (A, d). If A is of finite type, then $A^i = 0$ for $i > n$ and A is finite dimensional. Moreover if $\{a_1, \ldots, a_k\}$ is a homogeneous basis of A, then there is a dual homogeneous basis $\{a_j^*\}$ such that $\epsilon(a_i a_j^*) = \delta_{ij}$. We denote by $a^\#$ the dual of a in $A^\# = \mathrm{Hom}(A, \mathbb{Q})$. In particular $\omega_A = \epsilon^\# \in (A^\#)^\# \cong A$ is the fundamental class of A. Moreover the linear map $\pi_A : A^k \to (A^{n-k})^\#$ defined by $\pi_A(a)(x) = \epsilon(ax)$ is an isomorphism of A-modules of lower degree n.

If $(\wedge V, d)$ is the minimal Sullivan model of a simply connected space X, where $H^*(X, \mathbb{Q})$ satisfies Poincaré duality, then $(\wedge V, d)$ is quasi-isomorphic to a Poincaré duality algebra (A, d) [13]. In particular, a simply connected smooth manifold M of dimension m has a cdga-model (A, d) which satisfies Poincaré duality in dimension m.

Let $f : (A, d) \to (B, d)$ be a map between cdga's with Poincaré duality in dimensions m and n respectively. We can now relate isomorphisms $\pi_A : A \xrightarrow{\simeq} A^\#$ and $\pi_B : B \xrightarrow{\simeq} B^\#$.

Proposition 7. *If f is surjective, then there exists a morphism of A-modules $f_! : B \to A$ making the following diagram commutative.*

$$\begin{array}{ccc} B & \xrightarrow{f_!} & A \\ {\scriptstyle\simeq}\downarrow{\scriptstyle\pi_B} & & {\scriptstyle\pi_A}\downarrow{\scriptstyle\cong} \\ B^\# & \xrightarrow{f^\#} & A^\# \end{array}$$

Proof. Let $1 \in B$, then $\pi_B(1) = \omega_B^\#$, where ω_B is a cocycle which represents the fundamental class $[\omega_B] \in H^n(B)$. As π_A is bijective, there exists $\alpha \in A$ such that $\pi_A(\alpha) = f^\#(\omega_B^\#)$. As f is surjective, then given $b \in B$, there exists $a \in A$ such that $b = f(a)$. Recall that B is an A-module through the action induced by f, hence $b = f(a)1 = a * 1$. Therefore we define $f_!(b) = a\alpha$. In particular $f_! f(a) = a\alpha$.
We show that the above diagram commutes. Let $b \in B$ and $a \in A$ such that $b = f(a)$. On one hand

$$f^\#(\pi_B(b)) = f^\#(\pi_B(b \times 1)) = f^\#(b\omega_B^\#), \tag{2}$$

whereas

$$\pi_A(f_!(b)) = \pi_A(a\alpha) = a\pi_A(\alpha) = af^\#(\omega_B^\#). \tag{3}$$

Let $x \in A$. Then

$$f^\#(b\omega_B^\#)(x) = (b\omega_B^\#)(f(x)) = \omega_B^\#(bf(x)), \tag{4}$$

ISSN: 2521-2293

and

$$(5)\qquad \begin{aligned}(af^{\#}(\omega_B^{\#}))(x) &= (f^{\#}(\omega_B^{\#}))(ax) = \omega_B^{\#}(f(ax))\\ &= \omega_B^{\#}(f(a)f(x)) = \omega_B^{\#}(bf(x)).\end{aligned}$$

Hence $f^{\#}(b\omega_B^{\#}) = af^{\#}(\omega_B)$ and the diagram commutes.

Finally we show that $f_!$ is a morphism of A-modules. If $x \in A$ and $b \in B$, then

$$f_!(x * b) = f_!(f(x)b) = f_!(f(xa)) = (xa)\alpha = xf_!(b).$$

In particular $f_!(b) = f_!(b \times 1) = a * f_!(1)$. □

Remark 8. If ω_B is a cocycle representing the fundamental class of (B, d) and f is surjective, then there exists $x \in A$ such that $f(x) = \omega_B$. Then $f^{\#}(\omega_B^{\#}) = x^{\#} = \pi_A(x^*)$, where x^* is the dual of x under a choice of a basis $\{a_i\}$ of A and its dual $\{a_j^*\}$ (see Remark 6). If $dx = 0$, then $[x] \in H^*(A) \neq 0$ and $[x^*] \in H^{m-n}(A)$ is non zero.

Example 9. Consider the inclusion $i : \mathbb{C}P^n \to \mathbb{C}P^{n+k}$. As complex projective spaces are formal, a cdga model of the inclusion is

$$f : \wedge x_2/(x_2^{n+k+1}) \to \wedge y_2/(y_2^{n+1}),$$

where $f(x) = y$. Then $f_!$ is defined by $f_!(1) = x^k$. Hence $f_!(y^i) = x^{k+i}$, for $0 \leq i \leq n$.

3. Hochschild cohomology

If (A, d) is a graded differential algebra and (Q, d) a graded A-bimodule, then the Hochschild cohomology of A with coefficients in Q is defined by $HH^*(A, Q) = \mathrm{Ext}_{A^e}(A, Q)$, where $A^e = A \otimes A^{opp}$.

Let $A = (\wedge V, d)$ be the minimal Sullivan model of a simply connected space X. Then

$$(6)\qquad P = (\wedge V \otimes \wedge V \otimes \wedge \bar{V}, \tilde{D}) \to (\wedge V, d)$$

is a semi-free resolution of $\wedge V$ as a $\wedge V \otimes \wedge V$-module, where $\bar{V} = sV$ [5].

Moreover, the pushout

$$\begin{array}{ccc}(\wedge V \otimes \wedge V, d \otimes 1 + d \otimes 1) & \rightarrowtail & (\wedge V \otimes \wedge V \otimes \wedge \bar{V}, \tilde{D})\\ \downarrow{\scriptstyle \mu} & & \downarrow\\ (\wedge V, d) & \rightarrowtail & (\wedge V \otimes \wedge \bar{V}, D)\end{array}$$

yields a Sullivan model $(\wedge V \otimes \wedge \bar{V}, D)$ of the free loop space on X [17]. The differential is given by $Dv = dv$ for $v \in V$ and $D\bar{v} = -Sdv$, where

ISSN: 2521-2293

S is the unique derivation on $\wedge V \otimes \wedge \bar{V}$ defined by $Sv = \bar{v}$ and $S\bar{v} = 0$.

Hence if (Q, d) is a $\wedge V$-differential module, then the Hochschild cochains $CH(A, Q)$ are given by

$$CH^*(A,Q) \begin{array}{l} = (\mathrm{Hom}_{\wedge V \otimes \wedge V}(\wedge V \otimes \wedge V \otimes \wedge \bar{V}, Q), D) \\ \cong (\mathrm{Hom}_{\wedge V}(\wedge V \otimes \wedge \bar{V}, Q), D). \end{array} \tag{7}$$

As the differential of D on $\wedge V \otimes \wedge \bar{V}$ satisfies

$$D(\wedge V \otimes \wedge^n \bar{V}) \subset \wedge V \otimes \wedge^n \bar{V},$$

one gets a Hodge type decomposition

$$HH^*(A,Q) = \oplus_{i \geq 0} HH^*_{(i)}(A,Q),$$

where $HH^*_{(i)}(A,Q) = H^*(\mathrm{Hom}_{\wedge V}(\wedge V \otimes \wedge^i \bar{V}, \wedge V), D)$. Moreover, if $L = s^{-1}\,\mathrm{Der}\,\wedge V$, then the symmetric algebra $(\wedge_A L, d)$ is quasi-isomorphic to the Hochschild cochain complex $(\mathrm{Hom}_{\wedge V}(\wedge V \otimes \wedge \bar{V}, \wedge V), D)$ [9]. Furthermore if V is finite dimensional then $HH^*(\wedge V, \wedge V)$ is the homology of the complex $(\wedge V \otimes \wedge Z, D)$ where $Z \simeq s^{-1}V^{\#}$ [10].

Assume that M is a simply connected smooth manifold of dimension m and $(\wedge V, d)$ its minimal Sullivan model. Then there is an isomorphism of BV-algebras $\mathbb{H}_*(LM) \cong HH^*(\wedge V, \wedge V)$ [4, 8, 7]. For closed oriented submanifolds N and N' of M, we denote by $P_N^{N'}M$ the space of paths in M starting in N and ending in N'. Let N_1, N_2 and N_3 be submanifolds of M. When coefficients are rationals (or in $\mathbb{Z}/n\mathbb{Z}$) Sullivan showed that there is an intersection product

$$\mu : H_{p+d}(P_{N_1}^{N_2}M) \otimes H_{q+d}(P_{N_2}^{N_3}M) \to H_{p+q+d}(P_{N_1}^{N_3}M)$$

where $d = \dim N_2$ [15]. In particular if $N_1 = N_2 = N_3 = N$, one gets a graded commutative algebra structure on $\mathbb{H}_*(P_N^N M, \mathbb{Q}) = H_{*+d}(P_N^N M, \mathbb{Q})$. We consider the subset of $P_N^N M$ consisting of loops that originate in N. This is exactly $L_N M$ defined by the pullback of the diagram (1). The restriction yields a product on $\mathbb{H}_*(L_N M) = H_{*+d}(L_N M)$.

Let $e : N^n \hookrightarrow M^m$ be an embedding where N is simply connected and $f : (A, d) \to (B, d)$ a cdga model e, where both (A, d) and (B, d) satisfy Poincaré duality. Assume that f is surjective and let $[y] \in H^n(B)$ be the fundamental class. Let $x \in A$ such that $f(x) = y$. We will assume that x is a cocycle and consider $[x] \in H^n(A, d)$.

Theorem 10. *Under the above hypotheses, the composition*

$$HH^*(A,A) \xrightarrow{HH^*(f)} HH^*(A,B) \xrightarrow{HH^*(f_!)} HH^*(A,A)$$

BIUST Teaching, Research, & Innovation Symposium 2023 (TRDAIS 2023)
Botswana International University of Science and Technology
Palapye, Botswana, 18 - 19 September 2023
ISSN: 2521-2293

is the multiplication with the Poincaré dual $[x^*] \in H^{m-n}(A,d)$ *of* $[x]$.

Proof. We consider the minimal Sullivan model $\phi : (\wedge V, d) \to (A, d)$. By Eq. (7), $HH^*(A,A)$ is obtained as the cohomology of the complex

$$\begin{aligned}\mathrm{Hom}_{\wedge V\otimes\wedge V}(\wedge V\otimes\wedge V\otimes\wedge\bar{V},\wedge V) &\cong \mathrm{Hom}_{\wedge V}(\wedge V\otimes\wedge\bar{V},\wedge V)\\ &\simeq \mathrm{Hom}_{\wedge V}(\wedge V\otimes\wedge\bar{V},A).\end{aligned}$$

If $\gamma \in \mathrm{Hom}_{\wedge V}(\wedge V\otimes\wedge\bar{V},A)$, then

$$(CH(f_!)\circ CH(f))(\gamma)(x) = (f_!\circ f)(\gamma)(x) = \alpha\gamma(x),$$

where $\alpha = x^*$, by Remark 8. Therefore, if γ is a cocycle, then

$$HH^*(f_!)\circ HH^*(f)([\gamma]) = [x^*][\gamma].$$

□

Example 11. We consider the embedding $e : \mathbb{C}P^n \hookrightarrow \mathbb{C}P^{n+k}$ for which a Poincaré duality model is given by

$$f : A = \wedge x_2/(x_2^{n+k+1}) \to \wedge y_2/(y_2^{n+1}) = B, \text{ where } f(x_2) = y_2.$$

As f is surjective, the hypotheses of Theorem 10 are satisfied. The complex to compute $HH^*(A,A)$ is given by $(A\otimes\wedge(z_1, z_{2(n+k)}), D)$ where subscripts indicate the lower degree, and $Dz_{2(n+k)} = 0$, $Dz_1 = (n+k+1)x_2^{n+k}z_{2(n+k)}$ [10]. Here an element $x \in A^n = A_{-n}$ is assumed to be of lower degree $-n$. At chain's level, the composition

$$CH^*(f_!)\circ CH(f) : (A\otimes\wedge(z_1, z_{2(n+k)}), D) \to (A\otimes\wedge(z_1, z_{2(n+k)}), D)$$

is the multiplication by x_2^k.

Proposition 12. *Let* $e : N \to M$ *be an embedding between closed, oriented manifolds,* $(\wedge V, d)$ *the minimal Sullivan model of* M *and* $Z = s^{-1}V^{\#}$ *and* $L_N M$ *the pullback of Eq.* (1). *If* $f : (A,d) \to (B,d)$ *is a model of* $e : N \to M$, *then* $HH^*(C^*(M), C^*(N))$ *is computed by the complex* $(B\otimes\wedge Z, D)$ *which is the pushout of the following diagram.*

(8)
$$\begin{array}{ccc}(A,d) & \longrightarrow & (A\otimes\wedge Z, D)\\ \downarrow & & \downarrow\\ (B,d) & \longrightarrow & (B\otimes\wedge Z, D)\end{array}$$

Proof. Let $(\wedge V, d)$ be the minimal Sullivan model of M, where V is finite dimensional. Then $\mathbb{H}_*(LM)$ is the homology of the complex $(\wedge V\otimes\wedge Z, D)$ where $Z = s^{-1}V^{\#}$ and the differential D is induced by δ on $(\mathrm{Der}\wedge V, \delta)$, where $V^{\#} \subset \mathrm{Der}\wedge V$. As $(\wedge V, D) \to (A,d)$ is a quasi-isomorphism, then the pushout is a model of the pullback in Eq. 1. □

ISSN: 2521-2293

However, it is not known whether $\mathbb{H}_*(L_N M)$ and $H_*(B \otimes \wedge Z, D)$ are isomorphic as algebras.

4. Maps between manifolds of same dimension

Let $f : (A, d) \to (B, d)$ be a morphism of graded cochain algebras. An f-derivation of degree k is a linear map $\theta : A^* \to B^{*-k}$ such that $\theta(xy) = \theta(x)f(y) + (-1)^{k|x|} f(x)\theta(y)$. We denote by $\mathrm{Der}_k(A, B; f)$ the vector space of all f-derivations of degree k and $\mathrm{Der}(A, B; f) = \oplus_k \mathrm{Der}_k(A, B; f)$. Define a differential δ on $\mathrm{Der}(A, B; f)$ by $\delta\theta = d_B\theta - (-1)^{|\theta|}\theta d_A$. If $A = B$ and $f = 1_A$, we get the usual Lie algebra of derivations, $\mathrm{Der}\, A$, where the Lie bracket is the the commutator of two derivations. There is an action of A on $\mathrm{Der}\, A$, defined by $(a\theta)(x) = a\theta(x)$, making $(\mathrm{Der}\, A, \delta)$ a differential graded module over A.

Let M and N be compact, oriented manifolds of dimension n and $g : N \to M$ a smooth map such that $\deg g \neq 0$. Consider a Poincaré duality model $f : (A, d) \to (B, d)$ of g. Then f is injective and $B = f(A) \oplus Z$, where $dZ \subseteq Z$ and $f(A).Z$ [5]. Therefore Z is an A-submodule. Moreover the projection $p : B = f(A) \oplus Z \to A$ is a morphism of A-modules.

Theorem 13 ([5], Theorem 2)**.** *Consider a surjective Sullivan model $\phi : (\wedge V, D) \to (A, d)$. Then*

$$f_* : (\mathrm{Der}(\wedge V, A; \phi), \delta) \to (\mathrm{Der}(\wedge V, B; f \circ \phi), \delta) \tag{9}$$

induces an injective map in homology.

This can be interpreted in terms of rational homotopy groups of function spaces. Let $g : X \to Y$ be a continuous map between CW complexes where Y is finite and X of finite type and $\phi : (\wedge Z, d) \to (B, d)$ a Sullivan model of g. Consider $\mathrm{map}(X, Y; g)$ be the space of continuous mappings from X to Y which are homotopic to g. There is a natural isomorphism [1, 2, 14]

$$\pi_n(\mathrm{map}(X, Y; g)) \otimes \mathbb{Q} \cong H_n(\mathrm{Der}(\wedge V, B; \phi), \delta), \ n \geq 2.$$

Hence if $g : N \to M$ is a map between simply connected smooth manifolds such that $\deg g \neq 0$, then the map

$$j_M : \mathrm{aut}_1\, M = \mathrm{map}(M, M; 1_M) \to \mathrm{map}(N, M; g)$$

induces an injective map

$$\pi_*(j_M) \otimes \mathbb{Q} : \pi_*(\mathrm{aut}_1\, M) \otimes \mathbb{Q} \to \pi_*(\mathrm{map}(N, M; g)) \otimes \mathbb{Q}.$$

BIUST Teaching, Research, & Innovation Symposium 2023 (TRDAIS 2023)
Botswana International University of Science and Technology
Palapye, Botswana, 18 - 19 September 2023
ISSN: 2521-2293

Let $\phi : (\wedge V, d) \to (A, d)$ be a Sullivan model and $\rho = f \circ \phi$. We have the following commutative diagram

$$\begin{array}{ccc} H_*(\mathrm{Der}\,\wedge V, \delta) & \hookrightarrow & HH^*(A,A) \\ \downarrow & & \downarrow \\ H_*(\mathrm{Der}(\wedge V, B; \rho), \delta) & \hookrightarrow & HH^*(A,B), \end{array}$$

where horizontal maps are inclusions [11]. We show that the remaining vertical arrow is injective, which is a generalization of Theorem 13.

Theorem 14. *Let $g : N \to M$ be a smooth map of non zero degree between manifolds of same dimension n and $f : (A, d) \to (B, d)$ a Poincaré duality model of g. Then the induced map*

$$HH^*(A,A) \xrightarrow{HH^*(f)} HH^*(A,B)$$

is injective.

Proof. As $B = f(A) \oplus Z$, then $f(A) = \rho(\wedge V)$ is a submodule of B viewed as a $\wedge V$-module and Z is also a $\wedge V$-submodule of B. Therefore

$$\mathrm{Hom}_{\wedge V}(\wedge V \otimes \wedge \bar{V}, B) \cong \mathrm{Hom}_{\wedge V}(\wedge V \otimes \wedge \bar{V}, f(A)) \oplus \mathrm{Hom}_{\wedge V}(\wedge V \otimes \wedge \bar{V}, Z).$$

Moreover, the projection $p : B = f(A) \oplus Z \to f(A) \cong A$ is a morphism of $\wedge V$-modules. It induces a chain map

$$p_* : \mathrm{Hom}_{\wedge V}(\wedge V \otimes \wedge \bar{V}, B) \to \mathrm{Hom}_{\wedge V}(\wedge V \otimes \wedge \bar{V}, A)$$

such that $p_* \circ f_*$ is the identity. Therefore f_* is injective in homology. □

We can then deduce the following

Corollary 15. *Under the hypotheses of Theorem 14, there is an injective map $H_*(f)_! : H_*(LM, \mathbb{Q}) \to H_*(L_N M, \mathbb{Q})$*

Proof. Recall that there is an isomorphism $HH_*(A,A) \cong H^*(LM)$ [12]. Dualizing this isomorphism and using Poincaré duality yields an isomorphism $HH^*(A, A^\#) \cong H_*(LM)$. In the same way, there is an isomorphism $HH^*(A, B^\#) \cong H_*(L_N M)$. Hence $H_*(f)_!$ is given by the composition

$$HH^*(A,A^\#) \xrightarrow{(\pi_A)_*^{-1}} HH^*(A;A) \xrightarrow{f_*} HH^*(A,B) \xrightarrow{(\pi_B)_*} HH^*(A,B^\#).$$

Hence it is injective. □

ISSN: 2521-2293

References

1. J. Block and A. Lazarev, *André-Quillen cohomology and rational homotopy of function spaces*, Adv. Math. **193** (2005), 18–39.
2. U. Buijs and A. Murillo, *The rational homotopy Lie algebra of function spaces*, Comment. Math. Helv. **83** (2008), 723–739.
3. M. Chas and D. Sullivan, *String topology*, preprint math GT/9911159, 1999.
4. R.L Cohen and J.D.S Jones, *A homotopy theoretic realisation of string topology*, Math. Ann. **324** (2002), no. 4, 773–798.
5. Y. Félix, *Mapping spaces between manifolds and the evaluation map*, Proc. Amer. Math. Soc. **139** (2011), 3763–3768.
6. Y. Félix, S. Halperin, and J.-C. Thomas, *Rational Homotopy Theory*, Graduate Texts in Mathematics, no. 205, Springer-Verlag, New-York, 2001.
7. Y. Félix, J.-C. Thomas, and M. Vigué, *Rational string topology*, J. Eur. Math. Soc. (JEMS) **9** (2008), 123–156.
8. Y. Félix, J-C. Thomas, and M. Vigué-Poirrier, *The Hochschild cohomology of a closed manifold*, Publ. Math. Inst. Hautes Études Sci. **99** (2004), 235–252.
9. J.-B. Gatsinzi, *Derivations, Hochschild cohomology and the Gottlieb group*, Homotopy Theory of Function Spaces and Related Topics (Y. Félix, G. Lupton, and S. Smith, eds.), Contemporary Mathematics, vol. 519, American Mathematical Society, Providence, 2010, pp. 93–104.
10. J.-B Gatsinzi, *Hochschild cohomology of a Sullivan algebra*, Mediterr. J. Math. **13** (2016), 3765–3776.
11. J.-B. Gatsinzi, *Hochschild cohomology of Sullivan algebras and mapping spaces*, Arab J. Math. Sci. **25** (2019), 123–129.
12. J. D. S. Jones, *Cyclic homology and equivariant homology*, Inv. Math. **87** (1987), 403–423.
13. P. Lambrechts and D. Stanley, *Poincaré duality and commutative differential graded algebras*, Ann. Sci. Éc. Norm. Supér. **41** (2008), 495–509.
14. G. Lupton and S.B. Smith, *Rationalized evaluation subgroups of a map I: Sullivan models, derivations and G-sequences*, J. Pure Appl. Algebra **209** (2007), no. 1, 159–171.
15. D. Sulliivan, *Open and closed string field theory interpreted in classical algebaric topology*, Topology, Geometry and Quantum Field Theory, London Math.Soc. Lecture Notes, vol. 308, Cambridge University Press, 2004, pp. 344–357.
16. D. Sullivan, *Infinitesimal computations in topology*, Publ. I.H.E.S. **47** (1977), 269–331.
17. D. Sullivan and M. Vigué-Poirrier, *The homology theory of the closed geodesic problem*, J. Differential Geom. **11** (1976), 633–644.

Department of Mathematics and Statiscal Sciences, Botswana International University of Science and Technology.
Email address: gatsinzij@biust.ac.bw

BIUST Teaching, Research, & Innovation Symposium 2023 (TRDAIS 2023)
Botswana International University of Science and Technology
Palapye, Botswana, 18 - 19 September 2023
ISSN: 2521-2293

Submission Type: Full Paper

Track: Life Sciences and Environment

Microbiological and Physicochemical Characteristics of Effluents from Cocoa Processing Industry, Ile-Oluji, Nigeria

Yemisi A. Jeff-Agboola, Kehinde O. Adakan
Department of Biological Sciences, University of Medical Sciences, Ondo, Nigeria
yjeffagboola@unimed.edu.ng

James Oyedokun
Department of Food Science, Faculty of Food and Consumer Sciences, Ladoke Akintola University of Technology, P.M.B. 4000, Ogbomoso, Nigeria
Corresponding author: jimdokun@gmail.com

Abstract

This study investigated the microbiological and physicochemical properties; and heavy metal content; of effluent from the Cocoa Processing Industry, Ile-Oluji, Nigeria. Effluent samples from the reservoir (sample A) and discharge point (sample B) were aseptically taken and analysed for microbial properties, pH, conductivities (EC), total dissolved solids (TDS), total suspended solids (TSS) and heavy metal contents using standard methods. The data generated were subjected to Analysis of Variance and significance accepted at $p<0.05$. The probable organisms isolated from the two effluent samples and their percentages of occurrence were *Escherichia coli* (25%), *Salmonella* spp (25%), *Shigella* spp (12.5%), *Staphylococcus aureus* (12.5%) and *Proteus* spp (25%). The pH, EC, TDS and TSS were 6.77 and 7.90; 3420.33 and 52019.00 mS/cm; 480.33 and 400.00 mg/L; 40.00 and 18.50 mg/L for samples A and B, respectively. The freshly discharged effluent (Sample B) was higher in all the heavy metals, except nickel, than effluents from reservoir (sample A). The results from this study suggested that the effluents from the industry should be adequately treated before being discharged into the environment to forestall outbreak of diseases and heavy metal poisoning.

Keywords – Cocoa; effluent; microbiological and physicochemical characteristics

I. INTRODUCTION

Undoubtedly, industrialization in the developing world is accompanied by economic prosperity through wealth and job creation but concurrently exerts stress on life supporting systems such as atmospheric air and water bodies [1]. Industrialization aggravates environmental degradation [2]. While, effluents from industries discharged into a water body represent significant source of pollution in many Nigerian rivers. They have considerable deleterious effects on aquatic macro- and microflora alike [3]. Reference [4] noted that heavy metals from industries remain a major source of contamination of groundwater system in developing countries. Also, pathogenic microorganisms constitute the major contributors to numerous water-borne disease outbreaks with costly long-term effects. To mitigate this, indicator organisms are frequently used as a tool for determining the magnitude of risk the presence of a particular pathogen in wastewater can pose [5].

A number of studies have been conducted on effluents from cocoa processing industries. For instance, Akinnusotu and Arawande [6] conducted a study on the physicochemical properties, heavy metals and microbial load of effluents from different three cocoa processing factories in Nigeria, while Ogunleye and Izuagie [7] assessed the heavy metal contents in some industrial effluents including a cocoa processing industry. Hitherto, there is scanty work on the microbiological and physicochemical properties of effluents from different points within a cocoa processing industries. Therefore, this work was geared towards characterizing the effluents from reservoir and discharge point with a view of assisting the cocoa processing industries to take informed decisions as regards disposal of effluents for environmental safety.

ISSN: 2521-2293

II. MATERIALS AND METHODS

A. Study area

The effluent samples were collected from cocoa processing industry, Ile oluji, Nigeria. The town lies between longitudes 6º40 N, and 7º14 N, and latitudes 4º38 E and 4º53 E.

B. Preparation of media

The media used (nutrient agar and citrate agar) were weighed and prepared according to manufacturer's specification. The prepared media was carefully packed into the autoclave and sterilized at 121 ºC for 15 minutes. Prior to use, the media were cooled to about 45 ºC.

C. Isolation and identification of isolates

Plate growths were noticed after 24 hours of incubation, the isolates were then sub-cultured on fresh media plates until pure isolates were observed. The pure culture of isolates were stocked into MacCartney bottles. The isolates were identified based on their morphological appearance [8].

D. Gram staining techniques

A thin smear was made by emulsifying a little portion of organisms picked from stocked colony of 18–24 hours old pure culture into a drop of sterile distilled water on a grease free slide. The smear was air dried and heat fixed by passing it slightly over flame. The slide was carefully placed on the staining rack and was flooded with primary stain (crystal violet) for 30–60 seconds. Gram's iodine was added (mordant) for 30 seconds. The smear was gently rinsed with tap water. 70% ethanol was applied as decolouriser for 10–30 seconds; it was the stained with the secondary stain (safranin) for 30 seconds before rinsing with tap water and was allowed to dry. The smear was examined under the microscope using oil immersion objective (x100). Gram positive organisms appeared purple while Gram negative appeared red.

E. Biochemical characterization of the isolates

These tests were carried out to further identify and classify the isolates. They include; catalase test [8], citrate utilization test [9], indole Test [10], methyl red test, urea hydrolysis (urease test) [9], Voges Proskaurer test, sugar fermentation test (glucose, sucrose, lactose, galactose, maltose and fructose) [11], respectively.

F. Sugar fermentation test

The carbohydrate fermentation test is used to determine whether or not bacteria can ferment a specific carbohydrate. Carbohydrate fermentation patterns are useful in differentiating among bacterial groups or species. It tests for the presence of acid and/or gas produced from carbohydrate fermentation. Basal medium containing a single carbohydrate source such as glucose, lactose, sucrose or any other carbohydrate is used for this purpose. A pH indicator bromothymol blue (BTB), is also present in the medium; which will detect the lowering of the pH of the medium due to acid production. Small inverted tubes called Durham tube is also immersed in the medium to test for the production of the gas (hydrogen or carbon dioxide). It is a positive test for all members of *Enterobacteriaceae*.

G. Indole test

This test is used to identify microbes that can break down tryptophan to indole. It is used to identify bacteria of the family *Enterobacteriaceae*. Innocuate sterilized tubes containing tryptophan broth (4 ml) and incubate tubes for 24–28 hrs. After which 0.5 ml of Kovac's reagent is added. Presence/absence of ring indicates positive/negative test.

H. Citrate utilization test

This test is often used to differentiate organisms that are capable of utilizing citrate as a carbon source. Simmon's citrate agar medium was prepared in bijou bottle and allowed to set in a slanting position. A sterile wire loop was used to inoculate the test organism on to the slant medium and incubated at 37 ˚C for 48 hours after which it was examined for color change. A bright blue color in the medium gave a positive citrate test.

I. Catalase test

This test is used to identify organisms that produce the enzyme catalase. This enzyme detoxifies hydrogen peroxide (H_2O_2) by breaking it down into water and oxygen gas. This test demonstrates the presence of catalase, an enzyme characterized with the release of oxygen from hydrogen peroxide. A drop of 3% hydrogen peroxide solution was added to the sterile slide containing a loopful of the organism. Foaming or bubble indicates a positive result.

J. Urease test

This is used to identify those organisms that are capable of hydrolysing urea (bacteria that produce urease) to produce ammonia and carbon dioxide. It is primarily used to distinguish urease-positive protease from other Enterobacteriaceae. Organisms that hydrolyze urea rapidly (Proteus spp., *Morganel lamorganii*, and some *Providencia stuartii* strains) will produce strong positive reactions within 1 or 6 hours of incubation; delayed positive organisms (e.g. *Klebsiella* spp.and *Enterobacter* spp.) will produce weak positive reactions in the slant in 6 hours of

ISSN: 2521-2293

incubation which will be intense during further incubation. The culture medium will remain a yellowish color if the organism is urease negative e.g. *Escherichia coli*. If organism produces urease enzyme, the color of the slant changes from light orange to magenta. If organism do not produce urease the agar slant and butt remain light orange (medium retains original color).

K. Methyl red test

Methyl red broth was prepared and autoclaved in a test tube at 121 ºC for 15 min. The broth was allowed to cool and a colony of organism was inoculated into it and incubated at 37 ºC for 24 hours. About 2-3 drops of methyl red reagent were added to it. A positive result shows the presence of red ring in the test tubes while a negative result does not.

L. Voges-Proskaurer test

Voges-Proskaurer test was carried out by preparing MRVP broth or Clark and Lub's media in test tubes. The broth was inoculated aseptically with 2 loopful of respective bacterial culture. The test tubes were labelled with the name of organism inoculated. This was followed by incubation at 37 ºC for 48 h. Barrit's reagent A (α-napthol) and Barrit's reagent B (40% KOH) in the ratio 3:1 were added. The cotton plug was removed and the tubes were shaken for aeration. The result was observed after 15 min. Pinkish red colour at the surface was taken to be positive result.

M. Determination of physicochemical properties

1) Determination of pH

The pH of the collected samples were determined in the laboratory to cross check the field results using pH meter (Jenway 3505 model) after calibration with standard buffer solutions of pH 4 and pH 7 [12].

2) Determination of electrical conductivity

Electrical conductivity (EC) was measured using a portable Hanna Combo (combined) meter.

3) Determination of total suspended solid (TSS)

Filter paper was weighed and labelled A and B, dried in oven at 105 ºC for 30 mins and weighed again. 50 ml of the samples were measured and allowed to pass through the filter paper into a beaker and the filter paper was dried in the oven and was weighed.

4) Determination of total dissolved solid (TDS)

Evaporating dish was weighed and 50 ml sample was dispensed into the evaporating dish and the evaporating dishes were oven dried and weight of respective dishes were measured.

5) Determination of total solid (TS)

A 50 mL sample was weighed in petri-dish. The petri-dish and the sample was then transferred into the oven and dried at 105 ºC to a constant weight for 24 hours. The petri-dish and its content was later transferred into dessicator, cooled, weighed and calculated as described by Hewitt [12].

N. Determination of selected minerals

The selected minerals were determined as described by AOAC [13] by using atomic absorption spectrophotometer (Buck scientific, USA).

O. Statistical analysis

All determinations were carried out in triplicates and error reported as standard deviation from the mean. All data was subjected to analysis of variance and significance accepted at $p<0.05$. The means were separated using Fisher's least Significant difference test with Minitab statistical software package (version 21.1.0).

III. RESULTS

The cultural and biochemical characteristics of the isolates from cocoa processing effluents are presented (Table 1). The probable organisms and their percentage occurrence were *Escherichia coli* (25%), *Salmonella* spp. (25%), *Shigella* spp (12.5%), *Staphylococcus aureus* (12.5%) and *Proteus* spp. (25%).

The physico-chemical properties of the effluent samples are presented (Table 2). The pH of the two effluents ranged from 6.77 to 7.90 with effluents from reservoir (Sample A) having the lower value and the freshly discharged effluent (Sample B) having the higher value.

For electrical conductivities (EC) were 3420.33 mS/cm and 52019.00 mS/cm for sample A and B, respectively.

While, the total dissolved solids (TDS) for samples A and B were 480.33 mg/L and 400.00 mg/L, respectively. The total suspended solids (TSS) were 40.00 and 18.50 mg/L for samples A and B, respectively.

The selected heavy metals in the effluents are presented in Table 3. The freshly discharged effluent (Sample B) was higher in all the metals, except nickel, than effluents from reservoir (sample A).

ISSN: 2521-2293

Table 1. Cultural and biochemical characteristics of the isolates from effluents in Cocoa Industry, Ile-Oluji

Test	Isolate 1	Isolate 2	Isolate 3	Isolate 4	Isolate 5	Isolate 6	Isolate 7	Isolate 8
Gram staining	- rod	+ cocci	- rod	- rod	- rod	- rod	- rod	- rod
Catalase test	+	+	+	+	+	+	+	+
Methyl red test	+	+	+	+	+	+	+	+
Voges proskaurer	-	+	-	-	-	-	-	-
Urease	-	+	+	-	+	-	+	+
Citrate	-	+	+	-	+	-	+	+
Gas production	+	+	+	+	+	+	+	+
Indole	+	-	+	+	-	-	-	+
Galactose	+	+	+	+	v	v	v	+
Fructose	-	+	+	-	v	v	v	+
Sucrose	+	+	-	+	-	-	-	-
Mannitol	+	+	-	+	+	+	-	-
Organism	*Escherichia coli*	*Staphylococcus aureus*	*Proteus* spp.	*Escherichia coli*	*Salmonella* spp.	*Shigella* spp.	*Salmonella* spp.	*Proteus* spp.

Key: - = negative; + = positive; v = variable

Table 2. Physicochemical properties of effluents in Cocoa Industry, Ile-Oluji

Parameter	Sample A	Sample B
pH	6.77 ± 0.05^{b}	7.90 ± 0.05^{a}
Total suspended solid (mg/L)	40.00 ± 0.00^{a}	18.50 ± 0.10^{b}
Conductivity (mS/cm)	3420.33 ± 0.57^{b}	52019.00 ± 1.00^{a}
Total dissolved solids (mg/L)	480.33 ± 0.57^{a}	400.00 ± 0.00^{b}
Total solids (mg/L)	520.33 ± 0.57^{a}	418.50 ± 0.10^{b}

Values are Mean± SEM
Values with different alphabets within the row are significantly different $P<0.05$

ISSN: 2521-2293

Table 3. Selected heavy metals (mg/Kg) of effluents in Cocoa Industry, Ile-Oluji

Heavy metal	Sample A	Sample B	FME limit	NESREA limit
Cu	0.833±0.06[a]	0.407±0.01[b]	<1.00	0.5
Cd	0.002±0.00[b]	0.098±0.00[a]	-	0.2
Ni	0.010±0.00[b]	0.120±0.00[a]	-	0.01
Cr	0.002±0.00[b]	0.170±0.00[a]	-	0.05
Pb	0.000±0.00[b]	0.053±0.00[a]	<1.00	0.05

Values are Mean± SEM
Values with different alphabets within the row are significantly different $P < 0.05$
Cu = copper, Cd = cadmium, Ni = nickel, Cr =chromium, Pb = lead
FME = Federal Ministry of Environment, NESREA = National Environmental Standard and Regulation Enforcement

IV. DISCUSSION

The organisms have been reported by several authors to be causative organisms for several human and animal diseases. *Escherichia coli*, *Salmonella typhi* and *Shigella* species, are the most common food-borne disease causing organisms in developing countries [14]. The diseases such as diarrhea, dysentery and arthritis are caused by *Staphylococcus*, *Salmonella*, *Shigella* [15]. While hemorrhagic uremic syndrome could be caused by *Escherichia coli* and *Shigella* spp. [15]. *Proteus* spp., apart from being implicated in urinary tract infection, is one of the most important bacterial species associated with histamine poisoning in fish [15]. In most cases, foodborne illnesses are fatal as well as cause suffering, discomfort, and debilitation among the survivors with associated huge economic losses [15]. Therefore, effluents from cocoa processing industries should be treated before being discharged into the environment to forestall outbreak of diseases as indiscriminate discharge of untreated or poorly treated domestic and industrial wastewater effluents are major contributors to surface water pollution with its attendant health implications [16, 17].

The pH range is similar to the range (7.03 - 8.98) reported for wastewater from sewage works [18] but higher than the range (6.00 - 6.60) for effluents from some cocoa processing industries [6]. However, the pH values are within the recommended effluent discharge limit (6.00 – 9.00) stipulated by environmental regulatory agencies in Nigeria [19].

The high EC, especially for sample B, obtained in this study could be as result of high amount of dissolved ions in the effluents. The EC of the surface water is a valuable indicator of salinity with total salt content [18]. The EC values are higher than 60 - 1,095 mS/m reported for wastewater effluents in some communities in Africa [18] and 480 - 660 µs/cm for effluents from some cocoa processing plants [6].

The TSS for the samples were within the range (60-701 mg/L) reported for wastewater effluents in some communities in Africa [18], higher than the range (198 – 320 mg/ L) reported for effluents from some cocoa processing factories in Nigeria [6], and lower than range (848 – 1840 mg/L) for textile industries' effluents in Kaduna (Yusuf and Sonibare, 2004). However, the values for both samples are lower than the recommended limit (500 mg/L) stipulated by the National Environmental Standards and Regulation Enforcement Agency [20]. A high TDS could be lethal to aquatic organisms, leading to osmotic shock thereby, affecting the osmoregulatory strength of the organism [21]. The concentrations of TDS in irrigation water hinder plant growth, crop yield, and quality of product [22].

The difference in the TSS values could be as a result of precipitation of some solutes during stop-over of the effluent in the reservoir. The values for both samples are comparable to the range (24.80 – 30.20 mg/L) reported by Akinnusotu and Arawande [6] for effluents from different cocoa processing factories in Nigeria. While the TSS value for sample A is higher than the recommended limit (30 mg/L) that of sample B was lower than the limit stipulated by the Federal Ministry of Environment [6]. Meanwhile, the total solids (TS) for samples A and B were 520.33 mg/L and 418.50 mg/L, respectively. These values were lower than 116.60 – 350.20 mg/L reported by Akinnusotu and Arawande [6] for effluents from different cocoa processing factories in Nigeria. The high TSS and TS is an indication of contamination as

ISSN: 2521-2293

the solid materials may play host to different microorganisms.

For heavy metal contents, leaving the effluents in reservoir for a while could lead to reduction of the minerals in the effluents. The heavy metal contents of both samples are lower than the values (2.32, 0.14, 0.41, 1.00 and 0.9 mg/Kg for copper, cadmium, nickel, chromium and lead, respectively) reported by Okunola et al. [20] for wastewater from cocoa processing plant. The values for both samples are within the limits stipulated by the Federal Ministry of Environment. For sample A, the copper (Cu) content was above the limit stipulated by National Environmental Standard and Regulation Enforcement (NESRA) for effluent discharge. In the case of sample B, copper and cadmium contents were lower, while nickel (Ni), chromium (Cr) and lead (Pb) contents were higher, than the limits stipulated by NESRA for effluent discharge. Several authors have reported on the harmful effects of heavy metals including the ones involved in this study. For instance, Pb is highly toxic which has adverse effects on the neurological, biological, and cognitive functions in the bodies [23]. Cr can cause dermal, renal, neurological, GI diseases; and several cancers including lungs, larynx, bladder, kidneys, testicles, bone, and thyroid [24]. While Cd contamination of food and water supplies causes painful degenerative bone disease, kidney failure, GI and lungs diseases [25]. There is therefore, a need for treating the effluents, especially sample A, to reduce the levels of the heavy metals to meet the stipulated standards by regulatory agencies as they have harmful effects on human health [26].

V. CONCLUSION

This study showed that effluents from cocoa processing industry, Ile-Oluji, were laden with pathogenic microorganisms such as *Escherichia coli*, *Salmonella* spp., *Shigella* spp., *Staphylococcus aureus* and *Proteus* spp. Although, the pH of the effluents were within the stipulated limits set by regulatory agencies, the TSS and TS values of both sample were high. The heavy metal content of sample B was higher than the stipulated limits set for nickel, chromium and lead by NESRA for effluent discharge. The effluents should be adequately treated before being discharged into the environment to forestall outbreak of diseases and heavy metal poisoning.

ACKNOWLEDGEMENTS

The management of the Cocoa Processing Industry, Ile-Oluji, Ondo State, Nigeria, is appreciated for the maximum cooperation accorded the team of researchers during the collection of samples.

REFERENCES

1. P. Rasmi, “Impact of industrialization on environment and sustainable solutions – reflections from a south indian region,’’ IOP Conf. Ser.: Environ Earth Sci. vol. 120**,** pp. 012-016, 2018.
2. E.E.O. Opoku and O.A. Aluko, “Heterogeneous effects of industrialization on the environment: evidence from panel quantile regression,” Struct Chang Econ Dyn, vol. 59 pp. 174-184, 2021
3. I. Kanu and O.K. Achi, “Industrial effluents and their impact on water quality of receiving rivers in Nigeria, Journal of applied technology in environmental sanitation,” Vol. 1 pp. 75-86. 2011
4. O.O. Zacchaeus, M.B. Adeyemi, A.A. Adedeji, K.A. Adegoke, A.O. Anumah, A.M. Taiwo and S.A. Ganiyu, “Effects of industrialization on groundwater quality in Shagamu and Ota industrial areas of Ogun state, Nigeria,” Heliyon, 7:e04353. 2020
5. J.N. Okereke, O.I. Ogidi and K.O. Obasi, “Environmental and health impact of industrial wastewater effluents in Nigeria” - A Review, Int J Adv Res Biol Sci, vol. 6 pp. 55-67. 2016.
6. A. Akinnusotu and J.O. Arawande, “Qualities of Effluents from Three Cocoa ProcessingFactories in Ondo State, Southwest Nigeria,” Int J Environ Bioenerg, vol. 1 pp. 24-35. 2016
7. I.O. Ogunleye and A.A. Izuagie, “Determination of heavy metal contents in some industrial effluents from Ondo State, Nigeria,” J Environ Chem Ecotoxicol, vol. 8 pp. 216-219. 2013
8. H.J. Bennion, “Microbiological applications-a laboratory manual in general microbiology,” 5th ed. Brown Publishers, Boulevard, 1990
9. M. Cheesebrough, “District laboratory practice in tropical countries”, 2nd ed. Cambridge University press, Cambridge. 2006.
10. M. Kuffner, De S. Maria, M. Puschenreiter, K. Fallmann, G. Wieshammer, and M. Gorfer, “Culturable bacteria from Zn-and Cd-accumulating salix caprea with differential effects on plant growth and heavy metal availability,” J Appl Microbiol, vol 108, pp. 1471–84. 2010
11. J.F. McFaddin, “Biochemical test for identification of medical bacteria,” The Willims and Wilkinson, Baltimore. 2000

ISSN: 2521-2293

12. C.N. Hewitt, “Instrument analysis of pollutants”, Elsevier, London pp. 85-98. 2001.
13. AOAC, “Official Method of Analysis Association of Analytical Chemists,” 19th ed. Washington D.C. 2012.
14. A. Mengist, Y. Aschale and A. Reta,. “Bacterial and parasitic assessment from fingernails in Debre Markos, northwest Ethiopia’” Can J Infect Dis Med Microbiol, pp. 2-7. 2018
15. R. Bibek and B. Arun, “Fundamental food microbiology”, 5th ed. Taylor and Francis, Boca Raton, 2014.
16. A.W. Steel, A.J. Postgate, S. Khorsandi, J. Nicholls, L. Jiao, P. Vlavianos, N. Habib and D. Westaby, “Endoscopically applied radiofrequency ablation appears to be safe in the treatment of malignant biliary obstruction,” World J Gastrointest Endosc, pp. 1:149. 2011
17. H. Malassa, M. Al-Qutob, M. Al-Khatib and F. Al-Rimawi, “Determination of differenttrace heavy metals in ground water of South West Bank/Palestine by ICP/MS,” J Environ Prot Sci, vol. 08, pp. 818. 2013.
18. M.A. Agoro, O.O. Okoh, M.A. Adefisoye and A.I. Okoh, “Physicochemical properties of wastewater in three typical South African sewage works’” Pol J Environ Stud, vol. 2, pp. 491-499. 2018
19. O.F. Kayode, C. Luethi, and E.R. Rene, “Management recommendations for improving decentralized wastewater treatment by the food and beverage industries in Nigeria. Environments”, vol. 41, pp. 1-16. 2018.
20. A.A. Okunola, E.E. Babatunde, O.J. Temitope and O.O. Evelyn, “Assessment of environmental contamination by wastewater from a cocoa processing industry usinggenetic and reproductive biomarkers,” J Toxicol Risk Assess, vol.1 pp. 1-8. 2017
21. E.E. Odjadjare and A.I. Okoh, “Physicochemical quality of an urban municipal wastewater effluent and its impact on the receiving environment,” Environ Monit Assess, vol. 1 pp. 383. 2010.
22. J.S. Mcculloch and M. Robinson, “History of forest hydrology,” J. Hydrol, vol. 150, pp. 189. 1993
23. S. Kianoush, M. Balali-Mood, S.R. Mousavi, M.T. Shakeri, B. Dadpour, V. Moradi, “Clinical, toxicological, biochemical, and hematologic parameters in lead exposed workers of a car battery industry,” Iran J Med Sci, vol. 38, pp. 30. 2013
24. Z. Fang, M. Zhao, H. Zhen, L. Chen, P. Shi and Z. Huang, “Genotoxicity of tri-and hexavalent chromium compounds in vivo and their modes of action on DNA damage in vitro,” PLOS One 9 (8):e103194. 2014.
25. M. Nishijo, H. Nakagawa, Y. Suwazono, K. Nogawa and T. Kido, “Causes of death in patients with Itai-itai disease suffering from severe chronic cadmium poisoning: a nested case–control analysis of a follow-up study in Japan,” Brit Med J, vol. 7:e015694. 2017
26. M. Balali-Moo, K. Naseri, Z. Tahergorabi, M.R. Khazdair and M. Sadeghi, “Toxic mechanisms of five heavy metals: mercury, lead, chromium, cadmium, and arsenic,” Front Pharmacol, vol. 12643972. 2021

BIUST Teaching, Research, & Innovation Symposium 2023 (TRDAIS 2023)
Botswana International University of Science and Technology
Palapye, Botswana, 18 - 19 September 2023
ISSN: 2521-2293

Study of two Turbulence Models in Predicting the Drag of a Bluff Body

M.D. Koontse and N. Subaschandar*
Department of Mathematics and Statistical Sciences
Botswana International University of Science and Technology,
Private Bag 16,Palapye, Botswana

Abstract

Drag reduction on a two dimensional D-shaped bluff body is numerically studied. In this research, mesh independence study is carried out at the same velocity value of $10m/s$. The effect of Reynolds number on the drag coefficient is also carried out. This was done by increasing the inlet velocity from $10m/s$ to $60m/s$ hence increasing the Reynolds number. The k-ϵ and SST turbulence models are used and also their suitability for predicting the drag is compared in this study. Preliminary results on drag forces are presented here. The preliminary results suggest that the drag values obtained for our two-dimensional bluff body is mesh independent. The results also show that the drag coefficient remains nearly constant with increase in Reynolds number. The study show that the SST turbulence model underpredicts the drag coefficient compared to the k-ϵ turbulence model.

Keywords: Turbulence model, drag, Bluff body.

1 Introduction

It is believed that the Navier-Stokes equations can be used to fully describe turbulent flows, but current limitations in computational resourses have made direct solution of the Navier-Stokes equations impractical for all but very simple flows at low Reynolds numbers. The quest for the ultimate turbulence model has been ongoing for nearly a century now. Early turbulence models were emperically formulated algebraic relations. As computer speed, software capability and efficient numerical schemes developed and numerical simulation evolved, differential equation based transport type turbulence models became the turbulence simulation methodology of choice. The use of transport type turbulence models has become standard practice for most engineering applications. Many current researchers are now solving the unsteady Navier-Stokes

*corresponding author: raos@biust.ac.bw

ISSN: 2521-2293

equations for large-scale or grid realized, turbulence and modeling the smaller or subgrid, turbulent scales that cannot be captured on the computational grid.[1]
The subject of drag reduction of a bluff body is an interesting problem with a wide range of applications. Because of the difficulties associated with theoretical analysis, the study of drag reduction has been almost entirely experimental.[2] The flow over a bluff body is a common occurance associated with fluid flowing over an obstacle or with the movement of a natural or an artificial body. Evident examples are the flows past an airoplane, a submarine and a road vehicle. At much lower Reynolds numbers, the flow over a bluff body is highly viscous and the force exerted on the body is mainly attributed to the skin friction. However, when the Reynolds number exceeds a critical value, vortex shedding occurs in the wake, resulting in a significant pressure drop on the rear surface of the body.[3]
The main purpose of this paper is to predict the drag of a bluff body using two turbulence models,namely, the k-ϵ turbulence model and the Shear Stress Transport(SST) turbulence model. This is done based on the effect of grid/mesh size and the effect of Reynolds number against the drag coefficient(C_d).Preliminary results are presented here.

2 Mathematical Formulation

The flow around a D-shaped 2-dimensional rectangular cylinder of length $l = 0.355$ and height $h = 0.25$ is considered in this work. The effect of mesh/grid independence and the effect of Reynolds number on the drag of a bluff body are studied.
The flow domain is two dimensional and the fluid is air. This flow is steady, fully turbulent,incompressible with constant viscosity and constant density.
Figure 1 below shows the two-dimensional sketch of the computational domain. L is the length of the domain and H is the height of the domain. Lower case h is the height of the D-shaped rectangular cylinder, l is the length of the cylinder and $r = \frac{h}{2}$ is the radius of the semi-cycle.

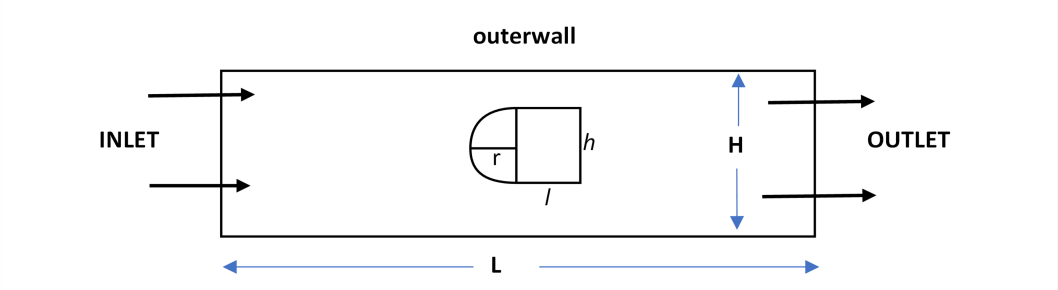

Figure 1: 2-D computational domain

The fundamental equations of fluid flow have been applied in this research. These equations results from the application of Newton laws to the moving fluid. The two dimensional form of

ISSN: 2521-2293

the transport equations for a general variable ϕ is given by

$$\frac{\partial(\rho\phi)}{\partial t} + \frac{\partial}{\partial x}(\rho u\phi) + \frac{\partial}{\partial z}(\rho w\phi) = \frac{\partial}{\partial x}\left(\Gamma\frac{\partial\phi}{\partial x}\right) + \frac{\partial}{\partial z}\left(\Gamma\frac{\partial\phi}{\partial z}\right) + S_\phi \tag{1}$$

where $\rho[kg/m^3]$ is the fluid density, $u(m/s)$ and $w(m/s)$ are the velocity components along the horizontal axis and along the vertical axis. Γ is the diffusion coefficient of ϕ and S_ϕ is the generation rate of ϕ per unit volume.
If ϕ in equation (1) was the velocity component we will now get the momentum conservation equations,The Navier Stokes Equations which for a two dimensional situation may be stated as

Horizontal component(x-direction):

$$\frac{\partial(\rho u)}{\partial t}+\frac{\partial}{\partial x}(\rho u^2)+\frac{\partial}{\partial z}(\rho wu) = \frac{\partial}{\partial x}\left[\Gamma\left(2\frac{\partial u}{\partial x} - \frac{2}{3}div\vec{V}\right)\right]+\frac{\partial}{\partial z}\left[\Gamma\left(\frac{\partial u}{\partial z}+\frac{\partial w}{\partial x}\right)\right]-\frac{\partial p}{\partial x}. \tag{2}$$

Vertical component(z-direction):

$$\frac{\partial(\rho w)}{\partial t}+\frac{\partial}{\partial x}(\rho uw)+\frac{\partial}{\partial z}(\rho w^2) = \frac{\partial}{\partial x}\left[\Gamma\left(2\frac{\partial w}{\partial z} - \frac{2}{3}div\vec{V}\right)\right]+\frac{\partial}{\partial x}\left[\Gamma\left(\frac{\partial u}{\partial z}+\frac{\partial w}{\partial x}\right)\right]-\frac{\partial p}{\partial z} \tag{3}$$

where $p[n/m^2]$ represents pressure and the diffusion coefficient in this case is given by

$$\Gamma = \mu + \mu_t$$

where $\mu(Ns/m^2)$ is the dynamic viscosity and μ_t is the turbulent viscosity.
The conservation of mass law, or continuity equation is also stated as:

$$\frac{\partial(\rho u)}{\partial t} + \frac{\partial(\rho u)}{\partial x} + \frac{\partial(\rho w)}{\partial z} = 0 \tag{4}$$

Turbulence Modelling
This section presents the mathematical equations of two turbulence models studied in this research. Each model will be presented separately.

Shear Stress Transport Turbulence model(SST)
The SST turbulence model was originally used for aeronautical applications but has since made its way into most industrial, commercial and many research codes. The starting point for its development was the need for the accurate prediction of the aeronautical flows with strong adverse pressure gradients and separation. Over decades, the available models had consistently failed to compute these flows[4]. The SST turbulence model[6] represents a combination of the k-ϵ and the k-ω models. According to [4], the k-ω model is more accurate near the wall but presents a high sensitivity to the ω values in the free stream region, where k-ϵ model shows

ISSN: 2521-2293

a better behaviour. The SST model represents a blend of the two, through a weighting factor computed based on the nearest wall distance. The governing equations for the SST model are as follows;

$$\frac{\partial(\rho k)}{\partial t}+\frac{\partial(\rho uk)}{\partial x}+\frac{\partial(\rho wk)}{\partial z}=\bar{P}_k-\beta^*\rho\omega k+\frac{\partial}{\partial x}\left((\mu+\sigma_k\mu_t)\frac{\partial k}{\partial x}\right)+\frac{\partial}{\partial z}\left((\mu+\sigma_k\mu_t)\frac{\partial k}{\partial z}\right) \quad (5)$$

and

$$\begin{aligned}\frac{\partial(\rho\omega)}{\partial t}+\frac{\partial(\rho u\omega)}{\partial x}+\frac{\partial(\rho w\omega)}{\partial z}=&\frac{\partial}{\partial x}\left((\mu+\sigma_\omega\mu_t)\frac{\partial\omega}{\partial x}\right)+\frac{\partial}{\partial z}\left((\mu+\sigma_\omega\mu_t)\frac{\partial\omega}{\partial z}\right)+\frac{\alpha\bar{P}_k}{v_t}\\&-\beta\rho\omega^2+2(1-F_1)\rho\sigma_{\omega2}\frac{1}{\omega}\left(\frac{\partial k}{\partial x}\frac{\partial\omega}{\partial x}+\frac{\partial k}{\partial z}\frac{\partial\omega}{\partial z}\right)\end{aligned} \quad (6)$$

where ω is the frequency of dissipation of turbulent kinetic energy.
The production of turbulent kinetic energy is limited to prevent the build-up of turbulence in stagnant regions:

$$\bar{P}_k=min(P_k,10\beta^*\rho k\omega)$$

The weighting function F_1 is given by

$$F_1=tanh\left\{\left\{min\left[max\left(\frac{\sqrt{k}}{\beta^*\omega y};\frac{500v}{y^2\omega}\right);\frac{4\rho\sigma_{\omega2}k}{CD_{k\omega}y^2}\right]\right\}^4\right\}$$

and

$$CD_{k\omega}=max\left(2\rho\sigma_{\omega2}\frac{1}{\omega}\frac{\partial k}{\partial x_j}\frac{\partial\omega}{\partial x_j},10^{-10}\right)$$

where y represents the distance to the neighbour wall and v is the laminar viscosity. F_1 is zero away from the wall(k-ϵ model) and changes to unit inside the boundary layer(k-ω model), with a smooth transition based on y.
The turbulent viscosity is computed as;

$$v_t=\frac{a_1k}{max(a_1\omega;SF_2)}$$

where S is the invariant measure of the strain rate given by

$$S=\sqrt{S_{ij}S_{ij}}\quad;\qquad S_{ij}=\tfrac{1}{2}\left(\tfrac{\partial u_i}{\partial x_j}+\tfrac{\partial u_j}{\partial x_i}\right)$$

and

$$F_2=tanh\left\{\left[max\left(\frac{2\sqrt{k}}{\beta^*\omega y};\frac{500v}{y^2\omega}\right)\right]^2\right\}.$$

ISSN: 2521-2293

The constants are computed as a blend of the k-ϵ and k-ω models, through the following generic equation;

$$\alpha = F_1\alpha_1 + (1 - F_1)\alpha_2.$$

The constants are

$\alpha_1 = \frac{5}{9}$ $\beta_1 = \frac{3}{40}$ $\sigma_{k1} = 0.85$ $\sigma_{\omega 1} = 0.5$

$\alpha_2 = 0.44$ $\beta_2 = 0.0828$ $\sigma_{k2} = 1$ $\sigma_{\omega 2} = 0.856$

$\beta^* = 0.09$

The Standard k-ϵ Turbulence model

A form of the standard k-ϵ turbulence model was first proposed by Harlow and Nakayana[5] and has since appeared in many reports. The model is often referred to as the standard k-ϵ turbulence model, where k stands for the turbulent kinetic energy and ϵ is the dissipation rate of the turbulent kinetic energy. The computation of the turbulent viscosity is made recurring to a turbulent model. The turbulent viscosity is given by the following equation

$$\mu_t = C_\mu \frac{\rho k^2}{\epsilon}.$$

The turbulence kinetic energy, k as well as its dissipation rate, $\epsilon(m^2/s^3)$ are computed using the following transport equations.

$$\frac{\partial(\rho k)}{\partial t} + \frac{\partial(\rho u k)}{\partial x} + \frac{\partial(\rho w k)}{\partial z} = \frac{\partial}{\partial x}[(\mu + \frac{\mu_t}{\sigma_k})\frac{\partial k}{\partial x}] + \frac{\partial}{\partial z}[(\mu + \frac{\mu_t}{\sigma_k})\frac{\partial k}{\partial z}] + P_k - \rho\epsilon \quad (7)$$

$$\frac{\partial(\rho \epsilon)}{\partial t} + \frac{\partial(\rho u \epsilon)}{\partial x} + \frac{\partial(\rho w \epsilon)}{\partial z} = \frac{\partial}{\partial x}[(\mu + \frac{\mu_t}{\sigma_k})\frac{\partial \epsilon}{\partial x}] + \frac{\partial}{\partial z}[(\mu + \frac{\mu_t}{\sigma_k})\frac{\partial \epsilon}{\partial z}] + \frac{\epsilon}{k}(C_1 P_k - C_2\rho\epsilon). \quad (8)$$

The term P_k represents the production rate of k as the results of the velocity gradients;

$$P_k = \mu_t[2(\frac{\partial u}{\partial x})^2 + 2(\frac{\partial w}{\partial z})^2 + (\frac{\partial u}{\partial z} + \frac{\partial w}{\partial x})^2] \quad (9)$$

The remaining model constants are given by

$C_\mu = 0.09$ $\sigma_k = 1.0$ $\sigma_\epsilon = 1.3$ $C_1 = 1.44$ $C_2 = 1.92$

ISSN: 2521-2293

Since the flow is considered steady, the $\frac{\partial}{\partial t}$ terms in all the above equations are considered to be zeros.
The above set of governing equations have been solved, along with appropriate boundary conditions for the computational domain using numerical methods. The boundary conditions are;

$u(0, z) = u_\infty(0m/s)$

$w(0, z) = u(x, 0) = u(x, +\infty) = w(x, 0) = w(x, +\infty) = 0$

At $x = L$, $\frac{\partial u}{\partial x} = \frac{\partial w}{\partial x} = \frac{\partial k}{\partial x} = \frac{\partial \epsilon}{\partial x} = 0$ for all z

At $x = 0$, $k = (\frac{3}{2} I \mu_\infty^2)$

I= Turbulence Intensity

$\epsilon = \left(\frac{C_\mu^{0.75} k^{1.5}}{L}\right)$ for all values of z

H=Inlet height(m)

The near wall treatment of momentum and turbulence equations as implemented in EasyCFD[7] obeys the suggestions explained in [8]. The basic motion behind the automatic wall functions is to change from a low-Reynolds number scheme to a wall function build on the mesh nodes nearness to the wall. The first order upwind method was used to discretize the momentum equations, turbulent kinetic energy and turbulence dissipation rate equations.
At the inlet of the computational domain, a uniform velocity condition is given. The exit was considered as a conservative outlet where the streamwise and normal gradients are zero for all parameters. On the walls the zero mean velocity condition was imposed. The computational fluid dynamics software EasyCFD[7] was chosen to solve these equations because of its capability, simplicity and user friendliness. This software uses a finite volume based discretization method. The computations are converged when the normalised residues for continuity and momentum equations are less than 0.0001.

3 Results and Analysis

The preliminary results shows that the drag of a bluff body is grid independent for both turbulence models. Figure 2 reflects that between the two models, as grid size increase the drag coefficient(C_D) for the SST turbulence model maintained less value as compared to the k-ϵ turbulence model. The graph also shows that both models maintained almost consistent value hence their graphs looking almost parallel as reflected in the graph.

ISSN: 2521-2293

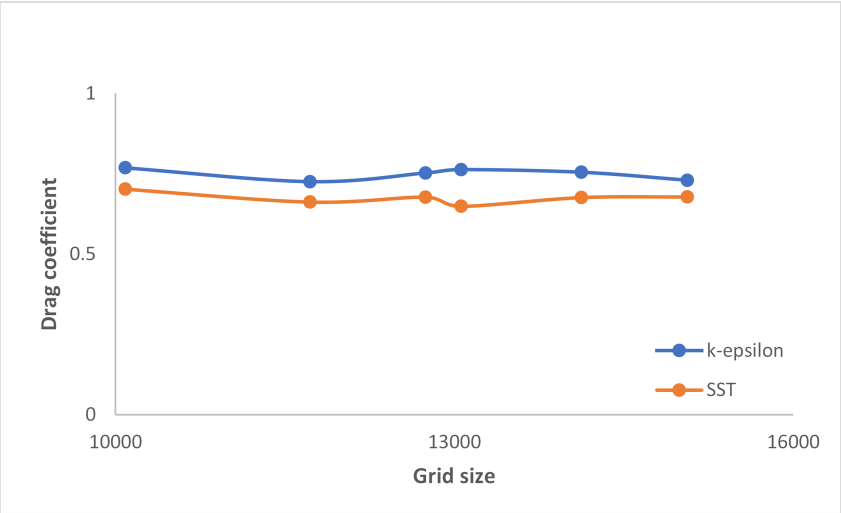

Figure 2: Effects of Mesh/Grid independence

The preliminary results also shows that as the inlet velocity increases(hence an increase in Reynolds number), the C_D maintained almost the same value as reflected in Figure 3. The SST turbulence model also maintained the least C_D value throughout as the Reynolds number increases.

ISSN: 2521-2293

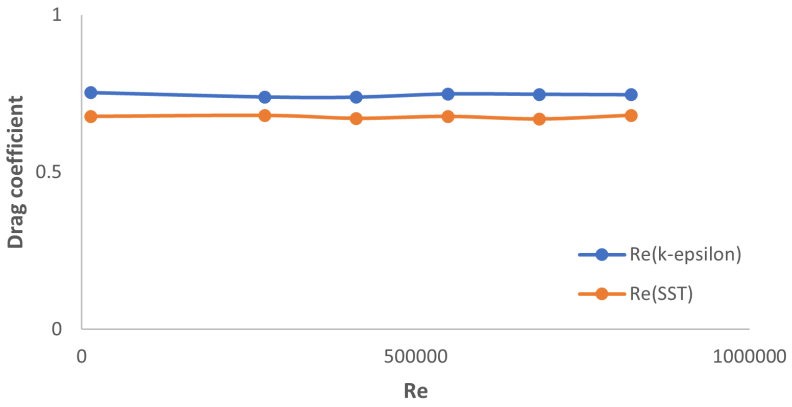

Figure 3: Effect of Reynolds number

4 Conclusion

The preliminary results suggest that between the two models for best results in predicting the drag of a bluff body, the SST turbulence model is the best model to use. The results also show that there was no any significant change in C_D for both models when increasing either the Reynolds number or grid size as reflected in figures 1 and 2.

References

[1] R.H Nicholas, *Turbulence models and their Applications to complex Flows*, University of Alabama at Birmingham,Revision 4.01.

[2] E. Rathakrishnam, *Effect of Splitter Plate on Bluff Body Drag*, AIAA Journal, Vol. 37, 1999.

[3] Choi,H. Jeon W and Kim J. *Control of Flow over a Bluff Body*,Annual Review of Fluid Mechanics, 40,2008, 113-139.

[4] F.R. Menter, M. Kuntz, R. Langtry, *Ten years of Industrial Experience with the SST Turbulence Model*, Turbulence Heat and Mass Transfer, 4(2003), 625-632. 10.4028, www.scientific.net/AMR.576.60.

ISSN: 2521-2293

[5] F.H. Harlow and P. Nakayama, *Transport of Turbulence Energy Decay rate*, Los Almos Science Lab, University of California Report LA-3854(1968).

[6] F.R. Menter, *Zonal two-equation k-ω Turbulence Model for Aerodynamic Flows*. AIAA Paper,1993-2906, 1993.

[7] A.G. Lopes, *EasyCFD: A Two-dimensional Computational Fluid Dynamics Software Manual.* Ver 4.4.4, www.easycfd.net, 2020.

[8] F.R. Menter, J.C. Ferreira and B. Konno, *The SST Turbulence Model with Improved Wall Treatment for Heat Transfer Predictions In Gas Turbines*, Proceedings of the International Gas Turbine Congress 2003, Tokyo, November 2-7,2003

BIUST Teaching, Research, & Innovation Symposium 2023 (TRDAIS 2023)
Botswana International University of Science and Technology
Palapye, Botswana, 18 - 19 September 2023
ISSN: 2521-2293

Energy Efficiency for Cloud Data Centers Using Machine Learning in Botswana

Nomsa Puso
Dept. of Computer Science and Information Systems
Botswana International University of Science & Technology
Palapye, Botswana
pn22100155@studentmail.biust.ac.bw

Tshiamo Sigwele
Dept. of Computer Science and Information Systems
Botswana International University of Science & Technology
Palapye, Botswana
sigwelet@biust.ac.bw

***Abstract*—Botswana is adopting cloud computing technology, and in the future, it will be dominated by more cloud data centers that will require more power supply from the grid. Botswana Fibre Networks (BoFinet) has planned to build the biggest cloud data center in the capital city with at least 400 racks, requiring more than 8MW from the power grid. Botswana government services will be hosted in this data center as virtual machines. Currently, Botswana's power supply is less than the demand, leading to power blackouts that have disrupted the subscribers like industrial and healthcare. These power blackouts have negatively impacted the economy of the country. More cloud data centers in Botswana will draw more electricity from the grid, which will cause more power blackouts unless sustainable sources like solar power are used. However, solar power adoption is shallow despite Botswana's high ultraviolet (UV) index of 9, indicating sufficient sunlight. There is a need for sustainable energy-efficient methods in cloud data centers. This paper proposes the most suitable machine learning approach to minimize energy consumption in cloud data centers which is applicable to Botswana. The proposed framework involves virtual machine placement optimization and shutting down low utilization data center servers to save energy while maintaining the quality of service (QoS). Machine Learning is a cutting-edge Industry 5.0 technology that can be applied to optimization for more accurate outcome predictions without being explicitly programmed to do so. The proposed framework will significantly reduce energy consumption and greenhouse gas emissions.**

Keywords*—Energy Efficiency; cloud computing; cloud data centers; virtual machine; quality of service (QoS), machine learning

I. Introduction

Cloud computing is a fast-growing technology that combines information technology (IT) efficiency and business agility major trends. High energy consumption poses as one of the major issues arising globally on cloud data centers. Hence, this paper is concerned with the development of a framework that minimizes or reduces energy consumption while maintaining the energy costs and QoS on the cloud using machine learning. The project basis lies on the utilization of deep reinforcement learning (DRL) as a machine learning algorithm for saving energy in cloud computing, it integrates the ability of feature learning and complex non-linear-function approximation deep learning (DL) ownership with the ability of decision-making reinforcement learning (RL) ownership, allowing the agent to perceive information in high-dimensional space, train models and make decisions based on the received information [1]. Machine learning (ML) has been on the forefront of other technologies when it comes to energy efficiency on cloud data centers.

The main aim of the study is to propose a framework that minimizes energy consumption while maintaining the energy costs and quality of service (QoS) on cloud data centers using machine learning. The overall goal of this study is achieved through the following contributions:

- Provide a literature review on the use of machine learning algorithms for saving energy in the cloud.
- Compare the performance results of each machine learning algorithm when solving energy efficiency problem.
- Develop a reinforcement learning model that would be able to minimize high energy consumption while maintaining energy costs and QoS on the cloud.
- Propose a prediction of underload or overload servers.
- Compare and test the framework with other models.
- Evaluate the proposed framework and publish its results or outcomes.

II. Literature Review

This section outlines state-of-art machine learning techniques and research related to green cloud computing, which reduces a significant portion of energy consumption in various aspects of a cloud computing system. Many researchers highlighted various innovations for energy efficiency in cloud computing. The author in [2] presented work, explored reinforcement learning algorithm for the virtual machine (VM) consolidation problem demonstrating their capacity to optimize the distribution of virtual machine across the data center for improved resource management. Author in [3] applied the random forest (RF) and multilayer perceptron (MLP)-based model to observe the low overhead and less energy consumption without significantly affecting the time to complete the tasks on the cloud. The author in [4] made use of machine learning technique called cooperative reinforcement learning (Q learning) agents for reducing user costs, reducing energy consumption, load balancing of resource, enhancing utilization of resources and improving availability and security.

ISSN: 2521-2293

Also, author in [5] used deep reinforcement learning to propose a novel hierarchical state space formulation coupled with a hybrid actor-critic technique for energy-efficient resource scheduling in edge-cloud environment. The author in [6] developed the ultra-low-power implementation of the DRL framework using stochastic computing technique, which has the potential of significantly enhancing the computation speed and reducing hardware footprint and therefore the power/energy consumption. Table 1 depicts different approaches of machine learning techniques in the field of energy efficiency and the metrics they have considered for the performance evaluation.

TABLE I. SUMMARY OF ENERGY EFFICIENCY-RELATED WORK IN CLOUD ENVIRONMENT

Authors	*Learning Model*	*Objective (Energy saving method)*	*Metrics*	*Limitations*	*Dataset*
Thein, et al., (2018) [7]	**Reinforcement learning and fuzzy logic**	Presented work provides the effective management of physical resources hosted by the infrastructure using dynamic resource demand patterns, Service Level Agreement, and resource utilization.	Accuracy (Power Usage Effectiveness in an efficient range from 1.79 to 1.96, resource utilization above 50%)	It considers only energy sources and the energy consumption for CPU and data centers. For a very large number of infrastructure resources, the scheduling process may become slow.	PlanetLab Virtualized Research datasets
McGough, et al., (2018) [3]	**Random Forest (RF) and MultiLayer Perceptron (MLP)**	Presented the work to observe low overhead and less energy consumption using ML techniques.	Accuracy (45.6-51.4% of the energy can be saved without significantly affecting the time to complete tasks)	The proposed approach uses real trace-logs allowing for complex situations to occur in the presented platform.	2010 exemplar datasets used with High Throughput Computing (HTC)-Sim
Rajalaksh-mi, et al., (2019) [8]	**Reinforcement Learning**	In the presented work, the learning agent improves the quality of the VM consolidation algorithm for energy consumption.	Correlation (the results shows that reinforcement learning (RLVC) algorithm gives minimum SLA violation compared to others by 8.5%)	The number of hosts can be increased to simulate the check the behavior of the proposed work.	The Cloudsim 3.0 use the PLANET LAB workload
Zhang et al., (2018) [9]	**Linear and Logistic Regression**	In the presented work, they use the classification of machine learning to model and analyze the multi-dimensional cloud resource allocation problem.	Response time (98% prediction accuracy)	A discussion on whether the resource allocation algorithm based on machine learning satisfies the strategy proof of the auction mechanism.	DAS-2 [ASCI (2017)] dataset from Grid Workloads Archive
Shaw et al., (2022) [2]	**Reinforcement Learning**	Presented work explores RL algorithm for the VM consolidation problem demonstrating their capacity to optimize the distribution of virtual machine across the data center for improved resource management.	Energy Consumption (energy efficiency is improved by 25% while also reducing service violations by 63% over the popular Power-Aware heuristic algorithm)	One of the fundamental challenges faced by model-free learning agents is tradeoff between exploration and exploitation.	Real workload data from PlanetLab
Madhusud han et al., (2021) [10]	**Genetic Algorithm (GA) and Random Forest (supervised machine learning technique)**	The aim of the work is to minimize power consumption while maintaining better load balance among available resources and maximizing resource utilization.	Energy Consumption, Execution Time, Resource Utilization, Average Start Time and Finish Time (GA-RF model improves energy consumption, execution time, and resource utilization of the data center and hosts as compared to the existing models).	The model was not tested with various machine learning and deep learning approaches for the better solutions and performance study.	Real workload traces from PlanetLab

ISSN: 2521-2293

Authors	*Learning Model*	*Objective (Energy saving method)*	*Metrics*	*Limitations*	*Dataset*
Yan et al., (2021) [11]	**Deep Q-learning (DQN)**	Using machine learning algorithm to achieve multiple optimization goals such as reducing power consumption, ensuring resource load balance, and improving user service quality.	Failure Rate, Average Reward, Power Consumption and SLA Violation (the proposed algorithm outperformed native DQN in terms of convergence speed, Q value estimation accuracy and stability. It has shown the flexibility to achieve multiple optimization goals including power consumption reduction, resource load balancing and SLA quality.)	Advanced DQN was compared with native DQN and simple heuristic algorithms which are easy to implement, but do not have specific optimization goals.	Used CloudSim 4.0 to simulate a cloud data center containing 32 heterogeneous PMs and dynamic arrival of VM requests for one hour
Jayanetti et al., (2022) [5]	**Deep reinforcement learning**	Proposed a novel hierarchical state space formulation coupled with a hybrid actor-critic technique for energy-efficient resource scheduling in edge-cloud environment.	Energy consumption, execution time, percentage of deadline hits and percentage of jobs have been used as evaluation metrics (Proposed DRL technique performed 56% better with respect to energy and 46% with respect to execution time compared to time and energy optimized baselines, respectively.)	The proposed reinforcement learning framework is designed to only operate in a centralized manner.	CloudSim simulation toolkit, dataset was created based on synthetic workflow structures provided by the popular Peagasus workflow framework.
Asghari et al., (2020) [4]	**Cooperative reinforcement learning (Q learning) agents**	Using machine learning technique to reduce user costs, reduce energy consumption, load balancing of resources, enhancing utilization of resources and improving availability and security.	Scheduling time, makespan, resource utilization, cost, power, and energy (The results of the experiments showed that the proposed model is more efficient in comparison with other methods in terms of makespan, resource utilization, cost, and energy consumption.)	Loss of accuracy due to discretization of state space.	Cloudsim, Workflowsim To evaluate the proposed method using real datasets, four classic and standard datasets of this area, namely Montage, Cybershake, SIPHT, and Inspiral have been used. The Pegasus Toolkit has been used also as an open-source toolkit to generate scientific workflows
Li et al., (2018) [6]	**Deep reinforcement learning**	In the presented work, they developed the ultra-low-power implementation of the DRL framework using stochastic computing technique, which has the potential of significantly enhancing the computation speed and reducing hardware footprint and therefore the power/energy consumption.	Power usage, average job latency, power usage and average job latency – achieve up to 54.1% energy saving compared with baselines (All tested cases can achieve at least 47.8% power consumption saving with only a slight increase in job latency. These results prove that weights of the reward function can take an effective control of the trade-off between power, latency, and resiliency)	DRL framework requires a relatively low-dimensional action space due to the fact that at each decision epoch the DRL agent needs to enumerate all possible actions under current state and perform inference using DNN to derive the optimal Q(s, a) value estimate, which implies that the action space in the general DRL framework needs to be reduced.	Real data center workload traces extracted from Google cluster usage traces over month-long period in May 2011. TensorFlow 0.10 is adopted for DNN construction.

ISSN: 2521-2293

A. *Summary of related works*

Deep reinforcement learning, support vector machine regression, k-means, random forest, linear and logistic regression were among the machine learning models used in the literature review, 60% of the authors used DRL technique to solve energy efficiency problems on the cloud. With 40%, CloudSim simulation toolkit is the most frequently adopted for data generation whilst other datasets are taken from different sources and databases. For evaluation purposes, energy consumption 13%, accuracy 9%, power consumption 4%, execution time 4%, resource utilization 4%, average reward 4%, makespan 4%, power usage 4%, average latency 4% and others were used as performance metrics by the authors.

The significant research has been made in recent years to reduce energy consumption in cloud computing. The author in [7] addressed the issue of energy-efficient resource allocation in cloud data centers. Nevertheless, the reinforcement learning, and fuzzy logic-based model had limitations, it only considered energy sources and energy consumption for central processing unit (CPU) and data center, which can be valid for the analysis, however other resources may also influence the scheduling method's outcome. One of the fundamental challenges faced by model-free learning agents is tradeoff between exploration and exploitation [2]. Author in [10] aimed at minimizing power while maintaining better load balance among available resources and maximizing resource utilization, but the model was not tested with various machine learning and deep learning approaches for the better performance study and solutions.

There was a loss of accuracy due to discretization of state space [4]. The author in [6] used a DRL framework which required a relatively low-dimensional action space due to the fact that at each decision epoch the deep reinforcement learning agent needs to enumerate all possible actions under current state and perform inference using deep neural network (DNN) to derive the optimal value estimate, which implies that action space in the general DRL framework needs to be reduced for more accurate results. Compared to the other work, this study proposes a dynamic virtual machine optimization and shutting down low utilization data center servers through the deep reinforcement learning model for saving the energy while maintaining the quality of service.

III. METHODOLOGY

Deep Reinforcement Learning (DRL) which is a combination of RL and deep learning, has overcome many issues through the function approximation, thereby eliminating the need for agents to visit all states during the training process and for storing state transition data in space-consuming tabular formats [5]. The inherent characteristics of the reinforcement learning paradigm, such as learning through experience combined with the use of neural networks for function approximation, make DRL an ideal candidate for dealing with the unpredictable dynamicity associated with cloud computing environments. A DRL technique is widely used for managing complex computing and networking infrastructures because it overcomes the curse of dimensionality by using neural networks as function approximators [12]. Deep reinforcement learning is very popular today because of its ability to solve complex consequential decision-making problems. The DRL model is pre-trained and used in real time for obtaining the scheduling decisions.

Caviglione et al., 2021, states that DRL belongs to a family of reinforcement learning methods that is well suited to dealing with sequential decision making problems. In more detail, they are based on an agent interacting with an environment in discrete steps via actions taken in response to an observation of the environment's state. The environment returns a reward as a result of an action, which is a scalar value measuring the effectiveness of the action. The goal is to maximize the total reward, which is calculated as the sum of the rewards obtained at each iteration. In contrast to supervised learning, rewards do not assign a label to a correct or incorrect answer [12].

The deep reinforcement learning model will be adopted to save energy in the cloud with reasons that it is the most used machine learning model from the literature. It is well known for cost reduction, minimizing energy consumption with high accuracy, easy to scale up and finally it uses deep neural networks function approximators solve energy efficiency issues on cloud data centers.

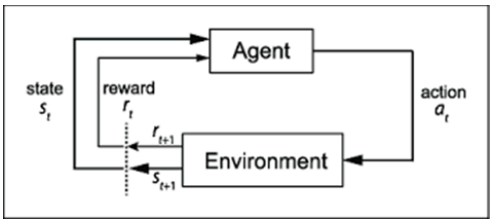

Fig. 1. Illustration of a simple flow of the agent-environment interaction in a Markov decision process

A. *DRL model's five key elements:*

- Agent: The model's algorithm/function that performs the requested task.
- Environment: The environment in which the agent operates. It uses the agent's current states and actions as input, rewards, and the agent's next states as output.
- State: It refers to the agent's position in the environment. There are two states: current and future/next.
- Action: The agent chooses and executes the moves in order to gain rewards.
- Reward: The agent's desired behaviors are referred to as rewards. Rewards, also known as feedback for the agent's actions in a given state, are described in the model as results, outputs, or prizes.

ISSN: 2521-2293

B. *Proposed Methodology*

Fig. 2. Steps of the proposed methodology

1. Gathering data: As the first step, data is collected from various sources, and the type of data collected is determined by the desired project.

2. Preparing that data: Data preparation is the process of cleaning raw data because it may contain missing values, inconsistent values, and duplicate instances, it cannot be used directly to build a model.

3. Choosing a model: The best performing learning algorithms are being researched, and their effectiveness is determined by the type of problem that needs to be solved.

4. Training: This is whereby the model is trained to improve its ability and the training dataset is fed to the learning algorithm.

5. Evaluation: In this stage, the model is evaluated to see if it is any good. To assess performance, metrics such as accuracy, precision, recall, and others are used.

6. Hyperparameter Tuning: Since this is an experimental process stage, increasing the number of testing cycles may result in more precise results.

7. Prediction: Finally, the created system or model is now used to solve real world problems, and this is where the true value of machine learning is realized.

IV. Evaluation

The key cloud performance metrics that are going to be used to evaluate the effectiveness of the proposed algorithm are energy/power consumption, accuracy, makespan, resource utilization, average reward, power usage effectiveness, execution time and average job latency. DRL-based model will be developed as a result of this study and it will involve the virtual machine placement optimization and shutting down low utilization for minimizing high energy consumption, excessive carbon emissions while maintaining the costs and QoS in cloud data centers. The proposed model will surpass the prediction accuracy ranging from 16.20-98% that was taken from the literature review.

V. Conclutions

Due to the ever expanding size of cloud computing facilities and ever-increasing number of users, high energy consumption has become a growing concern in the operation of complex cloud data centers. It does not only result in high costs, but it also produces excessive carbon emissions, which often leads to system unreliability and performance degradation. Energy efficiency is one of the main critical issues in the current cloud computing but since it lowers costs and adheres to green computing principles, ensuring energy efficiency is therefore a significant goal in Botswana. In this paper, DRL model was proposed as the most suitable machine learning technique that can be used for minimizing energy consumption in cloud data centers while maintaining the costs and quality of service. DRL has overcome many energy efficiency problems through the neural networks function approximation method that eliminates the need for the agents to visit all states during the training process. Energy/power consumption, accuracy, makespan, resource utilization, average reward, power usage effectiveness, execution time and average job latency will be used as performance metrics for evaluation. CloudSim simulation as used in the literature, will be adopted in this study to generate the data The proposed model will be better to surpass the prediction accuracy ranging from 16.20-98% that is taken from the literature.

Acknowledgment

I would like to express my deepest gratitude to my supervisor who is always there to guide me in every step of the way. This work is supported by the department of Computer Science and Information Systems, Botswana International University of Science & Technology.

References

[1] H. Fan, L. Zhu, C. Yao, J. Guo, and X. Lu, “Deep reinforcement learning for energy efficiency optimization in wireless networks,” in 2019 IEEE 4th International Conference on Cloud Computing and Big Data Analytics, ICCCBDA 2019, 2019. doi: 10.1109/ICCCBDA.2019.8725683.

[2] R. Shaw, E. Howley, and E. Barrett, “Applying Reinforcement Learning towards automating energy efficient virtual machine consolidation in cloud data centers,” Inf Syst, vol. 107, p. 101722, Jul. 2022, doi: 10.1016/j.is.2021.101722.

[3] A. S. McGough, M. Forshaw, J. Brennan, N. al Moubayed, and S. Bonner, “Using Machine Learning to reduce the energy wasted in Volunteer Computing Environments,” Oct. 2018, [Online]. Available: http://arxiv.org/abs/1810.08675

[4] A. Asghari, M. K. Sohrabi, and F. Yaghmaee, “A cloud resource management framework for multiple online scientific workflows using cooperative reinforcement learning agents,” Computer Networks, vol. 179, p. 107340, Oct. 2020, doi: 10.1016/j.comnet.2020.107340.

[5] A. Jayanetti, S. Halgamuge, and R. Buyya, “Deep reinforcement learning for energy and time optimized scheduling of precedence-constrained tasks in edge–cloud computing environments,” Future Generation Computer Systems, vol. 137, pp. 14–30, Dec. 2022, doi: 10.1016/j.future.2022.06.012.

[6] H. Li, R. Cai, N. Liu, X. Lin, and Y. Wang, “Deep reinforcement learning: Algorithm, applications, and ultra-low-power implementation,” Nano Commun Netw, vol. 16, pp. 81–90, Jun. 2018, doi: 10.1016/j.nancom.2018.02.003.

ISSN: 2521-2293

[7] T. Thein, M. M. Myo, S. Parvin, and A. Gawanmeh, "Reinforcement learning based methodology for energy-efficient resource allocation in cloud data centers," Journal of King Saud University - Computer and Information Sciences, vol. 32, no. 10, 2020, doi: 10.1016/j.jksuci.2018.11.005.

[8] N. R. Rajalakshmi, G. Arulkumaran, and J. Santhosh, "Virtual machine consolidation for performance and energy efficient cloud data center using reinforcement learning," Int J Eng Adv Technol, vol. 8, no. 3 Special Issue, 2019.

[9] J. Zhang, N. Xie, X. Zhang, K. Yue, W. Li, and D. Kumar, "Machine learning based resource allocation of cloud computing in auction," Computers, Materials and Continua, vol. 56, no. 1, 2018, doi: 10.3970/cmc.2018.03728.

[10] M. H. S, S. Kumar T, S. M. F. D. S. Mustapha, P. Gupta, and R. P. Tripathi, "Hybrid Approach for Resource Allocation in Cloud Infrastructure Using Random Forest and Genetic Algorithm," Sci Program, vol. 2021, pp. 1–10, Oct. 2021, doi: 10.1155/2021/4924708.

[11] J. Yan, J. Xiao, and X. Hong, "Dueling-DDQN Based Virtual Machine Placement Algorithm for Cloud Computing Systems," in 2021 IEEE/CIC International Conference on Communications in China (ICCC), Jul. 2021, pp. 294–299. doi: 10.1109/ICCC52777.2021.9580393.

[12] L. Caviglione, M. Gaggero, M. Paolucci, and R. Ronco, "Deep reinforcement learning for multi-objective placement of virtual machines in cloud datacenters," Soft comput, vol. 25, no. 19, pp. 12569–12588, Oct. 2021, doi: 10.1007/s00500-020-05462-x.

BIUST Teaching, Research, & Innovation Symposium 2023 (TRDAIS 2023)
Botswana International University of Science and Technology
Palapye, Botswana, 18 - 19 September 2023
ISSN: 2521-2293

Effect of harvest date on the yield and chemical composition of *Croton gratissimus* leaf essential oil

Eniah Lemogang Serame*, Wellington Masamba, Tshepo Pheko-Ofitlhile
Department of Chemical and Forensic Sciences
Botswana International University of Science and Technology
Palapye, Botswana
- Corresponding author *eniah.serame@studentmail.biust.ac.bw,*

Abstract
Essential oils are sensitive and complex mixtures which are composed of volatile secondary metabolites. The chemical profile of essential oils harvested from a particular plant vary with different parameters such as climate, soil type, methods of extraction, geographical origin, plant part and harvest conditions. As such, it is of paramount necessity to profile the essential oils extracted under different conditions as this can determine their potential applications. This study explored for the first time, the chemical composition of *Croton gratissimus* essential oil extracted by hydrodistillation from fresh leaves harvested on different dates. There was no difference in the essential oil yields obtained from the leaves harvested on different dates. The chemical profiling using gas chromatography mass spectrometry showed that the most dominant component in the essential oils extracted from the leaves harvested on different dates was cis-muurola-4(15),5-diene although its percentage abundance varied significantly. The essential oil extracted from the leaves harvested on different days also showed significant variation in the percentage composition of other major compounds such as camphor, germacrene D, β-himachalene, caryophyllene, α-muurolol and aromadendrene. The most abundant class of secondary metabolites for the essential oils harvested on all dates studied was the sesquiterpenes which also varied significantly in its percentage composition. These results point to a significant variation in the chemical profile of essential oils harvested from the same plant on different dates. Consequently, it is important to determine the chemical profile of the leaves of *Croton gratissimus* as it can vary depending on the conditions.

Keywords: Croton gratissimus, harvest date, essential oil, Croton zambesicus, chemical profile

INTRODUCTION

Essential oils are heterogenous mixtures of numerous volatile secondary plant metabolites which are mostly present in different concentrations depending on various factors [1]–[7]. These secondary metabolites are produced for the purposes of adaptation and mediation of interactions between plants and biotic environment[8], [9]. It has been widely reported that the chemical profiles of the essential oils are influenced by the plant species, climate, seasonal variation, growth conditions, agricultural methods, altitude, harvesting time, plant part used, sample size, processing methods and chemotype[8]. The chemotypes vary due to endogenous and exogenous factors and this may lead to differences in the oil quality of the same species [10][1]. Chemical variability and chemotype determination of the essential oils from a species, help in determining their pharmacological activities and toxicity levels [1]. Furthermore, the activities of essential oils may result from a synergistic action of all its chemical components[1] [11]. However, intraspecific variability of chemical constituents of essential oils of an individual plant has been reported[10]. This is mainly caused by the environmental factors[10]. *Croton gratissimus* essential oil is evidently receiving research attention due to its attractive yield and biological activity as well as the ethnomedicinal use of the plant[12]–[17]. Essential oils extracted from the leaves, bark, and roots of *Croton gratissimus* plant exhibit antimicrobial, vasorelaxant and antioxidant activities [ref]. Nevertheless, *Croton gratissimus* essential oils from different parts of the world have demonstrated significant variability in their chemical compositions[6], [12], [18]–[24]. The variation has even been reported in essential oils extracted from plants within the same

ISSN: 2521-2293

geographical origin and region[5], [8], [10], [19]. It is a challenge to establish the cause of chemical variability in essential oils due to many varied parameters during harvesting of the plant part, extraction, processing, and analysis of essential oils[19], [24]–[26]. Therefore, this study explored for the first time, the effect of harvest date on the chemical composition of *Croton gratissimus* essential oil extracted by hydrodistillation from fresh leaves harvested on different dates. To reduce interferences caused by many variables, the essential oils were extracted from the leaves of a single plant which were harvested on the same time of the day, and the oil was extracted and analyzed under similar conditions.

MATERIALS AND METHODS

Plant Collection and Authentication

The *Croton gratissimus* plant harvested at the Botswana International University of Science and Technology (BIUST), in Palapye, Botswana was authenticated by a botanist in the department of biological sciences in BIUST. The leaves of *Croton gratissimus* were harvested on three different dates in October 2018 [Table 1] from a single plant between 0940 and 1010 hours.

Sample Preparation

The fresh leaves of *Croton gratissimus* plant were crushed immediately after harvesting and the oil was extracted on the same day of harvest.

Extraction of Essential Oils by Hydrodistillation

The fresh leaves of *Croton gratissimus* plant were crushed immediately after harvesting and the oil was extracted on the same day of harvest. Extraction of essential oils from fresh leaves of *Croton gratissimus* was carried out by hydrodistillation using Clevenger-type apparatus. The crushed leaves (50.00 g) were placed in a 2.0 L conical flask after which 1200 mL of cold distilled water was added. The mixture was distilled for 3 hours after collecting the first drop of the distillate. After cooling, the oil was separated from the distillate using liquid-liquid extraction with pentane. The oil obtained was dried on anhydrous sodium sulphate, weighed, placed in an amber bottle, and stored in a refrigerator at 4 °C until further analysis.

Determination of Chemical Components of essential oils by Gas Chromatography Mass Spectrometry

The chemical composition of essential oils obtained from the leaves of *Croton gratissimus* were determined using gas chromatography interfaced with mass spectrometry (GC-MS). One microliter samples of essential oils diluted in the ratio of 1:100 (v/v) in hexane were injected on an Agilent Technologies 7890 gas chromatograph system coupled to an Agilent 5977A MSD. Separation of components was done on HP-5MS column (30 m × 0.25 mm id × 0.25 µm film thickness) with helium being the carrier gas. The flow rate of helium was set at 1 mL/ minute. The injector was set at 250 °C with a split ratio of 25:1. The column oven was initially set at 60 °C for 2 minutes, and then ramped to 125 °C at 1 °C/ minute, held there for 2 minutes, and finally ramped to 220 °C at 2 °C/ minute and held at 220 °C for 2 minutes. The mass spectra data was acquired in the electron impact mode (70 eV) in the m/z range of 40–400 a.m.u and scan time of 1.5 s. Normal alkanes C_7-C_{30} standard was also run under the same conditions and method. Identification of oil components was achieved through the analysis of their retention indices calculated from the C_7-C_{30} n-alkane standard as well as comparing their mass spectral fragmentation patterns with those reported in the literature and stored on the MS library and the NIST Chemistry Webbook.

Statistical Analysis

Two-way ANOVA was performed on the compositional data. The p-value was found to be less than 0.05 and the F critical was greater than F. This shows that the observed differences in chemical compositions are statistically significant.

RESULTS AND DISCUSSION

The effect of harvest date on the chemical composition of *Croton gratissimus* essential oil extracted by hydrodistillation from fresh leaves harvested on 03/10/18, 19/10/18 and 23/10/18 was investigated using

ISSN: 2521-2293

gas chromatography mass spectrometry. There was no difference on the essential oil yields obtained from the leaves harvested on different dates (0.12 -0.13%). However, the yield was lower than the literature values[12], [21]–[25]. The chromatograms of all sample essential oils obtained from GC-MS displayed more than 40 peaks [Figure 1 and 2]. Percentage compositions of compounds were calculated from the peak areas. The oils include cis-muurola-4(15),5-diene, β-himachalene and caryophyllene. Additionally, cis-muurola-4(15),5-diene was the most dominant compound in all sample oils. Its relative abundance ranged from 12.5% to 24.9%, the highest being from the oil extracted from the leaves harvested on 23/10/18. There was a noticeable difference in the percentage compositions of other major compounds such as germacrene D, aromadendrene, α-muurolol, γ-muurolene and camphor in the sample oils [Table 1 and Figure 3]. Germacrene D, caryophyllene and 1,8 cineole have been reported to be amongst the most abundant compound in *Croton gratissimus* essential oils[12], [25], [26]. The most dominant compound in the major classes of compounds include cis-muurola-4(15),5-diene sesquiterpene, camphor monoterpene and α-muurolol sesquiterpenoid [Figure 5]. The most abundant class of secondary metabolites for the sample essential oils was sesquiterpenes which ranged from 35.3 to 58. 5 % and being highest in sample

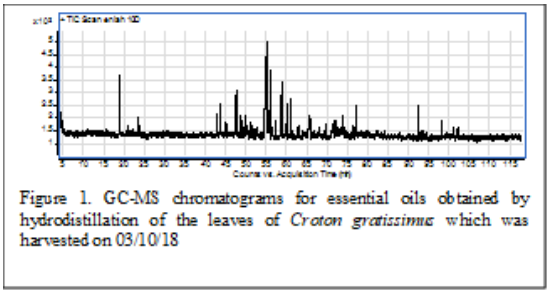

Figure 1. GC-MS chromatograms for essential oils obtained by hydrodistillation of the leaves of *Croton gratissimus* which was harvested on 03/10/18

results showed that all sample oils contained similar chemical compounds which varied in percentage compositions as depicted in Table 1. The most abundant compounds in each sample essential oil were identified and their percentage compositions were compared. The top three common major compounds identified in all sample essential oil from 23/10/18, as Figure 4 illustrates. The monoterpenoids 1,8 cineole and camphor were the most predominant in their class in all oils but the oil from 23/10/18 contained trace amount of 1,8 cineole. These results point to a significant variation in the percentage compositions of secondary metabolites found in essential oils harvested from the same plant on different dates. Intraspecific variability of chemical constituents of essential oils of an individual plant has been reported[10]. This has been attributed to environmental factors[10]. As such the variation in the percentage composition of the compounds in the sample essential oils in this study is thought to have been caused by environmental factors such as the amount of light, humidity or water, temperature, and weather conditions which the plant was subject to prior to harvesting. In the process of adapting to the environmental changes, the plant may have increased or decreased its production of some of the secondary metabolites.

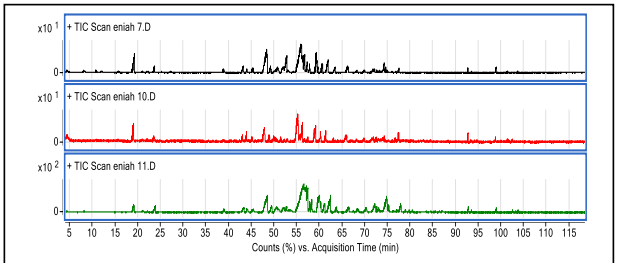

Figure 1. GC-MS chromatograms for essential oils obtained by hydrodistillation of the leaves of *Croton gratissimus* which were harvested at different dates: 7. D= 19/10/18, 10. D= 03/10/18, 11. D= 23/10/18, Zoomed chromatogram for purposes of clear illustration.

ISSN: 2521-2293

Table 1. Percentage composition of *Croton gratissimus* essential oils obtained by hydrodistillation of the leaves *Croton gratissimus* which were harvested at different dates.

KI	Class	Compound Identity	3/10/18	19/10/18	23/10/18	SD
1032	OM	1,8 Cineole	0.4	0.8	tr	0.4
1142	OM	Camphor	5.4	5.9	1.8	2.3
1189	OM	α-Terpineol	1.3	1.3	1.6	0.2
1373	S	Bourbonene	1.8	0.9	0.8	0.6
1416	S	Caryophyllene	5.3	9.1	8.6	2.1
1451	S	Aromadendrene	0.3	6.1	1.3	3.1
1472	S	cis-Muurola-4(15),5-diene	12.5	21.9	24.9	6.5
1475	S	γ-Muurolene	1.8	2.9	5.8	2.1
1480	S	Germacrene D	5.8	3.4	4.1	1.2
1503	S	β-Himachalene	5.4	5.8	7.3	1.0
1535	S	α-Cadinene	2.4	2.4	5.7	1.9
1647	OS	α-Muurolol	0.7	3.2	5.9	2.6
		Class				
		Monoterpenoids	7.1	8.0	3.4	
		Sesquiterpenes	35.3	52.5	58.5	
		Sesquiterpenoids	0.7	3.2	5.9	

Key OM = Monoterpenoids, S = Sesquiterpenes and OS =Sesquiterpenoids KI=Kovats retention index. GC-MS= Gas chromatography mass spectrometry, HP-5MS column, tr=trace Percentage composition of each class reported in this table was derived from the compounds in this table only.

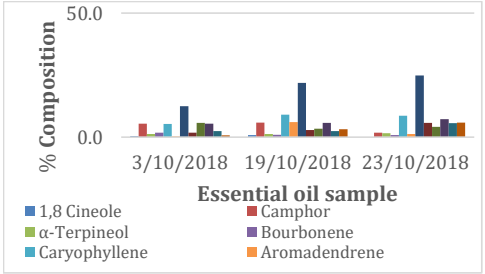

Figure 3. Major components of *Croton gratissimus* essential oils from the leaves harvested at different dates.

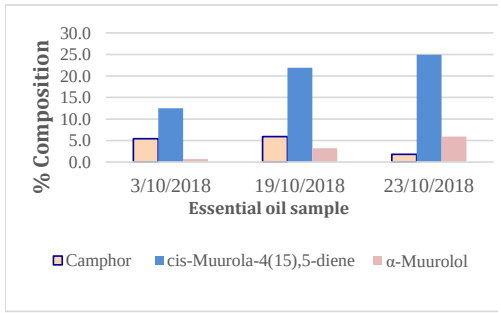

Figure 2. Comparison of selected major chemical components in *Croton gratissimus* essential oils harvested at different dates.

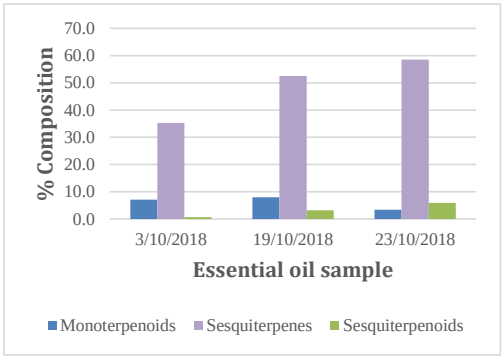

Figure 4. Major chemical classes of essential oils obtained by hydrodistillation of the *Croton gratissimus* leaves harvested at different dates.

CONCLUSIONS

The results of this study showed that all sample oils contained similar chemical compounds. However, there

ISSN: 2521-2293

was a significant variation in the percentage proportions of secondary metabolites in the essential oils obtained from the leaves of *Croton gratissimus* harvested on different days. Consequently, for a reproducible chemical profile to be obtained, the leaves of *Croton gratissimus* need to be collected on the same day and time then be processed under similar conditions.

REFERENCES

[1] N. Zouari, "Essential Oils Chemotypes: A Less Known Side," *Med. Aromat. Plants*, vol. 02, no. 02, 2013, doi: 10.4172/2167-0412.1000e145.

[2] N. Sadgrove and G. Jones, "A Contemporary Introduction to Essential Oils: Chemistry, Bioactivity and Prospects for Australian Agriculture," *Agriculture*, vol. 5, no. 1, pp. 48–102, 2015, doi: 10.3390/agriculture5010048.

[3] M. A. Hanif, S. Nisar, Z. Mushtaq, and M. Zubair, "Essential Oil Research," *Essent. Oil Res.*, no. June, 2019, doi: 10.1007/978-3-030-16546-8.

[4] S. Roohinejad *et al.*, "Extraction Methods of Essential Oils From Herbs and Spices," *Essent. Oils Food Process. Chem. Saf. Appl.*, pp. 21–55, 2017, doi: 10.1002/9781119149392.ch2.

[5] C. Turek and F. C. Stintzing, "Stability of essential oils: A review," *Compr. Rev. Food Sci. Food Saf.*, vol. 12, no. 1, pp. 40–53, 2013, doi: 10.1111/1541-4337.12006.

[6] N. J. Sadgrove, G. F. Padilla-González, and M. Phumthum, "Fundamental Chemistry of Essential Oils and Volatile Organic Compounds, Methods of Analysis and Authentication," *Plants*, vol. 11, no. 6, 2022, doi: 10.3390/plants11060789.

[7] C. Franz and J. Novak, *Sources of Essential Oils*. 2015.

[8] M. Moghaddam and L. Mehdizadeh, *Chemistry of Essential Oils and Factors Influencing Their Constituents*, no. October. 2017.

[9] K. D. Magwilu, J. M. Nguta, I. Mapenay, and D. Matara, "Phylogeny, Phytomedicines, Phytochemistry, Pharmacological Properties, and Toxicity of Croton gratissimus Burch (Euphorbiaceae)," *Adv. Pharmacol. Pharm. Sci.*, vol. 2022, 2022, doi: 10.1155/2022/1238270.

[10] A. Barra, "Factors affecting chemical variability of essential oils: A review of recent developments," *Nat. Prod. Commun.*, vol. 4, no. 8, pp. 1147–1154, 2009, doi: 10.1177/1934578x0900400827.

[11] S. F. van Vuuren and A. M. Viljoen, "In vitro evidence of phyto-synergy for plant part combinations of Croton gratissimus (Euphorbiaceae) used in African traditional healing," *J. Ethnopharmacol.*, vol. 119, no. 3, pp. 700–704, 2008, doi: 10.1016/j.jep.2008.06.031.

[12] O. A. Lawal, I. A. Ogunwande, F. O. Osunsanmi, A. R. Opoku, and A. O. Oyedeji, "Croton gratissimus Leaf Essential Oil Composition, Antibacterial, Antiplatelet Aggregation, and Cytotoxic Activities," *J. Herbs, Spices Med. Plants*, vol. 23, no. 1, pp. 77–87, 2017, doi: 10.1080/10496475.2016.1270245.

[13] S. Block, G. Flamini, D. Brkic, I. Morelli, and J. Quetin-Leclercq, "Analysis of the essential oil from leaves of Croton zambesicus Muell. Arg. growing in Benin," *Flavour Fragr. J.*, vol. 21, no. 2, pp. 222–224, 2006, doi: 10.1002/ffj.1558.

[14] O. A. Ajayi and I. E. Omomagiowawi, "Antimicrobial Activity of Croton zambesicus on Staphylococcus aureus and Streptococcus species," no. November, 2018.

[15] A. Salatino, M. L. F. Salatino, and G. Negri, "Traditional uses, chemistry and pharmacology of Croton species (Euphorbiaceae)," *J. Braz. Chem. Soc.*, vol. 18, no. 1, pp. 11–33, 2007, doi: 10.1590/S0103-50532007000100002.

[16] C. Baccelli, A. Martinsen, N. Morel, and J. Quetin-Leclercq, "Vasorelaxant activity of essential oils from croton zambesicus and some of their constituents," *Planta Med.*, vol. 76, no. 14, pp. 1506–1511, 2010, doi: 10.1055/s-0030-1249820.

[17] C. Baccelli, I. Navarro, S. Block, A. Abad, N. Morel, and J. Quetin-Leclercq, "Vasorelaxant Activity of Diterpenes from Croton zambesicus and Synthetic Trachylobanes and Their Structure−Activity Relationships," *J. Nat. Prod.*, vol. 70, no. 6, pp. 910–917, Jun. 2007, doi: 10.1021/np0603976.

[18] J. L. L. Cucho-Medrano, S. W. Mendoza-Beingolea, C. M. Fuertes-Ruitón, M. E. Salazar-Salvatierra, and O. Herrera-Calderon, "Chemical profile of the volatile constituents and antimicrobial activity of the essential oils from croton adipatus, croton thurifer, and croton collinus," *Antibiotics*, vol. 10, no. 11, 2021, doi: 10.3390/antibiotics10111387.

ACKNOWLEDGEMENTS

BIUST for research grants and Department of Chemical and Forensic Sciences, an incubation and breeding place.

ISSN: 2521-2293

[19] S. van Vuuren, "The Antimicrobial Activity and Essential Oil Composition of Medicinal Aromatic Plants Used in African Traditional Healing," pp. 1–305, 2007.

[20] M. S. Owolabi, L. A. Oladipupo, L. Lajide, R. M. Hauser, and W. N. Setzer, "Leaf oil composition of Croton zambesicus Muell . Arg . growing in southwestern Nigeria : essential oil chemotypes of C . zambesicus," *Am. J. Essent. Oils Nat. Prod.*, vol. 1, no. 1, pp. 14–17, 2013.

[21] S. Yagi, R. Babiker, T. Tzanova, and H. Schohn, "Chemical composition, antiproliferative, antioxidant and antibacterial activities of essential oils from aromatic plants growing in Sudan," *Asian Pac. J. Trop. Med.*, vol. 9, no. 8, pp. 763–770, 2016, doi: 10.1016/j.apjtm.2016.06.009.

[22] F. F. Boyom *et al.*, "Essential oils from Croton zambesicus Muell. Arg. growing in Cameroon," *Flavour Fragr. J.*, vol. 17, no. 3, pp. 215–217, 2002, doi: 10.1002/ffj.1081.

[23] C. Menut *et al.*, "Aromatic plants of tropical Central Africa. XXII. volatile constituents of Croton aubrevillei J. Léonard and C. Zambesicus Muell. Arg.," *J. Essent. Oil Res.*, vol. 7, no. 4, pp. 419–422, 1995, doi: 10.1080/10412905.1995.9698552.

[24] M. P. Moremi, F. Makolo, A. M. Viljoen, and G. P. Kamatou, "A review of biological activities and phytochemistry of six ethnomedicinally important South African Croton species," *J. Ethnopharmacol.*, vol. 280, no. May, p. 114416, 2021, doi: 10.1016/j.jep.2021.114416.

[25] N. J. Sadgrove, L. G. Madeley, and B. E. Van Wyk, "Volatiles from African species of Croton (Euphorbiaceae), including new diterpenes in essential oil from Croton gratissimus," *Heliyon*, vol. 5, no. 10, p. e02677, 2019, doi: 10.1016/j.heliyon.2019.e02677.

[26] A. Ogundajo, I. Ogunwande, H. Gbadamosi, R. Giwa, and G. Flamini, "Chemical Composition of the Leaf Essential Oils of Croton zambesicus Müll.-Arg. Grown in Lagos, South-West Nigeria," *European J. Med. Plants*, vol. 4, no. 12, pp. 1524–1533, 2014, doi: 10.9734/ejmp/2014/7099.

BIUST Teaching, Research, & Innovation Symposium 2023 (TRDAIS 2023)
Botswana International University of Science and Technology
Palapye, Botswana, 18 - 19 September 2023
ISSN: 2521-2293

Chemical composition, antimicrobial and antioxidant activity of *Schinus molle* essential oil from Palapye

[1]Dagmai H. Mehreteab, [1]Naumie Gasemodimo, [1]Mpho Mabutho, [2]Eniah Serame, [2]Tshepo Pheko-Ofitlhile, [1]Abdullah Makhzoum and [1]Kabo Masisi*
[1]Department of Biological Sciences and Biotechnology; [2]Chemical and Forensic Sciences
Botswana International University of Science and Technology, Palapye, Botswana
masisik@biust.ac.bw

Abstract- Plants have been a source of medical relief for diseases and ailments for millennia, and among this large list of medicinal plants includes the Peruvian pepper tree (Schinus molle). This species produces various compounds with antibacterial properties, such as alkaloids, flavonoids, phenols, and terpenes. This study was aimed at investigating the chemical composition, antioxidant, and antimicrobial activity of S. molle essential oil extracts collected from Palapye on bacterial and yeast colonies as a means to determine the antimicrobial efficacy. Fruit and leaf essential oils of S. molle were extracted using ultrasonic-assisted hydrodistillation. Using gas-chromatography mass spectrometry (GC-MS), 19 compounds were identified from fruit essential oil while only two were identified from the leaf essential oil. Antioxidant activity measured by 2,2-diphenyl-1-picryl-hydrazyl (DPPH), 2,2'-azino-bis-3-ethylbenzothiazoline-6-sulfonic acid (ABTS) and total phenolic content (TPC) showed significantly higher antioxidant activity in the fruit essential oil as compared to the leaf counterpart. Furthermore, antimicrobial activity of the essential oils was determined against bacterial colonies of Staphylococcus aureus and Escherichia coli, and the fungi C. albicans using agar disc diffusion assay. Our results showed one-third efficacy against bacteria as compared to the commercial broad-spectrum antibiotic Gentamicin, while there was no antibiotic activity observed against the fungi.

Keywords*: Antioxidant, antimicrobial, Gas chromatography-mass spectrometry, essential oil, *Schinus molle

I. INTRODUCTION

Antibacterial resistance of pathogenic microorganisms has become a global dilemma, leading to large number of diseases and deaths [1]. Drug resistance patterns observed in various types of bacteria have led to infectious cases that are virtually untreatable by commonly applied antimicrobial methods [2]. This is mainly caused by the excessive, and at times, unnecessary, use of broad-spectrum antibiotics, as the identification and customized treatment plans for specific microbial infections is greatly lacking in most healthcare settings [1]. Bacterial resistance to antibiotics and the development of resistant bacteria have been increasing exponentially, causing many tried and tested treatments to be rendered ineffective against such diseases-causing microorganisms. This has led to the need to develop new, revolutionary treatments [3]. Plants, including the Peruvian pepper tree (*Schinus molle*), produce various compounds with antibacterial properties, such as alkaloids, flavonoids, phenols, and terpenes, known to target the cell membrane of different microorganisms as their bactericidal mechanism of action. It has been recently established that essential oils, when administered at varying concentrations, respond to microbial action in different ways. For example, through blockage or interruption of bacterial communication, known as quorum sensing [4].

A. Distribution, properties, and uses of Schinus molle

The Peruvian or Californian pepper tree (*Schinus molle*) is an evergreen shrub native to Peru and has become widespread in many parts of the world [5]. *S. molle* is a member of the Anacardiaceae family,

ISSN: 2521-2293

comprising of over 30 species that are native to Central and South America [6, 7]. *S. molle* is commonly used as traditional medicine in South America because of its antifungal, analgesic, antitumoral, antispasmodic, and topical antiseptic properties. It has also been used to treat hypertensive disorders, wounds, asthma, and septic infections [5, 8, 9]. The success of this species' distribution worldwide is credited to its resilience against drought and heat, ability to outcompete native species for nutrients and light, and its quick growth rate and high seed proliferation [10, 11]. The *S. molle* tree has been used as an ornamental plant in Southern African countries including Mozambique, Malawi, South Africa, Botswana, Zambia, and Zimbabwe [12, 13]. The pepper tree, locally known as "Pepere" in Botswana, grows up to between 3-15 m tall, with dark brown, deeply fissured bark. Its leaves are imparipinnate, possessing long, thin leaves, present in clusters of 20-40 leaflets [14]. It produces an edible fruit which, when ripe, is about 5 mm in diameter and often pink-reddish to red in color. Thus far, there are limited to no reports in literature regarding the chemical composition, antioxidant, and antimicrobial activity of *S. molle* from Botswana on bacterial and fungal colonies to combat pathogenic microorganisms. Considering the connection between chemical composition, antioxidant activity, climatic and geographical factors, this study aimed to investigate the chemical composition, antioxidant activity and antimicrobial activity of *S. molle* essential oils (extracted from fruits and leaves) from Palapye on bacterial colonies of *Staphylococcus aureus, Escherichia coli* and the yeast *Candida albicans*. Previous research on *S. molle* has shown that essential oil composition can be greatly affected by soil type, harvest time and the extraction method used [15, 16].

II. METHODOLOGY

A. Sample and extraction of essential oil

Leaves and fruits of female *Schinus molle* were collected in the Palapye area of Botswana. Plant fruits and leaves were later cleaned and dried using liquid nitrogen, and afterwards ground to powder and stored at 4°C until further analysis.

Extraction was done as previously described by Jadhav et al. [17]. About 100 g of powder samples in triplicates was mixed with 300 mL of water and sonicated for 1 hour at 40°C. After an hour, the samples were taken to a simple distillation apparatus set at 100°C and oils were obtained after 6 hours. Essential oils were collected and kept at 4°C until further analysis.

B. Chemical composition, antimicrobial and antioxidant analyses

1. GC-MS analysis of the essential oils

Chemical composition analysis of the essential oils from the fruits and leaves of *S. molle* were performed on gas chromatography-mass spectrometry (GC-MS), with an Agilent GC System 7890B, MSD 5977A, using a 30 m long capillary column (30 m × 0.25 mm × 0.25 µm, calibrated). The carrier gas used was helium at 11.1 psi, at constant pressure and the split ratio was 1:10. The column temperature was programmed from 70°C to 300°C at 5°C/min, with no holding temperature. The fruit essential oil samples were dissolved in n-hexane at a ratio of 1:100 µL; leaf essential oil samples were dissolved at a ratio of 1: 50 µL. Duplicate samples of the essential oils were prepared for GC-MS. Sample volumes of 1 µL of each oil sample were injected manually at a split ratio of 1:10. Chemical components of the essential oils were identified through comparison of their mass spectra and retention indices contained in the NIST MS Search 2.0 (Contributor: NIST Mass Spectrometry Data Centre, 1990).

2. Antioxidant activities: DPPH radical scavenging assay

The free radical scavenging activity of each essential oil was measured using a 2,2-diphenyl-1-picryl-hydrazyl (DPPH) assay as previously reported by Stankovic et al. [18]. Shortly, 0.1 mL of the oil was vortexed vigorously with DPPH solution (60 µM) (in triplicates). The mixture was incubated in the dark for 30 minutes at room temperature and absorbance was measured against blank at 517 nm. The DPPH was presented as mg ferulic acid equivalence/mL of the oil sample (mg FAE/mL of oil sample).

3. Antioxidant activities: ABTS radical scavenging assay

The free radical scavenging activity of each sample was also determined using 2, 2'-azino-bis-3-ethylbenzothiazoline-6-sulfonic acid (ABTS) solution following a well-established method [19]. Shortly, 0.1 mL of the oil was vortexed vigorously with ABTS solution (in triplicates). The mixture was then incubated in the dark for 30 minutes at room temperature and absorbance was measured against a blank at 735 nm. The ABTS was presented as mg

ISSN: 2521-2293

ferulic acid equivalence/mL of the oil sample (mg FAE/mL of oil sample).

4. Antioxidant activities: Total phenolic content

Total phenolic content (TPC) was assessed as described previously [20]. In short, 2.5 mL Folin-Ciocalteu reagent (10 folds) and 2.5 mL sodium carbonate (60 g/L) were added to 0.5 mL of each oil extract (in triplicates). The mixtures were incubated in the dark for 15 minutes at 45°C and absorbance was measured against a blank at 765 nm. The TPC was presented as mg ferulic acid equivalence/mL of the oil sample (mg FAE/mL of oil sample).

5. Antimicrobial activity assay: Agar disc diffusion method (Kirby-Bauer Test)

To determine the antimicrobial activity of *S. molle* essential oil extracts, an agar disc diffusion method was conducted. Agar plates containing Mueller-Hinton agar (MHA) for bacterial cultures of *S. aureus* and *E. coli*, and yeast extract peptone dextrose (YPD) for yeast cultures of *C. albicans* were prepared, autoclaved and poured into Petri dishes and stored before use. All microorganisms used were cultured in Mueller-Hinton broth (MHB) at 37°C for 18 hours before use in a VWR 3500 Incubating Orbital Shaker (12620-948, VWR International, Radnor Township, Pennsylvania, USA) at 160 rpm, after which the microbial suspensions were diluted with MHB until a McFarland turbidity standard of 0.5 was achieved. Sterile discs were made from Whatman No. 3 filter paper (6 mm discs) and imbibed with 10 µL of pure essential oils and placed onto the MHA and YPD plates using sterilized forceps. For the bacterial samples, a positive control of Gentamicin antibiotic disc (10 µg/disc), was chosen with 10 µL discs of Mueller Hinton Broth (MHB) used as negative controls. The positive control for yeast was 10 µL discs of cycloheximide 200 µg/mL (prepared from ultra-pure grade crystalline cycloheximide), with the same negative control used as in the antibacterial assays. Commercially sold eucalyptus oil (purchased from a local pharmacy) was used as a secondary positive control as it is a well-established antibacterial [21] and antifungal essential oil [22]. The agar plates were incubated at 37ºC for 24 hours and antimicrobial activity was determined by measurement of the inhibition zones (in millimeters). Measurements for each oil, positive and negative controls were done in triplicates.

C. Statistical analysis

Results were subjected to one-way analysis of variance (ANOVA) by social survey research information (SSRI) statistical software-excel statistics. Values are represented as means ± standard error (SE). Statistical significance of the difference among means was estimated at $P < 0.05$, using Tukey-Kramer's multiple range test. Graphical representation of data was done using OriginPro 8.

III. RESULTS AND DISCUSSION

A. GC-MS analysis: chemical composition of the essential oils

Twenty-one compounds were identified in total, with 19 compounds identified in the fruit essential oils (Table I) and only two identified in the leaf essential oils (Table II). Monoterpenoids (D-limonene, β-pinene, α-phellandrene, β-phellandrene, and ascaridole,) and sesquiterpenoids (caryophyllene, humulene, α-muurolene, tau-cadinol, tau-muurolol, α-cadinol and 6-epi-shyobunol) formed a significant fraction of the *S. molle* fruit essential oil, and the monoterpene β-phellandrene in the leaf oil.

Found in the essential oils of many plants, including culinary staples such as fruits, vegetables, and herbs, monoterpenes are known to be effective in the treatment of several cancers in the early and advanced stages, including mammary, lung and liver cancers, having been used to treat breast and pancreatic carcinomas in mice [23]. Monoterpenes have also been shown to be of great use in the preservation of tropical fruits from fungi [24], and also possess strong antibacterial and antimicrobial activity, with research showing bactericidal and antimicrobial activities of β-pinene, limonene, and α-phellandrene, to name a few [25-28]. Sesquiterpenoids are relevant secondary metabolites found in the natural world, mostly in volatile plant oils, microbes, and some insects [29]. While there has been extensive research in the use of plants in traditional and folk-medicine, very few findings exist with regards to sesquiterpenoids. Among those that do, however, show that sesquiterpenoids are crucial in the treatment of various bacterial and fungal infections [30, 31].

ISSN: 2521-2293

TABLE I: THE COMPOSITIONS OF THE FRUIT ESSENTIAL OIL EXTRACTS FROM *S. MOLLE* L.

No.	Retention Time (RT)	Name
1	3.11	o-Cymene
2	3.236	D-Limonene
3	3.865	β-Pinene
4	4.123	α-Phellandrene
5	5.559	Octanoic acid, methyl ester
6	8.941	Ascaridole
7	12.528	Cyclohexane, 1-ethenyl-1-methyl-2,4 bis(1-methylethenyl)-
8	12.677	Cyclohexane, 1-ethenyl-1-methyl-2,4-bis(1-methylethenyl)-, [1S-(1α, 2β, 4β)]-
9	12.963	1H-Cycloprop(e)azulene, 1a,2,3,4,4a,5,6,7b-octahydro-1,1,4,7-tetramethyl-, [1aR-(1aα,4α,4aβ,7bα)]-
10	13.209	Caryophyllene
11	14.056	Humulene
12	14.954	1H-Cycloprop(e)azulene, decahydro-1,1,7-trimethyl-4-methylene-
13	15.201	α-Muurolene
14	15.538	Naphthalene, 1,2,3,4,4a,5,6,8a-octahydro-7-methyl-4-methylene-1-(1-methylethyl)-, (1α, 4aβ, 8aα)-
15	15.859	Naphthalene, 1,2,3,5,6,8a-hexahydro-4,7-dimethyl-1-(1-methylethyl)-, (1S-cis)-
16	18.525	.tau.-Cadinol
17	18.554	.tau.-Muurolol
18	18.845	α-Cadinol
19	19.675	6-epi-shyobunol

TABLE II: THE COMPOSITIONS OF THE LEAF ESSENTIAL OIL EXTRACTS FROM *S. MOLLE* L.

No.	Retention Time (RT)	Name
1	4.054	β-Phellandrene
2	22.525	Isobutylamine

B. Antioxidant activities: DPPH radical scavenging assay

DPPH antioxidant activities of leaf and fruit essential oils from *S. molle* in Palapye are shown in Figure 1. Free radical scavenging activity of DPPH is based on electron transfer, that produces a violet solution in alcohols such as methanol and ethanol [32]. In the presence of an antioxidant molecule, the free radicals in DPPH experience a reduction of electrons, causing a colourless solution. The stronger the antioxidant, the higher its free radical scavenging activity, which is used to represent the free radical reduction activity of antioxidants [32]. From the standard calibration curve against ferulic acid (linear with $y = 1.1145x + 0.0354$, $R^2 = 0.9295$), the scavenging capacity of the leaf and fruit essential oils of *S. molle* were determined to be 142.8 ± 1.80 mg and 139.4 ± 3.74 mg of ferulic acid equivalent (FAE)/g of sample, respectively (*Fig. 1*). Our data shows significantly high antioxidant activity (value; $P < 0.05$) in leaf essential oil extract when compared to fruit essential oil extract from *S. molle*. While it was expected that the fruit oil extracts should possess higher antioxidant activity, previous research has shown that higher antioxidant activity in leaves may be attributed to the presence of hydroxyls group in oxygenated sesquiterpenes found in the leaf oils [5], which may have not been identified in our GC-MS.

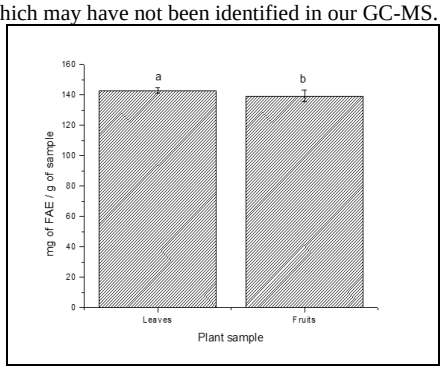

ISSN: 2521-2293

Fig. 1. DPPH scavenging activity (ferulic acid equivalent) per gram of sample. Values are mean ± standard error (n = 3). Significant differences among the extracts are indicated by different letters (P < 0.05, Tukey-Kramer's range test).

C. *Antioxidant activities: ABTS radical scavenging assay*

The ABTS antioxidant assay measures the scavenging ability of antioxidants in ABTS generated in the aqueous phase. Generation of ABTS occurs by reacting the ABTS salt with potassium persulfate, which is a strong oxidizing agent [33]. The antioxidant activity of *S. molle* using ABTS was determined from the standard calibration curve (linear with y = 0.6733x + 0.159, R^2 = 0.9554) to be 128.1 ± 9.74 and 211.2 ± 33.9 mg of ferulic acid equivalent (FAE)/g of sample for leaf essential oil extracts and fruit essential oil extracts, respectively (*Fig. 2*). Our data shows significantly high antioxidant activity (value; P < 0.05) in leaf essential oil extracts when compared to fruit essential oil extracts from *S. molle*. While it was expected that the fruit oil extracts should possess higher antioxidant activity, previous research has shown that higher antioxidant activity in leaves may be attributed to the presence of hydroxyls group in oxygenated sesquiterpenes found in the leaf oils [5], which may have not been identified in our GC-MS.

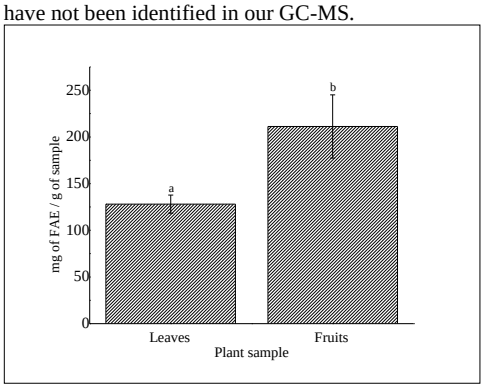

Fig 2. ABTS free-radical scavenging activity (ferulic acid equivalent) per gram of sample. Values are mean ± standard error (n = 3). Significant differences among the extracts are indicated by different letters (P < 0.05, Tukey-Kramer's range test).

D. *Antioxidant activities: Total phenolic content*

The total phenolic content of the essential oils, calculated from the standard calibration curve against ferulic acid (linear with y = 0.9911x + 0.0524, R^2 = 0.9987), were determined to be 250.9 ± 13.5 mg of ferulic acid equivalent (FAE)/g of sample for fruits, while no phenolic content was found in the leaves (*Fig. 3*). Samples were run in triplicates. Phenolic compounds are known to possess reductive-oxidative (redox) properties, granting free radical scavenging capabilities, and permitting them to function as antioxidants [34]. The absence of results in the leaf essential oils may be due to the organic compounds found in the leaves not being phenolic compounds (β-phellandrene and isobutylamine). The results obtained from the fruit essential oils, however, suggest that ultrasonic-assisted hydrodistillation is very effective at extracting phenolic compounds from the fruits of *S. molle*, with a relatively high yield of total phenolic compounds obtained, as displayed by our GC-MS results.

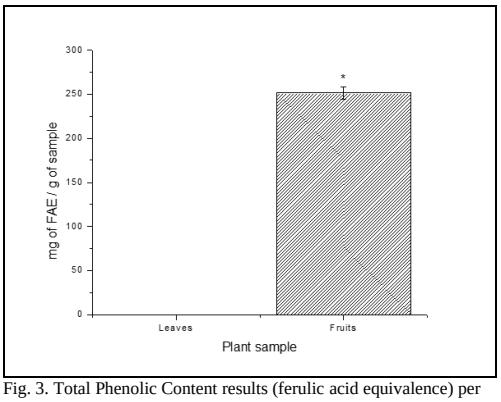

Fig. 3. Total Phenolic Content results (ferulic acid equivalence) per gram of sample. Values are mean ± standard error (n = 3). Significant differences among the extracts are indicated by different letters (P < 0.05, Tukey-Kramer's range test).

E. *Antimicrobial activity assay: Agar disc diffusion method (Kirby-Bauer Test)*

The antimicrobial activity of the fruit essential oil extracts showed promising antibacterial potency against Gram-positive (*S. aureus*) and Gram-negative (*E. coli*) bacteria, with no effect observed in yeast (*C. albicans*). The Gentamicin positive control yielded inhibition zones of (on average) 23.3 ± 0.33 mm and 18.7 ± 0.33 mm in *E. coli* and *S. aureus*¸ respectively, with the corresponding inhibition zones of the fruit essential oil extracts being 7.7 ± 0.33 mm and 6.0 mm (*Fig. 4-7*). According to Hosni et al. [35], if the inhibition zone is the size of the disc, i.e., 6 mm, the antimicrobial is considered inactive. These results suggest that pure essential oil extracts from *S. molle* fruits found in Palapye are 33% as effective as the broad-spectrum antibiotic Gentamicin, showing promising potential for their use as antibacterial treatments in medicine and food processing, and plant metabolites have been documented to possess multi-target activity which, unlike commercial antibiotics, does not result in antibiotic resistance [36].

ISSN: 2521-2293

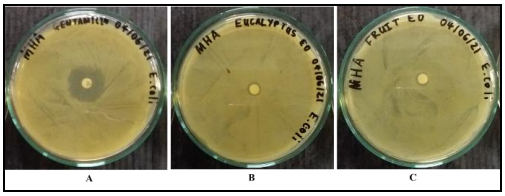

Fig. 4. Agar disc diffusion assays of *E. coli* – Gentamicin 10 µg with an inhibition zone of 23 mm (A); eucalyptus essential oil with an inhibition zone of 8 mm (B); and *S. molle* fruit essential oil with an inhibition zone of 8 mm (C).

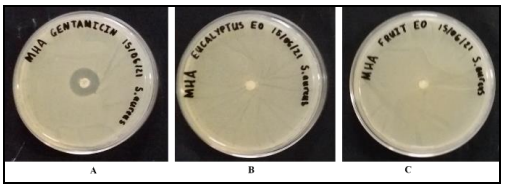

Fig. 5. Agar disc diffusion assays of *S. aureus* – Gentamicin 10 µg with an inhibition zone of 18 mm (A); eucalyptus essential oil with no inhibition zone (B); and *S. molle* fruit essential oil with an inhibition zone of 6 mm (C).

The leaf essential oil extracts did not induce any inhibition, as was also seen by the eucalyptus oil control samples in *S. aureus*¸ although an average inhibition zone of 8 mm was recorded in *E. coli* assays by eucalyptus essential oil. No inhibition of growth was observed in *C. albicans*.

The lack of antimicrobial and antioxidant activity in leaf essential oil extracts could perhaps be attributed to seasonal variations as well as soil composition found in Palapye, as several researchers have already established that *S. molle* leaf essential oils do possess antioxidants and antimicrobial activities of high efficacy [5, 35, 37]. Alternatively, due to the high volatile nature of essential oils, the oils found in the leaves may have volatilized in the 100ºC hydrodistillation setup, leaving us with fewer organic compounds than were initially present.

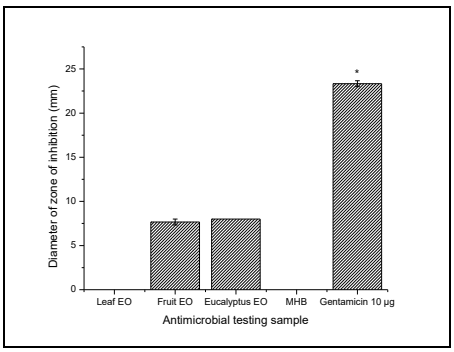

Fig. 6. *E. coli* antimicrobial activity. Values are mean ± standard error (n = 3). Significant differences among the extracts are indicated by an asterisk (P < 0.05, Tukey-Kramer's range test).

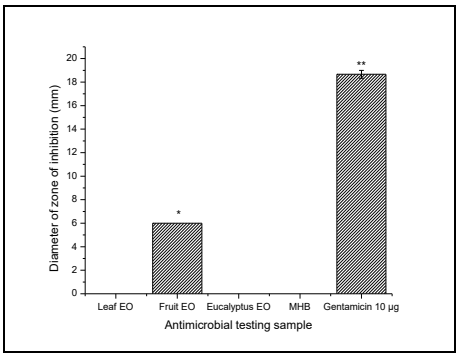

Fig. 7. *S. aureus* antimicrobial activity. Values are mean ± standard error (n = 3). Significant differences among the extracts are indicated by an asterisk (P < 0.05, Tukey-Kramer's range test).

IV. CONCLUSIONS

The essential oil extracts from *S. molle* found in Palapye were successfully extracted and their chemical compounds were identified and analyzed. Qualitative analysis of *S. molle* fruit essential oil extracts have shown promising antimicrobial potential against Gram-positive *S. aureus* and Gram-negative *E. coli*, functioning at approximately one-third the bactericidal capacity of commercial broad-spectrum antibiotics (Gentamicin 10 µg). The antioxidant activities of this plant species found in Palapye have also been established, with results showing a high phenolic content, which are attributed to the distinctive aroma which *S. molle* is well known for, and may be responsible for the antimicrobial activities observed by the Kirby-Bauer tests. The use of medicinal plants to treat a variety of ailments has been a worldwide practice for many generations, and even after the discovery, mass production and distribution of modern-day broad-spectrum antibiotics, still hold a relevant place in the field of medicine and pharmacology. While this research has shone light on the fact that *S. molle* essential oil extracts from trees found in Palapye do possess antimicrobial and antioxidant activities, quantitative work is further required to establish the minimum inhibitory concentration (MIC) and minimum bactericidal concentration (MBC) of these oils, as well as research on *S. molle* samples obtained from different points of the country and at different seasons to assess efficacy as influenced by environmental and seasonal variations. The use of alternative extraction techniques may also prove to yield much better results, such as hydrodistillation by means of a Clevenger-type apparatus.

ISSN: 2521-2293

ACKNOWLEDGMENT

We are grateful to Messrs BIBIZA M and LEKUTLANE D, and Mlles MGIDISWA N and MODIRWAGALE G for their technical support. The project was supported by Ministry of Tertiary Education, Research, Science and Technology (MOTE); Botswana International University of Science and Technology (BIUST)

REFERENCES

[1] M. Akova, "Epidemiology of antimicrobial resistance in bloodstream infections", Virulence, vol. 7, pp. 252–266, April 2016.
[2] M. Frieri, K. Kumar, and A. Boutin "Antibiotic resistance", J. Infect. Public Health, vol. 10, pp. 369-378, July-August 2017
[3] S. Mühlen, and P. Dersch, "Anti-virulence Strategies to Target Bacterial Infections", Curr. Top. Microbiol. Immunol., vol. 398, pp. 147-183, January 2016.
[4] M. Cáceres, W. Hidalgo, E. Stashenko, R. Torres, and C. Ortiz, "Essential oils of aromatic plants with antibacterial, anti-biofilm and anti-quorum sensing activities against pathogenic bacteria", Antibiotics, vol. 9, pp. 147, March 2020.
[5] M.R. Martins, S. Arantes, F. Candeias, M.T. Tinoco, and J. Cruz-Morais, "Antioxidant, antimicrobial and toxicological properties of *Schinus molle* L. essential oils" J. Ethnopharmacol., vol. 151, pp. 485-492, January 2014.
[6] F.A. Barkley, "Schinus L." Brittonia, vol. 5, pp. 160-198, September 1944.
[7] D.J. Mabberley, The Plant Book: A Portable Dictionary of the Higher Plants, Utilising Conquist's An Integrated System of Classification of Flowering Plants (1981), and Current Botanical Literature Arranged Largely on the Principles of Editions 1-6 (1896/97-1931) of Willi's a dictionary of the following plants and ferns, 1-6th ed, vol. 1, Cambridge, Cambridge University Press, 1990, pp. 637-674.
[8] D.J. Goldstein, and R.C. Coleman, "*Schinus molle* L. (Anacardiaceae) Chicha production in the Central Andes", Econ. Bot., vol. 58, pp. 523-529, December 2004.
[9] L.P. Maema, M. Potgieter, and S.M. Mahlo, "Invasive alien plant species used for the treatment of various diseases in limpopo province, South Africa", Afr. J. Tradit. Complement. Altern. Med., vol. 13, pp. 223-231, July 2016.
[10] L. Demelash, M. Tigabu, and P.C. Odén, "Enhancing germinability of *Schinus molle* L. seed lot from Ethiopia with specific gravity and IDS techniques" New Forests, vol. 26, pp. 33-41, July 2003
[11] D.M. Iponga, S.J. Milton, and D.M. Richardson, "Superiority in competition for light: A crucial attribute defining the impact of the invasive alien tree *Schinus molle* (Anacardiaceae) in South African savanna", J. Arid Environ, vol. 72, pp. 612-623, May 2008.
[12] K.C. Palgrave, Trees of southern Africa, 3rd ed., vol. 1, Cape Town, Penguin Random House South Africa, 2015, pp. 957-1212.
[13] G.W.B. van der Lingen, "South African pepper tree oil", J. Perf. Essent. Oil. Res., vol. 21, pp. 154. January 1930.
[14] M. Martínez-Millán, and S.R.S. Cevallos-Ferriz, "Arquitectura foliar de Anacardiaceae", Rev. Mex. Biodiv., vol. 76, pp. 137-190, July 2005.
[15] R.A. Bernhard, T. Shibamoto, K. Yamaguchi, and White, E. "The Volatile Constituents of *Schinus molle* L.", J. Agric. Food Chem., vol. 31, pp. 463-466, March 1983.
[16] J.A. Duke, Handbook of medicinal herbs, CRC press, 2002.
[17] H. Jadhav, A. Jadhav, Y. Morabiya, P. Takkalkar, S.S. Qureshi, A.G. Baloch, and N.M. Mubarak, "Combined Impact of Ultrasound Pre-treatment and Hydrodistillation on Bioactive Compounds and GC–MS Analysis of Cinnamomum cassia Bark Extract", Waste Biomass Valor., vol.12, pp. 807-821, March 2020.
[18] M.S. Stankovic, N. Niciforovic, V. Mihailovic, M. Topuzovic, and S. Solujic, "Antioxidant activity, total phenolic content and flavonoid concentrations of different plant parts of Teucrium polium L. subsp. Polium", Acta Soc. Bot. Pol., vol. 81, pp. 117-122, January 2012.
[19] P. Nicoletta, "Screening of dietary carotenoids and carotenoid-rich fruit extracts for antioxidant activities applying 2, 2'-azinobis (3-ethylbenzothiazoline-6-sulfonic acid) radical cation decolorization assay", Method Enzymol., vol. 299, pp. 379-389, October 1999.
[20] V.L. Singleton, R. Orthofer, and R.M. Lamuela-Raventós, "Analysis of total phenols and other oxidation substrates and antioxidants by means of folin-ciocalteu reagent", Methods in Enzymol., vol. 299, pp. 152-178, October 1999.

ISSN: 2521-2293

[21] R.G. Bachir, and M. Benali, "Antibacterial activity of the essential oils from the leaves of Eucalyptus globulus against *Escherichia coli* and *Staphylococcus aureus*", Asian Pac. J. Trop. Biomed., 2(9), 739-742, September 2012.
[22] A. Elaissi, Z. Rouis, N.A. Salem, S. Mabrouk, Y. ben Salem, K.B. Salah, M. Aouni, F. Farhat, R. Chemli, and M.L. Khouja, "Chemical composition of 8 eucalyptus species' essential oils and the evaluation of their antibacterial, antifungal and antiviral activities", BMC Complement Altern. Med., vol. 12, pp. 81, June 2012.
[23] M.N. Gould, "Cancer chemoprevention and therapy by monoterpenes", Environ. Health Perspect., vol. 105, pp. 977-979, June 1997.
[24] R. Garcia, E.S. Alves, M.P. Santos, G.M. Aquije, A.A. Fernandes, R.B. Dos Santos, and P.M Fernandes, "Antimicrobial activity and potential use of monoterpenes as tropical fruits preservatives", Braz. J. Microbiol., vol. 39, pp. 163-168, March 2008.
[25] Y. Han, Z. Sun, and W. Chen, "Antimicrobial susceptibility and antibacterial mechanism of limonene against Listeria monocytogenes", Molecules, vol. 25, pp. 33 December 2018.
[26] Y.W. Kim, M.J. Kim, B.Y. Chung, D.Y. Bang, S.K. Lim, S.M. Choi, K. Yoon, H.S. Kim, Y.S. Kim, S.J. Kwack, and B.M. Lee, "Safety evaluation and risk assessment of d-limonene", J. Toxicol. Environ. Health- BCrit., vol. 16, pp. 17-38, January 2013.
[27] A.C. Rivas da Silva, P.M. Lopes, M.M. Barros de Azevedo, D.C. Costa, C.S. Alviano, and D.S. Alviano, "Biological activities of α-pinene and β-pinene enantiomers", Molecules, vol. 17, pp. 6305-6316, May 2012.
[28] J. Zhang, H. Sun, S. Chen, L. Zeng, and T. Wang, "Anti-fungal activity, mechanism studies on α-Phellandrene and Nonanal against Penicillium cyclopium", Bot. Stud., vol. 58, pp.1-9, March 2017.
[29] L. Chen, X. Lu, H. El-Seedi, and H. Teng, "Recent advances in the development of sesquiterpenoids in the treatment of type 2 diabetes", Trends Food Sci. Tech., vol. 88, pp. 46-56, June 2019.
[30] M. Canales, T. Hernández, J. Caballero, A.R. De Vivar, G. Avila, A. Duran, and R. Lira, "Informant consensus factor and antibacterial activity of the medicinal plants used by the people of San Rafael Coxcatlán, Puebla, México", J. Ethnopharmacol., vol. 97, pp. 429-439, March 2005.
[31] D.E. Wedge, J.C. Galindo, and F.A. Macıas, "Fungicidal activity of natural and synthetic sesquiterpene lactone analogs", Phytochemistry, vol. 53, pp. 747-757, April 2000.
[32] D. Huang, O.U. Boxin, and R. L. Prior, "The chemistry behind antioxidant capacity assays", J. Agric. Food Chem., vol. 53, pp. 1841-1856, February 2005.
[33] C.V. Ratnavathi, and V.V. Komala, Sorghum grain quality. In Sorghum biochemistry, 1st ed, vol. 1, Academic Press, 2016, pp. 1-61.
[34] S.A. Baba, and S.A. Malik, "Determination of total phenolic and flavonoid content, antimicrobial and antioxidant activity of a root extract of Arisaema jacquemontii Blume", J. Taibah Univ. Sci., vol. 9, pp. 449-454, October 2015.
[35] K. Hosni, M. Jemli, S. Dziri, Y. M'rabet, A. Ennigrou, A. Sghaier, H. Casabianca, E. Vulliet, N.B. Brahim, and H. Sebei, "Changes in phytochemical, antimicrobial and free radical scavenging activities of the Peruvian pepper tree (*Schinus molle* L.) as influenced by fruit maturation", Ind. Crops Prod., vol. 34, pp. 1622-1628, November 2011.
[36] B. Adorjan, and G. Buchbauer, "Biological properties of essential oils: An updated review", Flavour Fragr. J., vol. 25, pp. 407-426, September 2010.
[37] C. Díaz, S. Quesada, O. Brenes, G. Aguilar, and J.F. Ciccio, "Chemical composition of *Schinus molle* essential oil and its cytotoxic activity on tumour cell lines", Nat. Prod. Res., vol. 22, pp. 1521-1534, December 2008.

BIUST Teaching, Research, & Innovation Symposium 2023 (TRDAIS 2023)
Botswana International University of Science and Technology
Palapye, Botswana, 18 - 19 September 2023
ISSN: 2521-2293

Comparison of mouse embryonic fibroblasts proliferation in culture media comprising different concentrations of components

Malebogo C. Moseki, Monica M. Mazebedi, Keagile Bati and Goabaone Gaobotse
Department of Biological Sciences and Biotechnology Botswana International University of Science and Technology, Palapye, Botswana
gaobotseg@biust.ac.bw

Abstract **- The discovery of embryonic stem cells (ESCs) has brought hope to medicine because ESCs can form different specialized cells and tissues. Mouse embryonic fibroblasts (MEFs) are a primary cell line derived from E13.5 murine embryos that are used as substrates during the culture of ESCs. They help maintain healthy and undifferentiated human embryonic stem cells (hESCs), mouse embryonic stem cells (mESCs) and induced pluripotent stem cells (iPSCs) *in vitro* by secreting vital growth factors into ESC culture media, aiding in maintaining ESC pluripotency and providing a cellular matrix for ESCs to proliferate. For MEFs to function optimally, they need to proliferate optimally. This study aimed to determine the concentrations of different components of MEF medium that support the optimal proliferation of MEFs in culture. We hypothesized that there are specific concentrations of MEF medium components that are optimal for MEF culture. Using sterile instruments and solutions, MEFs were derived from 13.5-day old pregnant Murphy Roths Large (MRL) mice in the animal house of the Department of Biological Sciences and Biotechnology, BIUST. Then, MEFs were cultured in five media formulations comprising different concentrations of penicillin/streptomycin (PenStrep), DMEM, L-Glutamine and foetal bovine serum (FBS). The viability of MEFs undergoing cell culture protocols in the different media formulations was determined using 3-(4,5-dimethylthiazolyl-2)-2,5-diphenyltetrazolium bromide (MTT) assay. Media 3, comprising 89.5% DMEM, 2% L-glutamine and 10.75% FBS, was the most efficient in enhancing MEF proliferation and displayed 5% more viability than normal media. Standardized media formulations can enhance MEF culture protocols and boost ESCs proliferation during culture. This promotes the increased turnover of ESCs in culture which is precious for their clinical applications.**

Keywords-human embryonic stem cells; mouse embryonic fibroblasts; cell viability; mouse embryonic stem cells; pluripotency; clinical application

I. INTRODUCTION

The recent COVD-19 pandemic has rubberstamped the global need for novel medicinal strategies that will supplement conventional medicine. The progression of biomedical knowledge as well as the use of human embryonic stem cells (hESCs) after their derivation from blastocysts [1] has brought about renewed optimism, inspiring additional studies in human cell differentiation and development. Human ESCs are pluripotent cells sourced from the inner cell mass (ICM) of the early human blastocyst that embodies the prototype of all types of cells in the human body [2]. It is this pluripotency, which can differentiate into different specialized cells, that has made stem cells so appealing in medicine for potential treatment of different disorders.

A. Properties, regulation, and applications of embryonic stem cells (ESCs)

Although mouse embryonic stem cells (mESCs) and human embryonic stem cells (hESCs) were initially derived and cultured in the presence of bovine serum on a layer of mouse embryonic fibroblasts (MEFs), aspects that sustain the growth and proliferation of these two cell types seem to be dissimilar [3]. Stem cells are well known for their development into tissues and cells of the three primary germ layers: the endoderm, mesoderm, and the ectoderm. Even though hESCs are derived from the fetal tissue or embryo, they are not themselves embryos. The innate biological qualities of these cells are pluripotency, which is their ability to differentiate into cell types of the three germ layers as well as self-renewal, which is their division into more of themselves while maintaining their progeny. These properties of hESCs have permitted their

ISSN: 2521-2293

boundless application in regenerative medicine, disease treatment and cell therapy [4].

Because hESCs proliferate without limit and can differentiate into any cell type, they have greater potential to enhance research on the function and differentiation of human tissues and aid in performing tests that will most likely advance the efficiency of drugs [5, 6].

The pluripotency of ESCs suggests possible widespread applications of these cells and their derivatives [7]. ESC-derived cells can potentially be used to replace or restore tissues that have been damaged by injury or diseases such as diabetes, heart attacks, Parkinson's disease, and spinal cord injury. The differentiation of ESCs also provides model systems to study early events in human development [8]. Because of possible harm to the developing child, it is not ethically acceptable to experimentally manipulate post-implantation human embryos. Therefore, most of what is known about the mechanisms of early human embryology and human development, especially in the early post-implantation period, is based on histological sections of a limited number of human embryos and their analogy to the experimental embryology of the mouse [9].

B. Properties, applications, and culture of mouse embryonic fibroblasts (MEFs)

Mouse embryonic fibroblasts (MEFs) are a primary cell line derived from E13.5 murine embryos [6]. MEFs comprise a heterogenous mixture of cells known as fibroblasts. These cells display morphological characteristics including a high nucleus: cytoplasm ratio as well as a prominent nucleolus. The cells are also flat and adherent [10]. They spread to form numerous kinds of shapes with various projections. Feeder cells are important in the *in vitro* culture of human and mouse embryonic stem cells (ESCs) as well as induced pluripotent stem cells (iPSCs). Most ESC procedures depend on harnessing a monolayer of primary MEFs. MEFs accomplish two vital roles in stem cell culture [11]. They secrete several vital growth factors and provide extracellular matrix (ECM) factors that help to maintain stem cell properties [12]. To serve as feeder cells, MEFs must be inactivated by treatment with mitomycin C or by irradiation to inhibit cell proliferation. The inactivation of MEFs prevent them from competing for nutrients with ESCs in culture. Treated MEFs can also be used to generate conditioned medium for the feeder free culture of pluripotent cells [7, 13].

Preparation of MEFs involves trypsinization which is a process of dissociating cells using a proteolytic enzyme called trypsin [14]. It also involves the seeding of embryos into culture medium following the removal of internal organs as well as the limbs, head, and tail. The resulting cultures after several passages are, in most cases, regarded as largely homogeneous populations [15]. Cultures of MEFs are widely perceived to proliferate in response to mitogenic factors that ascend from platelet degranulation because of coagulation from whole blood [16]. Among the growth factors that have been recognized from platelet releases are TGF-β1, PDFG-β, angiopoietin 1, ECM protein 1, and vascular endothelial growth factor (VEGF)-C. Most of these growth factors are thought to be significant in the proliferation of tumour stromal fibroblasts [11].

MEF medium comprises of different constituents including Dulbecco's modified eagle medium (DMEM), L-Glutamine, fetal bovine serum (FBS) as well as penicillin/streptomycin (PenStrep). DMEM is one of the most widely used modification of Eagle's medium [17]. It is used for supporting the growth of many different mammalian cells and is a modification of basal medium eagle (BME) that contains four-fold concentration of amino acids and vitamins. Additionally, the formulation also includes glycine, serine, and ferric nitrate [18]. The original formulation contains 1000mg/L of glucose and was originally used to culture embryonic mouse cells. DMEM high glucose is a further modification of the original DMEM that contains 4500mg/L of glucose. The additional glucose has proved to be useful in cultivating various other cell lines including primary cultures of mouse and chicken cells as well as various normal and transformed cell lines [6].

FBS is another important component of MEF medium. It is a complex mixture with low and high molecular weight biomolecules exhibiting optimal growth-enhancing and growth-suppressing functions. It contains molecules such as growth factors, proteins, vitamins, trace elements and hormones [19] that are important during the culture of MEFs. These molecules are important for the growth and maintenance of these cells. FBS is a common cell culture media supplement that is derived from calf blood and is devoid of fibrin and clotting factors. Heat inactivation of FBS blocks the complement system. L-glutamine plays a key role in the synthesis of proteins while penicillin/streptomycin are essential antibiotics that aid in the prevention of contamination [19] during MEF culture.

C. Aim

To determine concentrations of different components of MEF medium that optimally support the proliferation of MEFs in culture.

D. Objectives

• To perform 7-day culture protocols of MEFs in five different MEF media formulations.

ISSN: 2521-2293

• To determine the effect of the five different MEF media formulations on the morphology and proliferation of MEFs in culture.

• To determine, using MTT assay, the viability of MEFs that have undergo 7-day cell culture protocols in the five different MEF media formulations.

E. Hypothesis

There are specific concentrations of different components of mouse embryonic fibroblast (MEF) medium that optimally support the proliferation of MEFs in culture.

F. Significance of study

The study seeks to determine, among different five media formulations, the most optimum MEF medium formulation that will enhance the optimal proliferation of MEFs. MEFs are important substrates for the proliferation of human embryonic stem cells (hESCs). For hESCs to be applied clinically, millions and millions of these cells are required. To get this many hESCs, there is a need for highly efficient substrates that can provide optimal nutrition to hESCs. MEFs are traditionally used as feeder substrates during hESC culture. For them to do this effectively, they need to proliferate optimally. This study, therefore, seeks to determine the optimum medium formulation for the culture of MEFs. MEFs are crucial for the optimum culture of hESCs which are required in high clonal densities for their clinical application in the potential alleviation of diseases such as HIV/AIDS, cancer, diabetes, and the recent COVID-19 pandemic.

II. METHODOLOGY

A. Derivation and culture of mouse embryonic fibroblasts (MEFs)

1. Derivation of MEFs

All animal studies were conducted following protocols approved by institutional Animal Care and Usage committee of BIUST. Using sterile instruments and solutions, MEFs were derived from 13.5-day old pregnant Murphy Roths Large (MRL) mice in the animal house of the Department of Biological Sciences and Biotechnology, Botswana International University of Science and Technology (BIUST) in Palapye, Botswana. The mice were sacrificed by suffocation with Diethyl ether. Briefly, the abdomen of the mice was sterilized with 70% ethanol. Uterine horns were then exposed by cutting through the abdominal skin and the peritoneum. They were then placed in a petri dish containing phosphate buffered saline (PBS). Fetuses were then removed from the embryonic sac and the placenta followed by the removal and discarding of membranes. The foetuses were decapitated, and the remaining carcasses were washed three times with PBS. The carcasses were then placed in a clean petri dish and minced finely with a clean scalpel blade. Two (2) mL of trypsin: EDTA (0.25% trypsin w/v, Gibco; 5mM EDTA, Sigma) was added to the petri dish. The dish was then incubated for 15 minutes at 37°C. After incubation, 5 mL of normal MEF medium (Table 1) was added followed by the transfer of the mixture into a 15 mL centrifuge tube and mixing using a pipette. The mixture was then divided into 40ml culture flasks and a further 10 mL of MEF medium was added to each flask. The flasks were then incubated overnight at 37°C. After overnight incubation, media in the flasks was replaced with fresh media to remove any floating cellular debris. MEFs were then allowed to reach at least 90% confluency before being passaged.

TABLE I. CONCENTRATIONS OF DIFFERENT CONSTITUENTS OF MEF MEDIA FORMULATIONS USED IN THIS STUDY

Constituents	**1st Media Concentrations (Normal media)**	**2nd Media Concentrations**	**3rd Media Concentrations**	**4th Media Concentrations**	**5th Media Concentrations**
DMEM Medium	88.5%	89%	89.5%	88%	87.5%
L-Glutamine 2mM (L-Glu)	1%	1.5%	2%	0.5%	0.25%
Fetal Bovine Serum (FBS)	10%	9.25%	8.5%	10.75%	11.25%
Penicillin/Streptomycin (Pen/Strep)	0.5%	0.25%	0%	0.75%	1%

ISSN: 2521-2293

2. Culture of MEFs

After MEFs had reached at least 90% confluency, media in culture flasks was discarded followed by washing of the MEFs with PBS. To detach MEFs from the culture flask, 5 mL of TrypLE™ Express was added to every flask and the flasks were then incubated for about 2 minutes in a 37°C, 5% CO^2 incubator. To neutralize the TrypLE™ Express, 10ml of normal MEF media was added to each of the flasks. The cell suspensions were then transferred into 15 mL tubes and pipetted gently up and down to make single cell suspensions. The suspensions were then centrifuged for 5 minutes at 2000rpm. After centrifugation, the supernatant in the flasks was discarded and the pellets were each resuspended in 9 mL of normal MEF medium. MEFs were then plated in T150 culture flasks and incubated at 37°C, 5% CO^2 until the cells attained at least 90% confluency. The remaining MEFs in the culture flasks were frozen down for future use.

To freeze the MEFs, they were washed with PBS. Then, they were dissociated with the application of TrypLE™ Express. They were then centrifuged for 5 minutes and re-suspended in ice-cold freezing solution (90% FBS, 10% DMSO-Dimethyl Sulfoxide). One (1) mL volumes of the cell suspension were transferred into 1.6 mL cryopreservation vials. The vials were stored overnight at -80°C before being transferred to a liquid nitrogen tank for long-term storage. This protects cells from cell shock.

To culture the MEFs in different media formulations, five 40 mL gelatin coated culture flasks were used. Gelatin enhances the adhesion of MEFs to culture plates. Cells in the gelatin coated culture flasks were cultured in 5 pre-prepared media formulations (Table 1). Cells cultured in normal MEF media were regarded as a control. The flasks were incubated at 37°C, 5% CO^2. Each of the five MEF media formulations was replaced after 48 hours. After the MEFs had reached about 90% confluency, they were passaged and excess MEFs were frozen down.

B. Determination of the effect of different media formulations on the morphology and proliferation of MEFs

1. Observation of cell morphology during MEF culture protocol

The MEFs undergoing 7-day cell culture protocols in the five different MEF media formulations were observed under the microscope and cell morphology images were captured every day of the 7-day protocols to observe and record any morphological changes during cell proliferation.

C. Determination of the viability of MEFs after 7-day cell culture protocols using MTT assay

MTT assay (Thermo Fisher Scientific Inc., NYSE: TMO) involves the conversion of the water soluble MTT (3-(4,5-dimethylthiazol-2-yl)-2,5-diphenyltetrazolium bromide) to an insoluble formazan. The formazan is then solubilized, and the concentration determined by optical density at 570 nm.

First, 1000-100000 cells were plated in a 96-well plate and incubated for 48 hours using a seeding density of 1:1. The medium was then removed, and cells were washed with PBS. Following this was the addition of MTT made up in medium to a final concentration of 0.5 mg/mL. The cells were then incubated for 2 hours at 37°C, until intracellular purple formazan crystals were visible under the microscope. The MTT was then removed and followed by the addition of a solubilizing solution and triturated. The cells were then incubated at 37°C for 2 hours until they had lysed, and purple crystals had dissolved. Finally, absorbance was measured at 570 nm using the microplate reader.

To interpret the results, the absorbance reading of the blank was subtracted from all samples. Absorbance readings from test samples were divided by those of the standard media formulation (control) and multiplied by 100 to give percentage cell viability or proliferation (formula below). Absorbance values greater than the control indicate cell proliferation, while lower values suggest cell death or inhibition of proliferation.

$$\%\ \text{Viabile cell} = \frac{(\text{abs sample} - \text{abs balnk})}{(\text{abs control} - \text{abs blank})} \times 100 \quad (1)$$

D. Ethical considerations

• This study was approved by the Ministry of Tertiary Education, Research, Science and Technology (MOTE) through research permit no: MOTE 1/18/6 IX (14).
• There were no human subjects involved in this study.
• A minimal number of mice was used in this study.
• The number of mice used was the least number required to obtain reliable data and a thorough literature search was done to avoid unnecessary duplication of the experiment.
• Pain and discomfort to the mice used in this study was minimized by using anesthesia.
• All sources used in this study have been acknowledged.

III. RESULTS AND DISCUSSION

A. Culture of MEFs after derivation

Following their derivation, the MEFs did not have any definite morphology. They appeared to be circular and

ISSN: 2521-2293

shiny when observed under the microscope. The cells were also floating and did not attach immediately after derivation on day 0. However, the MEFs rapidly attached to the gelatin coated flasks after being left in the incubator overnight. They were about 80% confluent after the first 24 hours post derivation (Day 1) (*Fig. 1*). Also, on day 1, the cells had also developed a definite morphology. They appeared to be flat with spindle shape. This is in line with the studied morphology of MEFs which has been described as stellate shaped or plump spindle-shaped with round or centrally placed nucleus [20].

The morphology of the MEFs as well as their rate of cell growth changed drastically from day 2 to day 3. On day 2, the MEFs were about 85-90% confluent and appeared to be large, elongated, and flat (*Fig. 1*). The MEFs progressively exhibited a change in morphology on day 3 as they appeared to be larger with a more defined flat and round nucleus at 90-95% confluency. This is in line with the findings of [21] who report that active fibroblasts become larger and more defined during the first few days of isolation and culture. Additionally, [3] state that it takes about two or three days before confluent cultures can be observed. This corresponds to the observations of this study as a consistent reduction of spaces between the MEFs in culture was observed from day 2 to day 3. This was due to an increase in sizes of the cells.

After 3 days of culture post derivation, the MEFs were put through a few days of culture to determine if they would withstand a few days in culture during the 7-day cell culture protocols. The MEFs underwent 3 passages before the 7-day protocols so that they could adapt to the culture conditions since primary cell lines are generally volatile.

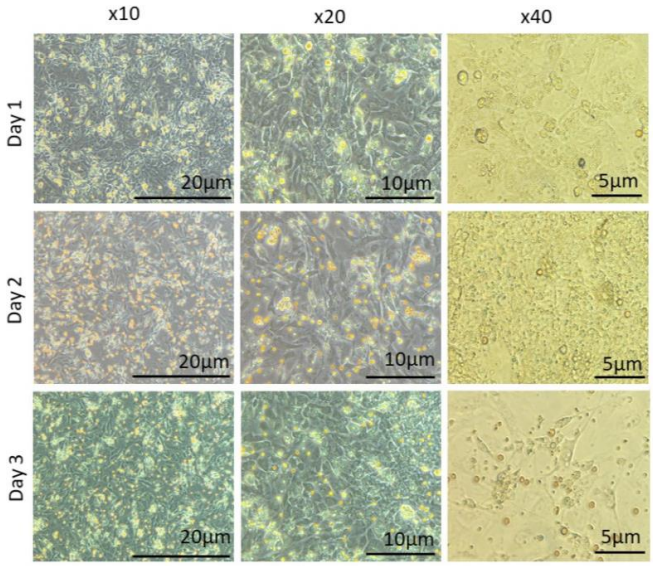

Fig. 1. Culture of MEFs after derivation. P0 MEFs were cultured in normal MEF medium. *Cell culture images were captured at days 1, 2 and 3 (Day of derivation is Day 0 on which cells were plated). Images were captured at x10, x20 and x40 magnifications.*

B. Cell morphology during a 7-day MEF culture protocol

Relative to medium 1 (normal medium), the MEFs in media 2, 4 and 5 showed slow growth. On the other hand, the MEFs in media 1 and 3 displayed increased growth and more confluency (*Fig. 2*). Cell morphology showed that cells that had been cultured in media 3 were slightly more confluent than those cultured in media 1 which is the normal MEF media. Media 3 appeared to support both early and late proliferation of the MEFs when compared to media 2, 4 and 5. This was confirmed by the superior growth and confluency of cells in media 3 at day 7 compared to cells that were cultured in other media. This growth superiority may be due to media 3 containing the highest concentration of L-glutamine which is responsible for the promotion of cell growth. L-glutamine is used as an energy source for cultured cells and is also used as a

ISSN: 2521-2293

reservoir of nitrogen that aids in the production of proteins, nucleic acids as well as nucleotides. Additionally, glutamine enhances cell growth by synthesizing a greater number of proteins and nucleic acids when compared to other components [22].

Media 4 appeared to support faster attachment of the MEFs when compared to the other media formulations. After the first 24 hours (day 1), most fibroblasts in media 4 were attached to the gelatin coated flasks. This is possibly due to the high FBS content of media 4. In fact, media 4 had the second highest FBS content (10.75%) behind media 5 (11.25%). FBS aids in the provision of attachment molecules including activin A, TGF β2 and fibroblast growth factors (FGF). It also provides shear force protection that is important for cell cultures that are difficult to grow [23].

As the protocol continued, the cells appeared to get darker in color in all the 5 media formulations. During culture, the internal complexity of the cells increased every day. This is because of the development and maturation of the components of MEFs. Furthermore, there were no traces of contamination observed due to proper aseptic cell culture techniques as well the use of PenStrep which is a vital antibiotic responsible for the prevention of contamination in mammalian cell culture [24]. Interestingly, it was only in media 3 where antibiotics were not used. However, this media still exhibited optimum support of the MEFs. This may be an indication of the relative dispensability of antibiotics during MEF culture when compared to ESC culture.

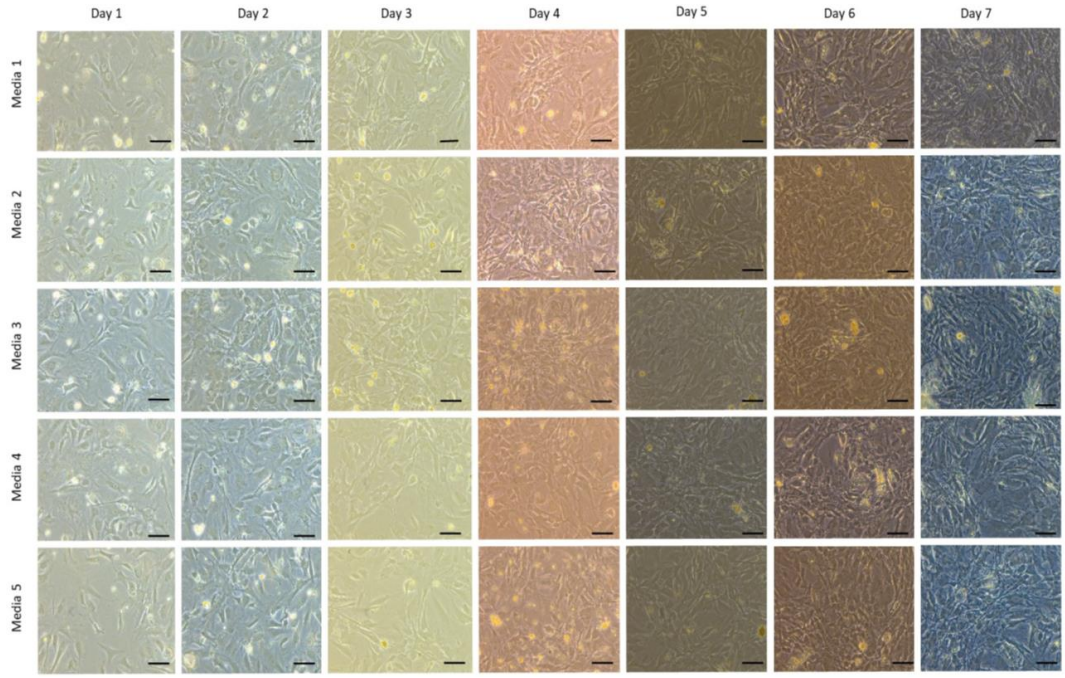

Fig. 2. Cell morphology during a 7-day MEF culture protocol. *Passage 3 (P3) MEFs were cultured in 5 different MEF medium for 7 consecutive days. Cell culture images were captured every day. Images were captured at x20 magnification. Scale bars= 10 μm.*

C. Viability of MEFs after 7-day culture protocol

Cell viability assay indicated that cell cultured in media 3 were almost as viable as MEFs cultured in normal media (media 1). Media 3 cells were the most viable when compared to all the other media formulations. The least percentage viability was obtained in cells from media 4 (92.6%), followed by media 5 cells (93.4%) and media 2 cells (98.3%).

ISSN: 2521-2293

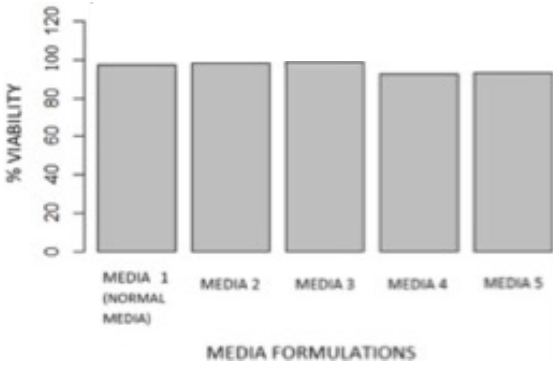

Fig. 3. Viability of MEFs. *Assayed with MTT after 7-day cell culture protocol in 5 different MEF media formulations comprising different concentrations of components. Values are expressed as mean ± standard error (SE).*

IV. CONCLUSION

By comparing the proliferation of MEFs in 5 media formulations comprising different concentrations of components, this study found that media formulation 3 which comprised of 89.5% DMEM, 2% L-glutamine and 8.5% FBS exhibited greater capacity to enhance the proliferation of MEFs. The percentage viability of cells cultured in this media was 5% higher than that of cells cultured in normal or standard media formulation. This gives inference to the potential superiority of this media formulation during high-throughput MEF propagation for the culturing of clinically viable ESCs.

To better understand the implications of these results, future studies could perform gene expression analysis in MEFs undergoing such cell culture protocols to determine if the culture of MEFs in different media formulations has any effect on the genotype of the MEFs. This is important because homogenous MEFs are the most ideal for ESC culture.

ACKNOWLEDGMENT

Department of Biological Sciences and Biotechnology, Botswana International University of Science and Technology (BIUST).

REFERENCES

[1] J.A. Thomson, J. Itskovitz-Eldor, S.S. Shapiro, M.A. Waknitz, J.J. Swiergiel, V.S. Marshall, and J.M. Jones, “Embryonic stem cell lines derived from human blastocysts,” Science, vol. 282, pp. 1145-1147, 1998.

[2] J.E. Lee and D.R. Lee, “Human embryonic stem cells: derivation, maintenance and cryopreservation,” Int. J. Stem Cells, vol. 4, pp. 9, 2011.

[3] J. Jozefczuk, K. Drews, K, and J. Adjaye, “Preparation of mouse embryonic fibroblast cells suitable for culturing human embryonic and induced pluripotent stem cells,” J. Vis. Exp., 64, 2012.

[4] N. Nakatsuji, and H. Suemori, “Embryonic stem cell lines of nonhuman primates,” Sci. World J., 2, pp. 1762-1773, 2002.

[5] K. Kim, A. Doi, B. Wen, K. Ng, R. Zhao, P. Cahan, and G.Q. Daley, “Epigenetic memory in induced pluripotent stem cells,” Nature, vol. 467, pp. 285-290, 2010.

[6] G.R. Martin, “Isolation of a pluripotent cell line from early mouse embryos cultured in medium conditioned by teratocarcinoma stem cells,” Proc. Natl. Acad. Sci. U.S.A, vol. 78, pp. 7634-7638, 1981.

[7] E. Fuchs, T. Tumbar, and G. Guasch, “Socializing with the neighbors: stem cells and their niche,” Cell, vol. 116, pp. 769-778, 2004.

[8] M. Crisan, S. Yap, L. Casteilla, C.W. Chen, M. Corselli, T.S. Park, and B. Péault, “A perivascular origin for mesenchymal stem cells in multiple human organs,” Cell Stem Cell, vol. 3, pp. 301-313., 2008.

ISSN: 2521-2293

[9] G. Martello, and A. Smith, "The nature of embryonic stem cells," Annu. Rev. Cell Dev. Biol., vol. 30, pp. 647-675, 2014.

[10] S. Kern, H. Eichler, J. Stoeve, H. Klüter, and K. Bieback, "Comparative analysis of mesenchymal stem cells from bone marrow, umbilical cord blood, or adipose tissue," Stem Cells, vol. 24, pp. 294-1301, 2006.

[11] N. Barker, R.A. Ridgway, J.H. Van Es, M. Van De Wetering, H. Begthel, M. Van Den Born, and H. Clevers, "Crypt stem cells as the cells-of-origin of intestinal cancer," Nature, vol. 457, pp. 608-611, 2009.

[12] X.S. Yue, M. Fujishiro, C. Nishioka, T. Arai, E. Takahashi, J.S. Gong, and Y. Ito, "Feeder cells support the culture of induced pluripotent stem cells even after chemical fixation," PloS One, vol. 7, e32707, 2012.

[13] P.K. Datta, "Murine teratocarcinoma-derived neuronal cultures,". in Neuronal Cell Culture, vol. III, New Jersey: Humana Press, 2013, pp. 35-44.

[14] M. Hirota, M. Ohmuraya, and H. Baba, "The role of trypsin, trypsin inhibitor, and trypsin receptor in the onset and aggravation of pancreatitis," J. Gastroenterol., vol. 41, pp. 832-836, 2006.

[15] T. Reya, S.J. Morrison, M.F. Clarke, and I.L. Weissman, "Stem cells, cancer, and cancer stem cells," Nature, vol. 414, pp. 105-111, 2001.

[16] Q.L. Ying, J. Wray, J. Nichols, L. Batlle-Morera, B. Doble, J. Woodgett, and A. Smith, "The ground state of embryonic stem cell self-renewal," Nature, vol. 453, pp. 519-523, 2008.

[17] A. Berns, "Stem cells for lung cancer?," Cell, vol. 121, pp. 811-813, 2005.

[18] T. Sato, J.H. Van Es, H.J. Snippert, D.E. Stange, R.G. Vries, M. Van Den Born, and H. Clevers, "Paneth cells constitute the niche for Lgr5 stem cells in intestinal crypts," Nature, vol. 469, pp. 415-418, 2011.

[19] R.A. Young, "Control of the embryonic stem cell state," Cell, vol. 144, pp. 940-954, 2011.

[20] P.S Ravikanth, K. Manjunath, T.R. Saraswathi, and C.R. Ramachandran, "Heterogenecity of fibroblasts," J. Oral Maxillofac. Pathol., vol. 15, pp. 247, 2011.

[21] D. Pei, M.A. Esteban, T. Wang, B. Qin, J. Yang, D. Qin, and J. Cai, "Vitamin C enhances the generation of mouse and human induced pluripotent stem cells," Cell Stem Cell, vol. 6, pp. 71-79, 2010.

[22] P. Newsholme, J. Procopio, M.M.R. Lima, T.C. Pithon-Curi, and R. Curi, "Glutamine and glutamate—their central role in cell metabolism and function," Cell Biochem. Funct., vol. 21, pp. 1-9, 2003.

[23] J. Van der Valk, K. Bieback, C. Buta, B. Cochrane, W. Dirks, J. Fu, and G. Gstraunthaler, "Fetal bovine serum (FBS): past–present–future," Altex, vol. 35, pp. 1-20, 2018.

[24] H.G. Drexler, and C.C. Uphoff, "Mycoplasma contamination of cell cultures: Incidence, sources, effects, detection, elimination, prevention," Cytotechnology, vol. 39, pp. 75-90, 2002.

BIUST Teaching, Research, & Innovation Symposium 2023 (TRDAIS 2023)
Botswana International University of Science and Technology
Palapye, Botswana, 18 - 19 September 2023
ISSN: 2521-2293

Application of geological data analysis and assessment techniques for coal resource evaluation

Nonduduzo B. Mamba
Department of Mining and Geological Engineering
BIUST
Palapye, Botswana
nonduduzo.mamba@studentmail.biust.ac.bw

Bonny B. Matshediso
Department of Mining and Geological Engineering
BIUST
Palapye, Botswana
matshedisob@biust.ac.bw

Rahul Verma
Department of Mining and Geological Engineering
BIUST
Palapye, Botswana
vermar@biust.ac.bw

***Abstract*—Coal mine development relies on the availability of accurate geological data, its analysis and the application of geological data to coal mine design. The collection, analysis and official use of drillhole and coal quality data are crucial for deriving meaningful resource estimates. This study presents a step-by-step approach for geological data analysis for an area that was extensively explored by Shell Coal Botswana between 1974 and 1982, where significant coal resources were identified. While much exploratory data is available, computer-aided geological modeling and data analysis has not been carried out as the resource estimation was carried out using the traditional resource estimation and modeling methods.The methodology for determining coal resources has been refined, taking advantage of improvements in geologic and mining model computer software. This study, therefore, helps in understanding the applicability of geological data analysis for the purposes of determining coal Seams boundaries, generation of 3D solid coal seam models of the deposit, which is evaluated to determine in-place coal resources. Following this methodology, three coal seams were identified and evaluated. These seams covered a total area of 52,492,911 m^2, occupying a total volume 560,030,268 m^3 at various depths.The estimated tonnage of the coal mineralization for the three coal Seams was 728 039 348.4 tonnes of mineable coal.**

***Keywords*—Geological data analysis; coal seam modeling**

I. INTRODUCTION

Geological data and interpretations form the basis for the coal resource evaluation process by delineating the mineralization, estimating the resource and providing information for mine design [1]. Botswana Government has embarked on a journey since independence which focused on an aggressive nationwide geological and geophysical mapping which resulted in 90% of the land area covered in high resolution aeromagnetic and relatively high-resolution gravity survey in the northern part, central part and the Molopo farms areas [2]. The current total geological mapping has covered 48% of the country. The purpose of exploration work is to provide information on the coal seam thickness, coal quantity, structure and mechanical properties of the rock associated with the coal deposit, and the distribution and quality of groundwater.

Geological data is obtained through exploration drilling programs, often augmented by down hole geophysical logging and the analysis and testing of core samples. This geological data is then assimilated using computer database and modeling systems: this is then used to develop a 3-dimensional (3D) illustration of the deposit which is used in mine planning as a basis for the evaluation of the in-situ, recoverable and marketable coal resource. The data obtained is processed, interpreted and computerized: a database is created and managed to ensure retrieval of data when needed. A software that has come into use with the application of information technology in the mining industry is GEOVIA Surpac, having multiple high-end functions of mine modeling [3]. It is a complete software of geological data analysis, coal seam modeling, and mine planning and designing. Use of these techniques and data collected assist in the design and operation of effective systems of coal mining, coal preparation and utilization.

II. RESEARCH OBJECTIVES

The main objective is to develop a step-by step approach for geological data analysis and interpretation. This study also helps in understanding the applicability of geological data analysis for the purposes of determining mine boundaries, generation of 3D solid coal seam models of the deposit, which is evaluated to determine in-place coal resources

III. STUDY AREA

The geological data of a limited area (142 km^2) that was extensively explored by Shell Coal Botswana between 1974 and 1982, was provided for the purpose of this analysis and modeling. A total of 201 boreholes had been drilled in the lease area by 1984, at an average density of one borehole per 0.97km2 (Fig. 1). NQ wire-line equipment was used to core most of the boreholes. Core for geotechnical testing was sourced from thirteen individual boreholes, three clusters of 10 large diameter boreholes, and a further 3 single large diameter bores, each providing 150mm core which was used for bulk core sampling. Of the 201 boreholes drilled in the area, data for 15 drill holes was utilised for demonstration of this analysis.

ISSN: 2521-2293

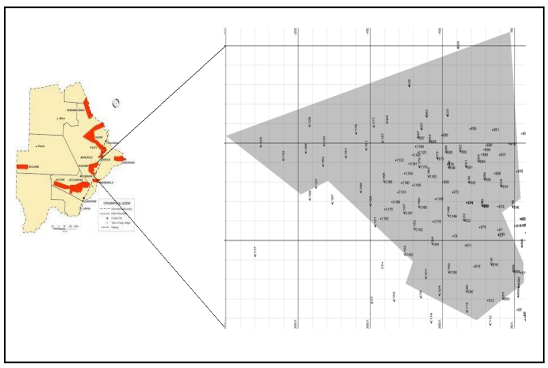

Fig. 1. Location of drill holes

IV. METHODOLOGY

Study was carried out based on borehole information sourced from the coal mine database. Information such as the property history and regional and property geology was sourced from a previous technical report which was revised and updated as required. This paper illustrates the development of a graphical representation of the coal deposit from borehole data, computing of coal reserves and estimation of coal grade suitable for coal mine design.

A. Drill hole data management

Data used was based on information obtained from drilling, lithological logging, core sampling, and the descriptions of stratigraphic sections measured in the field. This data also included collar information of drill holes coordinates; drill holes angles (dip and azimuth); coal seam intercepts; coal grades information; and geological and sampling data such as: lithology of samples taken from drill holes, calorific value, ash content, and moisture content. Data was presented in Microsoft Excel Comma Separated Values format so that the GEOVIA Surpac software understood the type of information that was fed into its system and results could be computed and displayed in graphical form. For the geological data provided, the collar, survey, lithology and assay tables were required (Tables I, II,III and IV).

TABLE I. COLLAR TABLE AND ASSOCIATED FIELDS

Drill hole ID	y	x	z	Max depth
Unique code for each borehole	Northing	Easting	Elevation	Drill hole path length

TABLE II. SURVEY TABLE AND ASSOCIATED FIELDS

Drill hole ID	Max depth	Dip	Azimuth
Unique code for each borehole	Drill hole path length	Angle of inclination of a drill hole w.r.t vertical	Direction of inclination

TABLE III. SAMPLE TABLE AND ASSOCIATED FIELDS

Drill hole ID	Sample ID	Depth from	Depth to	Calorific value	Other coal qualities
Unique code for each borehole	A number identity assigned to a sample extracted from the drill hole	From what depth the sample started	From what depth the sample ended	Coal calorific value from the sample in MJ/kg	Percentage of other coal qualities i.e ash, moisture, volatiles, sulphur, and carbon

TABLE IV. GEOLOGY TABLE AND ASSOCIATED FIELDS

Drill hole ID	Depth from	Depth to	Lithology
Unique code for each borehole	From what depth the sample started	From what depth the sample ended	Description of the different lithologies using rock codes obtained from the sample

B. Creation of geological database

Geological database is created from raw data acquired from drill holes presented in Microsoft Excel CSV files so that the software understands the type of information fed into its system and can compute the results or display any graphical form according to the user's requirements. The data in the Microsoft Excel CSV files is imported into GEOVIA Surpac version 2022 (x64) software The importing of data is mandatory for the processing of the database, as well as data validation to eliminate inconsistencies between the input data and the database descriptions made during database creation.

C. Generation of string files

A string file from the given borehole set, indicates the depths in the boreholes which can be considered as ore for the creation of sections. Firstly, the drill holes are displayed, and color constrained in terms of the geology and calorific value selecting the parameters of cut-off grade.The boreholes are then sectioned in the North South direction at 400m interval and digitized by selecting only the grades within and above the cut off value inside the digitized region using the section method to form ore strings which are further connected in a series to cover the entire deposit . The creation of sections is done for all the drill holes row sets using import data from the geology file.

D. Compositing

Once the ore strings are created, they are composited to; find basic statistics of the deposit enabling the proper solid modeling, create a block model, ensure proper resource evaluation and determine the resource estimate using estimation techniques. The process of compositing entails combining the assay values of adjacent samples from the drill

ISSN: 2521-2293

holes in order to determine the assay values of longer drill holes intervals. Compositing is performed on samples contained within the drill hole with respect to the intercepted contacts rather than the entire hole. Six types of compositing methods used in Surpac software- downhole, bench elevation, by grade constraints, by geological constraints, from end of hole and from multiple elements. Downhole drill compositing has been done with a fixed length of 1.5 m composite length, with minimum percentage of samples to be included as 75% and no zone selection method.

The sample database used contained a total of 138 assay samples representing 386.11m of core. To minimize dilution and over smoothing due to compositing, a composite length of 1.5m was selected as an appropriate composite length for resource estimation based on the average sample length. Using the downhole compositing method; compositing resulted in a total of 307 composite samples. Of the total assay population, approximately 25% are 1.1 meters or less with approximately 75% of the samples from 1.2 to 1.5 meters in length. Each composite sample was assigned a rock code corresponding with the mineralized solid in which it occurred, and each composite was used for grades interpolation onto the block within the individual solid by only placing additional constraints on the model.

E. Statistical analysis

Statistical analysis investigates the presence of high-grade outliers and a binomial distribution (two non-adjacent peaks) on the composite data presented in histograms. The reason for checking for outliers is that extreme grades (whether low or high) can bias the calculation of averages towards the extreme value especially in cases where there are few samples. This effect is even greater when the distribution is positively skewed. Histogram plots and cumulative probability plots of the composite data are also used to understand the degree of skewness and the need to apply top cut if the coefficient of variation is greater than 1.2.

The compositing string data and the statistics of the raw data were plotted, i.e. the statistical trends of grades vs number of samples for the sample data. Fig. 2 illustrates an example of a histogram plot for the coal calorific value sample data. The histogram has no outliers and no binomial distributions meaning the sampling data is representative with a normal distribution.

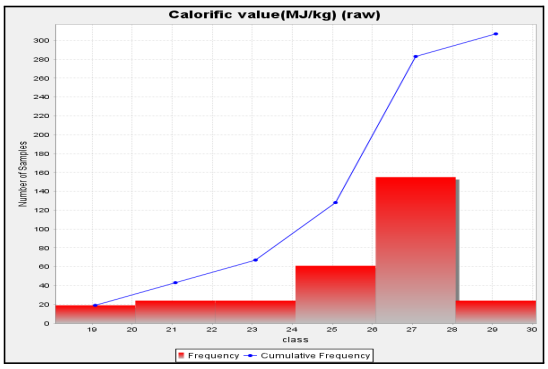

Fig. 2. Statistical analysis of coal calorific value

F. Spatial analysis

Spatial analysis shows how data values change over distance and direction. Variograms are used to illustrate the sample differences (variance) against distance (lag) for the various coal qualities. Several directional variograms are drawn to ascertain the direction of anisotropy of the deposit. Firstly, an experimental variogram is created from the population data (represented by the black data points), then afterwards fitted with a variogram model represented by the red curve. The variograms were drawn at 0° dip, 0° azimuth with 90° spread. Based on the composited data files, the following variogram was obtained for the coal calorific value sample data (Fig. 3).

The variograms modeled, indicated a strong negative spatial correlation as most of the variogram points were above the sill. Worth considering also is that if the nugget value is larger relative to the sill indicates that there is not enough correlation between the data points. In the variogram model for the calorific value, the nugget value was less than the sill value, meaning the correlation between the data points was adequate.

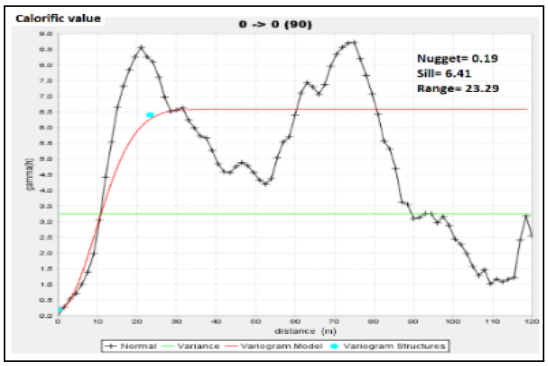

Fig. 3. Spatial analysis of coal calorific value

ISSN: 2521-2293

G. Creation of a solid 3-D coal seam model

A 3-D coal seam model in the form of a surface digital terrain model (DTM) is generated from the previously created ore string files. The ore strings are oriented in the clockwise direction (applicable if strings were digitizing anti-clockwise). Then, using the function of triangulation inside a segment and triangulation between segments for the extreme two sections, ore strings are oriented in clockwise direction and triangulated by connecting them to form a wireframe model of the deposit. After triangulation, the wireframe model is validated to check for the presence of invalid edges, triangles, repetition of edges, etc. Once validation is completed and accepted, the wireframe model is set to solid Fig. 4. The reported surface area and volume of the coal seams for the given sample data are given in Table V.

TABLE V. COAL SEAMS SURFACE AREA AND VOLUME

	Surface area (m^2)	Volume(m^3)
Coal Seam1	15 501 637	135 142 695
Coal Seam2	18 632 260	199 188 878
Cola Seam3	18 359 014	225 698 695
Total	52,492,911	560,030,268

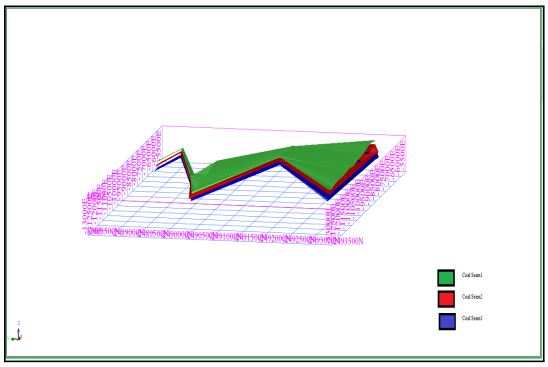

Fig. 4. 3-D model of the coal seams

H. Block model

Wireframes are used to constrain composite values chosen for grade interpolation and the coal blocks reported in the Mineral Resource estimate. The block size is chosen based partially on the average spacing between drill holes (borehole spacing), composite assay length, the tentative starting mining method, as well as the estimated minimum bench height achievable on the coal mine area. A block model of size 20m x 20m x 20 m was created to encompass the known areas of coal resources. At the scale of the sample deposit, this provided a block size reasonable for discerning grade distribution, but still big enough not to mislead when considering a higher cut-off grade distribution within the model. The extents of the model were a factor of the concession boundaries and the geometry of the mineralized solid (Table 6).

TABLE VI. BLOCK MODEL REPORT

Parameter	Value
y- coordinate	2493200
x- coordinate	12765.781
z- coordinate	696.822
Block size	20x20x20
Total blocks	58 303

I. Adding constraints to block model

Constraints are added to the empty block model to control the blocks from which interpolations were made i.e., restricting influence from surrounding samples through interpolating grades according to solid precedence. By incorporating the solid model to the overall block model, the extra blocks available in the area which fall outside the ore deposit are removed for a better estimation of the coal resource. The block model is also intersected with an overburden model and a surface topography model in order to exclude blocks that extend above the bedrock surface. The solid model generated was incorporated in the block model to form a constraint model.

J. Cut-off grade selection

Coal prices, reasonably assumed mining costs, metal recoveries and grades (used for comparable deposits in the region), are some of the several factors considered in determining the appropriate cut-off grade. Table 6 lists the price and recovery percentage used for coal equivalent calculations and cut-off grade determination. Based on the coal price of US$80 and recovery of 78%, a cut-off grade of 22MJ/kg was applicable to mineable blocks.

K. Filling constraint block model with attribute values

Interpolation of coal grades (calorific values) onto the block model is completed using the nearest neighbour estimation technique. The block model is filled with attribute values, these are, the coal qualities values (calorific value, ash content, carbon content and Sulphur content), specific gravity, air, waste and rock type. The block model is further intersected with an overburden model and surface topography to exclude blocks or portions of blocks that extend above the bedrock surface (air).

Coal grades are assigned to all blocks with a percent greater than zero, also flagged with a lithology code. Blocks within the model with a grade value less than the cut-off are considered waste (i.e blocks where no parts of a mineralized solid are captured, and no grades assigned) whilst those with values above the cut-off grade are considered as ore. The constraint block model modeled with assigned attributes as per the cut-off grade of 22MJ/kg thus obtained is shown in Fig. 5. The estimated tonnage of the coal mineralization for the three coal Seams was 728 039 348.4 tonnes.

ISSN: 2521-2293

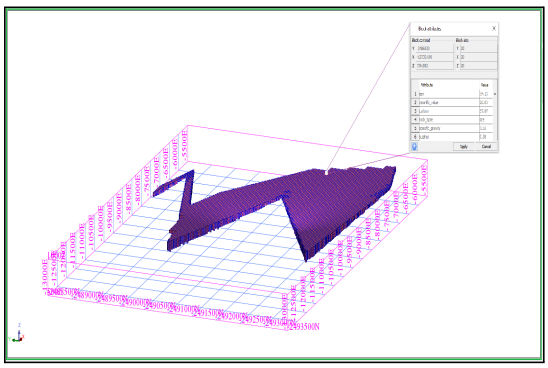

Fig. 5.Block model of the deposit showing grades through nearest neighbour method

V. RESULTS

The summarized methodology for geological data analysis and assessment as well as determining coal resources estimate is illustrated in Fig. 7.The coal mineralization in the study area was found to be widely distributed with even grade. Following this methodology, three coal seams were identified and evaluated. These seams covered a total area of 52,492,911 m^2, occupying a total volume 560,030,268 m^3 of at various depths.

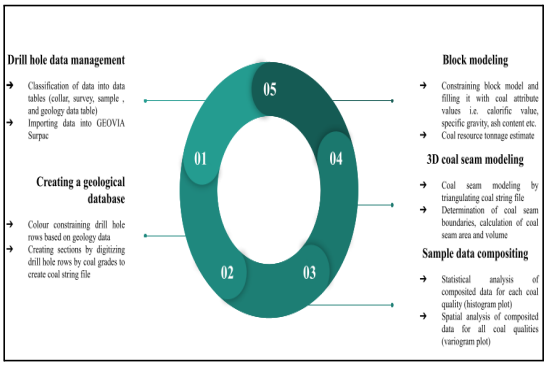

Fig. 7. Summarized methodology for geological data analysis

VI. CONCLUSION

In order to complete an updated Mineral Resource estimate for the coal seam block, with the help of a mine planning and design software Surpac, a geological database consisting of a series of comma limited spreadsheets was created into which the coordinates and alignment of the borehole points and their constituents along with their individual grades were fed into. The database included drill hole location information, specific gravity data, survey data, assay data and lithology data which were imported to GEOVIA Surpac. The borehole data was composited using downhole compositing method and statistical and spatial trends of individual constituents of coal.

Three-dimensional grade-controlled models were built by visually interpreting mineralized intercepts from cross sections using coal calorific values. Polygons of mineral intersections, snapped to drill holes, were made on each cross section and were wire framed together to create continuous resource wire frame models, the volume of the total block model was calculated, and the tonnage estimated. Mine models can then be formulated based on the resource estimates.

For the chosen study area, following the formulated methodology, coal seam boundaries were determined, a 3D solid model of coal Seams generated, and in-place coal resources evaluated. Following this methodology, three coal seams were identified and evaluated. These seams covered a total area of 52,492,911 m^3, occupying a total volume 560,030,268 m^3 at various depths.The estimated tonnage of the coal mineralization for the three coal Seams was 728 039 348.4 tonnes of mineable coal.

VII. REFERENCES

[1] Rupprecht, S., (2004). Establishing the feasibility of your proposed mining venture. In Proceedings of the International Platinum Conference 'Platinum Adding Value'. The South African Institute of Mining and Metallurgy. pp. 243-247.

[2] Sefemo, M.D., (2021). The 2018/19 Botswana mineral accounts technical report. Retrieved from The 2018-19 Botswana Mineral Accounts Technical Report.pdf (bgi.org.bw)

[3] Sahoo, M. M., & Pal, B. (2017). Geological modelling of a deposit and application using Surpac. J Mines Metals Fuels, 417.

BIUST Teaching, Research, & Innovation Symposium 2023 (TRDAIS 2023)
Botswana International University of Science and Technology
Palapye, Botswana, 18 - 19 September 2023
ISSN: 2521-2293

Prediction of blast-induced rock fragmentation at Orapa Diamond Mine using hybrid ANN models

Onalethata Saubi[1], Kesalopa Gaopale[1], Rodrigo S. Jamisola, Jr[2], Raymond S. Suglo[1], Oduetse Matsebe[2]*
[1]Dept. of Mining and Geological Engineering
[2]Dept. of Mechanical, Energy and Industrial Engineering
Botswana International University Science and Technology
Palapye, Botswana
onalethata.saubi@studentmail.biust.ac.bw, gaopaleg@biust.ac.bw, jamisolar@biust.ac.bw, suglor@biust.ac.bw, matsebeo@biust.ac.bw*

Abstract – This paper presents predictive models for blast-induced fragmentation at Orapa Diamond Mine in Botswana using machine learning algorithms namely artificial neural networks (ANN), particle swarm optimization artificial neural networks (PSO-ANN), and genetic algorithm artificial neural networks. A dataset consisting of 50 blasts with eight blast design parameters such as burden, spacing, hole depth, hole diameter, maximum charge per delay, stemming length, powder factor, distance from the monitoring point as input parameters, and fragmentation as the output parameter are used. The main goal of production blasting is to achieve proper fragmentation. Rock fragmentation has a direct influence on the mill throughput and diggability which in turn affect the overall mine economics. Hence accurate prediction of fragmentation is crucial in arriving at an economical outcome. Root mean square error and determination coefficient (R^2) indices were used to validate and compare the performance of the models. PSO-ANN demonstrated superiority over the other hybrid models in predicting fragmentation with the highest accuracy and lowest error. The results of sensitivity analysis showed that hole depth has the most influence on fragmentation while maximum charge per delay has the least influence on fragmentation.

Keywords - Rock fragmentation; blasting; artificial neural network; particle swarm optimisation; genetic algorithm; sensitivity analysis.

I. *INTRODUCTION*

The main goal of production blasting in the mining industry is to achieve proper rock fragmentation. Subsequent processes such as loading, hauling, and crushing are significantly influenced by production blasting. The quality of fragmentation is used as an indicator of the efficiency of a blast. As a result, blast design parameters play a significant role in producing the desired fragmentation [1]. Uniform particle size distribution leads to increased mill throughput due to the increased diggability of the fragmented rock that translates into the performance of the loader and excavator used. In addition, proper fragmentation eliminates the need for secondary blasting [2]. All these lead to improved overall plant or mine economics. Hence accurate prediction of rock fragmentation plays a significant role in the economies of operating the mines.

Parameters influencing rock fragmentation are divided into three categories, namely, rock mass properties, blast geometry, and explosive properties [3-6]. From the literature, there are several empirical models developed for forecasting blast-induced rock fragmentation [7-10]. Empirical models are only able to consider a few effective parameters thus making them inaccurate and unreliable. Furthermore, acquiring all the relevant effective parameters is not possible as their non-linear relationships are not known or are difficult to quantify [11-12].

To overcome the limitations of empirical models, the application of artificial intelligence techniques has been highlighted by several researchers in the field of engineering and rock mechanics [13-18]. Zhou et al. [19] predicted blast-induced rock fragmentation using artificial neural network (ANN), support vector regression (SVR), adaptive neuro-fuzzy inference system (ANFIS), adaptive neuro-fuzzy inference system combined with genetic algorithm (ANFIS-GA), and adaptive neuro-fuzzy inference combined with firefly algorithm (ANFIS-FFA). ANFIS-GA performed better compared to the other models in predicting rock fragmentation. ANN and multivariate regression analysis (MVRA) was applied in forecasting rock fragmentation by Monjezi et al. [20]. Burden-to-spacing ratio, hole diameter, stemming, total charge per delay, powder factor, maximum holes per delay, point load index, and delays between the rows were considered as inputs in their study. The ANN method showed superiority over MVRA in predicting rock fragmentation with an R^2 value of 0.985 and an RMSE value of 0.995.

Bahrami et al. [21] proposed an ANN model for estimating rock fragmentation. A four-layer neural network was found to be optimum in predicting rock fragmentation. Sensitivity analysis from the same study revealed that blastability index, charge per delay, burden, and powder factor are the most effective parameters for fragmentation. Shams et al. [12] offered a fuzzy inference system (FIS) and MVRA model for predicting rock fragmentation. The results showed that the FIS model was more accurate in predicting fragmentation than MVRA, with an RMSE of 2.423 and a variance account (VAF) of 92.195%. sShi et al. [22] predicted the mean particle size of rock fragmentation due to

ISSN: 2521-2293

bench blasting using support vector machine (SVM), MVRA, and the Kuznetsov empirical model. The prediction accuracy of SVM was more acceptable than the other methods.

Hasanipanah et al. [23] offered ANFIS combined with particle swarm optimization (PSO) model to predict rock fragmentation. In their study, SVM and nonlinear multiple regression (NLMR) methods were used. About 72 blasts were investigated, and the results showed that ANFIS-PSO is more accurate in predicting fragmentation than SVM and NLMR.

This study presents three data-driven models for predicting rock fragmentation. We used three methods, namely, ANN with gradient descend, ANN with PSO, and ANN with GA. The contributions of this paper are:

- A blast dataset consisting of 8 blast design parameters were collected from Orapa Diamond Mine, in Botswana for training and testing the models. The data sample size is 50.
- ANN is optimised by using GA and PSO to predict rock fragmentation, instead of the usual gradient descend method.
- Sensitivity analysis is conducted to determine the most effective parameters on rock fragmentation.

II. *DATA SETS*

In this study, a database consisting of 50 blasts has been collected from the Orapa Diamond Mine, in Botswana, to construct and verify the proposed PSO-ANN, GA-ANN, and ANN models. The parameters considered in this study are burden, spacing, hole depth, hole diameter, maximum charge per delay, stemming length, powder factor, and distance from the monitoring point as inputs and fragmentation as the output. The blast geometry parameters are shown in Fig. 1. Split desktop software was used to analyse the images obtained using a digital camera. Before implementing the modelling process, the data was first pre-processed which included cleaning and normalisation. It was then divided into train and test sets, 80% and 20%, respectively. Table 1 shows the range of parameters used in this study.

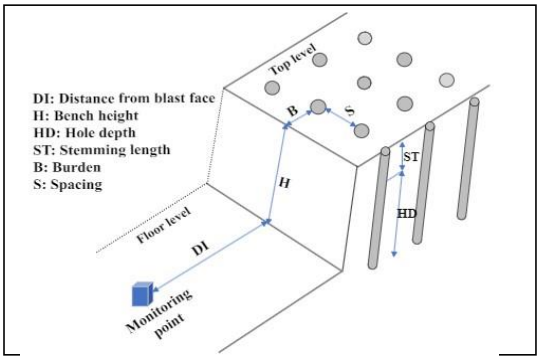

Fig. 1. Schematic Diagram of Blast Geometry

I. *METHODS*

Hybrid algorithms are used that combine the search properties of ANN with that of PSO and GA algorithms as a way of optimizing its performance in solving the given problem.

TABLE I. THE RANGE OF THE INPUT AND OUTPUT PARAMETERS

Parameter	Type	Unit	Symbol	Min	Max
Burden	input	m	B	4	8
Spacing	input	m	S	4	7
Stemming length	input	m	St	4	8
Hole depth	input	m	HD	12.28	16.29
Hole diameter	input	mm	D	127	250
Distance - blast face	input	m	DI	438	1500
Charge per delay	input	kg	MC	27	61.4
Powder factor	input	kg/m^3	Pf	0.3	1
Fragmentation	output	%	F	70	81

A. *ARTIFICIAL NEURAL NETWORKS*

The machine learning algorithm ANN was initially introduced by McCulloch and Pitts in 1943 and it has gained popularity due to the rise in computing capacity [24]. ANNs are inspired by the way neurons in the human brain process information. Three main constituents make up a typical ANN, namely, the network architecture, the transfer function, and the learning rule [25]. A simple neural network architecture consists of neurons in three layers (input, hidden, and output), connected by weights. The weighted total of the inputs and the bias is computed using a transfer function. After the transfer function computes the sum, the activation function gets the outcome and provides threshold values over which the neurons of the network will fire. The most applied learning rule for training ANNs is the backpropagation (BP) algorithm [26]. In the BP-ANN, input data is first forward propagated in the input layer, through the hidden layer, to the output layer. The error is computed in the output layer by taking the difference between the actual and predicted output as shown in (1)

ISSN: 2521-2293

$$E_n = \frac{1}{2}\sum_{n=1}^{n}\sum_{i=1}^{i}(A_{ni} - P_{ni})^2 \quad (1)$$

where A_{ni} and P_{ni} are actual and predicted values of the ith neuron, i is the total number of neurons, and n is the dataset number.

The result is then backpropagated to update the individual weights as shown in (2) and (3). The process is iterated until the error is minimised [27]

$$\Delta W_{jk} = \mu \frac{\delta E_n}{\delta W_{jk}} Out_k \quad (2)$$

$$W_{jk}^{new} = W_{jk}^{old} + \Delta W_{jk} \quad (3)$$

where Out_k is the output of the kth neuron, u is the learning rate, and E_n is the mean square error (MSE) of the ANN.

B. PARTICLE SWARM OPTIMISATION

Kennedy and Eberhart et al. [28] are credited with developing PSO, which was first designed to simulate social behaviour by mimicking the movement of a flock of birds or a fish school. A population of potential solutions, called particles are used to solve the problem, and these particles are moved across the search space over the particle's position and velocity ~~shown~~ expressed in equations (4) and (5)

$$V_{new} = wV + r_1C_1 * (P_{best} - X) + r_2C_2 * (G_{best} - X) \quad (4)$$

$$X_{new} = X + V_{new} \quad (5)$$

where Vnew, X, and V are the new velocity, current position, and current velocity of particles, respectively. The symbol w is the inertial weight coefficient, and r_1 and r_2 are random values in the range (1,0). The symbols C_1 and C_2 are predefined acceleration coefficients, P_{best} is the particle's personal best position, and G_{best} is the global best position among all particles.

In addition to being led toward the best-known positions in the search space, which are updated as other particles find better positions, each particle's movement is also influenced by its local best-known position. The swarm migrates toward a better solution as a result of this [29]. PSO is a metaheuristic because it can search very huge areas of potential solutions and makes little to no assumptions about the problem being optimised.

1) *Implementation of PSO-based ANN:*

According to Jadav and Panchal [30], ANN has the drawback of getting stuck in local minima. PSO can search a much wider space and find global minima. Therefore weights and biases of the neural network are updated using the best positions found by the PSO algorithm.

C. GENETIC ALGORITHM

Holland [31] introduced a genetic algorithm that is normally employed as a method for optimisation and stochastic search. GA was influenced by Charles Darwin's theory of natural selection. The selection of the fittest individuals in a population is the first step in the process of natural selection. They give birth to offspring who carry on their parent's traits and will be added to the following generation. Parents who are more physically fit will produce offsprings who will outperform the offspring from parents who are not as fit and have a higher chance of surviving [32]. The fittest generation will eventually emerge because of this process' continual iterations. The algorithm terminates when the population has converged (does not produce offspring which are significantly different from the previous generation) [33]. Five phases are considered in a genetic algorithm. These are:

- Initial population - The process begins with a set of individuals which are known as a population. These individuals are a potential solution to the problem. Genes are a set of parameters (variables) that define an individual. A chromosome (solution) is made up of a string of genes.
- Fitness function - The fitness function gauges an individual's level of fitness which is the ability of an individual to compete with other individuals. Based on its fitness score, an individual's likelihood of being chosen for reproduction is determined.
- Selection - The purpose of the selection phase is to choose the fittest individuals based on their fitness ratings and allow them to pass on their genes to the following generation.
- Crossover - A crossover point is picked at random from the genes for each set of parents to mate. A crossover can be a single point or double point. Parents' genes are exchanged among one another until the crossover point is achieved, at which time the offsprings are produced.
- Mutation - Some of the newly produced offspring's genes are subjected to a low-probability random mutation. When using binary values, mutation entails changing string 1 to 0 and string 0 to 1. To preserve variety throughout the population and avoid early convergence as mutation takes place.

2) *Implementation of GA-based ANN*

ISSN: 2521-2293

The algorithm GA has the significant advantage of being able to perform a multidirectional search and avoid being trapped in local optima [34-35]. Therefore, the weights and biases are updated using GA.

II. *RESULTS AND DISCUSSIONS*

To assess the performance of all the models, the determination coefficient (R^2) and the root mean square error (RMSE) were utilised as the performance indices. These are expressed by equations (6) and (7):

$$R^2 = \left[\frac{\sum_{i=1}^{N}(y-\bar{y})(y'-\bar{y}')}{\sum_{i=1}^{N}(y-\bar{y})^2 \sum_{i=1}^{N}(y'-\bar{y}')^2}\right]^2 \quad (6)$$

$$\text{RMSE} = \sqrt{\frac{1}{N}\sum_{i=1}^{N}(y-y')^2} \quad (7)$$

where y and y' are measured and predicted values, respectively; $\bar{y}$ and $\bar{y}'$ are mean measured and mean predicted values, respectively and N is the dataset number.

A good RMSE is a value close to or equal to 0 while a good R^2 is a value close to or equal to 1. Table 2 summarises the performance indices for all the models with their hyper-parameters. It is observed that the PSO-ANN model with 30 particles and 10 neurons in the hidden layer gives the highest R^2 value of 0.88 and the lowest RMSE of 1.97 compared to other models. It is therefore considered the optimum model for predicting rock fragmentation. A comparison is shown between the measured and predicted fragmentation by all models in Fig. 2.

The predicted results of the PSO-ANN model are in close agreement with the actual rock fragmentation, proving the capability of this model in forecasting blast-induced rock fragmentation compared to other models. Figs. 3 to 5 show the correlations between the measured and predicted fragmentation by all the models. Most of the data points are close to the line of best fit for the PSO-ANN model compared to other models indicating that it gives the highest correlation and highest accuracy than other models. Fig. 3 shows that the ANN model data points are the farthest from the line of best fit showing that the ANN model gives the lowest correlation and accuracy. Hence the performance of the ANN is significantly improved by being optimised by PSO.

TABLE II. PERFORMANCE INDICES FOR ALL THE MODELS

GD-ANN			GA-ANN			PSO-ANN		
Neurons	R^2	*RMSE*	*Population*	R^2	*RMSE*	*Particles*	R^2	*RMSE*
10	0.81	2.56	10	0.63	1.54	10	0.78	2.90
	0.77	2.81	20	0.52	2.30	30	0.88	1.97
	0.52	2.92	40	0.84	2.45	60	0.73	2.88
	0.61	3.67	60	0.61	4.89	90	0.65	3.61
12	0.75	2.78	10	0.65	3.66	10	0.79	2.63
	0.68	3.05	20	0.59	3.90	30	0.62	2.99
	0.63	3.97	40	0.40	4.11	60	0.54	3.43
	0.54	4.21	60	0.47	4.26	90	0.56	3.73
14	0.63	4.16	10	0.46	2.29	10	0.63	3.41
	0.66	4.23	20	0.48	3.45	30	0.59	3.66
	0.51	4.66	40	0.40	3.98	60	0.65	4.05
	0.44	3.54	60	0.39	3.67	90	0.60	4.11
16	0.61	4.27	10	0.43	4.24	10	0.55	4.72
	0.55	4.39	20	0.50	4.55	30	0.48	4.23
	0.43	4.51	40	0.55	4.73	60	0.45	4.56
	0.38	5.67	60	0.41	4.12	90	0.52	4.79

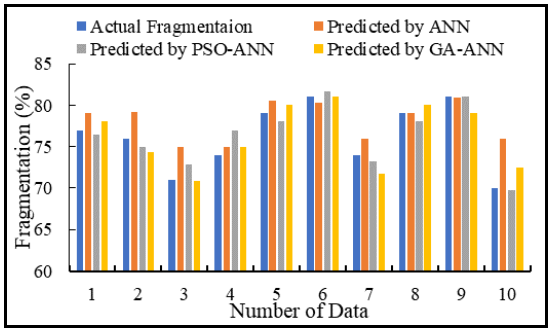

Fig. 2. Comparison of the Measured and Predicted Fragmentation by all the models

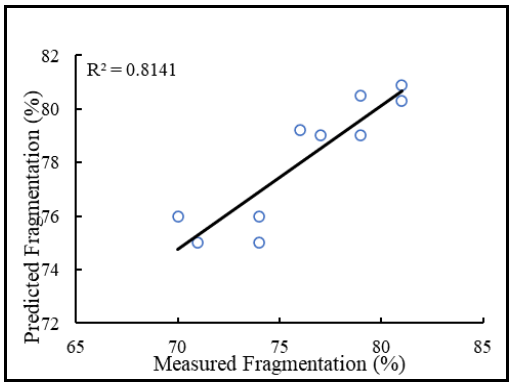

ISSN: 2521-2293

Fig. 3. ANN Model Performance

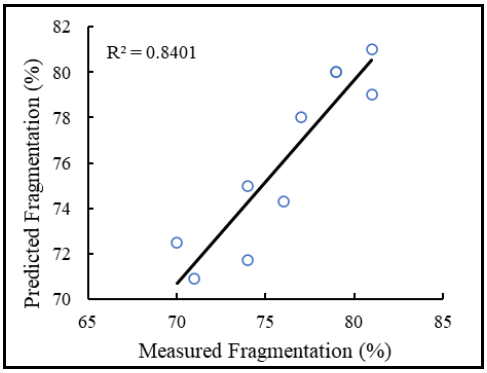

Fig. 4. GA-ANN Model Performance

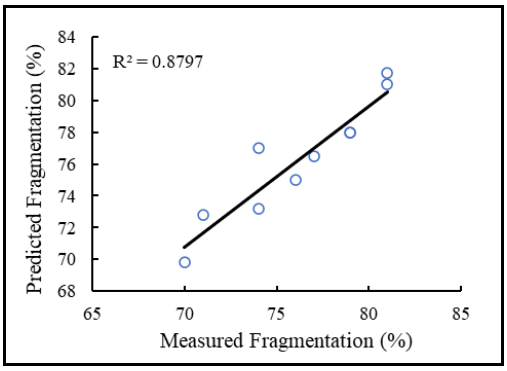

Fig. 5. PSO-ANN Model Performance

III. SENSITIVITY ANALYSIS

Sensitivity analysis is conducted using the cosine amplitude method [36]. It is used to determine the relative influence of the input parameters on the output. This can be calculated using equation (8) and the calculated results are plotted in Fig. 6

$$R_{ij} = \frac{\sum_{k=1}^{m} x_{ik} x_{jk}}{\sqrt{\sum_{k=1}^{m} x_{ik}^2 \sum_{k=1}^{m} x_{jk}^2}} \quad (8)$$

where X_i and X_j are the input and output parameters respectively, and m represents the number of data samples.

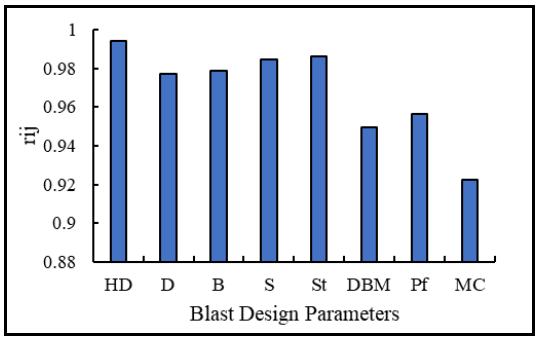

Legend: HD = Hole depth, D = Hole diameter, B = Burden, S = Spacing, St = Stemming, DBM = Distance from blast point, Pf = Powder factor and MC = Maximum charge per delay.

Fig. 6. Strength of Relation Between Input and Output Parameters

From Fig. 6, it can be inferred that hole depth is the most effective parameter on fragmentation while maximum charge per delay is the least influential parameter on fragmentation.

IV. CONCLUSIONS

In this paper, a PSO-ANN model was developed for forecasting blast-induced rock fragmentation at Orapa Diamond Mine in Botswana. In this regard, blast design parameters as well as rock fragmentation of 50 blasting operations were used. For comparison purposes, ANN and GA-ANN models were also developed using the same dataset. The blast design parameters considered in this study for predicting rock fragmentation are burden, spacing, hole depth, hole diameter, the maximum charge per delay, powder factor, stemming length, and distance from the blast point to the monitoring point. It was observed that the PSO-ANN model is more efficient in predicting fragmentation than ANN and GA-ANN. The R^2 and RMSE values obtained for the PSO-ANN model are 0.88 and 1.97 respectively, while the values for the least performed ANN model were computed as 0.38 and 5.67 respectively. The results of sensitivity analysis indicated that maximum charge per delay is the most influential parameter on rock fragmentation while hole depth is the least effective parameter on fragmentation.

ACKNOWLEDGMENT

The authors wish to extend their appreciation to the Debswana Diamond Company, Project No. P00064 for making this research possible. The authors would also like to thank Orapa Diamond Mine for providing the required data for this research.

REFERENCES

[1] M. Monjezi, M. Rezaei, and A.V. Yazdian, “Prediction of rock fragmentation due to blasting in Gol-E-Gohar iron mine using fuzzy logic,” Int. J. Rock. Mech. Min. Sci, vol. 46, no. 8, pp. 1273–1280, December 2009.

ISSN: 2521-2293

[2] P.H, Kulatilake, W. Qiong, T. Hudaverdi, and C. Kuzu, "Mean particle size prediction in rock blast fragmentation using neural networks," Eng. Geol, vol. 114, no. 3-4, pp. 298-311, August 2010.

[3] D. Thornton, S.S. Kanchibotla, and I. Brunton, "Modelling the impact of rock mass and blast design variation on blast fragmentation," Int. J. Blast. Fragment, vol. 6, no. 2, pp. 169–188, October 2002.

[4] M. Monjezi, A. Bahrami, and A.Y. Varjani, "Simultaneous prediction of fragmentation and flyrock in blasting operation using artificial neural networks," Int. J. Rock. Mech. Min. Sci, vol. 47, no. 3, pp. 476–480, April 2010.

[5] E. Bakhtavar, H. Khoshrou, and M. Badroddin, "Using dimensional regression analysis to predict the mean particle size of fragmentation by blasting at the Sungun copper mine," Arab. J. Geosci, vol. 8, no. 4, pp. 2111–2120, April 2015.

[6] X.Z. Shi, J. Zhou, B. Wu, D. Huang, and W. Wei, "Support vector machines approach to mean particle size of rock fragmentation due to bench blasting prediction, " Trans. Nonferrous. Met. Soc. China, vol. 22, pp. 432–441, February 2012.

[7] V.M. Kuznetsov, "The mean diameter of the fragments formed by blasting rock," Sov. Min. Sci, vol. 9, no. 2, pp. 144–148, March 1973.

[8] C.V.B. Cunningham, "The Kuz-Ram model for prediction of fragmentation from blasting," In Proc.1st Symp. on Rock Fragmentation by Blasting, pp. 439–453, Lulea 1983.

[9] P.P. Roy, and B.B. Dhar, "Fragmentation analyzing scale–A new tool for rock breakage assessment," InRock Fragmentation by Blasting, CRC Press, pp. 448-448, December 2020.

[10] P.A. Rosin, "Laws governing the fineness of powdered coal, " J. Inst. Fuel, vol. 7, pp. 29-36, 1933.

[11] N.K. Dumakor-Dupey, S. Arya, and A. Jha, "Advances in blast-induced impact prediction - A review of machine learning applications," Minerals, vol. 11, no. 6, p. 601, June 2021.

[12] S. Shams, M. Monjezi, V.J. Majd, and D.J. Armaghani, "Application of fuzzy inference system for prediction of rock fragmentation induced by blasting," Arab. J. Geo, vol. 8, no. 12, pp. 10819-10832, December 2015.

[13] K. Kaklis, O. Saubi, R. Jamisola, and Z. Agioutantis, "Machine learning prediction of the load evolution in three-point bending tests of marble," Min. Metall. Expl, vol. 39, no. 5, pp. 2037-2045, October 2022.

[14] M. Mohammadhassani, H. Nezamabadi-Pour, M. Suhatril, and M. Shariati, "An evolutionary fuzzy modelling approach and comparison of different methods for shear strength prediction of high-strength concrete beams without stirrups," Smart. Struct. Syst, vol. 14, no. 5, pp. 785-809, November 2014.

[15] M. Wang, X. Shi, J. Zhou, and X. Qiu, "Multi-planar detection optimization algorithm for the interval charging structure of large-diameter long hole blasting design based on rock fragmentation aspects," Eng. Opt, vol. 50, no. 12, pp. 2177- 2191, December 2018.

[16] K. Kaklis, O. Saubi, R. Jamisola, Z. Agioutantis, "A preliminary application of a machine learning model for the prediction of the load variation in three-point bending tests based on acoustic emission signals," Proced. Strct. Int, vol. 33, pp. 251-258, January 2021.

[17] T. Petso, R.S. Jamisola, D. Mpoeleng, E. Bennitt, W. Mmereki, "Automatic animal identification from drone camera based on point pattern analysis of herd behaviour," Ecol. Infor, vol. 66, p.101485 December 2021.

[18] M. Wazha, R.S. Jamisola, D. Mpoeleng, T. Petso, "YOLOv3-based human activity recognition as viewed from a moving high-altitude aerial camera," 7th Int. Conf. Auto. Robt. Appl, pp. 241-246, 2021.

[19] J. Zhou, C. Li, C.A. Arslan, M. Hasanipanah, and H.A. Bakhshandeh, "Performance evaluation of hybrid FFA-ANFIS and GA-ANFIS models to predict particle size distribution of a muck-pile after blasting," Eng. Com, vol. 37, no. 1, pp. 265-274, January 2021.

[20] M. Monjezi, H. Amiri, A. Farrokhi, K. Goshtasbi, "Prediction of rock fragmentation due to blasting in Sarcheshmeh copper mine using artificial neural networks," Geotech. Geol. Eng, vol. 8, no. 4, pp. 423-430, July 2010.

[21] A. Bahrami, M. Monjezi, K. Goshtasbi, and A. Ghazvinian, "Prediction of rock fragmentation due to blasting using artificial neural network," Eng. Com, vol. 27, no. 2, pp. 177-181, April 2011.

[22] X.Z, Shi, J.H, Jian, B.B, Wu, D. Huang, and W.E. Wei, "Support vector machines approach to mean particle size of rock fragmentation due to bench blasting prediction," Trans. Nonferr. Mtl So. Chn, vol. 22, no. 2, pp.432-441, February 2012.

[23] M. Hasanipanah, H.B. Amnieh, H. Arab, and M.S. Zamzam, "Feasibility of PSO–ANFIS model to estimate rock fragmentation produced by mine blasting," Neurl. Comp. Appl, vol. 30, no. 4, pp. 1015-1024, August 2018.

[24] W.S. McCulloch, and W. Pitts, "A logical calculus of the ideas immanent in nervous activity," Bulletin. Math. Biophysc, vol. 5, no. 4, pp. 115-133, 1943.

[25] S.M. Al-Alawi, "Development and Application of Back-Propagation-Based Artificial Neural Network Models in Solving Engineering," Sultan Qaboos University Journal for Science [SQUJS]. 2002 Jun 1; 7(1):55-70.

[26] E. Momeni, D.A., Jahed, M. Hajihassani, M., and F.A. Mohd, "Prediction of uniaxial compressive strength of rock samples using hybrid particle swarm optimization-based artificial neural networks," Measurement, vol. 60, pp. 50–63, 2015.

[27] K. M. Neaupane, and S.H. Achet, "Use of backpropagation neural network for landslide monitoring: a case study in the higher Himalaya," Engg. Geol, vol. 74, no. 3-4, pp.213-226, August 2004.

[28] J. Kennedy and R. Eberhart, "Particle swarm optimization," In Proc. Int. Con. Neur. Net, vol. 4, pp. 1942-1948, November 1995.

[29] Y. Shi, "Particle swarm optimization: developments, applications, and resources," In Proc. Cong. Evol. Comp, vol. 1, pp. 81-86, May 2001.

[30] K. Jadav, and M. Panchal, "Optimizing weights of artificial neural networks using genetic algorithms," Int. J. Adv. Res. Comput. Sci. Electron. Eng, vol. 1, pp. 47–51, 2012.

[31] J. Holland, "Adaptation in natural and artificial systems," University of Michigan Press, Ann Arbor, p232, 1975.

[32] K.E. Kinnear, "A Perspective on the Work in this Book", Advances in Genetic Programming, pp.3-19, 1994.

[33] J. Carr, "An Introduction to Genetic Algorithms," Sen. Proj, vol. 40, no. 1, p.7, 2014.

[34] S. Rajasekaran, and G.A.P. Vijayalakshmi, "Neural networks, fuzzy logic and genetic algorithms, synthesis and applications," Prentice-Hall of India, New Delhi. p121, 2007.

[35] L.D. Chambers, "Practical handbook of genetic algorithms: complex coding systems," CRC Press, Boca Raton, p. 592, 2010.

[36] T.J. Ross, "Fuzzy logic with engineering applications," John Wiley and Sons, p. 652, 2005.

BIUST Teaching, Research, & Innovation Symposium 2023 (TRDAIS 2023)
Botswana International University of Science and Technology
Palapye, Botswana, 18 - 19 September 2023
ISSN: 2521-2293

Development of an African National Cybersecurity Strategy Development Guide (ANCSDG): Botswana context

Violet Lebogang
Department of Computer Science and Information Systems
Botswana International University of Science and Technology
Palapye, Botswana
lv20100141@studentmail.biust.ac.bw

Oteng Tabona
Department of Computer Science and Information Systems
Botswana International University of Science and Technology
Palapye, Botswana
tabonao@biust.ac.bw

Thabiso Maupong
Department of Computer Science and Information Systems
Botswana International University of Science and Technology
Palapye, Botswana
maupongt@biust.ac.bw

***Abstract*—Botswana, like many other African countries, is undergoing a digital transformation. Whilst this transformation presents a vast amount of opportunities to greatly improve citizens' lives, there are associated risks. One of which is cybercrime. Cybercrime is a growing phenomenon that can not only disrupt businesses or personal systems but can also affect the national critical ICT infrastructure such as the supply of water, electricity, as well as business and government applications. Although efforts by the government have been made to secure the cyberspace through publishing a national cybersecurity strategy, establishing a cybersecurity incident response team, and adopting cybersecurity-related legal frameworks, a holistic approach to cybersecurity is still lacking and there is still a gap in terms of interoperability and shared understanding within the cybersecurity strategic environment. This research proposes the development of a semantic-based National Cybersecurity Strategy Development Guide (African National Cybersecurity Strategy Development Guide- ANCSDG). This ontology will help address the interoperability issues within the cybersecurity environment and it can also be used as a model for the development and implementation of the National Cybersecurity Strategy (NCS) in Botswana. The guide will be developed per the International Telecommunications Union (ITU) 's national cybersecurity development guide. The guide will cover six different components: Critical Infrastructure Protection, Governance, Cybercrime Reporting, and Intelligence, Risk Management, Regional and International Cooperation, Capacity, and capability building.**

Keywords—component; Cybersecurity; cybercrime; strategy development guide; security ontology

A. INTRODUCTION

Botswana is increasingly being targeted by cybercriminals. (Serianau, 2018). In an initiative to counter these attacks, the Government has formulated a national cybersecurity strategy that was approved by parliament in October 2020 (ITU, 2022). This strategy was developed by the Ministry of Transport and Communication in collaboration with other government and private stakeholders. International partners such as Great Britain Government's Foreign & Commonwealth Office and USA State Department through MITRE and Carnegie Mellon University also played a part in the development (Lebogang, Tabona and Maupong 2022). A national cybersecurity assessment was carried out in 2012 with the assistance of the ITU and International Multilateral Partnership Against Cyber Threats (IMPACT) to assess the country's readiness for establishing a National Incident Response Team (BwCIRT). Since then, Botswana has enacted cybersecurity-related laws like the Cybercrime and Computer-related crimes act of 2018, Data Protection Act of 2018, Consumer Protection Act of 2018, and Electronic Records (Evidence) Act of 2014, and it has also set up a Cybersecurity Incident Response Team.

Overall, the National Cybersecurity Strategy does not provide good evidence of a comprehensive assessment especially outlining the threat landscape and there is not much emphasis on using a holistic approach for the implementation of the NCS and how its progress will be monitored (Lebogang, Tabona, and Maupong 2022). On the Global Cybersecurity Index (GCI) report compiled by ITU in 2020, Botswana ranked 88th out of 198 countries globally and 12th of 43 countries in Africa. In another cybersecurity index compiled by e-Governance Academy, as of 2022, Botswana has been ranked 113th out of 160 countries globally. This is a decrease from the 100th ranking which was recorded in 2020. This indicates that there is low cyber maturity in the area. A strategy development guide is needed to help Botswana develop robust cybersecurity strategies.

Although various structures have been established to deal with cybersecurity in Botswana, they are still by e-

ISSN: 2521-2293

Governance Academy, as of 2022, Botswana has been ranked 113th out of 160 countries globally. This is a decrease from the 100th ranking which was recorded in 2020. This indicates that there is low cyber maturity in the area. A strategy development guide is needed to help Botswana develop robust cybersecurity strategies.

Although various structures have been established to deal with cybersecurity in Botswana, they are still inadequate and the implementation of the strategy is at an infant stage. Additionally, there is still a gap in terms of interoperability and shared understanding within the cybersecurity environment. (Rantos, 2021).

In trying to address this problem, Jansen van Vuuren et al. (2013) developed a cybersecurity policy implementation framework for South Africa. The framework is based on previous work by Jansen van Vuuren et al. (2012), an implementation framework proposed by Otoom & Atoum (2012), guidelines for the implementation of national cybersecurity strategies by Ghernouti-Helie (2010), and a cybersecurity Awareness toolkit by Phahlamohlaka et al., 2011.

This paper describes a semantic-based National Cybersecurity Strategy development guide to support Botswana in the development and implementation of a comprehensive and effective National Cybersecurity Strategy (NCS). This will map an ideal cybersecurity strategic environment. It will capture the complexity of the interactions required between different stakeholders to develop and implement a National Cybersecurity Strategy (NCS). The ultimate goal of this effort is to develop an ontology of the cybersecurity strategic environment expressed in OWL language. The availability of a formally encoded cybersecurity strategic environment will enable …

The rest of the document is structured as follows: section 2 will provide a brief literature review and related works. Section 3 will describe the methodology employed to develop the proposed solution, section 4 will describe the proposed model and the research will be concluded in section 5.

. RELATED WORKS

Despite the fact that several ontologies have been developed for the cybersecurity domain, the use of ontologies to model the complexities of cyber governance, in particular, has received limited attention in the research community. Greiman (2018) reflected on how ontological research methodologies contribute to the understanding of cyber governance at the global level. One of the numerous motivations the author highlights for using an ontology to model the complexity of the cyber governance environment is the ability of an ontology to formally define a vocabulary for the domain. Greiman found out that although there have been a number of research activities on the development of cybersecurity ontologies (Obrst, Chase, & Markeloff, 2021), there are very few investigations on the use of ontological development to support the interoperability of cyber governance at the international level. Greiman explored an ontological approach to analyze cyber governance with the motivation that ontological models can provide insight into the entities, attributes, and processes in this domain.

Previous works have used qualitative approaches including interviews and literature review to develop a national cybersecurity strategy development framework or provide suggestions for the improvement of the existing cybersecurity frameworks. Some of the works by J C Van Vuuren et al., 2013; Kulikova et al., 2012; K. 2012; and Amir Mohammed Talib et al., 2018 are discussed below;

.TABLE STYLES

Past related works in literature		
Researchers	***Methods***	***Findings***
J C Van Vuuren et al. (2013)	Literature review	This paper describes a cybersecurity policy implementation framework for South Africa which is based on previous work of the authors as well as guidelines and other frameworks in the literature.
J C Van Vuuren et al. (2019)	Literature review	This paper presents a framework for African countries to develop and implement a national cybercrime. It includes elements such as Governance, Cooperation, Reporting and Intelligence, Education and Awareness as well as High- tech crime and other specialized units.
Otoom & Atoum, 2012	Literature review	This paper proposes an implementation framework that lays out the ground for a coherent, systematic, and comprehensive approach to implementing the National Information Assurance and Cyber Security Strategy (NIACSS) of Jordan. The Framework 1). Suggests a methodology to analyze the NIACSS, 2). Illustrates how the NIACSS analysis can be utilized to design strategic moves and develop an appropriate functional structure, and 3). proposes a set of adaptable strategic controls that govern the NIACSS implementation and allow for achieving excellence, innovation, efficiency, and quality.
Khosraw Salamzada et al. (2015)	Qualitative approach using semi-structured interviews	This paper presented a framework for cybersecurity strategy for developing countries. This paper particularly focused on Afghanistan.
Kulikova (2012)	Interview and Literature review	This paper presented a cybersecurity framework and validated testing, defining two security incident scenarios and interviews.
Government of the Republic of South Africa		The National Cybersecurity Policy Framework (NCPF) proposed in this paper outlines policy guidelines related to

ISSN: 2521-2293

Past related works in literature		
Researchers	***Methods***	***Findings***
		cybersecurity in SA and requires the government to develop detailed cybersecurity policies and strategies. It aims to address national security in terms of cyberspace security, for example, cyber-warfare, cybercrime, cyber-terrorism, and cyber-espionage.

Table 1: Related works

B. ONTOLOGY CONSTRUCTION

In this section, the methodology that was employed for the development of the ANCSDG ontology is described.

. *Methodology*

In order to achieve the main objective of this research, which is to develop a semantic-based National Cybersecurity Strategy Development Guide (African National Cybersecurity Strategy Development Guide-ANCSDG), a research methodology proposed by (Fernández-López et al., 1997) called 'METHONTOLOGY' was used. This methodology is based on the idea of software engineering, which defines a set of tasks to be performed to develop a consistent and complete conceptual model. The authors of this paper also considered other methodologies like the one proposed by (Grüninger and Fox, 1995), (Noy and McGuinness, 2001), (Ahmed et al., 2007), and (Kumara, 2006) but because methontology is widely adopted, provides support in building ontologies from scratch, can be applied for the reuse of existing ontologies and it is flexible and easy to adopt. Below are the tasks that were followed to develop the ontology.

. *Specification*

The goal of the specification phase was to produce an informal ontology specification document written in natural language, using a set of competency questions. The technique used in the knowledge acquisition phase of the ANCSDG ontology was informal text analysis. Its purpose was to study the main concepts given in books and handbooks. This study enables you to fill in the set of intermediate representations of the conceptualization.

b. *Conceptualization*

In this activity, domain knowledge was structured in a conceptual model that describes the problem and its solution in terms of the domain vocabulary identified in the ontology specification activity. After most of the knowledge was acquired, there was a vast amount of unstructured knowledge that needed to be organized. Conceptualization organizes and structures the acquired knowledge using external representations that are independent of the implementation languages and environments. Specifically, this phase organizes and converts an informally perceived view of a domain into a semi-formal specification, using a set of intermediate representations that the domain expert and ontologist can understand. These IRs bridge the gap between how people think about a domain and the languages in which ontologies are formalized. This set of IRs is based on those used in the conceptualization phase of the ideal methodology for knowledge-based systems development.

The first task was to build a complete Glossary of Terms (GT). Terms include concepts, instances, verbs, and properties. So, the GT identifies and gathers all the useful and potentially usable domain knowledge and its meanings. Terms were further grouped as concepts and verbs. Each set of concepts/verbs included concepts/verbs that are closely related to other concepts/verbs inside the same group as opposed to other groups. For each set of related concepts and related verbs, a concepts classification tree and a verbs diagram are built.

After they have been built, the ontology development process was split into different but related, teams. Those related to concepts should follow the guidelines presented by G6mezPtrez and colleagues in (G6mez-Ptrez, Fern;indez, & De Vicente 1996), and those encharged of conceptualizing verbs are presented at (Vicente 1997). Concepts will be described using (G6mez-Ptrez, Fern;tndez, & De Vicente 1996): Data Dictionary, which describes and gathers all the useful and potentially usable domain concepts, their meanings, attributes, instances, etc.; tables of instance attributes, which provide information about the attribute or about its values at the instance; tables of class attributes, to describe the concept itselL, not its instances; tables of constants, used to specify information related to the domain of knowledge that always take the same value; tables of instances, which define instances; and attributes classification trees, to graphically display attributes and constants related in the inference sequence of the root attributes, as well as the sequence of formulas or rules to be executed to infer such attributes. Verbs represent actions in the domain. They could be described using (Vicente 1997): Verbs Dictionary, to express the meaning of verbs in a declarative way; tables of conditions, which specify a set of conditions to be satisfied before executing an action, or a set of conditions to be guaranteed after the execution of an action. Finally, to say that tables of formulas and tables of rules gather knowledge about formulas and rules. Note that both branches use these two intermediate representations.

c. *Integration*

Rather than building the ontology from scratch, the authors made use of some definitions that were already built into the ontology which was proposed by (van Vuuren et al., 2014). For the missed definition, justification and benefits of their inclusion are provided.

d. *Implementation*

Ontologies implementation requires the use of an environment that supports the meta-ontology and ontologies selected at the integration phase. During this stage, the ontology was codified in a formal language

ISSN: 2521-2293

called Ontology Web Language (OWL). The implementation environment that was chosen was protege desktop v5.5.0 software tool. Protégé is a free, open-source ontology editor and a knowledge management system.

e. Evaluation

Evaluation includes verification and validation. Verification refers to the technical process that guarantees the correctness of an ontology. Validation guarantees that the ontologies, software environment, and documentation correspond to the system they represent.

The output proposed by METHONTOLOGY for this activity is many evaluation documents in which the ontologist will describe how the ontology has been evaluated, the techniques used, the kind of errors found in each activity, and the sources of knowledge used in the evaluation.

In this research, a corpus based approach or data-driven approach will be used to evaluate the accuracy, conciseness and completeness of the NCSs.

f. Documentation

There are no set guidelines on how to document ontologies. In many instances tthe only documentation available is in the code of the ontology, the natural language text attached to formal definitions, and papers published in conference proceedings and journals setting out important questions of the ontology already built. In this research, documentation was done as an activity throughout the ontology development process.

C.

C. THe ANCSDG ONTOLOGY

This section has been divided into two parts. Subsection A gives a brief overview of what ontologies are and subsection B presents the ANCSDG ontology.

. *What is an ontology?*

In literature, there exist many definitions of what an ontology is. Noy and McGuinness (2001) describe ontology as “a formal explicit description of concepts of discourse classes, with the properties of each class describing various attributes of the concepts (slots) and their restrictions”. Other researchers describe ontology as a technology that provides a way to exchange semantic information between people and systems. However, in this research, the definition of ontology as described by Grüber (1993) will be adopted. Grüber (1993) defines an ontology as a “formal, explicit specification of a shared conceptualization”.

Ontologies provide many benefits, some of which is that they facilitate reuse of domain knowledge, they make domain assumptions clear, they separate domain knowledge from operational knowledge and they allow sharing of a common understanding of the structure of information.

This research will harness the power of ontologies to map an ideal cybersecurity strategic environment. The ANCSDG ontology will provide a single shareable model of the cybersecurity strategic environment. During the development and implementation of the cyber security strategy, the ontology can be used to map relevant aspects of the strategy to actors and functions as described in the ontology.

B. ANCSDG Ontology

This section describes the ANCSDG ontology. This ontology was developed as per ITU’s National Cybersecurity Strategy Development Guide and also a text corpus that was created using Sketch Engine. Sketch Engine is a corpus manager and text analysis software developed by Lexical Computing. The corpus and ITU’s strategy development guide were used to identify the main concepts of the ontological model as well as their subclasses.

The model was then implemented on Protege Desktop v5.5.0. Protege is a free, open-source ontology editor and a knowledge management system. The table below describes the logical axioms for the ANCSDG ontology.

Table 1 Axioms of the ANCSDG Ontology

Logical Axioms for the ANCSDG Ontology	
Concept name	***Axiom Description***
Governance	This component looks at laws and other technical structures developed by the government to secure cyberspace.
Risk Management	This component looks at structures and methods that have been put in place to manage cyber risks.
Capacity and Capability Building	This component looks at building local, regional and international cooperation among African countries.
Regional and International Cooperation	This component looks at efforts that have been put in place to support local, regional and international cooperation
Critical Infrastructure Protection	This component looks at the structure and measures that have been put in place to secure cyberspace.
Cybercrime Reporting and Intelligence	This component looks at cybercrime reporting and intelligence gathering and sharing.

ISSN: 2521-2293

Axioms provide a formal way to add logical expressions to an ontology. These logical expressions can be used to refine the concepts and relationships in the ontology. Axioms are used to design an explicit way of expression that is always true. Axioms can be used for defining the meaning of several components of the ontology, defining complex relationships and verifying the correctness of the information of obtaining new information. Table shows some of the axioms on the ANCSDG ontology.

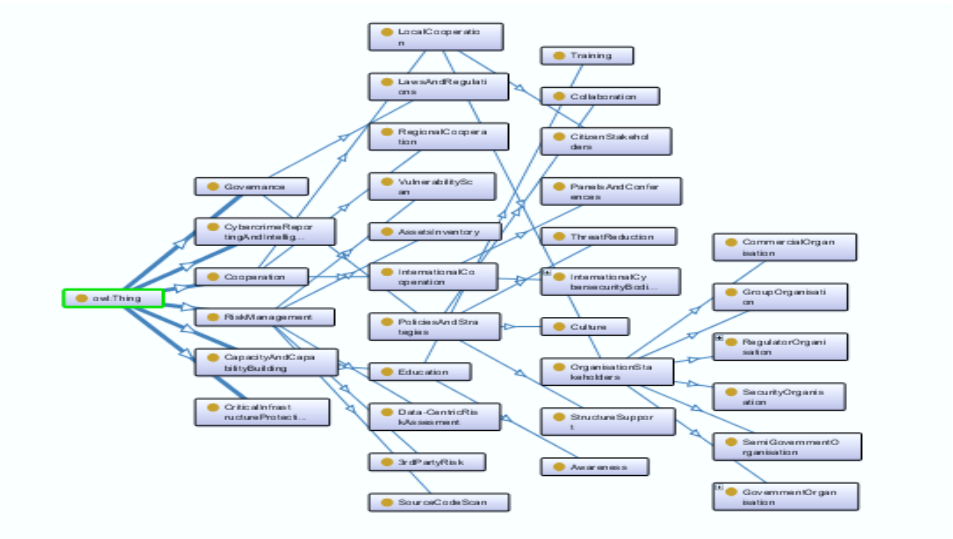

Fig. 1. The ANCSDG Ontology

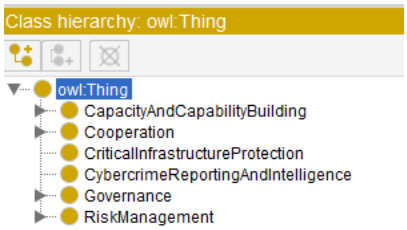

Figure 1 Main Concepts of the ANCSDG Ontology

Figure 1 above describe the main concepts of the ANCSDG ontology. These concepts were extracted from different relevant published papers, the Cybersecurity Policy Implementation ontology (CPIO) by and the ITU's cybersecurity development guide.

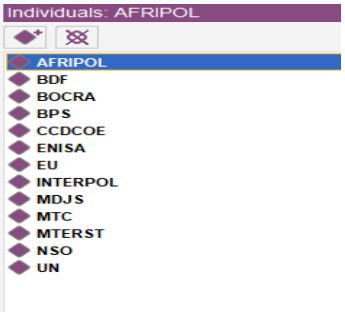

Fig. 2. In of the ANCSDG Ontology

Figure 2 above describes individuals of the ANCSDG ontology. Individuals or instances represent the objects in the domain. In this study, the individuals represent the different stakeholders that are relevant to NCS development and implementation. Figure 4 shows some individuals of the ANCSDG ontology.

ISSN: 2521-2293

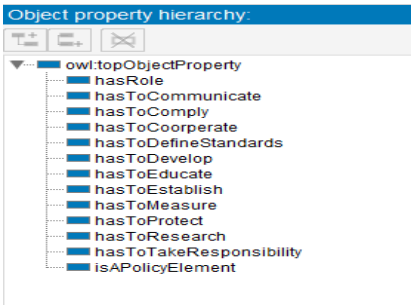

Fig. 3. Object properties of the ANCSDG

Figure 3 above describes the object properties of the ANCSDG ontology. Object properties refer to the relationships among concepts.

B. CONCLUSIONS

In this paper, the authors presented a semantic-based cybersecurity strategy development guide (ANCSDG) that is tailored to support Botswana in the development and implementation of a comprehensive National Cybersecurity Strategy (NCS). The first task was to assess existing solutions and their shortcomings. Thereafter, an ontology mapping the cybersecurity domain was implemented on Protégé Desktop v5.5.0. This ontology was developed as per ITU's National Cybersecurity Strategy Development guide. In addition to ITU's development guide, a text corpus that was created using the Sketch Engine was also utilized. The availability of a formal, encoded description of the cybersecurity strategic environment allows policymakers and other stakeholders that are relevant to the development of the NCS to identify which concepts are critical in NCS formulation and also how these concepts are related to one another. During the implementation of the strategy, the model will be used to map relevant aspects of the strategy to actors and functions as described in the ontology. Furthermore, an ontology for the cybersecurity strategic environment will help deal with issues of interoperability and knowledge sharing in the cybersecurity strategic environment. To the best of our knowledge, there only exists one other solution of this kind in the literature and the main difference between the presented solution and the one that already exists is the addition of new concepts, relationships, and data properties. These components were necessary for a holistic approach to the development and implementation of NCSs. Although this solution was initially developed for Botswana, it is applicable to be used by other African countries.

ACKNOWLEDGMENT

I would like to thank my supervisors and everyone who contributed to the successful completion of this research.

REFERENCES

[1] Serianu, (2018), African Cybersecurity Report- Botswana, Retrieved on September 22 from: https://africancyber.com/Botswana%20Cyber%20Crime%20Report%202018-2019.pdf

[2] Cybersecurity Capacity Centre for Southern Africa (C3SA), (2021), Southern African Development Community Cybersecurity Maturity Report 2021, Retrieved on September 22 from:https://open.uct.ac.za/bitstream/handle/11427/36211/SADC%20CYBERSECURITY%20CAPACITY%20MATURITY%20REPORT%202021.pdf?sequence=5

[3] Jansen van Vuuren, J.C., Leenen, L., Phahlamohlaka, L.J. and Zaaiman, J.J., 2013. Development of a South African cybersecurity policy implementation framework. Academic Conferences and Publishing International.

[4] Rantos, K., Spyros, A., Papanikolaou, A., Kritsas, A., Ilioudis, C. and Katos, V., 2020. Interoperability challenges in the cybersecurity information sharing ecosystem. *Computers*, *9*(1), p.18.

[5] Atoum, I., Otoom, A. and Ali, A.A., 2014. A holistic cyber security implementation framework. *Information Management & Computer Security*.

[6] Salamzada, K., Shukur, Z. and Bakar, M.A., 2015. A framework for cybersecurity strategy for developing countries: Case study of Afghanistan. *Asia-Pacific Journal of Information Technology and Multimedia*, *4*(1), pp.1-10.

[7] South Africa Government Information. (2012). Statement on the Approval by Cabinet of the Cybersecurity Policy Framework for South Africa. Retrieved on 21 October 2012 from http://www.info.gov.za/speech/DynamicAction?pageid=461&sid=25751&tid=59794

[8] Gcaza, N., von Solms, R. and van Vuuren, J.J., 2015. An Ontology for a National Cyber-Security Culture Environment. In *HAISA* (pp. 1-10).

[9] Lebogang, V., Tabona, O. and Maupong, T., 2022. Evaluating Cybersecurity Strategies in Africa. In *Cybersecurity Capabilities in Developing Nations and Its Impact on Global Security* (pp. 1-19). IGI Global.

[10] Fernández-López, M., Gómez-Pérez, A. and Juristo, N., 1997. Methontology: from ontological art towards ontological engineering.

[11] Grüninger, M. and Fox, M.S., 1995. Methodology for the design and evaluation of ontologies.

[12] Noy, N.F. and McGuinness, D.L., 2001. Ontology development 101: A guide to creating your first ontology.

[13] Nanda, J., Simpson, T.W., Kumara, S.R. and Shooter, S.B., 2006. A methodology for product family ontology development using formal concept analysis and web ontology language.

[14] Ahmed, S., Kim, S. and Wallace, K.M., 2007. A methodology for creating ontologies for engineering design.

[15] Fernández-López, M., Gómez-Pérez, A. and Juristo, N., 1997. Methontology: from ontological art towards ontological engineering.

[16] Van Vuuren, J.J., Leenen, L. and Zaaiman, J., 2014, March. Using an ontology as a model for the implementation of the National Cybersecurity Policy Framework for South Africa. In *9th International Conference on Cyber Warfare and Security* (pp. 107-115).

[17] Raad, J. and Cruz, C., 2015, November. A survey on ontology evaluation methods. In *Proceedings of the International Conference on Knowledge Engineering and Ontology Development, part of the 7th International Joint Conference on Knowledge Discovery, Knowledge Engineering and Knowledge Management*.

[18] Protégé. The Prot´eg´e project, http://protege.stanford.edu, (2002)

[19] Gruber, T.R., 1993. A translation approach to portable ontology specifications. *Knowledge acquisition*, *5*(2

ISSN: 2521-2293

BIUST Teaching, Research, & Innovation Symposium 2023 (TRDAIS 2023)
Botswana International University of Science and Technology
Palapye, Botswana, 18 - 19 September 2023
ISSN: 2521-2293

An Interpretation of the Transitions in EEG Signals Based on the Five Frequency Bands with Increasing Alcohol Content in the Human Body

Kaloso M. Tlotleng and Rodrigo S. Jamisola Jr
Department of Mechanical, Energy and Industrial Engineering
Botswana International University of Science and Technology
Palapye, Botswana
kaloso.tlotleng@studentmail.biust.ac.bw, jamisolar@biust.ac.bw

Berdakh Abibullaev
Department of Robotics and Mechatronics
Nazarbayev University
Astana, Kazakhstan
berdakh.abibullaev@nu.edu.kz

***Abstract*—We present an interpretation of the transitions of the brain signals harnessed from an electroencephalogram (EEG) headset attached to the user while increasing alcohol intake by drinking alcoholic beverages. These transitions can be traced to an individual's cognitive and behavioral changes under the influence of alcohol that may affect the individual's decisions and motor control. The EEG headset is a wireless 32-channel Emotiv Epoc Flex brain wear. The data were recorded during experiments where an individual was given alcoholic beverages to consume within two hours. The individual was given a six-pack of beer with an alcohol content of 6%. We establish the variations of epoched data within a specific timeframe, starting from the first bottle of alcohol intake until the last bottle is finished. We use five frequency bands namely, delta, theta, alpha, beta, and gamma to observe and create visualizations based on the power spectrum of the EEG signals. The data is segmented into time-locked segments called epochs that represent the process of alcohol intake. These results can lead to a better understanding of transitions that occur in brain activity as the amount of alcohol consumption increases within a fixed timeframe.**

***Index Terms*—Electroencephalogram (EEG) signals, alcohol consumption, 32-channel headset, frequency bands, epochs**

I. Introduction

The analysis of electroencephalogram (EEG) signals has become a prominent research area in understanding different brain activities. EEG shows a record of continuous time electrical activity that takes place in the brain [1]. These signals are harnessed using a brain-computer interface (BCI) device that directly records from an individual and stores them in a computer [2]. Based on the type of application, EEG data can be interpreted and the results can be used to reflect an individual's mental activity [3].

In more studies using the application of EEG, [4] explains that brain activity can be monitored to understand the dynamics that occur during cognition. Standard tests and measurements are readily available to identify the different waveforms of the EEG signals. In their study, the power spectral density (PSD) of the theta, alpha, beta, and gamma bands was measured during baseline and cognitive tests.

A study by [5] further explains the significance of EEG analysis over the subjective assessment approach. The research concludes that the latter is not reliable in developing clinical diagnosis as it is prone to patient and expert bias. Furthermore, the study demonstrates that EEG signals can be interpreted by focusing on the analysis of the power spectrum of the five brain rhythms.

All these studies show that based on the type of application for EEG analysis, PSD still remains a powerful tool in interpreting the activity of the brain. PSD is a method of EEG data analysis in which the power intensity of the brain signals is measured across the frequency bands [6]. There are many risk factors that impact the normal function of the brain, that include the excessive use of alcohol. Consuming alcoholic beverages has been proven to disrupt normal brain activity and if it is taken more than 48g per day or 144g then it can be regarded as risky [7]. The changes caused by alcohol intake on signal activity can be analyzed by observing its power spectra. This information can be obtained in the frequency bands of the brain that include, delta, theta, alpha, theta, and gamma. These rhythms are classified based on their range of frequency as follows: delta (0.5-4Hz), theta (4-7Hz), alpha (8-13Hz), beta (13-36Hz), and gamma (36Hz and above) [8].

Section 2 of this paper describes the proposed methodology of our study and Section 3 introduces the materials and methods used. Section 4 focuses mainly on results while Section 5 outlines the analysis and interpretations of our results. The last section discusses future recommendations in relation to this study.

II. Methodology

The flowchart in Fig. 1 depicts the logical sequence of our proposed methodology. The first step is EEG data recording which includes recording using the Emotiv Epoc Flex brain wear. In this step, the volunteers were given a six-pack of beer with 6% of alcohol and the experiment took a maximum of two hours. The second step includes preprocessing the raw EEG data by first importing the data in CSV format, then detecting and dropping the bad channels, and finally filtering the data. Two types of filtering were applied that includes notch filtering and band-pass filtering. In the third step, epoching was applied

ISSN: 2521-2293

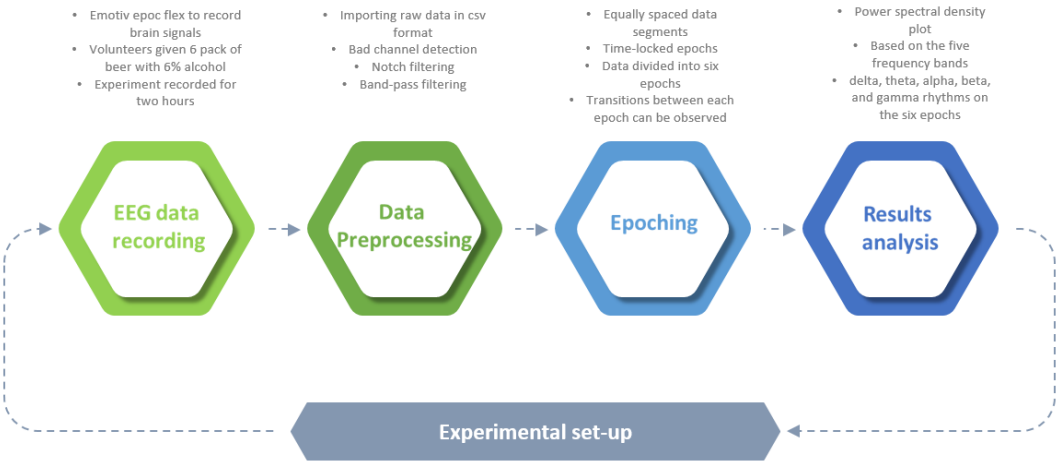

Fig. 1. *The proposed methodology of our study showing all the steps. It depicts the logical sequence followed from the recording of the EEG data until the analysis of the results. We use a power spectral density plot for all five frequency bands that are, delta, theta, alpha, beta, and gamma. The variations of these rhythms are observed in the six epochs.*

by creating six equally spaced data segments. These are time-locked such that the transitions between each epoch can be observed. The final step of the methodology includes the analysis of the results by spectral density plot based on the five frequency bands. These delta, theta, alpha, beta, and gamma rhythms were observed across all six epochs.

III. Materials and Methods

In this section, we outline the process we used to derive the required output, as outlined in the methodology below:

A. Experimental setup and device

Data were recorded using a wireless 32-channel Emotiv Epoc Flex EEG headset. During the experiment, the individual was given alcoholic beverages to consume within two hours. They were given a six-pack of beer with an alcohol content of 5.5% The BCI experiments were approved by the Ministry of Health and Wellness and, the Human Ethics Research Committee. The study participants include male volunteers aged between 22-44 years who are alcoholics. Each individual signed a consent form indicating that he agreed to participate in the experiments. The method of recruitment was random and participants were briefed on the experimental setup. The Alcohol Use Disorder Identification Test was administered to the volunteers to evaluate their frequency of use of alcohol.

The Emotiv Epoc Flex Headset was positioned based on the 10-20 standard electrode placement as shown in Fig.2.

B. Data Preprocessing

This step involves transforming our data into a format that is easier to manipulate and analyze. Artifact removal is carried out such that we can have clean EEG data separated from the noisy data [9]. This is because EEG data can be easily contaminated by various artifacts that include, muscle movement, eye blinks, and measuring instruments. It is desirable to filter out this type of data [10].

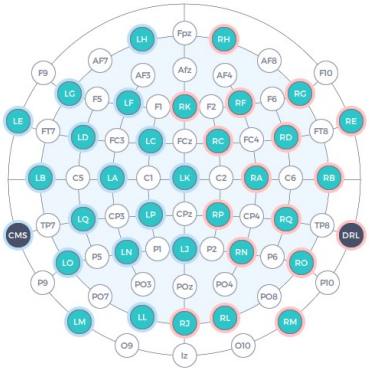

Fig. 2. *In the figure, the highlighted green positions represent the electrode placement using the 10-20 standard electrode placement. It also shows the number of channels from which the EEG data was recorded. They are 32 positions representing the 32-channel headset.*

1) Importing raw data: The data was imported in a CSV format through the use of the MNE library which is python based. It provides a way to convert any type of data into a format that can be used by the library [11]. Only data from the 32-channels was retained and all other columns were dropped.

ISSN: 2521-2293

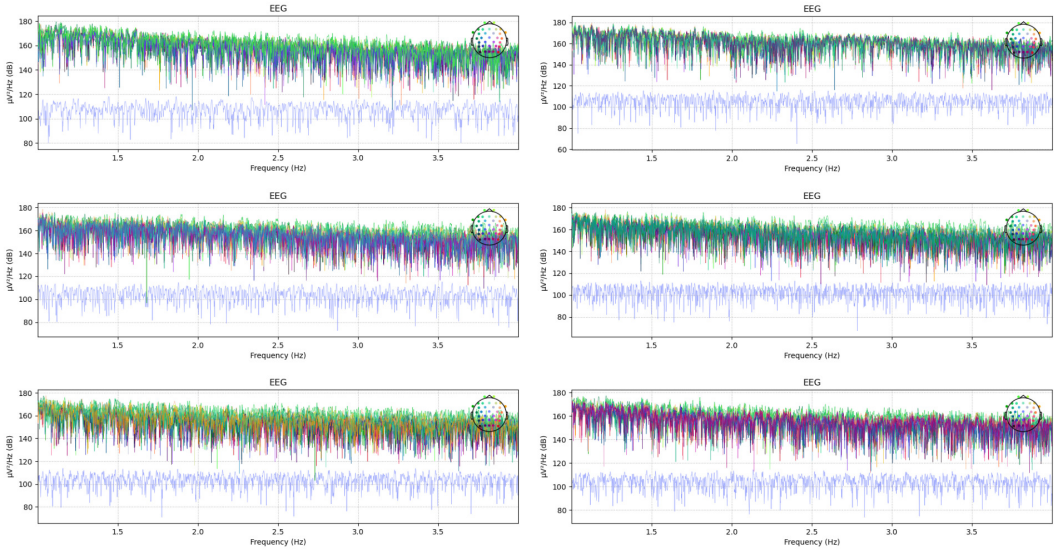

Fig. 3. *The power spectral density plots for the six epochs of the delta band are shown in Fig.3. The frequency range for this band lies between 1Hz and 4Hz. We can observe that the power of the delta band stays constant across all the epochs.*

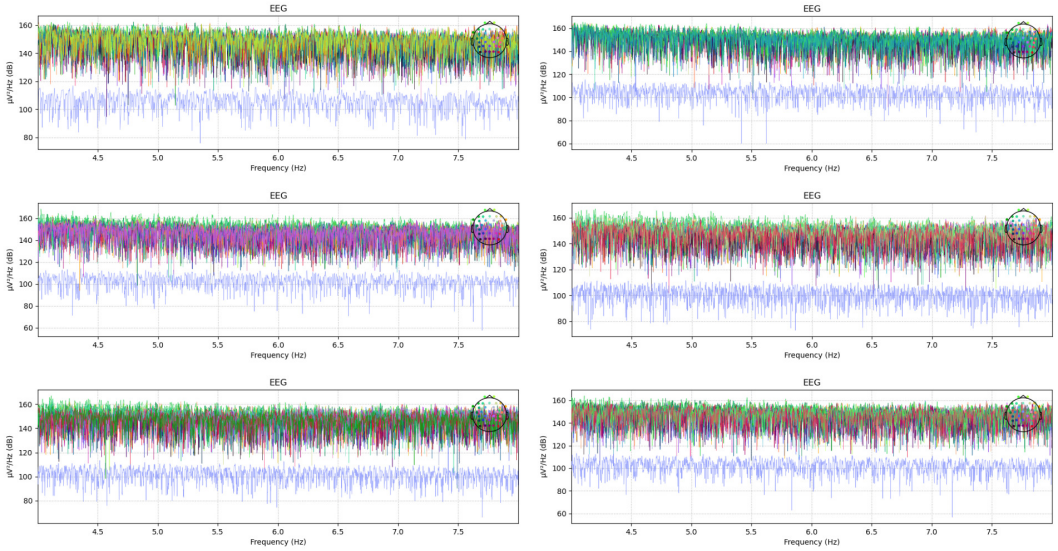

Fig. 4. *The graph in Fig.4 represents the power spectral density of the theta band across the six epochs. This frequency band ranges between 4Hz and 8hz. The power spectrum is constant in all six epochs.*

2) Bad channel detection: These are channels that do not provide enough information to be considered for analysis. They may be caused by various reasons that include, poor contact between the scalp and the electrode, poor electrode

ISSN: 2521-2293

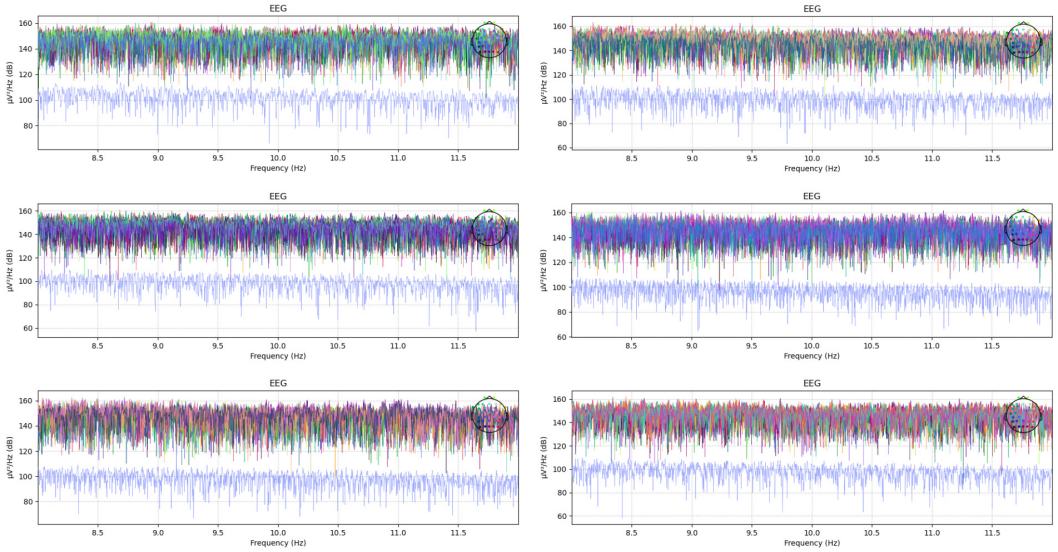

Fig. 5. *The graph in Fig.5 depicts the power spectral density plot for the alpha band across the six epochs. This band ranges between 8Hz and 12Hz. The power in this rhythm is constant across all six epochs.*

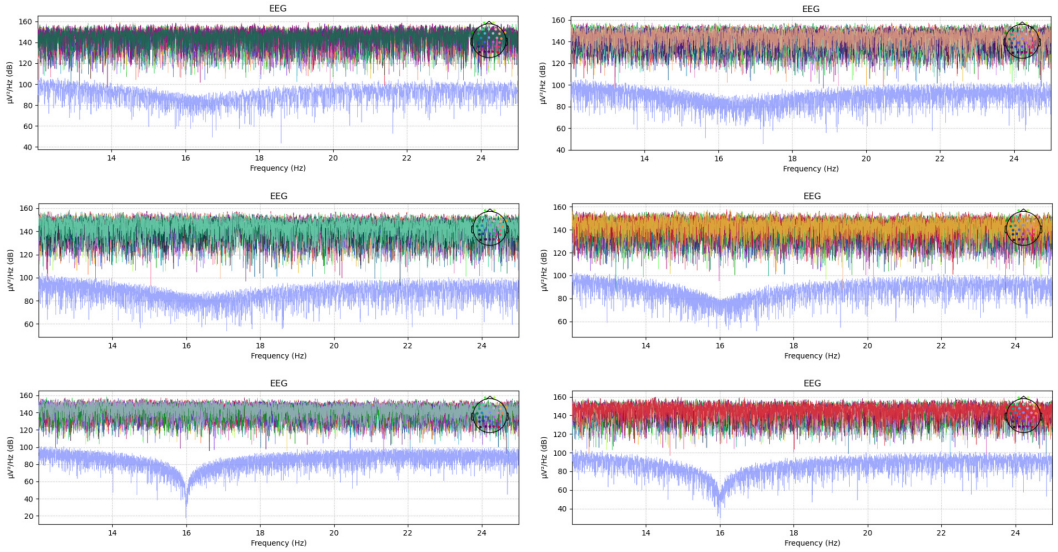

Fig. 6. *In the beta band the visualizations are shown in this graph on Fig.6. Its frequency ranges between 12Hz and 25Hz. The power in this band can be observed to have a slight reduction in power at 16Hz.*

placement, and malfunction. These may affect the interpretation and analysis of the EEG data [12]. No bad channels were spotted in our data.

ISSN: 2521-2293

3) Notch Filtering: This step is very crucial to remove the power line or electrical noise in our EEG data [13]. The artifacts are usually around 50Hz or 60Hz. A notch filter was introduced to reject all the frequencies from 60Hz and above.

4) Band-pass Filtering: In a band-pass filter, minimum and maximum frequencies are chosen such that any signal that falls outside the range will be rejected. It can help eliminate noise from eye blinks, muscle movements, and probable electrocardiography data [1]. We applied a band-pass filter to keep frequencies between 1Hz and 55Hz.

5) Epoching: This process allows us to create segments of data that are equally spaced. It divides the data into equal epochs that are time-locked such that we can analyze the transitions that occur from one segment to the other. The data was segmented between six equally spaced epochs that correspond to the increasing amounts of alcohol intake. That is, they represent the time a participant started drinking until the time they finished drinking. Within each epoch, we obtain the results for the power spectra of the five frequency bands and interpret these changes.

IV. Results

In this section, we present the visualizations from the power spectral density of each epoch. We show the results of the changes in the frequency bands starting with delta, then theta, alpha, beta, and lastly gamma. We observe the transitions of these rhythms from the first epoch to the last epoch.

A. Delta band

This frequency band is mostly associated with deep sleep and is only active when the body is fully at rest in that state. It is the smallest rhythm with a frequency range from 1Hz to 4Hz [14].

B. Theta band

The theta band is found mostly in frequencies ranging from 4Hz and 8Hz. It is also associated with learning and inhibitory control processes [15]. It can be generated and recorded across all the parts of the cortex.

C. Alpha band

The alpha rhythm is found within the frequency band from 8Hz to 12Hz and is mostly associated with sensory and memory functions [16]. Its power spectrum is mostly suppressed during body activities with eyes open.

D. Beta band

This frequency band is mostly associated with sensory-motor control processing and tasks [17]. It is usually generated in the frontal regions of the brain and ranges between 12Hz to 25Hz.

E. Gamma band

This rhythm is mostly associated with very high frequencies ranging from 25Hz upwards. It is still an active research area and therefore it is still unclear where it is generated [18].

V. Interpretation of Results

Based on these visualizations, we can observe obvious changes in the power spectra from epoch one to epoch six in all rhythms shown in Fig.3 to Fig.7. In figures 3 to 5 we can observe the color changes in the graph. Each signal color corresponds to an eeg channel. The change in the color in the graph means that some channels are becoming more prominent than others for their signal color to dominate the graph. We can interpret this as some parts of the brain are suppressed due to alcohol consumption. And this suppression increases as the alcohol content increases. It is observed further that the power spectrum of the graph has no observable changes.

In Fig.6 to Fig7 the same observed change of colors in the graph is shown. However, for some channels, there are observed changes in the power of the signals as shown in the lower set of signals that dips. This dipping of the signal increases with increasing alcohol content.

Based on these results, we can interpret that, the volunteer has higher alcohol tolerance. We can also conclude that the individual is projecting symptoms of alcohol use disorder. According to [19], increased spectral power in the beta band is expected from people who are alcoholics. In our results, the participant had a slight reduction in the spectral power of the beta rhythm which is in contrast to the expected results. This implies that at the time the volunteer had the last bottle of alcohol, there were no induced effects, and the body could potentially have more consumption.

VI. Future work

In the future, we plan to increase the data visualization by presenting the data per channel or combining the signals for several channels. We also plan to improve the filtering to further remove white noise. Some presentations will also be shown for the brain signal topography map. Feature extraction is to be implemented and the results will be clustered using unsupervised machine learning. We will compare the results for all seventeen volunteers.

References

[1] A. Khosla, P. Khandnor, and T. Chand, "A comparative analysis of signal processing and classification methods for different applications based on eeg signals," *Biocybernetics and Biomedical Engineering*, vol. 40, no. 2, pp. 649–690, 2020.

[2] M. C. Guerrero, J. S. Parada, and H. E. Espitia, "Eeg signal analysis using classification techniques: Logistic regression, artificial neural networks, support vector machines, and convolutional neural networks," *Heliyon*, vol. 7, no. 6, p. e07258, 2021.

[3] S. Ullah and Z. Halim, "Imagined character recognition through eeg signals using deep convolutional neural network," *Medical & Biological Engineering & Computing*, vol. 59, no. 5, pp. 1167–1183, 2021.

[4] J. G. Foy and M. R. Foy, "Dynamic changes in eeg power spectral densities during nih-toolbox flanker, dimensional change card sort test and episodic memory tests in young

ISSN: 2521-2293

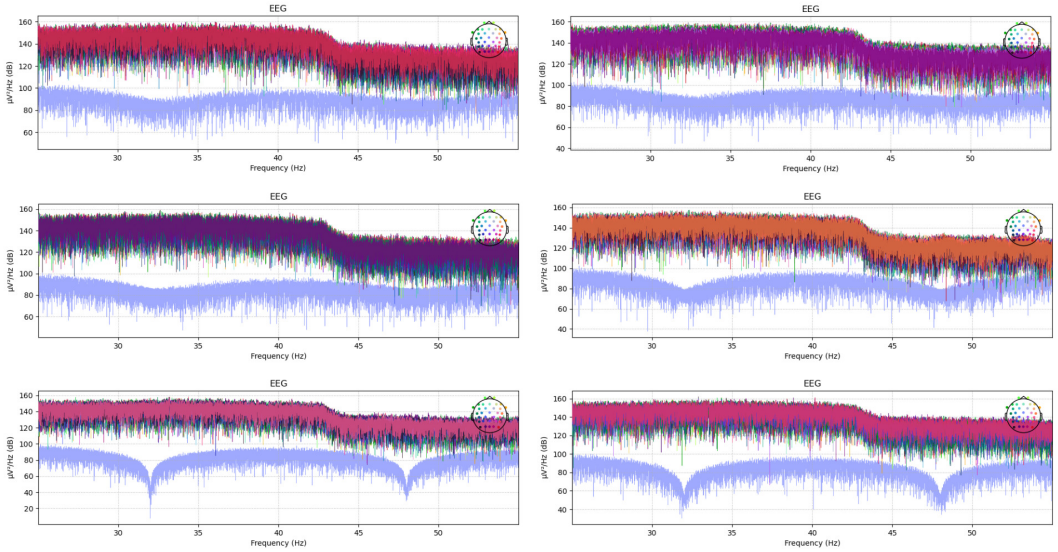

Fig. 7. *The graph for the power spectral density of the gamma band is shown in Fig.7. It ranges between 25Hz and 55Hz. The results show a distinctive structure in relation to the power of the rhythm.*

adults," *Frontiers in human neuroscience*, vol. 14, p. 158, 2020.

[5] J. J. Newson and T. C. Thiagarajan, "Eeg frequency bands in psychiatric disorders: a review of resting state studies," *Frontiers in human neuroscience*, vol. 12, p. 521, 2019.

[6] M. N. Alam, M. I. Ibrahimy, and S. Motakabber, "Feature extraction of eeg signal by power spectral density for motor imagery based bci," in *2021 8th International Conference on Computer and Communication Engineering (ICCCE)*. IEEE, 2021, pp. 234–237.

[7] W. Mumtaz, P. L. Vuong, L. Xia, A. S. Malik, and R. B. Abd Rashid, "Automatic diagnosis of alcohol use disorder using eeg features," *Knowledge-Based Systems*, vol. 105, pp. 48–59, 2016.

[8] A. Anuragi and D. S. Sisodia, "Alcohol use disorder detection using eeg signal features and flexible analytical wavelet transform," *Biomedical Signal Processing and Control*, vol. 52, pp. 384–393, 2019.

[9] S.-P. Kim, "Preprocessing of eeg," in *Computational EEG Analysis*. Springer, 2018, pp. 15–33.

[10] X. Jiang, G.-B. Bian, and Z. Tian, "Removal of artifacts from eeg signals: a review," *Sensors*, vol. 19, no. 5, p. 987, 2019.

[11] A. Gramfort, M. Luessi, E. Larson, D. A. Engemann, D. Strohmeier, C. Brodbeck, R. Goj, M. Jas, T. Brooks, L. Parkkonen, and M. S. Hämäläinen, "MEG and EEG data analysis with MNE-Python," *Frontiers in Neuroscience*, vol. 7, no. 267, pp. 1–13, 2013.

[12] V. Tuyisenge, L. Trebaul, M. Bhattacharjee, B. Chanteloup-Forêt, C. Saubat-Guigui, I. Mîndruţă, S. Rheims, L. Maillard, P. Kahane, D. Taussig *et al.*, "Automatic bad channel detection in intracranial electroencephalographic recordings using ensemble machine learning," *Clinical Neurophysiology*, vol. 129, no. 3, pp. 548–554, 2018.

[13] S. Leske and S. S. Dalal, "Reducing power line noise in eeg and meg data via spectrum interpolation," *Neuroimage*, vol. 189, pp. 763–776, 2019.

[14] F. Bröhl and C. Kayser, "Delta/theta band eeg differentially tracks low and high frequency speech-derived envelopes," *Neuroimage*, vol. 233, p. 117958, 2021.

[15] C. Pscherer, M. Mückschel, L. Summerer, A. Bluschke, and C. Beste, "On the relevance of eeg resting theta activity for the neurophysiological dynamics underlying motor inhibitory control," *Human Brain Mapping*, vol. 40, no. 14, pp. 4253–4265, 2019.

[16] B. Scally, M. R. Burke, D. Bunce, and J.-F. Delvenne, "Resting-state eeg power and connectivity are associated with alpha peak frequency slowing in healthy aging," *Neurobiology of aging*, vol. 71, pp. 149–155, 2018.

[17] H. Díaz, F. M. Cid, J. Otárola, R. Rojas, O. Alarcón, and L. Cañete, "Eeg beta band frequency domain evaluation for assessing stress and anxiety in resting, eyes closed, basal conditions," *Procedia Computer Science*, vol. 162, pp. 974–981, 2019.

[18] M. Sameer, A. K. Gupta, C. Chakraborty, and B. Gupta, "Epileptical seizure detection: Performance analysis of

ISSN: 2521-2293

gamma band in eeg signal using short-time fourier transform," in *2019 22nd international symposium on wireless personal multimedia communications (WPMC)*. IEEE, 2019, pp. 1–6.

[19] K. E. Courtney and J. Polich, "Binge drinking effects on eeg in young adult humans," *International journal of environmental research and public health*, vol. 7, no. 5, pp. 2325–2336, 2010.

BIUST Teaching, Research, & Innovation Symposium 2023 (TRDAIS 2023)
Botswana International University of Science and Technology
Palapye, Botswana, 18 - 19 September 2023
ISSN: 2521-2293

Predicting California Bearing Ratio Using Machine Learning to Model Soil Behavior for Road Construction in Tshimoyapula, Botswana

Botlhe B. Pule[1*], Jerome A. Yendaw[1], Rodrigo S. Jamisola Jr[2], Onalethata Saubi[1]
[1]Dept. of Mining and Geological
[2]Dept. of of Mechanical, Industrial and Energy Engineering
Botswana International University of Science and Technology (BIUST)
Palapye, Botswana
botlhe.pule@studentmail.biust.ac.bw, yendawj@biust.ac.bw, jamisolar@biust.ac.bw,*
onalethata.saubi@studentmail.biust.ac.bw

Abstract*— The present research work is carried out to predict California Bearing Ratio (CBR) values of soils from the Tshimoyapula area near Serowe in the Central District of Botswana based on the index properties using machine learning techniques. The CBR test is a very important and common test performed on soils to assess the stiffness modulus and shear strength of subgrade materials to determine the thickness of overlaying layers in pavement design. It is an expensive and time-consuming test in addition to difficulty in keeping the sample in the desired condition. The construction industry is one of the least digitized in the world, and using Artificial Intelligence could help achieve profitability, efficiency, safety, and security. Machine learning techniques, namely, Regression Analysis (RA) and Artificial Neural Network (ANN) were developed with different configurations using various laboratory soil properties comprising Liquid Limit (LL), Plastic Limit (PL), Plastic Index (PI), Maximum Dry Density (MDD), and Optimum Moisture Content (OMC) of 200 soil samples that laboratory CBR test was performed on. The index properties were used as input parameters for different models with the CBR as output. Results indicate a good correlation between the input parameters and the output. Artificial Neural Networks showed the least error and the highest accuracy followed by Linear Regression among the models.

Keywords*— California bearing ratio, index properties, machine learning, artificial neural network, linear regression.

I. I INTRODUCTION

In the construction of railroads, dams, buildings, and roads there is a lot of testing and analyses of soils to determine their suitability for the project. Variability in the soil conditions from one location to another makes it difficult to predict the behavior of soil. As a result, soil conditions at every point must be completely investigated for proper design. In Botswana, most of the road networks consist of flexible pavements which are made up of different layers namely sub-grade, sub-base, and surface layers [1]. The design and performance of the pavement substantially depend on the strength of the subgrade material based on the California Bearing Ratio (CBR) test on soil samples. The subgrade is the most bottom layer that serves as a foundation of road pavement and the wheel load from pavement surfaces is ultimately transferred to the subgrade. The CBR test is an empirical method of design of flexible pavement and can be defined as the ratio of resistance to penetration of a material to the penetration resistance of a standard crushed stone base material under controlled density and moisture content [2]. The test was originally developed in the 1920s by the California State Highway Department and later incorporated by the Army Corps of Engineers for the design of flexible pavements. Thereafter, the CBR test became so globally popular that it has been incorporated into many international standards like AASHTO T193 and ASTM D-1883, D-449. The significance of the CBR test emerged from the following two factors [3];

1. For almost all pavement design charts, unbound materials are characterized in terms of their CBR values when they are compacted in pavement layers.
2. The CBR value has been correlated with some fundamental properties of soils, such as plasticity indices, grain-size distribution, bearing capacity, modulus of subgrade, shear strength, density, and moisture content.

CBR test being crucial to construction projects is still laborious and time-consuming. Furthermore, the results occasionally aren't accurate due to the poor skill of the technicians testing the soil or the extreme erratic behaviour of the soil [4]. An alternative method which involves the use of the Nuclear Gauge for the measurement of density and moisture content. Is, however, both expensive and requires

ISSN: 2521-2293

special precautions against radioactive material. Other techniques, such as Vane Shear Test, Cone Penetration Test, Unified Compression, and Texas Triaxial Test have been reported in the literature to correlate well with the CBR test, but couldn't replace it due to either some inherent shortcomings of the tests or their limitations to laboratory applications [5].

II. LITERATURE REVIEW

With the development of technology throughout the years, Geotechnical Engineering processes nevertheless continue to be the least digitized and the use of Artificial Intelligence (AI) can push the industry ahead into the future. Most geotechnical engineering procedures use empirical correlations derived with the assistance of statistical methods using antique laboratory or field testing to assess the engineering properties of soils. Most geotechnical parameters which include relative density, compression index (Cu), and Atterberg Limits are determined within the laboratory and some are estimated in the field with some assumptions. Their calculations require specific laboratory equipment, and an experienced geotechnical engineer with a crew of skilled technicians [6]. Integrating AI into these methods through machine learning (ML) algorithms could help attain profitability, efficiency, safety, and accuracy. ML aims to develop methods that can automatically detect patterns in data, after which the uncovered patterns are used to predict future data or others of interest. With this goal, ML is therefore closely related to the fields of statistics but differs slightly in terms of emphasis. Machine learning algorithms can deal with non-linear and plastic issues of soils effectively and avoid the weakness that can be caused by traditional methods [7]. ML is thus well suited to model complex performances of most geotechnical engineering, which by its very nature, exhibits extreme erraticism [6].

Alternative methods such as Plate load test and Dynamic cone penetration test are not achieving the desired outcome, it inspired earlier researchers to develop various predictive models based on the existing data. The literature review showed how different correlations for estimating CBR values were developed and revealed that most of the empirical correlations could not be attained in many cases because most of the empirical equations neither had a high degree of accuracy nor had any generalized solution and the use of these equations in further studies yielded unacceptable results. A summary of previous studies based on the empirical modelling of CBR with parameters used is presented in Table 1. In the age of technology, modern-day researchers have resorted to the use of Artificial Intelligence (AI) as a potential alternative to predict the desired output. [8] further compiled previous studies on AI-based modelling of soil CBR as summarized in Table 2. The developed models resulted in maximum accuracies of R^2=0.9 with lowest values being R^2=0.78. The data sets used varied with different models, with one model having a small set of 20 samples and the other having a large data set of as many as 389 samples.

TABLE I. PREVIOUS EMPIRICAL CORRELATIONS ON CBR VALUES

References	Correlations	No. of samples	R^2
[9]	$Y = 28.79 - 0.61(OMC) + 0.44(PL) + 0.48(PI) - 0.82(\%sand)$	165	0.78
[10]	$Y = -0.1024(PI) + 6.1596$	105	0.94
[11]	$Y = -0.275(LL) + 0.118(PL) + 0.033F + 5.106G$	7	0.96
[12]	$Y = 1.045SPT + 1.653$	15	0.77
[13]	$Y = 198.63 - 3.78(OMC) - 73.37(MDD) + 0.34D_{60} + 1.64D_{30}$	8	0.97

TABLE II. PREVIOUS AI BASED MODELLING OF CBR OF SOILS

References	Models	No. of Samples
Taskiran [19]	ANN, GEP	151
Varghese et al. [20]	ANN	145
Kumar et al. [21]	ANN (GRNN, MLPN)	60
Sabat [22]	ANN, SVM	49
Yildirim and Gunaydin [23]	ANN	124

There are different machine learning algorithms which include Linear Regression (LR), Support Vector Machine (SVM), Random Forest (RF), Decision Trees, Artificial Neural Network, and so on. which can be used depending on the intended outcome and type of input. Each algorithm has its own advantageous and disadvantageous fields when it is utilized to deal with problems [7].

III. METHODOLOGY

The data used in this study was obtained from tests on 200 soil samples from different sites in the Tshimoyapula area of Central District of Botswana for the Mabeleapudi-Tshimoyapula-Serule road project from 2018 to 2019. The soil samples were tested to determine the liquid limit (LL), plasticity index (PI), and, compaction propertie characteristics (Maximum Dry Density (MDD) and Optimum Moisture Content (OMC)) of each sample. The range of value for some of the more significant parameters are given in Table 3. The results obtained were fed into the Machine Learning algorithms with the index properties as input parameters and the CBR value as the output and the correlations for different inputs against the CBR determined.

ISSN: 2521-2293

TABLE III. SUMMARY OF INPUT VALUES

Input Parameters	No. of Samples	Max	Mean	Min
CBR at 100% compaction	200	76	11.4	1.9
Maximum Dry Density (Kg/m^3)	200	2264	1938.03	1619
Optimum Moisture Content (%)	200	19	10.15	4.7
Liquid Limit (%)	200	53	26.73	16
Plastic Index (%)	200	27	10.77	2.3

A. CALIFORNIA BEARING RATIO

In a CBR test, the penetration is measured by applying the bearing load on the sample using a standard plunger of 50 mm at a rate of 1.25 mm/min. The CBR is expressed as a percentage of the actual load causing the penetration of 2 mm and 5 mm to the standard load on the crushed California Limestone at the same depth. A load penetration curve is then drawn. The load values on the standard crushed stone are shown in Table 4 above. A CBR value equal to 3% is for tilled farmland, while CBR equal to 4.75% for turf as moist clay and moist sand may have a CBR value of 10%. And in high-quality crushed rock, the CBR value is around 80% compared to standard material for this crushed stone which has a value of 100%. The CBR test equation is given as;

$$CBR = \frac{P}{Ps} \times 100 \quad (1)$$

Where:

P = Pressure applied for site soils (N/mm^2)

Ps = Pressure achieved at the same penetration for California crushed limestone (N/mm^2)

1) 1INPUT PARAMETERS

Soils are classified with different engineering properties which affect the behavior of soil under different conditions. Some of these properties which were used as input parameters are;

- Liquid Limit: The liquid limit (LL) is the water content at which a soil changes from plastic to liquid behavior. At this limit, the soil possesses a small value of shear strength, losing its ability to flow as a liquid. In other words, the liquid limit is the minimum moisture content at which the soil tends to flow as a liquid.
- Plasticity Index: The plasticity Index (PI) is the range of water content within which the soil exhibits plastic properties, that is, it is the difference between liquid and plastic limits. Plasticity Index (PI) = Liquid Limit (LL) -Plastic Limit (PL).
- Maximum Dry Density (MDD): Is the dry density of soil corresponding to the optimum moisture content during compaction.
- Optimum Moisture Content (OMC): Is the water content at which the soil attains maximum dry density.

TABLE IV. LOAD PENETRATION DATA FOR CRUSHED ROCK

Penetration depth (mm)	Load (KN)
2	11.5
2.5	13.24
4	17.6
5	19.96
6	22.2
8	26.3
10	30.3
12	33.5

.

B. MULTIVARIATE REGRESSION ANALYSIS

Multivariate regression was used to assess how linearly connected the different independent variables and different dependent variables were to one another. Due to the correlation between the variables, the relationship is considered to be linear [14]. Multivariate regression was applied to the dataset to forecast the behaviour of the response variable (CBR) based on its related predictor factors (LL, PI, MDD, OMC). The main form of MVRA is expressed mathematically in (2):

$$Y = \beta_0 + \beta_1 X_1 + \beta_2 X_2 + \ldots. + \beta_n X_n \quad (2)$$

In which, β1, β2, ..., βn are the coefficients of the regression model; β0 is a constant value; X1, X2, Xn are the independent variables and Y is the dependent variable.

C. ARTIFICIAL NEURAL NETWORK

ANNs which falls under the category of supervised learning, a branch of machine learning was used to model both input and output data. Artificial neurons are a group of interconnected nodes that form the basis of an ANN and aim to simulate the operation of biological brain neurons [15]. Like the synapses in a human brain, each link has the ability to send a signal to neighbouring neurons. An artificial neuron can signal neurons that are connected to it after processing signals that are sent to it. The output of each neuron is calculated using a transfer function of the sum of its inputs, and the signal at a connection is a real value. Typically, weights and a bias that changes as learning progresses are used to connect neurons. The weight alters a connection's signal intensity by increasing or decreasing it [16]. A neuron's threshold, which is provided by an activation function, may be

ISSN: 2521-2293

such that a signal is only transmitted if the total signal crosses it. The rectified linear activation function (ReLU), the log sigmoid, and the tan-sigmoid functions are a few examples of activation functions. Neurons are typically aggregated into layers. Three layers make up a basic neural network: the input layer, the hidden layer, and the output layer [17]. When trained on data that has both inputs and outputs, neural networks are able to identify the underlying patterns in the data [18]. The training of a neural network from a given data is usually conducted by determining the difference between the measured and predicted output. This difference is the error and is computed in the output layer. The network then adjusts its weights and bias according to a learning rule using this error value. Successive adjustments cause the neural network to produce the desired output. This is known as error minimisation, and the network is said to have learnt the data very well, when it produces a small error [17]. The equation for the analysis is as follows;

$x_i$represent the inputs, w_{ij} are the weights connecting layer i with layer j, b is the bias weight and n is the number of input units.

IV. RESULTS AND ANALYSIS

Table 5 gives the results of various soil properties from the laboratory experiments on two hundred soil samples which were used for the present investigation. The properties include liquid limit, plasticity index, and compaction characteristics (maximum dry density and optimum moisture content) and CBR conducted at optimum moisture content.

A. REGRESSION ANALYSIS

The various regression analysis between CBR value with respect to the different soil properties are presented in Figures 1 to 4. It shows the linear trend line, which shows the effect of the various soil properties on CBR value. These graphs show the different correlations together with their respective R2 values, with the highest R^2 being maximum dry density at 0.2018 and the lowest being Liquid Limit at 0.0245. Figure 5 shows the sensitivity analysis to support the data. This further shows from the single linear regression, maximum dry density has the greatest effect on the CBR value followed by optimum moisture content, plasticity index and liquid limit in that order. Also, the graphs trendlines show only maximum dry density is proportional to the CBR value and the rest are inversely proportional.

The multiple linear regression analysis was conducted with the results summarized in Table 5. The t-statistic and p-value of multiple linear regression analysis are shown in Table 6. Comparison between the measured CBR values and predicted CBR values from the regression model using a linear relationship shows a model with a correlation coefficient R^2 = 0.249 as in Figure 6.

TABLE V. SUMMARY OUTPUT

Regression Statistics	
Multiple R	0,453867
R Square	0,205995
Adjusted R Square	0,189708
Standard Error	10,15191
Observations	200

TABLE VI. SUMMARY OF MVRA

	Coefficients	***Standard Error***	***t Stat***	***P-value***
Intercept	-60.69	16.38	-3.70	0.000275
LL	0.137	0.205	0.671	0.503
PI	-0.206	0.216	-0.956	0.340
MDD	0.0371	0.00693	5.35	2.45E-07
OMC	-0.122	0.414	-0.295	0.768

B. ARTIFICIAL NEURAL NETWORK

Table 7 gives a summary of ANN results, in which the model with a Relu Function with a hidden layer with seven number of neurons gives the highest R^2 value of 0.83. The table also shows a model with a Tan-sigmoid Function with a hidden layer with fifteen number of neurons giving R^2 of 0.21. Comparison between the measured CBR values and predicted CBR values from the ANN model using a linear relationship is presented in Figure 7.

TABLE VII. SUMMARY OF ANN RESULTS

Model	Number of Neurons	Activation Function	R2	RMSE
		Relu		
ANN	5		0.69	2.23
	7		0.83	1.24
	13		0.62	3.74
	15		0.51	2.19
		Tan-sigmoid		
	5		0.55	3.69
	7		0.43	3.73
	13		0.34	4.78
	15		0.21	5.01
		Log-sigmoid		
	5		0.33	5.54
	7		0.56	4.36

ISSN: 2521-2293

	13		0.38	5.19
	15		0.22	6.9

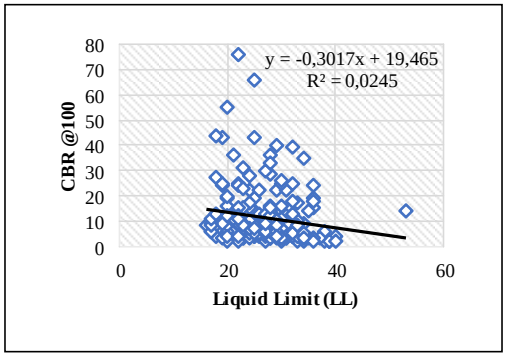

Fig. 1. *Regression model for CBR and LL*

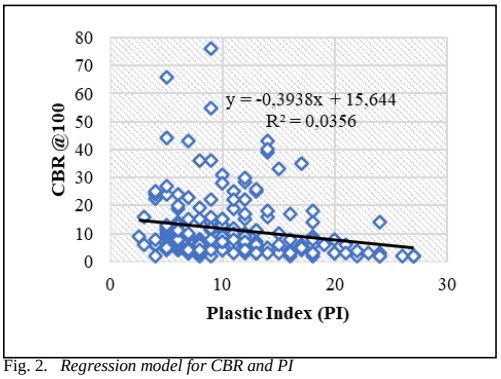

Fig. 2. *Regression model for CBR and PI*

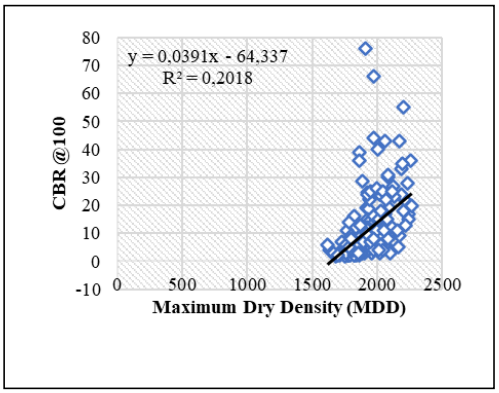

Fig. 3. *Regression model for CBR and MDD*

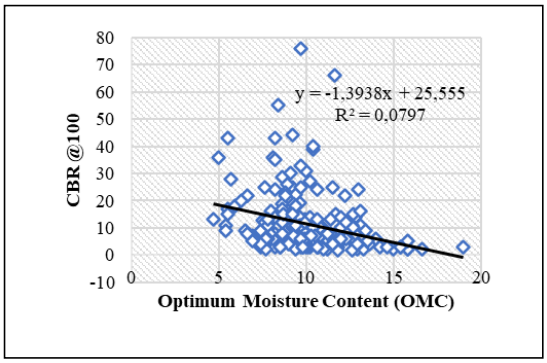

Fig. 4. *Regression model for CBR and OMC*

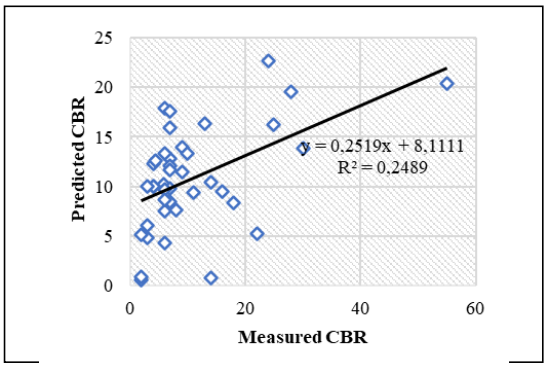

Fig. 5. *MVRA model performance*

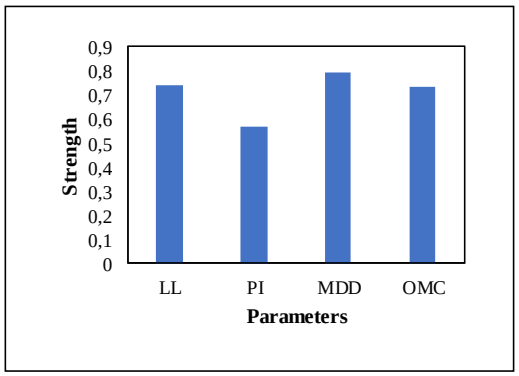

Fig. 6. MVRA model performance

ISSN: 2521-2293

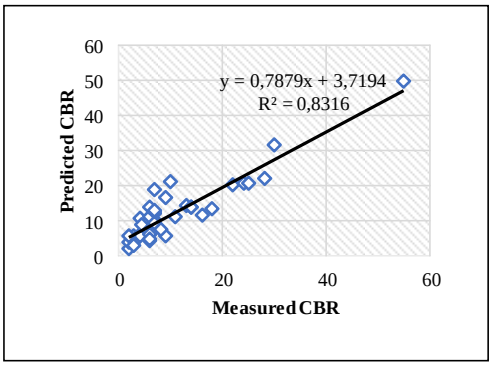

Fig. 7. *ANN Model Performance*

V. CONCLUSION

From the results of the research, the following conclusions are being drawn:

- Based on the above laboratory tests, there isn't any reliable Single linear relationship for predicting CBR value from index properties with relatively low R^2 values.
- The highest coefficient of determination obtained for CBR is 0.2018 with MDD.
- It is observed that CBR values increases with increase in MDD and decreases with increase in LL, PI and OMC.
- The correlation of CBR with LL, PI, MDD and OMC by utilizing MLRA approach gives a relationship with R2 = 0.249
- From the developed correlation, it can be seen that the CBR value is largely dependent on MDD of soil whereas, the effect of the other parameters is lower in comparison.
- The ANN analysis showed that ReLu function model with hidden of seven number of neurons, produced a good relationship with a R^2=0.83
- The results also showed that of the two types of algorithms, ANN has the best output of results

References

[1] O. Bassey Bassey, E. Ambrose, and R. K. Etim "Correlation between CBR Values and IndexProperties of Soils: A Case Study of Ibiono, Oron and Onna in Akwa Ibom State," vol. 7, no. 4, pp. 94–102, 2017,

[2] S. T. Torgano, M. S. Ali, E. T. Yenealem and A. T. Tumato, "CORRELATION BETWEEN CBR VALUES AND INDEX PROPERTIES OF SUBGRADE SOILS: IN THE CASE OF BODITI TOWN," International Journal of Advance Research and Innovative Ideas in Education, vol. 6, no.3, 2020

[3] C. R. Foster and R. G. Ahlvin, "Notes on the Corps of Engineers CBR Design Procedure," Us Army Engineer waterways experiment station, pp. 1-12, 1959.

[4] T. Abdulnabi and Z. Abdulrazzaq, "An Estimated Correlation between California Bearing Ratio (CBR) with some Soil Parameters of Gypseous Silty Sandy Soils," *Tikrit Journal of Engineering Sciences*, vol. 27, no. 1, pp. 58–64, Mar. 2020.

[5] O. S. B. Al-Amoudi *et al.*, "Clegg Hammer-California-Bearing Ratio Correlations Related papers St abilizat ion of a Saudi calcareous marl soil Met hod and Mechanisms of Soil St abilizat ion Using Elect ric Arc Furnace Dust Clegg Hammer-California-Bearing Ratio Correlations," 2002.

[6] N. Puri, H. D. Prasad, and A. Jain, "Prediction of Geotechnical Parameters Using Machine Learning Techniques," in *Procedia Computer Science*, 2018, vol. 125, pp. 509–517.

[7] Z. Chao, G. Ma, Y. Zhang, Y. Zhu, and H. Hu, "The application of artificial neural network in geotechnical engineering," in *IOP Conference Series: Earth and Environmental Science*, Nov. 2018, vol. 189, no. 2.

[8] A. Bardhan, C. Gokceoglu, A. Burman, P. Samui, and P. G. Asteris, "Efficient computational techniques for predicting the California bearing ratio of soil in soaked conditions," *Eng Geol*, vol. 291, Sep. 2021

[9] K. V. S. D. Jayamali, U. P. Nawagamuwa, and U. P. Nawagamuwa, "Empirical Correlations Between CBR and Index Properties for Sri Lankan Soils Determination of Age of MSW through Soil Tests View project Index properties of SL soils and CBR View project Empirical Correlations Between CBR and Index Properties for Sri Lankan Soils," 2015.

[10] P. Sharma, S. VSatyanarayana, S. ReddyN, and S. Venkata Satyanarayana, "Prediction of California Bearing Ratio through Empirical Correlations of Index Properties for Tropical Indian Soils," *International Journal of Innovations in Engineering and Technology*, 2020.

[11] P. G. Rakaraddi and V. Gomarsi, "ESTABLISHING RELATIONSHIP BETWEEN CBR WITH DIFFERENT SOIL PROPERTIES," 2015.

[12] T. Abdulnabi and Z. Abdulrazzaq, "An Estimated Correlation between California Bearing Ratio (CBR) with some Soil Parameters of Gypseous Silty Sandy Soils," *Tikrit Journal of Engineering Sciences*, vol. 27, no. 1, pp. 58–64, Mar. 2020.

[13] V. Chandrakar and R. K. Yadav, "'Study of correlation of CBR value with engineering properties and index properties of coarse grained soil.,'" 2016.

[14] J. F. Hair, W. C. Black, B. J. Babin, and R. E. Anderson, "MULTIVARIATE DATA ANALYSIS EIGHTH EDITION," 2019.

[15] W. S. Mcculloch and W. Pitts, "A LOGICAL CALCULUS OF THE IDEAS IMMANENT IN NERVOUS ACTIVITY* n," 1990.

[16] S. E. Dreyfus, "Artificial neural networks, back propagation, and the kelley-bryson gradient procedure," *Journal of Guidance, Control, and Dynamics*, vol. 13, no. 5, pp. 926–928, 1990.

[17] P. K. Simpson, Artificial neural systems : Foundations, paradigms, applications, and implementations, New York: Pergamon Press, 1989.

[18] Y. Li, Y. Fu, H. Li, and S. W. Zhang, "The improved training algorithm of back propagation neural network with selfadaptive learning rate," in *Proceedings of the 2009 International Conference on Computational Intelligence and Natural Computing, CINC 2009*, 2009, no. 1, pp. 73–76.

[19] Taskiran, T.,. Prediction of California bearing ratio (CBR) of fine grained soils by AI methods, 2010

[20] Varghese, V.K., Babu, S.S., Bijukumar, R., Cyrus, S., Abraham, B.M., Artificial neural networks: a solution to the ambiguity in prediction of engineering properties of fine-grained soils. Geotech. Geol. Eng. 31, 1187–1205, 2013.

[21] Kumar, S.A., Kumar, J.P., Rajeev, J., Application Of Machine Learning Techniques To Predict Soaked CBR Of Remolded Soils, 2, pp. 3019–3024, 2013

[22] Sabat, A.K., Prediction of California bearing ratio of a stabilized expansive soil using artificial neural network and support vector machine. Electron. J. Geotech. Eng. 20, 981–991, 2015.

[23] . Yildirim, B., Gunaydin, O.,. Estimation of California bearing ratio by using soft computing systems. Expert Syst. Appl. 38, 6381–6391, 2011.

BIUST Teaching, Research, & Innovation Symposium 2023 (TRDAIS 2023)
Botswana International University of Science and Technology
Palapye, Botswana, 18 - 19 September 2023
ISSN: 2521-2293

Seeing the Galaxy's central black hole with the Africa Millimetre Telescope

Rhodri Evans[1], Michael Backes[2], Heino Falcke[3], and Marc Klein-Wolt[4]

[1]Department of Physics and Astronomy, Botswana International University of Science and Technology. email: evansr@biust.ac.bw
[2]Department of Physics, Chemistry and Material Science, The University of Namibia
[3,4]Department of Astronomy, Radboud University

28th October 2022

Abstract

Using very long baseline interferometry Astronomers are able to link together telescopes in different parts of the world to obtain incredible angular resolution of millionths of an arc second. The Event Horizon Telescope (EHT) is such a network, and this collaboration has recently published the first-ever images of the supermassive blackholes at the centre of Messier 87 and our own Milky Way. The Africa Millimetre Telescope (AMT) will be the first millimetre-wave telescope on the African continent, and will be an important addition to the EHT network. The AMT will improve the EHT's resolution, thus enabling us to better understand these strange but important objects. The AMT will be located in Namibia, and will see first-light in early 2024.

1 Introduction

The idea that there could be black holes at the centres of some galaxies was first proposed in 1964 by Seyfert [1]. He suggested that the intense emission coming from the active nuclei of some galaxies, Active Galactic Nuclei (AGNs), could be due to the accretion of material onto a central massive object [1]. This idea was further developed by e.g. Lynden-Bell and Rees [2], who proposed models where the prodigious energy output from quasars was be due to material accreting onto a central massive blackhole. In a prescient paper in 1974, Rees [3] further suggested that there could be a supermassive blackhole (SMBH) at the centre of *all galaxies*, not just AGNs. This prediction has been found to be true [4],[5],[6],[7].

ISSN: 2521-2293

In 1974, a compact radio source in the direction of the inner 1-pc core of the Galactic nucleus was first observed at 2.7 GHz and 8.1 GHz (Figure 1), using the Very Large Array (VLA) by Balick and Brown [8]. It was realised that this source, which has become known as Sagittarius A*, lies at the centre of our Galaxy, and this source has now been studied at many other wavelengths.

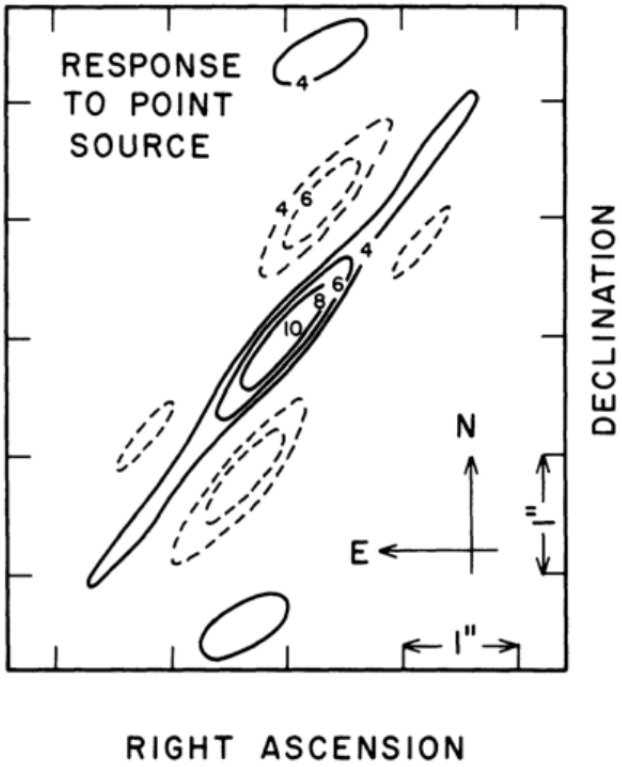

Figure 1: Sagittarius A* as observed at 2.7 GHz and 8.1 Gz ([8])

In the mid-1980s, a team at the Max Planck Institute for Extraterrestrial Physics (MPE)[9],[10] started making near-infrared observations of the motions of stars near Sagittarius A*. A second team, based at the University of California Los Angeles (UCLA), started a similar programme in the early-1990s [11],[12]. Observations by these two teams over several decades [13],[14] have enabled us to determine the mass of the central SMBH, it is found to have a mass of $M \approx 4.5 \times 10^6$ $M_\odot$ [13],[14]. Genzel and Ghez were awarded the 2020 Nobel Prize in Physics "for the discovery of a supermassive compact object at the centre of our galaxy"[15].

ISSN: 2521-2293

2 The Event Horizon of a black hole

Although General Relativity is necessary to correctly work out the details near the event horizon of a black hole, we can gain an idea of the size of the event horizon using simple Newtonian gravity. The event horizon is defined as the point where the escape velocity v_{esc} becomes equal to the speed of light c. The first solution of Einstein's field equations for a point mass were produced by Schwarzschild[16]. We therefore refer to the point in space where the event horizon is found as the *Schwarzschild radius* R_s.

Using Newtonian gravity, we can show that the escape velocity from any object is given by

$$v_{esc} = \sqrt{\frac{2GM}{R}} \tag{1}$$

where G is the universal gravitational constant, M is the mass of the object from which we are trying to escape, and R is radius we are considering. For a black hole, as $v_{esc} = c$ at R_S, so we can write

$$R_S = \frac{2GM}{c^2} \tag{2}$$

Although we cannot, by definition, observe the event horizon, we can observe light which passes very close to the event horizon[17]. The first person to do calculations of how light passing near a black hole would be bent was Hilbert in 1917[17]. Bardeen[18] calculated the geometrical properties of a rotating black hole's "shadow" against a bright background. Falcke, Melia and Agol[19] showed that an accreting black hole embedded in a plasma that is optically thin at millimetre wavelengths would produce a bright ring of emission, with a dim "shadow" created by the black hole's event horizon in its interior. They went on to suggest that such a shadow, while subtending too small an angle to observe conventionally, may be detectable towards the Galactic centre using the technique of very long baseline interferometry (VLBI).

Using the mass of the SMBH at the Galactic centre, we can calculate that the event horizon should have a physical diameter, using Equation (2), of $2R_S = 2.67 \times 10^{10}$ m. With the Sun lying 8 kpc [20] from the Galactic centre, this means that the event horizon subtends an angle of $\theta \sim 22$ micro arcseconds.

Such a tiny angle is *only* accessible using VLBI, where telescopes are linked together and make observations simultaneously. Although VLBI has been used for many decades at radio wavelengths, to achieve a resolution of a few tens of micro arcseconds would require baselines of millions of kms, which is currently not achievable. However, at millimetre wavelengths, the baseline of the Earth is sufficient, and therefore the Event Horizon Telescope (EHT) was conceived in 2009[21] to be a network of millimetre-wave telescopes spread across different continents. In 2017, the network comprised

ISSN: 2521-2293

millimetre-wave telescopes in Europe, the continental USA, Mexico, Hawai'i, the South Pole and Chile (Figure 2).

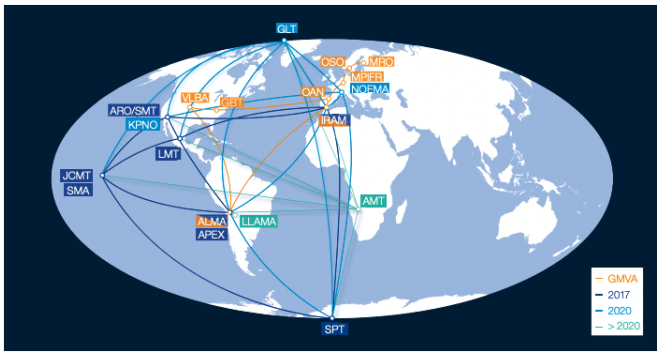

Figure 2: The EHT Network (from [17]). The 2017 network is shown in blue, with two new telescopes being added in 2020. The AMT will be added in 2024.

3 Imaging the event horizons of the SMBHs in Messier 87 and our Milky Way galaxy

In an observing campaign in April 2017, the SMBH at the centre of Messier 87 was imaged using the EHT. The images were released in April 2019[22]. Although M87 is $\sim$ 2000 farther away than our Galactic centre[17], it hosts a SMBH with a mass of $\sim$ 16 billion$M_{\odot}$[23]. Therefore, the angular diameter of its SMBH is only slightly smaller than for our Galaxy. Figure 3 shows the first-ever images of the shadow of a supermassive black hole.

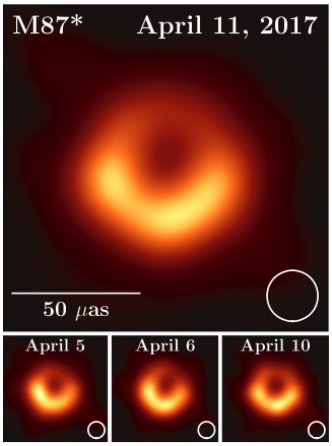

Figure 3: The shadow of the event horizon of M87 [22]

ISSN: 2521-2293

During the same observing campaign, the EHT also observed Sagittarius A*, and the first images of our own Galaxy's SHMB (Figure 4) were released in May 2022[24].

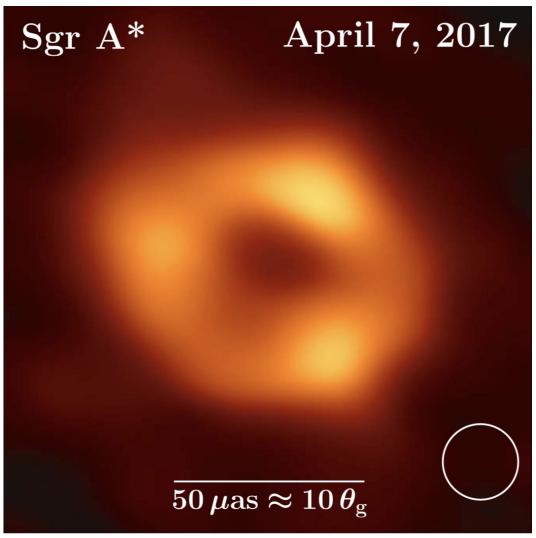

Figure 4: The shadow of the event horizon of Sagittarius A* [24]

4 The Africa Millimetre Telescope

Although the EHT has successfully produced images of the shadow of the SMBHs in both M87 and Sagittarius A*, simulations show that the resolution of the array will be greatly enhanced by the addition of a millimetre-wave dish on the African continent, specifically, on Mount Gamsberg in Namibia. Figure 5 shows simulations of the appearance of an input synthetic image with and without both ALMA and the AMT. Figure 6 shows where in Namibia Mount Gamsberg is located, it is approximately 150 km east-south-east of Windhoek, in one of the driest parts of the country. Figure 7 shows the mountain, with the current access road to the summit.

As can be seen from Figure 5, the improvement in resolution by adding the AMT is actually greater than the inclusion of ALMA. This is because the AMT briefly allows for the maximum possible baseline between its location in Namibia and the elements of the EHT which are in Hawaii, a full earth-diameter away.

Site testing of this site conducted by the European Southern Observatory (ESO) from mid-1994 to mid-1995[25] showed that Mount Gamsberg, at an elevation of 2400m, has low precipitable water vapour, particularly during the dry season from May to October (see Figure 8). This makes it ideal for millimetre-wave astronomy.

ISSN: 2521-2293

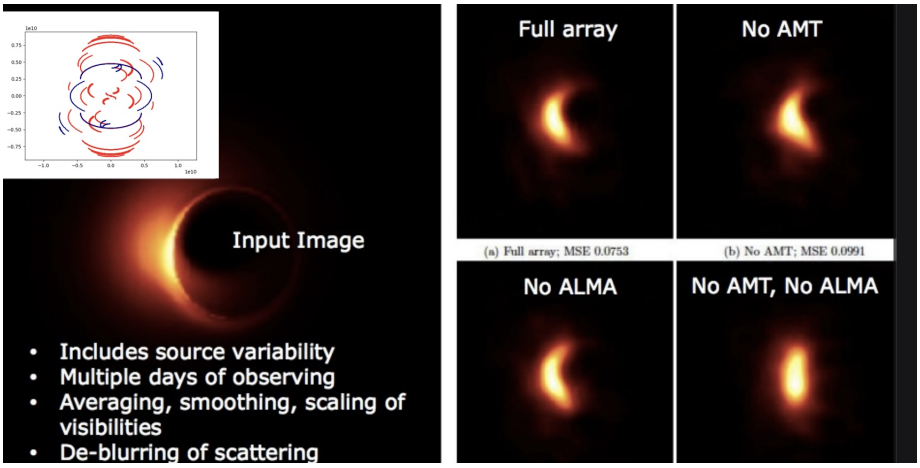

Figure 5: Simulated images and with and without the AMT

Figure 6: The location of Mount Gamsberg

ISSN: 2521-2293

Figure 7: Mount Gamsberg, with the access road to the summit in the foreground.

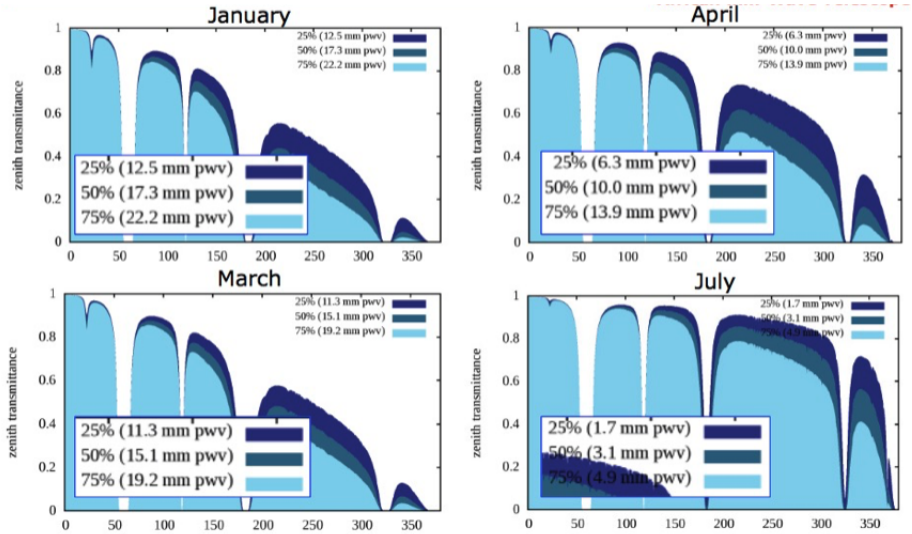

Figure 8: Precipitable water vapour at Mount Gamsberg as measured by ESO from mid-1994 to mid-1995 using a radiometer[25].

ISSN: 2521-2293

5 The Telescope

To reduce costs, the AMT project will use the decommissioned 15-metre Swedish-ESO Sub-millimetre Telescope (SEST). SEST was operated at La Silla in Chile from 1987 to 2003, when it was decommissioned[26],[27]. SEST will be dismantled, and initially shipped to France for repair and refurbishment. Then, it will be shipped to Namibia, where it will be transported in sections to the summit of Mount Gamsberg. The largest sections of the telescope are the gears, which are a few metres in size and weigh about 5 metric tonnes. In order for such large items to be transported to the summit, the access road shown in Figure 7 will need to be improved. Power at the summit will be provided by solar power with large storage batteries, and data communication will use the current communication mast on the mountain, with an upgrade for high data-rate transfers.

Figure 9: The Swedish ESO Sub-millimetre Telescope (SEST) at La Silla, Chile. This telescope operated between 1987 and 2003, when it was decommissioned[26],[27].

6 Summary and Conclusions

In the last few years we have entered a new era in millimetre-wave astronomy, obtaining images for the first time of the shadows of the supermassive black holes at the centres of Messier 87 and our own Milky Way. This has been achieved by linking together millimetre-wave telescopes on several continents and using the technique of very long baseline interferometry to produce resolutions of a few tens of a micro-arcsecond. Simulations show that the

ISSN: 2521-2293

resolution of the network of telescopes will be greatly improved by the addition of a telescope in Africa, and Mount Gambserg in Namibia has been chosen as the most suitable site. The Africa Millimetre Telescope will use the decommissioned 15-metre Swedish-ESO Submillimetre Telescope, and will see first light in April 2024.

References

[1] E.E. Salpeter. Accretion of interstellar matter by massive objects. *Astrophysical Journal*, 140:796–800, 1964.

[2] D. Lynden-Bell and M. Rees. On quasars, dust and the galactic centre. *Monthly Notices of the Royal Astronomical Society*, 152:461–475, 1971.

[3] M. Rees. Black holes. *The Observatory*, 94:168–179, 1974.

[4] L Ferrarese and D Merritt. A fundamental relation between supermassive black holes and their host galaxies. *Astrophysical Journal*, 539:L9–L12, 2000.

[5] K Gebhardt, Bender R, Bower G, and A Dressler etal. A relationship between nuclear black hole mass and galaxy velocity dispersion. *Astrophysical Journal*, 539:L13–L16, 2000.

[6] S Tremaine, K Gebhardt, and R Bender etal. A relationship between nuclear black hole mass and galaxy velocity dispersion. *Astrophysical Journal*, 574:740–753, 2002.

[7] A King. Black holes, galaxy formation, and the $m_{BH} - \sigma$ relation. *Astrophysical Journal*, 596:L27—L29, 2003.

[8] B. Balick and R.L. Brown. Intense sub-arcsecond structure in the galactic center. *Astrophysical Journal*, 194:265–270, 1974.

[9] R Genzel, N Thatte, A Krabbe, H Kroker, and L E Tacconi-Garman. The dark mass concentration in the central parsec of the milky way. *Astrophysical Journal*, 472:153–172, 1996.

[10] A Eckart and R Genzel. Stellar proper motions in the central 0.1 pc of the galaxy. *Monthly Notices of the Royal Astronomical Society*, 284:576–598, 1997.

[11] A M Ghez, B L Klein, M Morris, and E E Becklin. High proper-motion stars in the vicinity of satittarius a*: Evidence for a supermassive black hole at the center of our galaxy. *Astrophysical Journal*, 509:678–686, 1998.

ISSN: 2521-2293

[12] J R Lu, A M Ghez, S D Hornstein, M R Morris, E E Becklin, and K Matthews. A disk of young stars at the galactic center as determined by individual stellar orbits. *Astrophysical Journal*, 690(1463–1487), 2009.

[13] S. Gillessen, F. Eisenhauer, S. Trippe, T. Alexander, R. Genzel, F. Martins, and T. Ott. Monitoring stellar orbits around the massive black hole in the galactic center. *Astrophysical Journal*, 692:1075–1109, 2009.

[14] A.M. Ghez, S. Salim, N.N. Weinberg, J.R. Lu, T. Do, J.K. Dunn, K. Matthews, M.R. Morris, S. Yelda, E.E. Becklin, T. Kremenek, M. Milosavljevic, and Naiman. J. Measuring distance and properties of the milky way's central supermassive black hole with stellar orbits. *Astronomy and Astrophysics*, 689:1044–1062, 2008.

[15] R Genzel and A M Ghez. The nobel prize in physics, 2020, "for the discovery of a supermassive compact object at the centre of our galaxy", https://www.nobelprize.org/prizes/physics/2020/summary/, 2020.

[16] K Schwarzschild. Über das gravitationsfeld eines massenpuktes nach der einsteinschen theorie (on the gravitational field of a mass point according to einstein's theory). *Sitzungsberichte der Deutschen Akademie der Wissenschaften zu Berlin, Klasse fur Mathematik, Physik, und Technik*, page 189, 1916.

[17] C. Goddi, G. Crew, and V. etal. Impellizzeri. First m87 event horizon telescope results and the role of alma. *Messenger*, 177:25–35, 2019.

[18] J M Bardeen. Rapidly rotating stars, disks, and black holes. In C DeWitt and B S DeWitt, editors, *Black Holes*, pages 241–289. Summer School of Theoretical Physics of the University of Grenoble at Les Houches, Gordon and Breach, NY, 1973.

[19] J Falcke, F Melia, and E Agol. The shadow of the black hole at the galactic center. In *Cosmic Explosions*, volume 522, pages 317–320. American Insitute of Physics, 2000.

[20] R Abuter, A Amorim, and M Bauböck etal. A geometric distance measurement to the galactic center black hole with 0.3 *Astronomy and Astrophysics*, 625:L10, 2019.

[21] S Doelman, E Agol, and D Backer etal. Imaging an event horizon: submm-vlbi of a super massive black hole. In *Astronomy Decadal Review*, 2009.

[22] The Event Horizon Telescope Collaboration. First m87 event horizon telescope results. i. the shadow of the supermassive black hole. *Astrophysical Journal*, 875(L1), 2019.

ISSN: 2521-2293

[23] Jonelle L Walsh, A J Barth, L C Ho, and M Sarzi. The m87 black hole mass from gas-dynamical models of space telescope imaging spectrograph observations. *Astrophysical Journal*, 770:86–96, 2013.

[24] The Event Horizon Collaboration. First Sagittarius A* event horizon telescope results. i. the shadow of the supermassive black hole at the center of the milky way. *Astrophysical Journal*, 930:L12–32, 2022.

[25] S Sarazin. Environmental conditions on potential observatories - gambserg (namibia) for the months july 1994 to july 1995, 1995.

[26] R S Booth, M J de Jong, and P A Shaver. The swedish-eso submillimetre telescope. *Messenger*, 48:2–6, 1987.

[27] C Madsen. Swedish-eso 15m submillimeter telescope (sest), 2003.

BIUST Teaching, Research, & Innovation Symposium 2023 (TRDAIS 2023)
Botswana International University of Science and Technology
Palapye, Botswana, 18 - 19 September 2023
ISSN: 2521-2293

An economic analysis of a stand-alone solar system for an off-grid village shop in Majwanaadipitse, Botswana

Thabang T B Osupeng
Temogo P Mabaila
Davison Munyaradzi Murape
Department of Physics and Astronomy
Botswana International University of Science and Technology, Botswana
muraped@biust.ac.bw

Abstract

Electricity is one of the main requirements for sustainable development and the improvement of living standards for different nations. Remote areas in Botswana depend in the use of fossil fuels e.g., petrol, diesel and natural gas to produce electricity. However, the villagers encounter high fuel price from buying fossil fuels. On the other side, combustion of fuels creates air pollution that contributes to global warming which is accountable for climate change and disastrous effects. This is a study that explores replacing the fossil fuel used by a village shop in Majwanaadipitse, Botswana (22° 6' 50″ S, 26° 53 0″ E) with an off-grid PV system. This was done by designing, sizing, estimating the contribution to pollution by the fossil fuels and costing an off-grid solar PV system. The estimated energy requirement of a village shop was found to be 7.97 kWh/day. The design and sizing of the PV system equipment's depended on the estimated load. The proposed off-grid PV system required 5 PV modules each rated 330 W, 5 batteries each rated 100Ah, a charge controller and an inverter. The system capacity of an off-grid PV system to be installed was 1.6kW_p. The emitted pollution into the atmosphere to be avoided was found to be 2882 Kg of carbon dioxide per year. The payback period of the PV system was estimated to be 2 years. The NPV was also found to be favorable, showing that it is a profitable investment with a cost of P653 880. It The study revealed that an off-grid PV electricity is technically and economically feasible for electrifying a shop compared to the use of fossil fuels.

Keywords: Electricity, Majwanaadipitse shop, Botswana, off-grid photovoltaic (PV) system, pollution, net present value (NPV)

ISSN: 2521-2293

1. Background and Motivation

The United Nations Sustainable Development Goals (SDGs) of 2015 include goal No. 7 which unequivocally recognizes how access to affordable, reliable and modern energy is central to achieving economic growth and human development while ensuring a sustainable environment. More than a billion people live without access to electricity in developing countries according to energy access outlook 2017 (1) (2). Energy has long been considered as one of the key fundamentals of modern life and if one does not have energy, then they are poor (3). Absence of energy influences individuals from numerous points of view, students have less hours to study, medical clinics and facilities have no light to see patients and independent small business cannot power electronic gadgetry (4) (5). In Botswana, there are many villages in the rural areas that are without electricity as they are located far from the national electricity grid (6) (7). Clearly not all villages will be connected to the grid in the short term as such the use of alternative energy sources such as solar PV system emerges as the best solution. Solar photovoltaic is an innovation that changes sun's radiation into usable direct current (DC) power by utilizing the use of semi-conductors. It is one of technologies that can shape a clean, reliable, and affordable electricity systems for the future (8). This alternative source of energy is well supported by the fact that Botswana has a gigantic potential to wander into the utilization of solar energy. As it encounters yearly a direct normal light equivalent to 3000 kWh/m^2/a (6). Furthermore the use of solar PV system to replace fossil fuels has a positive impact on the environment (i.e., it helps to reduce CO_2 emission, generates no noise, and has positive health benefits) .It also helps to minimize the risk of global warming which is accountable for climate change and its disastrous effects (9), as well as to reduce depletion of fossil fuel (10).

2. Description of case

As pointed out earlier, access to electricity in remote villages is a challenge. Mr. Ontireletse Rebagamang is a sole trader operating a village shop in Majwanaadipitse village. He is currently using a generator and LP gas as sources of energy for his requirements. He has to procure these sources of energy from the nearest town of Serowe and in the process incurs further transport costs. The fossil fuels he uses in the form of petrol and gas for his energy requirement poses a big threat to health and environment He is not happy with his energy expenditure and complains that his income is being eroded as a result. As such Mr. Ontireletse Rebagang is keen to switch to a stand-alone solar PV system as an alternative. A need has therefore arisen to design and cost an appropriate solar PV system for Mr. Rebagamang and carry out an economic analysis that convinces him that he is indeed better off switching to solar energy. The off-grid PV system to be designed is to be installed in Botswana, Majwanaadipitse village shop (22˚ 6 ' 50 ″S, 26˚ 53' 0 ″E), bearing in mind that the PV system if designed well will minimize the cost compared to the use of fuel and LPG gas. Also, PV system if installed well will provide energy requirement for Mr. Ontireletse Rebagamang's shop at a lower cost as opposed to fuel and LP gas.

3. Experimental description

3.1 Load assessment

ISSN: 2521-2293

The load assessment involved finding out the daily load demand of the electrical appliances in the shop in ampere-hours (Ah). This was done through the following steps:

- All electrical appliances used at the shop (inside and outside) were listed down.
- The power ratings (wattages) of the individual appliances were noted.
- Special attention was given on whether an appliance was AC or DC.
- The hours of operation per day for each item were also noted

Table 3.2 Contains a list of electrical appliances at the shop, their daily hours of operation, rated power and the energy used by each of them on a typical day.

Table 1. Load Profile of the Appliances

Electrical Appliance	Operation Hour/day	Quantity	Rated power (W)	kW	KWh/day
Bar Fridge	6	1	320	0.32	1.92
Bar Fridge	7	1	320	0.32	2.24
Lights (CFL) indoor	5	3	15	0.045	0.225
Lights (CFL) outdoor	11	5	15	0.075	0.825
Radio	7	1	220	0.22	1.54
Tv	4	1	130	0.13	0.52
Smart Switch Machine	4	1	40	0.04	0.16
Phone Chargers	4	5	6	0.03	0.12
Long single twin tube CFL bulb	5	1	24	0.024	0.12
Small radio	6	1	50	0.05	0.30
Total	78	30	1140	1.254	7.97

Note: All electrical appliances were AC type

ISSN: 2521-2293

From the calculations of the energy load, it was found that the energy requirement of the village shop was 7.97 kWh per day.

3.2 PV system design and sizing

System sizing is a technique for determining enough voltage and current ratings for each component of the PV system, meeting the shop's electrical demand and, at the same time, calculating the total system cost from the design process to the operational of the system. The process involved calculating the system specifications e.g. battery bank, PV array, inverter etc. using the daily electrical load demand.

3.2.1 Selection of system voltage

Selecting the DC system voltage depends on different factors some of them being (11).

Peak load

- 12VDC is fine for peak loads up to 1000W
- 24VDC is good for peak loads up to 2000W
- 48VDC is best for peak loads over 2000W

The complete daily AC load is over 2000W, with 48VDC being the chosen voltage.

3.2.2 PV array sizing and selection of PV module

PV array is several PV panels electrically connected to convert sunlight rays to electricity. The size of the PV panel is calculated by considering the solar insulation available, the daily load requirement and the features of the PV modules.

The size of the PV array used for the project can be calculated as (12):

$$\text{System Capacity} = \frac{E_d}{G} \quad (1)$$

$$= \frac{7.97kwh}{6.2PSH} \times 1.25 \text{ (energy lost in the system)}$$

$$= 1.607\ kW_p$$

1607 is the minimum PV array watts. The module rated power used was 330 W

Number of needed PV module is given by:

$$\frac{System\ Capacity\ W_p}{\text{Module Rated Power } W_p} \quad (2)$$

Table 2. shows details of the PV module selected.

Table 2. Details of the PV module chosen

Brand and Model	Sunergy, SUN330-60M

ISSN: 2521-2293

Maximum Power P_{max} (W) At STC	330
Cell type	Mono crystalline module
No of cells	60 (6×10)
Dimensions (length, width, height)	(164 × 99 × 3.5) cm
Weights	19 Kg
Short circuit current I_{sc} (A) At STC	9.35
Open circuit voltage V_{oc} (V) At STC	38.2
Maximum power current I_{mp} (A) At STC	8.72
Maximum power voltage V_{mp} (V) At STC	32.1
Module efficiency	17.25
Max system voltage	1000 V DC
Operating temperature At STC	-45℃~+ 85℃

3.2.3 Battery bank sizing and selection

During the day, batteries store energy produced by the solar array and satisfy electricity requirements during the night and after successive rainy days. Battery size is a design variable usually based on the required period of autonomy, the maximum allowable depth of release and the low operating temperature. The battery's storage capacity is displayed in ampere-hours. The battery selected must be able to achieve greater depth. The permissible discharge depth for this application is 0.8 (11).

3.2.4 Battery sizing

The following formula is used to calculate battery storage capacity requirements

The daily load demand L_d in ampere-hours (Ah) (12):

$$L_d = \frac{E_d}{DODV_{nsv}} \quad (3)$$

3.2.5 Battery bank capacity:

C_{batt} = daily battery capacity demand × DOA (4)

Specification of battery

Capacity of the battery chosen is of 100Ah and nominal voltage is 12 V.

ISSN: 2521-2293

3.2.6 Number of batteries is given by (12):

$$\text{Number of batteries} = \frac{storage\ capacity}{Capacity\ selected} \quad (5)$$

Number of batteries in series is obtained by:

$$N_s = \frac{\text{system voltage}}{\text{battery voltage}} \quad (6)$$

Number of batteries in parallel is obtained by:

$$N_p = \frac{Number\ of\ battery}{N_s} \quad (7)$$

3.2.7 Charge controller design and selection

Regulates the voltage and current from the battery-powered PV panels, prevents overloading of the battery and extends battery life (11). The voltage regulator size can be acquired by multiplying the short circuit current of the horizontally linked modules by a safety factor. It can be calculated as follows (12):

The rated current of the regulator is given by:

$$\mathrm{I_{rated}} = N_{mp} \times I_{sc} \times F_{safety} \quad (8)$$

$$=5\times 9.35 \times 1.25$$

$$= \ 58\ \mathrm{A}$$

Number of voltage regulator is given by:

$$\text{Number of voltage regulator required} = \frac{I_{rated}}{I_{selected}} \quad (9)$$

3.2.8 Inverter design and selection

The inverter used must be capable of handling the highest anticipated energy of AC charges. It must also be at least 1.25 times the solar wattage maximum. In the scheme where AC Power is required, an inverter is used (11).

Therefore, the rated power of the inverter becomes:

= (5× 330W) × 1.25 = 2062.5 W

=2.06 kWh

The specification of required inverter will be 3000W, 12V, 100V and 50Hz

3.2.9 Determination of the system cables sizes:

Choosing the right size and sort of wire will improve a PV system's efficiency and efficiency (11).

ISSN: 2521-2293

$$I_{rated} = N_{mp} \times I_{sc} \times F_{safety} \quad (10)$$

$$= 5 \times 9.35 \times 1.25$$

$$= 58 \text{ A}$$

And the cross-sectional area is given by (11):

$$A = \frac{\rho L I}{V_d} \times 2 \quad (11)$$

Where ρ = resistivity of copper wire which was taken as 1.724×10^{-8} Ωm. For Ac and Dc, the wiring for off-grid PV system the voltage drop is taken to exceed 4% value.

Determination cable size between for PV modules through the battery voltage regulator

Maximum voltage drop

$$V_d = \frac{4}{100} \times 48 = 1.92v$$

Let the length of the cable (L) = 1m

Therefore $A = \frac{\rho L I}{V_d} \times 2$

$$A = \frac{1.724 \times 10-8 \times 1 \times 58}{1.92V} \times 2$$

$= 2.08 \text{ mm}^2$

Determination of cable size between battery bank and inverter

Let length of cable (L) = 3.5m, therefore maximum current from battery is given by (11)

$$I_{max} = \frac{inverter\ capacity}{\eta_{\text{inverter}} \times V_{system}} \quad (12)$$

$$= \frac{1000}{0.95 \times 48}$$

$= 21.9$ A

Maximum voltage drop $V_d = \frac{4}{100} \times 24$

$= 0.96$v

$$A = \frac{1.724 \times 10-8 \times 3.5 \times 21.9}{0.96} \times 2$$

$=2.75 \text{ mm}^2$

Table 3.7 below shows a summary of the proposed sizing of an off-grid system

ISSN: 2521-2293

Table 3. Summary of the proposed sizing of an off-grid PV system

Components	Description	Results	Cost (Pula)
Load estimation	Total estimated load	7.97 kWh/day	
PV array Model: Renewsys Solar panels	Capacity of PV array	1.6 kW	11 500
	Number of modules in series	3	
	Number of modules in parallel	2	
	Total number of modules	5	
Battery Bank Model: freedom Battery	Battery bank capacity	416 Ah	41 290
	Number of batteries in series	4	
	Number of batteries in parallel	1	
	Total number of batteries required	5	
Victron Energy Voltage Regulator	Capacity of voltage regulator	58A	2 300
	Number of voltage regulator required	1	
1.5kVA Victron Energy Inverter	Capacity of the inverter	2.06 kW	6 003
Wire	Between PV modules and batteries through the voltage regulator	2.08 $mm^{2,}$58A	2000

ISSN: 2521-2293

	Between battery and inverter	2.75 $mm^{2,}$ 21.9A	
Balance of system			3 400
Labour			1 800
		Total Cost	68 093

3.3 Cost benefit analysis of the solar PV system

Table 1. shows that in a day a village shop requires 7.97 kWh per day of energy. Thus, for a year the solar PV system will provide 95.64 kWh of energy. The working life span of a solar PV systems averages between 20 to 25 years. The average value of 25 years working life span was used in this project. The cost of fossil fuel used in a village shop was P28 500. The energy efficiency factor for a standard petrol generator was found to be 0.935. The cost of fossil fuel was adjusted using the efficiency factor of 0.935 and recorded in **Table 4.** The following **Table 4** shows the cost involved in using fossil fuels to provide a village shop with electricity.

Table 4. Shows annual energy requirement for a village shop with respective bills for using fossil fuels.

Village shop Annual energy (kWh)	Annual bill (P)	Inefficiency factored annual bill (P)
95.64	28 400	30 246

A cost-benefit analysis of a village shop in Majwanaadipitse to switch from using fossil fuels to using solar PV system is performed here. The maintenance costs for the system in this project was P700 for a year. The Net Present Value (NPV) and internal rate of return (IRR) were computed utilizing the aggregate money streams for the 25 years. Annual inflation rate in Botswana arrived at the midpoint of 4.3 percent from 2013 until 2016 (13) and this is the rate utilized as a part of this investigation. Avoided electricity costs of the year under consideration year (C_{av}) are calculated by applying the annual inflation rate to the previous year's avoided electric bill (C_{py}) as captured in the formula:

$$C_{av} = C_{py}(1 + i_{an}) \quad (13)$$

Where i_{an} is annual inflation?

ISSN: 2521-2293

Fossil Fuel	Quantity	Total Pollution of carbon dioxide
Petrol	960 litres	2208 kg
LP gas	228 kg	674 kg
	Total Pollution from fossil fuel	2882 kg

The annual cash flow is the energy cost that a shop is avoiding paying every year by having invested in the use of solar PV system; it is essentially the avoided electricity costs. The NPV (PV_n) of an annual cash flow is calculated using the formula:

$$PV_n = \frac{C_{av}}{[1+i_n]^n} \quad (14)$$

Where i_n the interest rate is for the period n, the interest rate in Botswana is 5.5 percent and this rate is used in the study.

3.4 Fossil fuel cost of petrol for a shop and litres used

The following table shows the cost of fossil fuel used by a village shop, it also shows amount of fossil fuel used per year and total emission of carbon dioxide.

Total cost of fossil fuels per year is given by:

Cost of petrol per year + Cost of LP gas per year

P 24 000 + P 4400 = P 28 440

3.5 Results

The cost benefit analysis was done using P 68 293 as the system cost and P 30 246 as the annual bill for a village shop. The results were presented in **Table 5.**

Table 5. Shows annual energy demand for solar PV system and the respective bill for a village shop in Majwanaadipitse.

Year(n)	System Cost (P)	Avoided Bill (P)	Annual Cash-Flow (P)	NPV of Annual Cash-Flow (P)	Cumulative NPV (P)
0	68293.67	0	68293.00	68293.67	68293.67
1	0	31546.58	31546.58	29901.97	38391.70
2	0	32903.08	32903.08	29561.85	8829.85
3	0	34317.91	34317.91	29225.60	-20395.76
4	0	35793.58	35793.58	28893.18	-49288.94
5	0	37332.71	37332.71	28564.54	-77853.47
6	0	38938.01	38938.01	28239.63	-106093.11

ISSN: 2521-2293

7	0	40612.35	40612.35	27918.42	-134011.53
HIDDEN CALCULATIONS					
20	0	70202.75	70202.75	24060.52	-469328.04
21	0	73221.47	73221.47	23786.84	-493114.89
22	0	76369.99	76369.99	23516.28	-516631.17
23	0	79653.9	79653.90	23248.80	-539879.96
24	0	83079.02	83079.02	22984.35	-562864.32
25	0	86651.41	86651.41	22722.92	-585587.24
Totals	68293.67	1368159		653 880	

Table notes

Annual Inflation	4.3 %		NPV	P 653 880
Interest Rate	5.5 %		Payback Period	2 Years
Base Annual bill	P 30 246		Avoided Bill	P 1 368 159
IRR	50.49			

3.6 Estimation of pollution caused by fossil fuels

3.6.1 For Petrol

The complete combustion of hydrocarbon fuel is given by the equation below (14):

$$\text{Fuel } (C_xH_y) + O_2 + \text{Spark} \longrightarrow H_2O + CO_2 + \text{Heat} \quad (15)$$

From the above equation, carbon dioxide is the waste produced

Carbon dioxide waste equation is given by:

$$C + O_2 \longrightarrow CO_2 \quad (16)$$

Carbon has an atomic weight of 12 while oxygen has 16 (14). The molecular weight of carbon dioxide is given by:

= (1 Carbon atom + 2 Oxygen atom)

= 12 + (2×16)

= 44

Therefore:

1 litre of gasoline produces 2.3 kg of carbon dioxide (14). As such 960 liters of petrol used for a village shop will give:

ISSN: 2521-2293

= 2.3 of carbon dioxide × 960 litres of petrol

= 2208 kg for a year into the atmosphere

3.6.2 For LP gas

Emission factor for LP gas is given by 1.51

LP gas Unit Conversion Formulas (Metric): (LP gas unit conversion of kg to litres is 1kg = 1.96L). Therefore 228 kg gives us 446.88 litres. We then multiply the emission factor by litres used

= 1.51 × 446.88 L

= 674 kg emission into the atmosphere for a year.

3.6.3 Total emission caused by fossil fuels is given by:

Petrol emission + LP gas emission

=2208 kg + 674 kg

= 2882 Kg of carbon dioxide is caused by fossil fuel used in a village shop into the atmosphere per year

4. Discussion

The purpose of this thesis was to provide a village shop in Majwanaadipitse, Botswana (22˚ 6 ' 50″ S, 26˚ 53' 0″E) with an energy throughout the whole year by designing, sizing and costing an off-grid solar PV system to replace fossil fuels.

In **Table 1.** the estimated energy requirement of a village shop was found to be 7.97 kWh/day.

The proposed off-grid PV system required 5 PV module rated 330 W, 5 batteries of 100Ah 12V nominal voltage, charge controller and inverter to power a village shop in Majwanaadipitse. The system capacity of a stand-alone PV system to be installed was 1.6 kWp.

Table 3. shows PV system components required for a proposed stand-alone system it also includes installation cost, maintenance cost, accessories, and total cost of P68 093. The total cost of the system is affordable if Mr. Ontireletse Rebagamang saved money for a year from fossil fuels.

In section 3.6 the amount of emitted pollution into atmosphere was found to be 2882 Kg of carbon dioxide per year. This implies that by installing stand–alone PV system the risk caused by pollution will be minimized.

The Net Present Value was also found to be favorable, showing that it is a profitable investment with a cost of about P653 880. This shows that the costs of the project are outweighed by the benefits because after 2 years, the project will have paid itself back and up to the 25th year shop owner Mr. Ontireletse Rebagamang will enjoy free energy for the shop. The shop owner avoids paying an electric bill of P 1 368 159 over the 25 years by installing a solar PV system.

ISSN: 2521-2293

The payback period of the PV system was estimated to be 2 years, which is shorter than the life span of selected PV modules which is 25 years. The Net Present Value was also found to be positive, showing it's a profitable investment with a value of about P653 880. This is indicated by the fact that the Botswana interest rates fluctuate at around 5.5%, which is always lower than the internal rate of return of the system valued at 50.49%.

5. Conclusion

Compared to the use of fossil fuels, it is concluded that stand-alone PV electricity is technically and economically viable to electrify a store. Majwanaadipitse stand as a best place for installing a PV system, to produce electricity for daily requirements. This is well supported by the fact that it gets plenty of solar energy around 6,211 kWh / kWp per day, making the PV system efficient. The installation of a solar photovoltaic system will therefore go a long way in eliminating the risk of pollution caused by fossil fuels, as it will not release any dangerous gas. By replacing fossil fuel with off-grid PV system after 2 years, the project will have paid itself back and up to the 25th year shop owner Mr. Ontireletse Rebagamang will enjoy free energy. The shop owner will avoid paying an electric bill of P 1 368 159 over the 25 years by installing a solar PV system.

5.1 Future Work

It is recommended that the proposed off-grid PV system to be installed in Majwanaadipitse to open access to others to venture into the use of solar energy. A PV simulator software may be used for verification of results before installing.

Funding: The research received no external funding

Acknowledgement: The work was supported by DR. M. Murape

Author Contributions: D.M. Murape formulated and designed this study, T.T. Osupeng wrote the paper. All authors read and approved the final manuscript.

Conflict of Interest: The author declares no conflict of interest.

Nomenclature

PV = Photovoltaic

E_d = Electrical load

G = Solar irradiation

W_p= Watts peak

DOD= Depth of discharge

DOA = Days of Autonomy

References

1. *Sustainability of Off-Grid Photovoltaic Systems for Rural Electrification in Developing Countries: A Review.* **Feron, Sarah.** 12, 2016, Sustainability, Vol. 8, p. 1.

BIUST Teaching, Research, & Innovation Symposium 2023 (TRDAIS 2023)
Botswana International University of Science and Technology
Palapye, Botswana, 18 - 19 September 2023
ISSN: 2521-2293

Design fabrication and characterization of a solar food dryer for Palapye, Botswana

Paida Muengwa
Davison Munyaradzi Murape
Department of Physics and Astronomy
Botswana International University of Science and Technology, Botswana
mp18000745@studentmail.biust.ac.bw

Abstract

Dehydration is a way to preserve food that may spoil. Drying removes water and thus prevents fermentation or the growth of molds. It also slows the chemical changes that take place naturally in foods as when fruit ripens. People in Botswana and the rest of the world have been drying food for thousands of years by placing the food on mats in the sun. This simple method, however, allows the food to be affected or ruined by dust, airborne molds and fungi, insects, rodents, and other animals. Furthermore, open air drying is often not possible in humid conditions. Solar food dryers represent a major improvement upon this ancient method of dehydrating foods.

This study profiles the design, fabrication and performance evaluation of an indirect cabinet solar dryer. The dryer consists of a separate solar collector that heats up ambient air entering the collector and creates a convectional current that drives warm air into a coupled drying chamber. Food samples comprising tomatoes and apples were used for the performance evaluation of the dryer. The comparison experiment sought to differentiate the performance of the dryer from the largely uncontrolled natural drying i.e., direct sun drying. The results from the experiment showed that the temperature inside the drying chamber was consistently higher than the ambient air temperature. The drying rate of the dryer and percentage moisture loss content were 0.18 kg/hr and 91 % respectively. For natural drying the drying rate and percentage moisture loss were found to be 0.14 kg/hr and 71 % respectively. The dryer revealed its ability to dry products without them losing most of their original color as compared to direct sun drying as well as protecting products from birds, insects, strong winds and being soiled. Some of the open-air dry samples were eaten up by birds.

Keywords: Solar dryer, design, fabrication, drying chamber, food dryer

ISSN: 2521-2293

Introduction

Drying food removes the moisture from the food that may otherwise cause spoilage of the food product. The growth of fungi and molds can also be prevented by drying as this organisms flourish in environments where there is more moisture. Drying also derails the chemical process that lead to the over ripening of fruits and thus increasing the shelf life of the fruits after they are harvested.[1]Over the years individuals and farmers have employed the traditional method of drying surplus grains which is now known as direct open air-sun drying. Although this method as way cheaper and simple it is not very efficient and one cannot rely on it, as it comes with disadvantages and limitations. The shortcomings of this method are that the products being dried are exposed to both wild and domestic animals that may eat the products being dried during the drying period. Insects and pests can also destroy the food being dried as the food is just in an open area and not enclosed. Dust and strong winds also affect the product being dried as strong winds can take the products being dried from the place where they are being dried to different locations. Unexpected rainfall can also derail the drying process as it can lead to reabsorption of moisture by the products. It is also time consuming as it needs close monitoring which most people living in the 21^{st} century do not have. Solar food dryers were an improvement that was done to this already existing method of drying. The only problem with solar food dryers is that they require a very low amount to fabricate as compared to the direct open air sun drying which does not require any expense. The cost is worth it though as solar dryers dry food products at a much higher rate than open air drying, solar dryers also produce food that are more appealing to the human eye and they provide an enclosure for the food being dried thus protecting the food from external damage . Additionally solar dryers produce food with a higher nutritional value and better tasting food s compared to open air. Because this food dryers use solar energy they contribute significantly in the conservation of non-renewable energy resources. Because the drying takes a shorter time there is very little room for spoilage. [2] The storage required after drying is cheaper than refrigeration. Storage requires protection from the growth of molds and fungi. Additionally, Botswana lies in a region that receives high solar irradiance, enough to provide adequate energy for solar drying [3]. Solar energy is cleaner, cheaper and more environmentally friendly compared to use of gas, oil and in some cases firewood. A well-designed solar food dryer could convince local farmers to embrace this largely proven but shunned technology. The aim of this project is to design, fabricate and characterize a solar food dryer to be used in Botswana. We hope that the test results will be positive and form a basis for which solar dryer technology will be promoted.

The specific objectives of this paper were to:

- design a natural convection solar food dryer
- fabricate the designed solar food dryer
- test and compare the solar food dryer with traditional open air sun drying

Dryer design:

Design considerations

The following points were taken into consideration for the design of the dryer.

1. Solar dryer to be used on a small scale (prototype)

ISSN: 2521-2293

2. Ability to exclude dust and foreign particles from product
3. Natural convection solar dryer
4. Ability to reduce moisture

Description:

A shelf type dryer with a separate solar collector and a drying chamber is the dryer that is going to be designed. The dryer will consist of three main components being:

- The solar energy collector
- Drying chamber
- Drying trays

The solar collector consists of the cover plate and the absorber plate that are discussed below.

Cover plate

This will be a 4mm thick glass that will collect the incident solar rays. Glass allows close to 90% of visible light to pass through which will ensure that the absorber plate absorbs maximum radiation that hits the collector. The glass also traps the heat inside the collector region and thus reducing heat loss to the ambient as glass is a very good insulator.

Absorber plate

It is an aluminum sheet of 1mm thickness painted black to absorb the incident solar radiation transmitted by the cover plate thereby heating the air between it and the cover. The aluminum sheet will be used because it is a very good absorber and emitter of heat. The distance between the absorber plate and the cover plate is 40 mm for proper heating of incoming air. [20]

Drying chamber

The drying chamber will be made using plywood which will be painted and vanished in order to avoid termite attack and damage from rain. The inside of the drying chamber will be insulated by aluminum foil to minimize heat loss by radiation. The drying chamber will house the drying trays which will be made from chicken wire mesh which is porous to allow heat from the absorber plate to pass through the food products being dried easily. Two drying trays made from wire mesh with wood frame will be housed in the drying chamber. The drying chamber will have a chimney with an internal diameter of 90 mm that will aid in the removal of air from the drying chamber. The chimney will be made from aluminum sheet with a height of 200 mm.

Design features of the solar dryer

The solar dryer is composed of two sections, the drying chamber which is the first section has the shape of a home cabinet and the flat collector which is the second section, is tilted to the North, the angle of the slope is 22.55˚ as stated that the best orientation for a solar collector in the southern hemisphere is due north and the best tilt angle is equal to its latitude [21] where the latitude of Palapye is 22.55˚. The solar collector has two openings, the inlet vent at the front and outlet vent at the back. The outlet vent is located at a high level while the inlet at a lower level

ISSN: 2521-2293

just at the opening of the solar collector. The flow of air is natural flow since hot air is less dense than cold air, so cold air will enter the solar collector through the air inlet and get heated then flows into the drying chamber. Figure 1 below shows schematic sketch of the dryer.

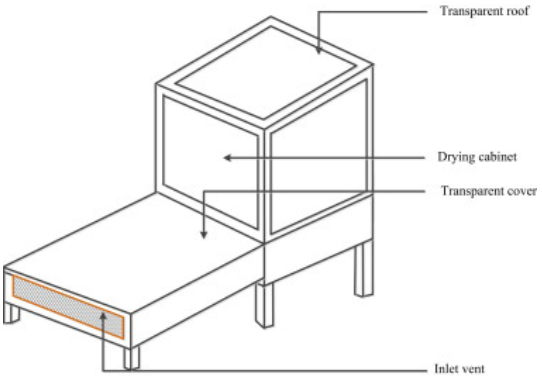

Figure 1: sketch of proposed solar dryer [22]

Design calculation and analysis:

1. Energy balance on the absorber

[17] States that energy absorber balance on a solar collector is found by equating the total heat gained to the total heat lost by absorber in the solar collector hence,

$$IA_C = Q_u + Q_{Cond} + Q_{conv} + Q_R + Q_P \quad (1)$$

Where: I = rate of total radiation incident on the absorber's surface (Wm^{-2});
A_C= collector area (m^2)
Q_U = rate of useful energy collected by the air (W);
Q_{cond} = rate of conduction losses from the absorber (W);
Q_{conv} = rate of convective losses from the absorber (W);
Q_R= rate of long wave re-radiation from the absorber (W);
Q_{p}= rate of reflection losses from the absorber (W).

Q_R, Q_{cond} and Q_{conv} are always combined into (Q_{L}), thus

$$Q_{\text{L}} = Q_{Cond} + Q_{conv} + Q_R \quad (2)$$

$$IA_C = \tau I_T A_C \quad (3)$$

Where: τ is the transmittance of the top glazing
I_T = total solar radiation incident on the top surface.

The expression for the reflected energy from the absorber is given by:

$$Q_{\text{p}} = \rho\tau\, I_T A_C \quad (4)$$

Where ρ is the reflection coefficient of the absorber
If we substitute equations (2), (3) and (4) into equation (1). We get

ISSN: 2521-2293

$$\tau I_T A_C = Q_{\mathrm{u}} + Q_{\mathrm{L}} + \rho\tau I_T A_C \quad (5)$$

Or we can write it as:

$$Q_{\mathrm{u}} = \tau I_T A_C (1 - p) - Q_{\mathrm{L}} \quad (6)$$

We know that for an absorber $(1 - \rho) = \alpha$

Where α is solar absorptance.

Therefore

$$Q_{\mathrm{u}} = (\tau\alpha) I_T A_C - Q_{\mathrm{L}} \quad (7)$$

2. Tilt and orientation of solar collector

Angle of orientation (β) = latitude of Palapye = 22.55° and orientation is due north.

3. Determining Collector Area and air vent dimensions.

The air vent was calculated by dividing the volumetric airflow rate by wind speed:

$$A_V = \frac{V_a}{V_w} \quad (8)$$

Where

V_a=Volumetric airflow rate

A_V = the area of the air vent, m^2,

V_w = wind speed, m/s.

The value used for the wind speed was 0.2 kilometers per hour as this was the average value of the wind speed forecasted for the month of May 2022 which was the duration of the drying period. This information was obtained from [23]

The expression for the width of the air vent is:

$$B_V = \frac{A_V}{L_V} \quad (9)$$

Where B_V is the width of air vent, *m*.

L_V = The length of air vent, *m*

Collector area

The collector area was determined by the dimensions of the glass cover that were found available at the local supplier and this was 1000 mm x 800 mm.

4. **Collector efficiency**:

[17]States that the collector efficiency is calculated using the formula:

$$\eta = \frac{\rho C_p V \Delta T}{A_C} \quad (10)$$

Where (ρ) is the density of air (kg/m^3),

(I_C) = the insolation on the collector,

(Δ) = the temperature elevation,

(C_p) = the specific heat capacity of air at constant pressure (J/kg K),

(V) = the volumetric flow rate (m^3),

ISSN: 2521-2293

(A_C) = the effective area of the collector facing the sun (m^3).

5. **Dryer rate**: This is given as:

$$\eta d = \frac{ML}{\Delta t} \quad (11)$$

(ML) = change in mass of the crop,

(Δt) = the time of drying.

6. **Moisture Content (M_C):** The moisture content is given as:

$$M_C = \frac{M_i - M_f}{M_i} \quad (12)$$

M_i = mass of sample before drying and

M_f = mass of sample after drying.

7. **Moisture loss M_L**:

$$M_L = (M_i - M_f) \quad (13)$$

M_i = the mass of the sample before drying

M_f = the mass of the sample after drying.

8. **The heat gained by the airQ_G**:

$$Q_G = M_a C_{pa}(T_c - T_a) \quad (14)$$

Where:

M_a = Mass of air leaving the dryer per unit time (kgs^{-1})

C_{pa} = specific heat capacity of air($KJKg^{-1}K^{-1}$)

9. **Percentage moisture loss**:

$$\%M_c = \frac{ML}{M_i} \times 100 \quad (15)$$

Where:

$\%M_c$ = percentage moisture loss

ML= change in mass of dried product

M_i= initial mass of dried product

Reference is made to [24]

ISSN: 2521-2293

Fabrication

Fabrication of the solar dryer was outsourced from a local manufacture. Figures 3-6 show the....

Figure 3: drying tray

Figure 4: solar collector

Figure 5: drying chamber

Figure 6: solar dryer

Experimental set-up and procedure:

ISSN: 2521-2293

Two specimens were chosen at random for the experiment. The chosen specimen were apples and tomatoes. The two products were washed with distilled water and wiped using paper towel. The tomatoes were cut into 10 slices of 3mm thickness as this is the recommended thickness by [19]. The apples were also cut into 10 slices of 3mm thickness. The two specimen were then labelled and weighed, the initial mass was recorded. The weighing of the specimen was done using an electronic digital balance with an accuracy of 0.01g. The tomatoes and the apples were separated into two groups with 5 slices each. 5 slices from both the specimen were collected and put into the drying chamber of the solar dryer. The remaining slices of the apples and tomatoes were laid flat on a card box for direct solar drying. When drying commenced the hourly changes of mass of the products were recorded until there was no change in mass and the duration for drying noted. The data from the variation of mass was used to plot the graph of mass loss against time .A temperature data logger with two temperature probes was used to measure the hourly variation of temperature inside the drying chamber and outside the drying chamber. The hourly variation of temperature was recorded and used to plot a graph titled hourly variation of temperature inside and outside the dryer. The color of the specimens before drying and after drying was observed and noted. A total of 4 parallel experiments were undertaken and the average from the experiments used for result and analysis.

Results discussion:

- **Temperature comparison:**

The graph below show that the ambient temperature (in blue) will always be lower than the temperature inside the drying chamber (red). That is to say at any given point in time the temperature that is drying the products inside the solar dryer will be greater than the temperature drying products outside the drying chamber, i.e. direct solar drying temperature. [24] States that drying rate of the products is directly proportional to the temperature drying the products. This graph goes to show that solar dryer drying uses a higher temperature and is therefore likely to be more effective and efficient than direct sun drying.

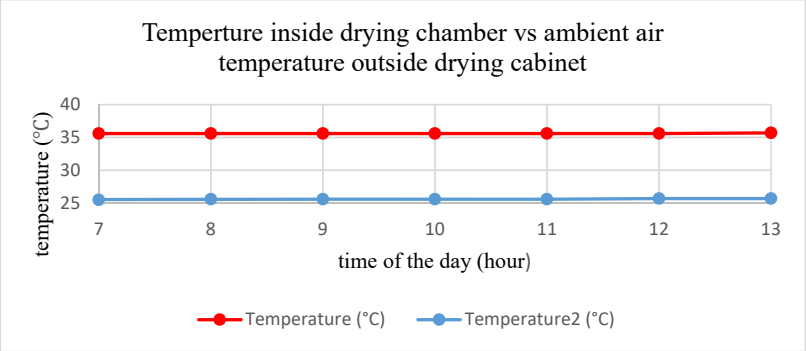

Figure 7: Graph of temperature comparison

- **Mass loss in the solar dryer and outside solar dryer:**

ISSN: 2521-2293

The graph below show variation in mass loss of the samples in the dryer and in the direct sun. The graph shows that more mass was lost in the dryer than in the direct sun at any given time. This shows that the solar dryer is more effective than direct sun drying in terms of mass loss per given time. The graph shows that after 48 hours there was no change in mass in the product in the dryer while there was still change in mass in the product in the direct sun, this tells that the drying time of the solar dryer is shorter than the drying time in the direct sun.

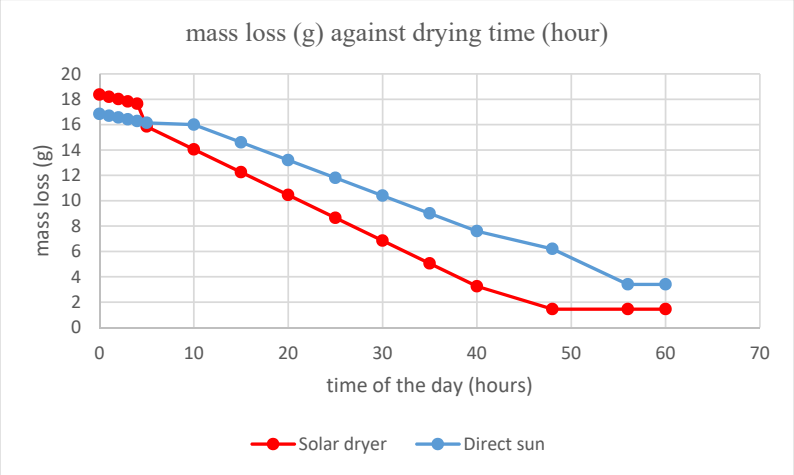

Figure 8: a typical variation of mass loss in the dryer and direct sun with respect to time

- **Drying rate and percentage moisture loss:**

Since there are 5 specimens, the average change in mass was calculated and used to determine the drying rate of both methods.

$$\eta d = \frac{ML}{\Delta t}$$

Where; ML = change in mass of dried product

Δt = time taken to dry crop

- **Drying rate for solar dyer**

$$\eta d = \frac{8.73\ g}{48 hours}$$

$$\eta d = 0.18\ g h^{-1}$$

$$\eta d = 0.18\ \times 10^{-3} kg h^{-1}$$

- **Drying rate for direct sun drying**

$$\eta d = \frac{7.94\ g}{56\ hours}$$

$$\eta d = 0.14\ g h^{-1}$$

ISSN: 2521-2293

$$\eta d = 0.14 \times 10^{-3} kgh^{-1}$$

The above results show that the drying rate of the solar dryer is higher than the drying rate of the direct sun drying method.
The percentage moisture loss for both methods was also calculated using the average data from the samples used in the experiment. The formula below was used

$$\%M_c = \frac{ML}{M_i} \times 100$$

Where: $\%M_c$ = percentage moisture loss
ML= change in mass of dried product
M_i= initial mass of dried product

- **Percentage moisture loss for solar dryer**

$$\%M_c = \frac{8.73g}{9.61} \times 100$$
$$M_c = 91\%$$

- **Percentage moisture loss for direct sun**

$$\%M_c = \frac{7.94\ g}{10.64} \times 100$$
$$M_c = 76\ \%$$

Color comparison of solar dryer dried product and direct sun dried:

- **Color comparison in apples**

One of the most easily spotted and distinguishing features that attracts the customers is the color or the overall physical appearance of the product or fruit they are purchasing. Figure 9 shows the color comparison of fresh, solar dryer dried and direct sun dried apple specimen from right to left respectively.

Figure 9: fresh, solar dryer dried and direct sun dried apple

The color difference from Figure 9 shows clearly that products dried by the solar dryer retain their color and they are more appealing to the human eye than products that are dried directly by

ISSN: 2521-2293

the sun. This is because products dried by the traditional open air drying are exposed directly to the sun ultraviolet rays. Direct solar drying leads to the sudden rise of the internal temperature of the fruit leading to damage to the tissues inside the product being dried, in our case apples hence the color of the direct sun dried apples was darker than the solar dryer dried apples which were not exposed to direct solar rays.

- **Color comparison in tomatoes.**

Figure 6 shows that the tomatoes in the solar dryer retained their most important feature, lycopene which is responsible for the darkening of the tomato i.e., the red pigmentation. The other tomato on the left from direct solar air drying shows low levels of lycopene and an overall dull appearance.

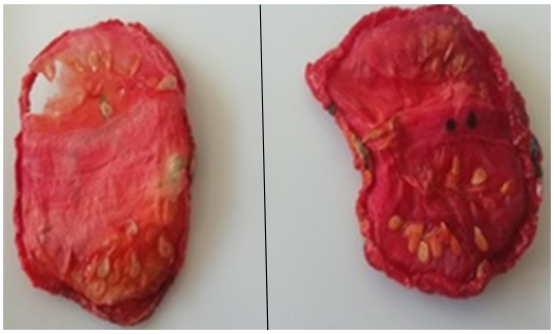

Figure 10: sun dried on the left and solar dryer dried on the right

Attack by animals:

The figure below shows some of the damages that were done by animals during and after drying. The picture on the bottom far right in Figure 11 shows apple specimens that were attacked by birds during drying. This on its own shows just how direct sun drying is not as conservative and reliable compared to solar dryer drying were the products being dried are enclosed in a drying chamber.

Figure 11: From the left, specimen before drying, after drying and apples after drying.

Figure 11 also goes to show how all the specimens that were being directly dried on the third trial of the experiment were all eaten by birds and insects. This shows that solar dryers are

ISSN: 2521-2293

needed to protect the products being dried from predators as all products being dried by the solar dryer were not attacked by any predator or animals.

Conclusion:

The project was a success and all the objectives of the project were accomplished. The hypothesis of the whole project was proved to be right by the results obtained from the experiment.

The results obtained from the experiment are:

It is easy to monitor the drying of the solar dryer compared to natural drying.

Solar dryer drying protects the products from animals and wind.

The drying rate of the solar dryer was found to be $0.18 \times 10^{-3} kgh^{-1}$ while the drying rate of direct sun was$0.14 \times 10^{-3} kgh^{-1}$.

Overall the mass loss was faster in the solar dryer than for direct sun drying. Percentage moisture loss was 91% in a period of 48hrs for tomatoes and apples in the solar dryer and 76% for direct sun drying for a period of 56 hours for the same fruits.

The loading capacity of the dryer was 500 g per tray making a total of 1kg since it had 2 trays.

The temperature in the dryer was found to be high as compared to direct sun drying.

Recommendation:

The department of physics should have more equipment's so that the students can be able to measure different parameters that are needed for evaluation of the results and collecting some results. Equipment like the food spectrometer, a contrast color analyzer (TPGI) etc.

More can be done to compare the two methods like people testing the dried samples.

Another area of improvement is the possibility of having energy storage capability of the solar dryer to improve its performance.

Reference:

[1] R. G. Gregoire, "Understanding solar food dryers," United States, 1984.

[2] P. Roger G. Gregcire, *UNDERSTANDING SOLAR FOOD DRYERS,* Virgina: Volunteers in Technical Assistance (VITA), 1984.

[3] Koketso Mosalagae,Davison M. Murape, *Potential for solar dryer application for food,* Gaborone,Palapye, 2017.

[4] A. e. a. Sridhar, "Food preservation techniques and nanotechnology for increased shelf life of fruits, vegetables, beverages and spices: a review," *Environmental Chemistry Letters,* vol. 19, no. 10, pp. 1715-1735., 2020.

[5] E. D. V. Belessiotis, "Solar drying," *solar energy,* vol. 85, no. 8, pp. 1665-1691, 2011.

[6] S. K. B. R. H. &. S. G. D. Gupta, "Gupta, S. K., Bhawalker, PERFORMANCE STUDY OF SOLAR DRYERS. In Passive and Low Energy Alternatives," *Pergamon.,* pp. 8-14, 1982.

ISSN: 2521-2293

[7] A. S. S. &. T. N. Hande, "Open-Air Sun Drying of Kokum (Garcinia indica) Rind and Its Quality Evaluation.," *Agricultural Research,* no. https://doi.org/10.1007/s40003-016-0229-3, pp. 373-385, 2016.

[8] Meekeetza, "| Dreamstime.com," [Online]. Available: https://www.dreamstime.com/stock-photo-open-air-drying-fish-spitsbergen-svalbard-oldest-traditional-way-preserving-was-to-let-wind-sun-dry-image53785787. [Accessed 04 07 2022].

[9] V. C. V. R. V. M. Abhay Bhanudas Lingayat, "A review on indirect type solar dryers for agricultural crops – Dryer setup, its performance, energy storage and important highlights," *Applied Energy,* vol. 258, pp. 0306-2619, 2020.

[10] S. S. M. C. S. Y. a. Suraj Pathak, "Solar Food And Seed Dryer," EasyChair Preprint, 2020.

[11] J. D. e. a. (2020)., " Energy Educatio. Nuclear fusion in the Sun [Online]," 2020. [Online]. Available: https://energyeducation.ca/encyclopedia/Nuclear_fusion_in_the_Sun. [Accessed 5 7 2022].

[12] C. Grigg, "The Science of the Sun," [Online]. Available: https://www.mrsd.org/cms/lib/NH01912397/Centricity/Domain/245/the%20science%20of%20the%20sun.pdf. [Accessed 1 May 2022].

[13] S. Ashok, "solar energy," *Britannica,* 2021.

[14] G. O'Brien, "Astronomy with Georgia O'Brien," [Online]. Available: https://sc663he-go.weebly.com/the-sun.html. [Accessed 5 7 2022].

[15] E.-. A. O. M. A. A. I.-F. A. A. W. Luecke, *Design and Construction of A Solar Dryer for Mango Slices.*

[16] O. A. K. a. M. F. A.O. Fagunwa, "Development of an Intermittent Solar Dryer for Cocoa," *International Journal of Engineering Research & Technology,* vol. 2, no. 1, pp. 2278-01816, 2013.

[17] B. O. B. a. A. P. Olalusi, "Performance Evaluation of a Mixed-Mode Solar Dryer," vol. 11, no. 4, pp. 225-231, 2008.

[18] M. M. P.Chandrasekar., *Drying of copra in a forced convection solar drier,* New Delhi: Pollachi-642003,, 2007.

[19] H. K. WEEFAR, *DESIGN, CONSTRUCTION, AND PERFORMANCE EVALUATION OF A SOLAR,* Abuja: African University of Science and Technology , 2017.

[20] D. Ajadi, "Determination of optimum distance between glass cover and absorber plate of a solar dryer," *Medwell journals,* vol. 3, no. 2, pp. 246-250, 2007.

[21] D. I. Ekadewi A. Handoyo, "The optimal tilt angle of a solar collector," *Energy Procedia ,* vol. 32, pp. 166-175, 2013.

ISSN: 2521-2293

[22] S. M. R. S. A.G.M.B. Mustayen, "Performance study of different solar dryers: A review,," *Renewable and Sustainable Energy Reviews,,* vol. 34, no. 1364-0321, pp. 463-470, 2014.

[23] J. N. K. James Diebel, "Weather Spark [Climate and Average Weather Year Round in Palapye]," Cedar Lake Ventures, Inc., [Online]. Available: https://weatherspark.com/y/94222/Average-Weather-in-Palapye-Botswana-Year-Round. [Accessed 6 6 2022].

[24] A. S. O. I.N. Itodo, "Evaluation of a solar crop dryer for rural applications in Nigeria," *Botswana Journal of Technology,* vol. 11, no. 2, pp. 58-62, 2011.

[25] D. D. Rooij, *Solar Panel Angle: how to calculate solar panel tilt angle?,* Shanghai, China, 2009.

[26] E. Matlotse, "A Multidisciplinary Examination of Solar Power in Botswana," Gaborone, 2016.

[27] N. N. P.V.C. Luhanga, "Investigation of solar radiation in Botswana and some anomalous phenomena observed," *Renewable Energy,* vol. 12, no. 4, pp. 401-408, 1997.

BIUST Teaching, Research, & Innovation Symposium 2023 (TRDAIS 2023)
Botswana International University of Science and Technology
Palapye, Botswana, 18 - 19 September 2023
ISSN: 2521-2293

Correlation analysis of tonnage and cost factors for productivity management: an open pit mine case study

Nonduduzo B. Mamba
Department of Mining and Geological Engineering
BIUST
Palapye, Botswana
nonduduzo.mamba@studentmail.biust.ac.bw

Desmond B. Munyadzwe
Department of Mining and Geological Engineering
BIUST
Palapye, Botswana
desmond.munyadzwe@studentmail.biust.ac.bw

***Abstract*— Correlation analysis is a data interpretation tool that draws inferences between two or more variables. Mine dispatch systems produce massive amounts of data that requires interpretation in order to identify contributing factors to both tonnage and cost losses. These losses are analysed to identify the significance of factors that contribute to these losses. Such factors as: loading rate, daily tonnage and truck loads, particle size distribution, fuel costs, labour costs, tyre costs, repairs and maintenance etc. For each analysis, the R (correlation coefficient) parameters were determined to classify the significance of each loss factor. A scatter graph was generated to determine the correlation factors for each key performance indicator (KPI) and corresponding loss. The scatter graphs illustrated the strength, direction, correlation coefficient and association of the relationship between the two variables. This analysis was run using data from an open pit mines' January 2021 to October 2021 production reports sourced from the mine's Modular Dispatch System. The analysis showed that labour costs and tyre costs both had the highest correlation factor of 1 when inferred to total mining costs, meaning they were the most significant contributors to mining costs and could contribute greatly to financial losses. Loading rate had the highest correlation factor (0.7147) out of all the other factors inferred to tonnage losses. The results showed the importance of correlation as a tool to reveal information about the root causes of productivity losses.**

***Keywords*— tonnage losses; cost losses; correlation**

I. INTRODUCTION

Data interpretation requires drawing inferences regarding the association between two or more variables, this is termed correlation. Statistical analysis methods can be used on data produced by mine dispatch systems to identify the contributing factors to tonnage and financial losses. In this case the inference is between the productivity key performance indicators (KPIs) with the associated losses or factors. Tonnage and cost factors are analysed to identify the significance of major contributors to costs and tonnage losses. These factors include loading rate, daily tonnage and truck loads, particle size distribution, fuel costs, labour costs, tyre costs, repairs and maintenance etc.

A. Key performance indicators

KPIs are used to standardise performance measurement. Tonnage and costs are studied as key performance indicators in materials handling processes. The equations used to calculate factors in each of the indicators are also established.

B. Tonnage

Tonnage is an important KPI in mining because it reflects the amount of work done by machinery and operators. Tonnage per given time as a performance indicator is mainly affected by fragmentation quality, loading techniques and operator skills[1]. Among the factors, the degree of fragmentation is usually quantitatively reported to express muck pile performance. The dig rate and loadability are the main parameters used to indicate fragmentation impact on load and haul performance [1]. Dig rate is measured by the percentage of particle size in range, the range of which is determined by the equipment that will be used for the load and haul operations. Loadability is measured by the loading rate expressed as tons per hour as shown in equation 1. It is difficult to express other factors quantitatively, but operator skill is usually loosely expressed as truck loads per ton.

$$\text{Loading rate} = \frac{Material\ moved}{Time\ taken\ to\ move\ the\ material} \quad (1)$$

C. Costs

Mining costs affect productivity and in turn, distribution of costs is affected by the production inputs. According to reference [2] , a capital-intensive mine has the cost of operating machinery being higher than labour costs. Conversely, a labour-intensive mine has higher labour costs. Reducing the mining cost is a direct goal to reduce the total production cost and increase the mine's profitability. It is important to ensure that minimum resources are utilised to achieve maximum results in order to achieve high productivity. Therefore, limiting the working time of employees or machinery reduces costs, increasing both productivity and profitability [3]. This might increase worker morale and wellbeing due to short working hours and reduce machine downtimes, but it can also drop the workers morale

ISSN: 2521-2293

due to less remuneration and reduce machine utilisation as these factors also affect productivity [4].

D. Correlation analysis

Reference [5] defines correlation as a way of denoting the association between two quantitative variables based on a linear relationship between the variables. The result of a correlation analysis is a correlation coefficient which is a single value or number which establishes a relationship between the two variables. These values generally range from -1 to +1. For analysis, the Karl Pearson's product moment correlation coefficient, r is utilised. Where r is calculated as in equation 2.

$$r = \frac{n\sum xy - \sum x \sum y}{\sqrt{\left\{n\sum x^2 - (\sum x)^2\right\}\left\{n\sum y^2 - (\sum y)^2\right\}}} \qquad (2)$$

where: y = variable 1

x = variable 2

Three assumptions used as the basis for the establishment of the Pearson's correlation coefficient are:

- The relationship is linear;
- Variables are independent of each other;
- Variables are normally distributed.

The correlation coefficient can further be interpreted and the relationship between the variables placed in perspective through a spectrum of the correlation coefficients as illustrated in Fig. 1. A correlation coefficient of +1 indicates that the two variables are perfectly related in a positive manner, a correlation of -1 on the other hand indicates that two variables are perfectly related in a negative manner, while a correlation coefficient of zero indicates that there is no relationship between the two variables being studied (Gotgay and Thatte, 2017). This statistical measure is integral in productivity management because inference is important when interpreting data.

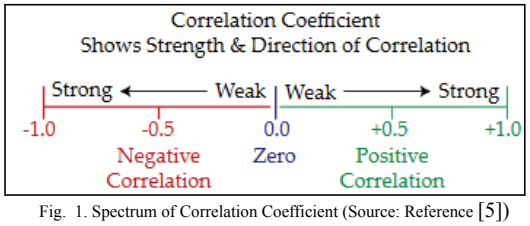

Fig. 1. Spectrum of Correlation Coefficient (Source: Reference [5])

II. OBJECTIVES OF RESEARCH

The objectives of this research paper are to firstly analyse different tonnage and cost factors to identify their significance as major contributors to costs and tonnage losses, and then run correlation analysis between the productivity key performance indicators (KPIs) and the associated tonnage and financial losses.

III. RESEARCH METHODOLOGY

Firstly, the general productivity KPIs were classified into tonnage and cost indicators. These indicators are the availability, utilisation, production rate, tonnage and mining costs. The trend of each indicator was analysed using line graphs, bar charts and stacked charts. Secondly, correlations between the losses and KPIs were then determined. The data used was obtained from January 2021 to October 2021 open pit mine production reports compiled from Modular Dispatch system..

The data was collected from databases as Excel files. The data was processed firstly in Microsoft Excel to sort, classify, analyse and interpret the data. The output data from Excel was inputted into R-software to ascertain the correlation for analysis. For each analysis the R (correlation coefficient) was determined.

IV. DATA ANALYSIS

The degree of correlation between the data sets was calculated from the data for each of the identified function parameters. Pearson's correlation factor analysis was run using Microsoft Excel and verified using R software.

A. Key performance indicators trend

The data collected from the Modular Dispatch System was analysed to find the production trends of the mine before analysing the details of productivity management.

Tonnage indicator

The tonnage produced reflects the performance equipment and workforce in a given period. The tonnage produced over a period of 10 months was studied. The results are shown in Fig. 2. It shows that there were wide fluctuations in production from January to October and the trendline shows a general slight declining trend with a gradient of -0.0456 over the period. The lowest value reported was 0-tonnes in May and highest value of 248,000 tonnes in March.

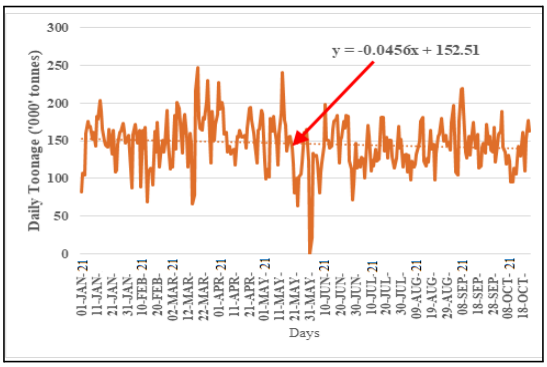

Fig. 3. Line Graph of daily material loaded for January - October 2021

ISSN: 2521-2293

Cost indicator

Mining costs have been classified into 5 groups namely labour, repair and maintenance, business expenses, fuel and tyres. Fig. 3 shows the trend of mining costs and the contribution of each type of cost to the total cost over time. The total mining cost declined from January to December (i.e., from BWP 3,552,150.05 to BWP 3,508,605.12). The contribution of each type of cost also varied with business expenses with the highest value of BWP 15,111,095.20 to tyres with the lowest value of BWP 1,868,330.64. Repairs and maintenance cost contributed the highest amount of BWP 1,383,037.54 from January to June and business expenses was the highest at BWP 1,784,257.93 from July to December.

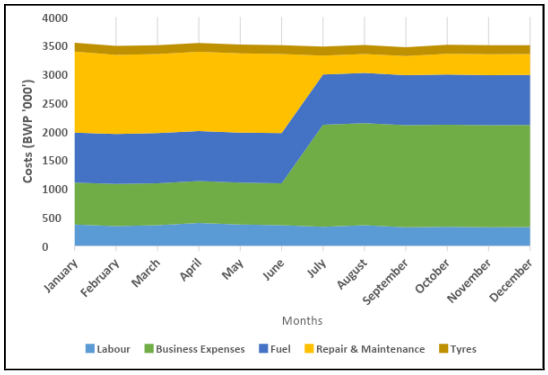

Fig. 3. Stacked graph of trend of mining costs in 2021

B. *Correlation analyses*

Pearson's correlation analysis was run in Microsoft Excel. The results are shown in scatter graphs and the correlation coefficient reported for each graph.

Tonnage correlation

Factors affecting tonnage were correlated with tonnage to find their linear relationship, and the results shown in scatter graphs.

Daily tonnage and loading rate correlation

The scatterplot of daily tonnage against loading rate is shown in Fig. 4. The strength, the form, the direction, correlation coefficient and the association of the relationship between the two variables are shown in the graph. The plot shows a strong significant relationship having points that strongly resembled a straight line as indicated by the concentration of points along the trend line.The loading rate and daily tonnage are strongly positively correlated with a correlation coefficient of 0.7147.

Correlation between daily tonnage and truck loads

Shown in Fig. 5 is a scatter plot of daily tonnage against the number of truck loads. It shows that there is a very strong correlation between the two variables. The plot shows a statistically significant relationship having points that strongly resembled a straight line as indicated by the concentration of points along the trend line. The slope of the trendline is close to 45°, meaning that as the value of the daily tonnage increased, there was a corresponding increase in the number of truck loads. It is important to note that there was a positive outlier which could have a strong impact on the correlation coefficient. The value of the correlation coefficient, measured as 0.4122 (including the outlier), indicates a positive linear relationship with a weak strength between the daily tonnage and truck loads.

Particle size distribution and loading rate correlation

A plot of particle size distribution of the muck pile against the loading rate produced the scatter graph shown in Fig. 6. With the limited data points, it is hard to detect any relationship between the two variables. The correlation coefficient of 0.5082 signifies a moderate strength relationship.

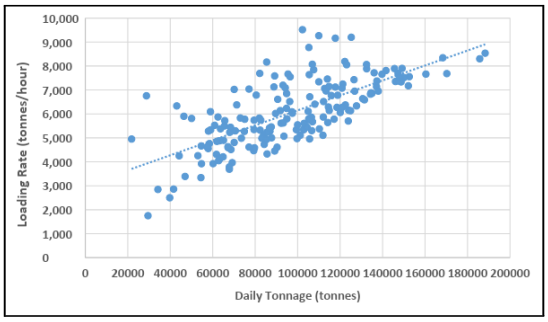

Fig. 4. Scatter graph for daily tonnage and loading rate

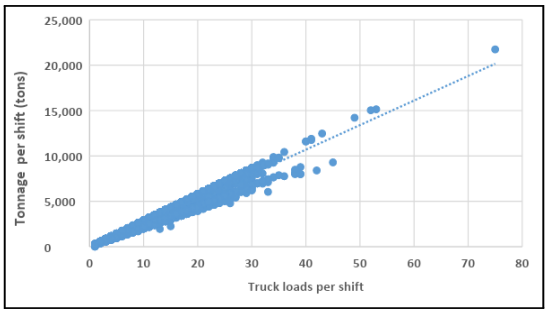

Fig. 5. Scatter graph for tonnage and truck loads

ISSN: 2521-2293

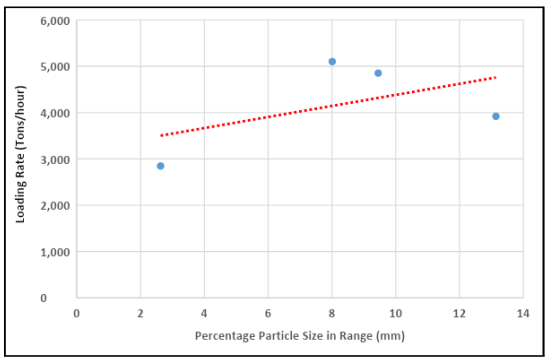

Fig. 6. Scatter graph of particle size and loading rate

Costs correlation

Categories of mining costs were correlated with total mining costs to find their linear relationship, and the results shown in scatter graphs.

Mining labour costs and total mining costs

Fig. 7 is a scatter plot of the mining labour costs against the total mining costs. It shows a linear positive association with correlation coefficient of 1.0000 which shows a perfect strong linear relationship between mining labour costs and total mining costs.

Mining business expenses and total mining costs

Fig. 8 is a scatter graph of mining business expenses against the total mining costs. It shows a negative relationship between them i.e. as the total mining costs decrease, the mining business expenses increase. The scatter graph slope was moderately dipping having equal number of points both below and above the trend line. The measured correlation coefficient is 0.9998 which shows a very strong linear relationship between the two parameters.

Mining fuel costs and total mining costs

A scatter plot of the total mining costs against the mining fuel costs is shown in Fig. 9, with points forming a vertical straight line, showing that the mining fuel costs were constant while the total mining costs increased. This shows that there is neither a positive nor a negative association between the two parameters. The correlation coefficient is 0.9906 which shows a very positive linear relationship between the two variables.

Repair and maintenance costs and total mining costs

Fig. 10 is a plot of the total mining costs against mining repair and maintenance costs. The data points are scattered in small clusters at the beginning and end of the trend line. The correlation coefficient is 0.9815 which shows a very strong relationship between the total mining costs and the mining repairs and maintenance costs.

Mining tyre costs and total mining costs

Fig. 11 is total mining cost versus mining tyre costs. The data points are clustered at almost the same point. This indicates that there is little or no linear relationship between mining costs versus mining tyre costs. The computation of the correlation coefficient gave a value of 1.0000, which clearly indicated a perfect strong relationship between the two variables.

Fig. 7. Scatter graph of mining labour costs and total mining costs

Fig. 8. Scatter graph of mining business expenses and total mining costs

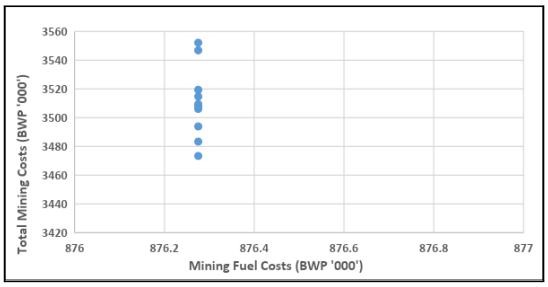

Fig. 9. Scatter graph of mining fuel costs and total mining costs

ISSN: 2521-2293

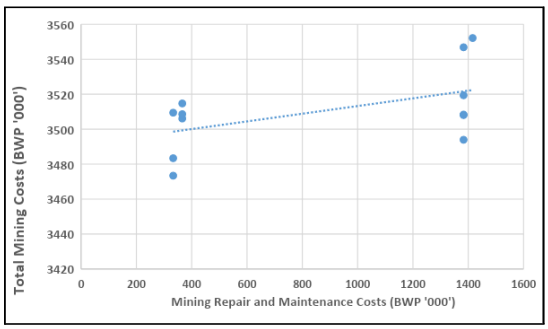

Fig. 10. Scatter graph of mining repair, maintenance costs and total mining costs

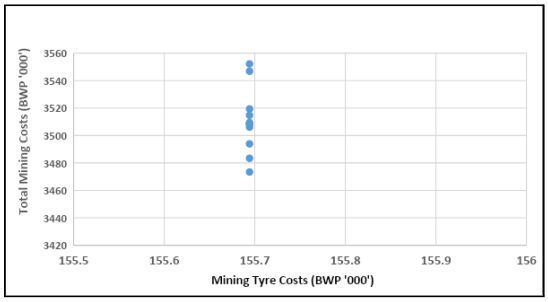

Fig. 11. Scatter graph of mining tyres costs and total mining costs

V. CONCLUSION

In this study, statistical methods were used to identify and analyse major tonnage and cost losses in an open pit mine. The parameters identified for analysis included loading rate, daily tonnage, degree of fragmentation (particle size distribution), labour costs, business expenses, fuel costs, repair and maintenance costs, and tyre costs. The Pearson correlation factors and R-values which measure the degree of relationship between data are sets were calculated from the data for each of the identified objective function parameters. All graphs showed a strong correlation with correlation coefficients ranging from 0.7147 to 1. The value of 1 clearly indicated a perfect strong relationship between the two variables. Labour costs and tyre costs both had the highest correlation factor of 1 when inferred to total mining costs, meaning they were the most significant mining costs and could contribute greatly to financial losses. Loading rate had the highest correlation factor (0.7147) out of all the other factors inferred to tonnage losses. The results showed the importance of correlation as a tool to reveal information about the root causes of productivity losses.

REFERENCES

[1] Beare, M. (2011). "Costcutters: Efficiency and Productivity in Mining", www.mining-technology.com/features/featurecostcutters-efficiency-and-productivity-in-mining. (Accessed: 14th March, 2022).

[2] Gogtay. N. J., Deshpandes. S., Thatte. U. M, (2016). Principles of Correlation Analysis. Journal of the Association of Physicians of India. Vol. 65, pp.78-81

[3] Khorzoughi, M. B. & Hall, a. R., (2016). A Study of Digging Productivity of an Electric Rope Shovel for Different Operators. Minerals, VI (1), p. 48.

[4] Sloan, D. A. (2013). Mine Management, Springer Science and Business Media, London, pp. 27.

[5] Walters, J. (2010). Positive Management: Increasing Employee Productivity. 2nd ed. Business Expert Press, Atlanta, pp. 54.

BIUST Teaching, Research, & Innovation Symposium 2023 (TRDAIS 2023)
Botswana International University of Science and Technology
Palapye, Botswana, 18 - 19 September 2023
ISSN: 2521-2293

GREEN SYNTHESIS OF COPPER OXIDE NANOPARTICLES USING MORULA LEAF EXTRACT AND THEIR APPLICATION IN ADSORPTION OF DYE.

T. Khao[1], *S. Odisitse*[1] *and C. K. Kingóndu*[1]

[1]Chemical and Forensic Sciences, Botswana International University of Science and Technology, Private Bag 16, Palapye, Botswana

ABSTRACT

Morula leaf extract was examined in the synthesis of Copper Oxide (CuO) nanoparticles in this study. The active morula agents are extracted using boiling water followed by hydrothermal treatment with the metal oxide precursors to synthesize the metal oxide nanoparticles. There were no other hazardous substances used apart from water which is considered to be green. X-ray diffraction (XRD) analysis showed that pure and crystalline structures of CuO were fully formed after calcination at 350 °C. CuO was determined by the doublet peak between 200 and 400 cm^{-1} using Raman spectroscopy. Scanning electron microscopy (SEM) and Brunauer–Emmet–Teller (BET) analysis were used to analyze the structural morphology and the adsorptive behaviour of the materials, respectively. Through these two methods, platelets were discovered in CuO and the material was discovered to have larger surface areas of 26.8 m^2/g.

CuO material was then applied in the adsorption of dyes. It was observed that methylene blue (MB) and rhodamine 6G (R6G), adsorb well onto CuO material in an adsorption process. CuO has a maximum adsorptive efficiency of 78 %.

Keywords: Green synthesis, morula leaf extract, adsorption, wastewater

I. INTRODUCTION

Water is one of the most critical resources worldwide, and it is the fundamental support of the existence of life. Therefore, the scarcity of good quality water has detrimental effects on every living creature [1]. Despite this fact, water pollution continues to be a significant problem in our rapidly growing world. This issue stems from the rapid explosion of industries, the global population's exponential growth, and climate change [2]. Rivers, dams, and oceans are daily getting contaminated with dyes, heavy metals, papers, and plastics [3]. Dyes such as methylene blue (MB), rhodamine B (RhB), methyl orange (MO), Congo red (CR) are increasingly being used and are now becoming some of the most important sources of industrial pollutants [4]–[6].

Several methods have been developed by scientists to tackle the dye pollution problem. Various physicochemical and biological methods have been used. These include adsorption, degradation, ion exchange, chemical precipitation, membrane filtration and microbial technologies [7], [8]. Adsorption is popular among these methods due to its simplicity, effectiveness, flexibility, and insensitivity to toxic pollutants. Also attributable to the reversibility of the processes, by using a suitable desorption process, the adsorbent can be reused multiple times [8]–[11].

ISSN: 2521-2293

Transition metal oxides (TMOs) being excellent choice of adsorbents has brought up a great deal of obsession amongst scientists to bring about synthesis methods that are environmentally friendly, cost-effective and easy to employ [12]–[15]. Numerous methods have thus far been developed, and some of them are Sol-gel, Electrospinning, Chemical vapor disposition (CVD), Pyrolysis and Biosynthesis. These methods involve the use of large sums of money, chemicals that are harmful to the environment, are time-consuming, and require high technical skills [16]–[19].

Recent developments in research have brought about the concept of green synthesis. This concept tries to efface the problems brought by the methods mentioned above [15]. Microorganisms, plants, plant extracts, sugars and biopolymers are currently being explored in green synthesis of nanosized TMOs [20], [21]. Plant extracts and other plant parts have gained much more popularity due to the biomass abundance of many plants and their ability to generate nanoparticles of varying size, shape, and stability [22],[23]

The aim of this research was to investigate the use of morula leaves to synthesize CuO as a green and cheaper alternative to already existing methods of synthesis.

II. EXPERIMENTAL

A. *Preparation of Morula leaf extract and characterisation*

The Morula leaves were collected from the tree and rinsed under running water before being dried in a 60 °C oven for 6 h. The leaves were then crushed and stored in a glass bottle for future use.

To obtain the extract, 4 g crushed leaves were cooked in 100 mL distilled water while constantly stirring for 5 mins. The leaves were then filtered, and the new filtrate characterised using contraAA 700 atomic absorption spectroscopy before being used for synthesis.

B. *Synthesis of nanomaterials*

The materials were prepared using a hydrothermal process. 100 mL leaf extract was combined with 20 g of different metal precursors (zinc nitrate, cupric nitrate, and potassium permanganate). After that, the mixture was placed in a hydrothermal reactor and transferred to an oven set at 150 °C. After that, the product was filtered, rinsed, and dried in a 60°C oven overnight.

C. *Characterization of the nanomaterials*

The crystalline structure of the materials was investigated using X-Ray diffractions (XRD) on a Bruker D8 Advance powder diffractometer. A Cu tube X-ray source (λ=1.54056 nm, 40 kV, 40 mA) was employed and the XRD was set at a scan rate of 0.500 sec/step covering 0.02 degrees of 2θ. Spectroscopic studies were performed using the LabRAM HR800 Raman spectrophotometer, which excited the samples with a 532 nm laser.

Morphological analysis of the materials was also done using the JEOL JSM-7500F Field Emission Scanning Electron Microscope (FE-SEM) Equipped with Energy Dispersive X-ray spectroscopy (EDX) which was also employed in further analysis of the materials' elemental composition. Finally, the materials surface area, pore size, and volume were determined using nitrogen at 77 K. Micromeritics Tristar II Brunauer-Emmett-Teller (BET) analyser was employed in this regard

ISSN: 2521-2293

D. Batch equilibrium studies (adsorption)

The impact of variables like contact time and temperature on dye removal from wastewater via adsorption onto metal oxide nanoparticles was investigated. For the investigation, batch adsorption procedures were used. 2 ppm mixtures of methylene and rhodamine dyes were prepared in 250 mL Erlenmeyer flasks. 20 mL of the mixture was then transferred into a beaker and 15 mg of the adsorbent dispersed into the mixture. The mixture was then constantly stirred with a magnetic stirrer until an equilibrium was attained. The supernatant liquids from the centrifuged mixtures were examined with a UV–vis spectrophotometer. The adsorption capacity and dye removal % were calculated using the formulae below:

$$Q_e = \frac{(C_o - C_e)}{W} V \quad (1)$$

$$dye\ removal\ \% = \frac{C_o - C_e}{C_o} \times 100 \quad (2)$$

The initial and equilibrium concentrations (mg/L) are C_0 and C_e, respectively. W is the mass of adsorbent employed (g), and V is the volume of solution (L).

III. Results and discussion

A. Characterization

Synthesis of CuO was initially attempted without the morula leaf extract. Distilled water was the only solvent utilized in the process. Copper Nitrate was mixed with distilled water and the mixture was hydrothermally treated at 150 °C. This reaction resulted in a blue solution without any precipitate as shown in Error! Reference source not found.a below. This shows that the CuO precipitation was aided by the morula leaf extract.

Error! Reference source not found.b depicts the XRD patterns of the CuO materials prepared using the morula leaf extract before and after calcination at temperatures of 250, 300, 325, and 350 °C. CuO was amorphous before calcination. After calcination at 250 °C, peaks began to emerge. Some of the peaks are indicative of CuO at calcination temperatures of 250 and 300 °C, but there are some contaminant peaks as well. Only samples calcined at 325 and 350 °C show XRD peaks, indicative of CuO with no impurities and matches Crystallography Open Database (COD) card no. 1011194. The strongest peaks were found at 34, 38, 49, 54, 59, 61, and 65° corresponding to the lattice planes (110), (111), (202), (020), (202), (202), and (022), respectively.

The particle size was determined using the Debye Scherrer equation. The average particle size of CuO was 10.8 nm after calcination at 350 °C. The sample was subsequently taken for further study using Raman spectroscopy after being calcined at 350 °C.

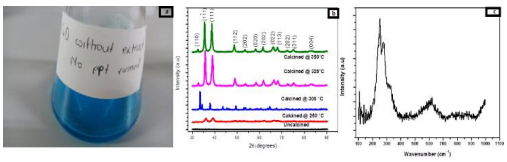

Fig. 1: (a) Optical image of the solution obtained after attempted synthesis of CuO using distilled water instead of morula leaf extract, (b) XRD pattern of CuO synthesized using the morula leaf extract, after calcination at different temperatures, (c) Raman spectrum of CuO synthesized using morula leaf extract and calcined at 350 °C.

The Raman spectra further indicated the formation of CuO during calcination at 350 °C. Nine zone-center optical phonon nodes of CuO with symmetries $4A_u + 5B_u + A_g + 2B_g$ have been reported. Only three of those

ISSN: 2521-2293

A_g and $2B_g$ are Raman active [24]. CuO Raman spectrum in Error! Reference source not found.c exhibits a doublet peak between 200 and 400 cm^{-1} and a singlet peak at 600 cm^{-1}. In the doublet peak, the 1st peak can be assigned to the A_g node and the secondone of the B_g nodes. The peak at 600 cm^{-1} could be attributed to the other B_g node. The peaks correspond to the A_g (296 cm^{-1}), B_g (346 cm^{-1}), and B_g (636 cm^{-1}) modes of bulk CuO crystals respectively and no Cu_2O modes are present [24]. This demonstrates the single-phase property of our CuO nanorods.

B. Morphological analysis

The morphology of the samples was examined using scanning electron microscopy (SEM). **Fig. 1**a-c below represents the SEM images of CuO nanoparticles obtained by calcining at 300, 325 and
350 °C, respectively. The morphology of the material calcined at 300 °C is composed of agglomerated platelet-like structures shape, **Fig. 1**a. At 325 °C, the platelet morphology transformed in thick slabs stacked into microcolumns, **Fig. 1**b. At 350 °C the stacking of the slabs was destroyed due to crystal growth via sintering of slabs, **Fig. 1**c.

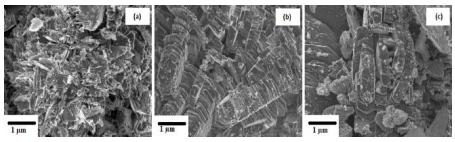

Fig. 1: (a) SEM image of CuO calcined at 300 °C, (b) SEM image of CuO calcined at 325 °C, (c) SEM image of CuO calcined at 350 °C.

Fig. 2a is a representation of the N_2 adsorption-desorption isotherms of the synthesized materials calcined at 300, 325, 350 °C. According to IUPAC classification, all produced materials have typical type V isotherms with an H3-type hysteresis loop. The observed hysteresis loop shape is typical of samples that are mesoporous. The Barret-Joyner-Halenda (BJH) pore size distribution (PSD) profiles are presented in **Fig. 2**b. PSD profiles for the materials calcined at the different temperatures show maxima around 100 Å corresponding 10 nm which falls within the 2–50 nm mesoporous range, meaning no microporosity [25].

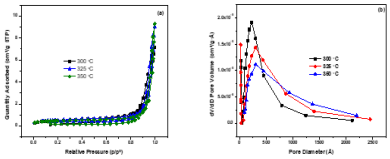

Fig. 2: (a) N_2 adsorption-desorption isotherms (b) Barret-Joyner-Halenda (BJH) pore size distribution curves of CuO materials at 300, 325, and 350 °C.

C. Application

The CuO material was applied as an adsorbent in dye adsorption from water. Figures 7 through 16 show how the material behaves as a dye adsorbent under different condition.

1. Effects of catalyst loading

The influence of adsorbent dose on the efficacy of removing a MB and R6G combination was investigated by adding varying amounts of CuO (0.15, 0.2, 0.25, 0.3, 0.35, and 0.4 mg) while keeping a constant 2 ppm dye concentration. The results are presented in **Fig. 3.** When the CuO dosage was increased from 0.15 to 0.35 mg, the dye adsorption effectiveness increased from 21 to 39% for MB and from 49 to 66% for R6G. The availability of more adsorption sites is responsible for the initial rapid increase in adsorption with increased adsorbent dosage. However, when the CuO dosage was increased beyond 0.35 mg, an equilibrium was reached. The "screening effect," which occurs at higher adsorbent dosage, could be used to explain this phenomenon. It is characterized by the accumulation

ISSN: 2521-2293

of adsorbent particles and a reduction in the distance between adsorbent molecules at the nanoadsorbent surfaces, which results in the formation of a dense screening layer. The dye molecules' binding sites were therefore hidden by the screening layer at the adsorbent's surface [26].

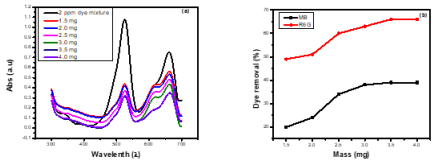

Fig. 3: (a) Effects of adsorbent dosage on adsorption of dye onto CuO, (b) Plot of % dye removal versus amount of adsorbent on adsorption of MB and R6G onto CuO.

2. *Effects of contact time*

Fig. 4 shows the influence of contact time on dye adsorption onto CuO at a starting concentration of 2 ppm. Data was collected at room temperature using a 0.35 mg adsorbent dose and a constant pH of 7.2. According to the graph, the adsorption of both dyes was slow in the first 15 mins. The adsorption rate increased rapidly after 30 mins before it dropped again at 45 mins. Beyond 60 mins, the adsorption rate plateaued. In the first 15 mins of the reactions, the adsorbent had not yet evenly dispersed throughout the dye solution, this caused the slow uptake of the dye molecules. Beyond 15 mins, the adsorbent was event distributed and there was a high number of active sites for dye adsorption, this resulted in increased dye uptake rate. The rate then slowed down and then became constant at 56 and 72% for MB and R6G, respectively, as the active sites of the material were getting filled up and there was no more room to accommodate more dye molecules [26].

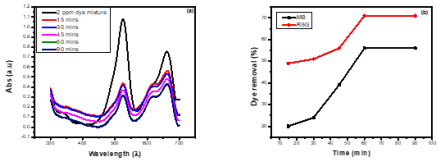

Fig. 4: Effects of contact time on adsorption of dye onto CuO

3. *Effects of temperature*

The impact of temperature on dye adsorption was investigated, and the results presented in Error! Reference source not found.. The temperature ranged from ambient temperature to 90 °C. At 25 °C, CuO adsorption capability was observed to be highest reaching about 56 and 72% for MB and R6G, respectively, at room temperature. The adsorption capacity declined from 56 and 72% to close to 0% when the temperature was increased from room temperature to 90 °C, demonstrating that the process was exothermic. Dye adsorption tends to decrease with increase in temperature as molecules adsorbed earlier tend to desorb from the surface at elevated temperatures. This is caused by the weakening of the attractive forces between the material and the dye molecules at high temperatures [27].

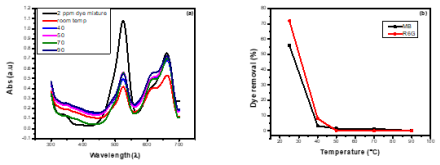

Fig. 6: (a) Effects of temperature on adsorption of a dye mixture onto CuO, (b) Plot of % removal versus temperature on adsorption of MB and R6G onto CuO.

4. *Effects of pH*

Error! Reference source not found. demonstrates the effects of pH on dye adsorption onto CuO. (0.35 mg at room temperature for 1 h). The graph shows that the dye uptake was initially slow from pH 2 to 9. The

ISSN: 2521-2293

adsorption capacity of the methylene blue and rhodamine mixture increased dramatically from pH 9 to 12, reaching 78% for MB and 86% for R6G. It is worth noting that the adsorption efficiency is influenced by the pH of the solution. The active group chemistry and surface charges of CuO changed when the pH was modified [90]. In basic aqueous media, hydroxyl (OH) groups occupy functional binding sites of the CuO material, while protons (H+) occupy functional binding sites of the material in acidic solutions. Between pH 2 and 7, more protons are occupying the hydroxyl vicinities of CuO surfaces. This promotes the initiation of repulsive force (between positive charged dye molecules and the CuO surface), which limits dye binding to some extent and produces a substantial drop in the rate of adsorption [4]. Between 7 and 9, there is an increase in the hydroxyl ions, but it is not yet enough to increase the rate of dye uptake. Beyond pH 9, the OH negative charges on CuO surfaces are widely spread which increases the electrostatic interaction potential between active binding sites and dye species. This resulted in the rapid increase in the dye uptake [28].

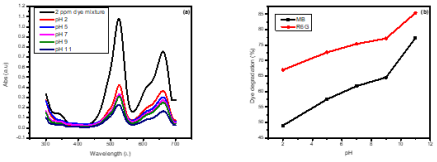

Fig. 7: (a) Effects of pH on adsorption of a dye mixture onto CuO, (b) Plot of % removal versus pH on adsorption of MB and R6G onto CuO.

5. Effects of initial concentration of contaminant

In **Error! Reference source not found.**, the effect of concentration on dye removal using CuO is shown. The results were collected at room temperature with a constant pH of 7.2 and an adsorbent dose of 0.35 mg. The contact time was similarly set at 30 mins. With increasing adsorbate concentration, the amount of dye absorbed (mg/g) was shown to decrease. The blocking action of dye molecules on pores and channels is thought to be the cause of the reduced absorption capacity. The adsorbent sites become totally saturated when the concentration of dye increases without increasing the surface area of the adsorbent, resulting in a decrease in dye removal [22].

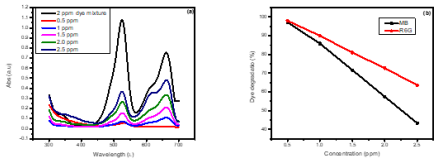

Figure 8: (a) Effects of concentration on adsorption of a dye mixture onto CuO, (b) Plot of % removal versus concentration on adsorption of MB and R6G onto CuO.

V. CONCLUSIONS

CuO possessing a platelets like structure was successfully synthesized using morula leaf extract and this was verified to be the case using XRD and Raman spectroscopy. The surface area of CuO was found to be 26.82 m^2/g which is larger than any previously reported in literature. This demonstrates that the extract was crucial in improving the surface area of the material. The material was then utilized as an adsorbent. Adsorption onto CuO is aided by increasing the adsorbent dose, pH, and contact time.

VI. ACKNOWLEDGMENTS

Authors wish to thank Botswana International University of science and Technology and the department of chemical and forensic sciences for providing instrument facilities to carry out the research work.

ISSN: 2521-2293

IV. REFERENCES

[1] "Botswana Water Sector Policy Brief 2012."

[2] D. Melissa, "Water Pollution: Everything You Need to Know," *Nrdc*, 2018.

[3] P. K. Raul, "CuO nanorods: A potential and efficient adsorbent in water purification," *RSC Adv*, 2014, doi: 10.1039/c4ra04619f.

[4] L. Pereira and M. Alves, "Dyes-environmental impact and remediation," in *Environmental Protection Strategies for Sustainable Development*, 2012, pp. 111–162. doi: 10.1007/978-94-007-1591-2_4.

[5] K. Hunger, *Industrial Dyes: Chemistry, Properties, Applications*. 2003. doi: 10.1021/ja0335418.

[6] D. Gola, "Silver nanoparticles for enhanced dye degradation," *Current Research in Green and Sustainable Chemistry*, vol. 4, Jan. 2021, doi: 10.1016/j.crgsc.2021.100132.

[7] S. Noreen, "ZnO, MgO and FeO adsorption efficiencies for direct sky Blue dye: equilibrium, kinetics and thermodynamics studies," *Journal of Materials Research and Technology*, vol. 9, no. 3, pp. 5881–5893, 2020, doi: https://doi.org/10.1016/j.jmrt.2020.03.115.

[8] J. H. Park, J. J. Wang, Y. Meng, Z. Wei, R. D. DeLaune, and D. C. Seo, "Adsorption/desorption behavior of cationic and anionic dyes by biochars prepared at normal and high pyrolysis temperatures," *Colloids Surf A Physicochem Eng Asp*, vol. 572, pp. 274–282, Jul. 2019, doi: 10.1016/j.colsurfa.2019.04.029.

[9] S. Noreen, "ZnO, CuO and Fe2O3 green synthesis for the adsorptive removal of direct golden yellow dye adsorption: Kinetics, equilibrium and thermodynamics studies," *Zeitschrift fur Physikalische Chemie*, vol. 235, no. 8, pp. 1055–1075, Aug. 2021, doi: 10.1515/zpch-2019-1599.

[10] Y. Kuang, X. Zhang, and S. Zhou, "Adsorption of methylene blue in water onto activated carbon by surfactant modification," *Water (Switzerland)*, vol. 12, no. 2, Feb. 2020, doi: 10.3390/w12020587.

[11] A. S. Elfeky, H. F. Youssef, and A. S. Elzaref, "Adsorption of Dye from Wastewater onto ZnO Nanoparticles-Loaded Zeolite: Kinetic, Thermodynamic and Isotherm Studies," *Zeitschrift fur Physikalische Chemie*, vol. 234, no. 2, pp. 255–278, Feb. 2020, doi: 10.1515/zpch-2018-1342.

[12] P. Tundo., "Synthetic pathways and processes in green chemistry. Introductory overview," 2000. doi: 10.1351/pac200072071207.

[13] S. K. Sharma, H. Demir, S. K. Sharma, and H. Demir, "Principles of Green Chemistry," in *Green Chemistry in Scientific Literature*, 2019. doi: 10.1201/9781003002352-3.

[14] V. Polshettiwar and R. S. Varma, "Green chemistry by nano-catalysis," *Green Chemistry*, 2010, doi: 10.1039/b921171c.

[15] O. O. E. US EPA, "Basics of Green Chemistry," *EPA.GOV*, 2013.

[16] C. Suryanarayana and B. Prabhu, "Synthesis of Nanostructured Materials by Inert-Gas Condensation Methods," in *Nanostructured Materials: Processing, Properties, and Applications: Second Edition*, 2006. doi: 10.1016/B978-081551534-0.50004-X.

[17] T. Guo, M. S. Yao, Y. H. Lin, and C. W. Nan, "A comprehensive review on synthesis methods for transition-metal oxide nanostructures," *CrystEngComm*, 2015, doi: 10.1039/c5ce00034c.

[18] A. Tavakoli, M. Sohrabi, and A. Kargari, "A review of methods for synthesis of nanostructured metals with emphasis on iron compounds," *Chemical Papers*. 2007. doi: 10.2478/s11696-007-0014-7.

[19] C. Dhand, "Methods and strategies for the synthesis of diverse nanoparticles and their applications: A comprehensive overview," *RSC Advances*. 2015. doi: 10.1039/c5ra19388e.

[20] S. Iravani, "Green synthesis of metal nanoparticles using plants," *Green Chemistry*, 2011, doi: 10.1039/c1gc15386b.

[21] M. Ioelovich, "GREEN CHEMISTRY AND TECHNOLOGY OF PLANT BIOMASS," 2018.

[22] H. R. El-Seedi, "Metal nanoparticles fabricated by green chemistry using natural extracts: Biosynthesis, mechanisms, and applications," *RSC Advances*, vol. 9, no. 42. Royal Society of Chemistry, pp. 24539–24559, 2019. doi: 10.1039/c9ra02225b.

[23] S. Lyubchyk, "Integrated Green Chemical Approach to the Medicinal Plant Carpobrotus edulis Processing," *Sci Rep*, vol. 9, no. 1, Dec. 2019, doi: 10.1038/s41598-019-53817-8.

[24] M. Rashad, M. Rüsing, G. Berth, K. Lischka, and A. Pawlis, "CuO and Co3O4 nanoparticles: Synthesis, characterizations, and raman spectroscopy," *J Nanomater*, vol. 2013, 2013, doi: 10.1155/2013/714853.

[25] M. P. Geetha, P. Pratheeksha, and B. K. Subrahmanya, "Development of functionalized CuO nanoparticles for enhancing the adsorption of methylene blue dye," *Cogent Eng*, vol. 7, no. 1, Jan. 2020, doi: 10.1080/23311916.2020.1783102.

ISSN: 2521-2293

[26] N. K. Soliman, "Experimentally and theoretically approaches for disperse red 60 dye adsorption on novel quaternary nanocomposites," *Sci Rep*, vol. 11, no. 1, Dec. 2021, doi: 10.1038/s41598-021-89351-9.

[27] P. Senthil Kumar, "EFFECT OF TEMPERATURE ON THE ADSORPTION OF METHYLENE BLUE DYE ONTO SULFURIC ACID–TREATED ORANGE PEEL," *Chem Eng Commun*, vol. 201, no. 11, pp. 1526–1547, Nov. 2014, doi: 10.1080/00986445.2013.819352.

[28] A. El-Maghraby, A. El-Maghraby, and H. A. el Deeb, "Removal of a basic dye from aqueous solution by adsorption using rice hulls Heba El deeb City of Scientific Researches and Technology Applications (SRTA) Newborg Al-Ara… REMOVAL OF A BASIC DYE FROM AQUEOUS SOLUTION BY ADSORPTION USING RICE HULLS," 2011. [Online]. Available: https://www.researchgate.net/publication/267384112

BIUST Teaching, Research, & Innovation Symposium 2023 (TRDAIS 2023)
Botswana International University of Science and Technology
Palapye, Botswana, 18 - 19 September 2023
ISSN: 2521-2293

Method development and validation of a rapid silica-based smart-phone assisted device in the detection of iron in water

Bame Sanah Senna*1, Wellington Masamba1 and Veronica Obuseng2
1Department of Chemical and Forensic Sciences, Botswana International University of Science and Technology, Palapye
2Department of Chemistry, University of Botswana, Gaborone
sb18100151@studentmail.biust.ac.bw

***Abstract*—** A new method of rapidly detecting iron in water using a smartphone assisted device is introduced. Currently, point-of-need devices have largely explored patterned paper as a substrate. While paper is affordable and detection is rapid, its sensitivity is compromised by its fast-wicking nature hence the need for methods of retaining and immobilizing analytes. Silica generally has a higher absorptive power than paper therefore can better immobilize analytes for better detection. The improvement of sensitivity in such devices is important in the monitoring of heavy metals such as iron that can be dangerous to plant and animal life. Testing of such metals not only requires rapid methods of detection but those with low detection limits. The pairing of these devices with smartphones contributes to their rapidity. The aim of this paper is to present findings on the method development and validation of silica-based smart-phone assisted rapid detection of iron in water. Iron standards were prepared in various amounts (0-60 ng) and converted to iron (II). A silica plate was prepared by adding 1,10-phenanthroline that would turn bright orange on reacting with iron (II). A box structure was built around the silica plate to control light and the distance of the light source (smartphone). The standards and reference material were tested by depositing on the treated silica plate before capturing with the smartphone and analyzed using a software called ImageJ. Detection limit, linear range, accuracy and precision were determined. The results showed a limit of detection of 0.2 ng, a limit of quantification of 0.6 ng, a linear range of 0.6 ng to 30.0 ng and RSD of <5%. The results also showed that for silica not only are complex immobilizing reagents not necessary but they in fact, lead to worse precision, accuracy and sensitivity. From this study we conclude that silica-based substrates make a more sensitive detection method while requiring less reagents. The settings of the software were found to be unique to the substrate.

Keywords*— *Silica, rapid testing, iron detection, ImageJ, heavy metals, method validation

I. Introduction

Analytical chemistry methods are an important part of everyday life including areas such as medical diagnostics, product development, quality control and environmental monitoring [1], [2]. The ability to carry out tests and analyses in and out of the laboratory is a big part of informed decision making that in many cases can be life-saving.

Currently, the detection of toxic substances like heavy metals is done through Inductively Coupled Plasma – Mass Spectrometry (ICP-MS) and Atomic Absorption Spectroscopy (AAS) among others. These methods have low detection limits, good sample throughput and are a reliable way of analysis in the laboratory [3]–[5]. However, the cost of using these can be very high. Cate (2016), notes that the cost of these instruments can exceed USD150 for just one sample. Additionally, transportation and sample processing drive up the costs of testing with these instruments [6]. The turnaround time for using such instruments may range from a couple of weeks to a few months [3], [7]–[10]. In the case of environmental monitoring, there is a need for high frequency testing in order to capture what is happening in real time [7], [11]. This means there is a need to increase rapidity of testing. The current methods of analysis consume significant amounts of reagents while requiring highly skilled personnel to operate. These challenges have significant implications on accessibility especially for developing countries and their communities.

In recent years, there has been a growing interest in improving environmental monitoring through lab-on-a-chip and point-of-need devices [3], [7]–[10], [12], [13]. Such devices have been around since the early 90s and researchers have been advancing on their construction and development. Point-of-need devices can use micro litre (or even less) levels of analyte and reagents. They can be rapid in detection and allow for analysis to be carried out at the outside the laboratory. Most have a designated point of introducing a solution, a pre-treatment zone and a detection zone. These zones are usually connected by small channels that have attributes of driving solutions without the need of an external driver such as gas (e.g capillary movement in paper devices). Some of the substrates commonly used in the construction of point-of-need devices include paper, carbon, alumina and silica. The method of detection may be electrochemical, chemiluminescent or colorimetric among many others.

Heavy metals make up some of the most ubiquitous and potentially toxic pollutants globally (Kaur et al. 2019)(WHO). Many of these metals can cause cancer in humans even at low concentrations (WHO). Poisoning of communities and their livestock has been reported in many instances after drinking groundwater laden with some toxic metals especially arsenic, lead, iron and chromium. Iron is one of the most significant heavy metals for its effects to human physiology and concentrations in the environment. As a micronutrient, iron is the major component in the heamoglobin molecule that helps to transport oxygen in the body [14]. Iron at higher concentrations in the environment has been reported to pollute underground

ISSN: 2521-2293

water sources [15]. This poses a threat as water reserves are said to be steadily dwindling, globally [16]. Additionally, iron plays a major role in the release and attenuation of other toxic metals such as arsenic [17]. The rapid detection of this metal in the environment is important.

The aim of this paper is therefore to present findings of method development and validation of a new rapid method of iron analysis. This paper specifically explores silica as a substrate for out-of-the-lab iron analysis in water with the assistance of a smartphone.

II. MATERIALS AND METHODS

A. Chemicals and materials

Analytical grade chemicals were used as is in this study. AAS grade Iron standard 1000ppm, hydroxylamine hydrochloride, 1,10-phenanthroline, poly (acrylic acid), TLC silica plate on aluminium base.

B. Sample Preparations

The samples were prepared in concentrations ranging 0-30 mg/L of Fe from the 1000 ppm standard solution. To each sample was then added 2mL of hydroxylamine hydroxide solutions (5g prepared in 50mL water) to convert all Fe into Fe (II).

C. Fabrication on Silica Plate

On the silica plate, circles representing detection points were drawn using an HB (hard black) lead pencil. 2H (too hard) pencils were damaging to the silica plate. 3 aliquots of 1,10-phenanthroline (0.52g in 100mL water) were deposited on these detection points. The plate was allowed to dry before each deposition. Poly (acrylic acid) was added to detection points for immobilization of the ferroin complex that would be formed from Fe reacting with 1,10-phenanthroline. The silica plate was then ready for rapid detection.

D. Fe detection

The prepared standard samples were deposited in designated detection points in triplicate. That it, one concentration had 3 detection points. The blank and a standard reference material (TraceCERT CRM Iron in water (ISO/IEC 17025)) were also included. A second silica plate that did not have poly (acylic acid) as a ferroin complex immobilizer, was done in a similar manner.

E. Image Processing

Images of the silica plate after color development, were captured using an iPhone 11 Pro® in wide camera mode, aperture f/1.8, 26 mm, 12 MP, 3024 x 4032. The images were also scanned using the smartphone's notes application scanning component for comparison. The images were then sent to a laptop through email to be processed. The image software used was ImageJ, a public domain software developed by the National Institute of Health (US). For use with this software, all images had to be converted to JPEG format. Upon being loaded on the software, images were first inverted to negatives such that the areas outside the color development are black and measure zero in color intensity as done previously [18] [19]. After inverting, the image was set to an auto color contrast in contrary to color thresholding in previous studies [18] as this gave a clearer image. Color intensity was measured in gray intensity and integrated density for comparison.

III. RESULTS AND DISCUSSION

A. Color Development on Silica Plate

A bright orange color developed upon introducing samples to the prepared silica showing the formation of a ferroin complex. The detection points that were also treated with poly (acrylic acid) to immobilize the complex, resulted in poor color development. This is in contrast to the effect of poly (acrylic acid) in literature [18], [19]. While these studies found that treating paper substrate with poly (acrylic acid) improves the color development, in this study, it did the opposite and made the color development worse (Figure 1). Poly (acrylic acid) is said to have low mobility particularly on paper [20]. It is a weak anion therefore making is highly mobile on silica substrate [1]. This explains its failure to immobilize ferroin complex on silica.

B. Results of Image Processing

Although image processing methodology from literature was followed, results show that the type of substrate has an effect on the output of the software. Figure 2 shows the results of the image of the silica plate when color thresholding as done by [18]. It is observed that this method leads to loud background noise and is not suitable for silica substrate (Figure 2a). A better image was obtained from manually adjusting the color contrast (Figure 2b) with much of the background noise eliminated. The best image resulted from setting the color contrast to "Auto" i.e. allowing the software to correct the color contrast (Figure 2c). Through this setting, the background noise was successfully reduced to zero. This was evidenced by color intensity measurements in non-detection zones recording zero.

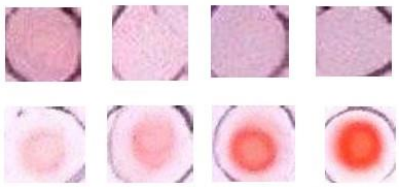

Fig. 1: Detection points of ferroin complex color development with poly (acrylic acid) (top) and without poly (acrylic acid) (bottom)

ISSN: 2521-2293

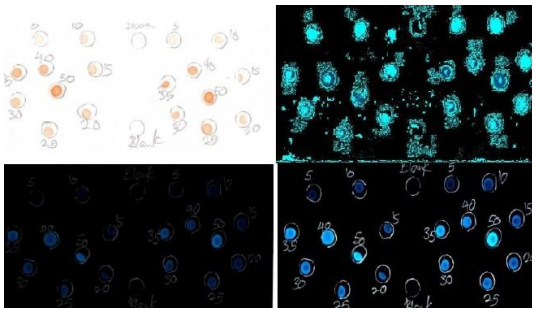

Fig. 2: Images of the silica device after color detection (a), after color thresholding (b), after manual contrast adjustment (c) and after automatic contrast adjustment (d)

C. Color Intensity Measurements

As the software had already showed specificity for type of substrate, the color intensity of the ferroin complex was measured in both mean gray and integrated density. Results show that both measurements successfully measured color intensity on silica substrate. However, there were differences noted in the two methods. Figure 3 shows calibration curves from both methods. Results show no statistical difference ($p<0.05$), between mean gray and integrated density. Despite this, all measurements of integrated density seemed to have a coefficient of determination (R^2) that is closer to 1 than those measure in mean gray. In other studies mean gray has been the choice of measurement in this software due to the accurate results it yielded [13], [21]–[27]. With scanty information of integrated density as a measurement for color intensity, this study found it equally accurate. A trend was also observed where images higher background noise seem best measured in mean gray while those with lower background are best measured in integrated density. According to literature [28], [29], integrated density captures bright and dim colors more accurately while mean gray "corrects" the dim colors to be brighter and the brighter colors to be dimmer.

Figure 4 presents the calibration curve from the image being scanned instead of photographed. It is clear that scanning produced better images for analysis in the improved R^2 value. This was attributed to how the scanning application automatically adjusts lighting to illuminate shadows on the silica plate. A box enclosure was therefore not as needed.

D. Method Validation

To validate the method, figures of merit were determined and are presented. Table 1 shows the relative standard deviation (RSD) was found to be under 5% in all test samples. A good analytical method is generally considered to have an RSD of less than 20% [30]–[32].

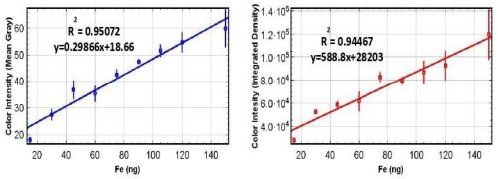

Fig. 3: Color intensity of ferroin complex measured in mean gray and measured in integrated density

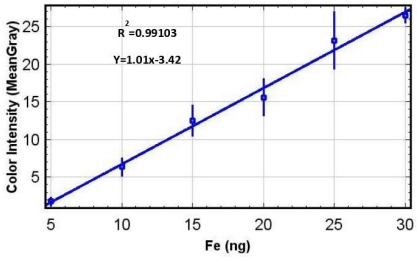

Fig. 4: Fe calibration curve measured in mean gray from scanned silica device

TABLE 1: Relative Standard Deviations of Fe standards (5 mg/L, 15 mg/L and 30 mg/L) in %

Measurement Tool	Calculated RSD in %		
	5 mg/L	*15 mg/L*	*30 mg/L*
Mean Gray	3.14	3.26	0.96
Integrated Density	3.77	2.42	2.96

N=10

TABLE 2: Certified reference material concentration determination with silica device compared to AAS analysis in mg/L

TraceCERT ® CRM Iron in water (ISO/IEC 17025) (mg/L)	AAS Analysis (mg/L)	Silica Device analysis (mg/L)
20.00	20.03 ± 0.17	20.13 ± 0.29

N=10

Results show that this method was accurate as measurements of CRM was were statistically not different ($p<0.05$, $n=10$) from those of AAS (Table 2). The CRM which was Fe of concentration 20.0 mg/L was measured to be 20.09 ± 0.17 mg/L using AAS and 20.13 ± 0.29 mg/L using the silica device.

The limit of detection and limit of quantification (calculated on equation (1) and equation (2) were determined as 0.2 and 0.6 µg of Fe, respectively. This LOD is less than that previously reported for paper using the same method [33]

$$\left(\frac{3s}{m}\right) = LOD \qquad (1)$$

ISSN: 2521-2293

$$\left(\frac{10s}{m}\right) = LOQ \quad (2)$$

IV. CONCLUSION

The development and method validation of a new smartphone assisted method was successfully done. With an LOQ of 0.6 ng of Fe, good precision (RSD of <5%), accuracy against AAS using certified reference material and a linear range of 0.6 – 30.0 ng of Fe. The developed method proved more sensitive than methods in literature for paper substrate. This study also found that with silica as a substrate, ferroin complex immobilization with poly (acrylic acid) is not necessary. The software ImageJ is unique to the substrate in its settings. Going forward, the same method may be applied to other metals and environmental samples.

ACKNOWLEDGMENT

The authors thanks Botswana International University of Science and Technology for funding with the Initiation Grant and the University for laboratory space

REFERENCES

[1] F. W. Fifield and D. Kealey, *Principles and practice of analytical chemistry*. Blackwell Science Hoboken, 2000.

[2] D. A. Skoog, D. M. West, F. J. Holler, and S. R. Crouch, *Fundamentals of analytical chemistry*. Cengage learning, 2013.

[3] N. A. Meredith, C. Quinn, D. M. Cate, T. H. Reilly, J. Volckens, and C. S. Henry, "based analytical devices for environmental analysis," *Analyst*, vol. 141, no. 6, pp. 1874–1887, 2016.

[4] G. Tyler and S. Jobin Yvon, "ICP-OES, ICP-MS and AAS Techniques Compared," *ICP Optical Emission Spectroscopy Technical Note*, vol. 5, 1995.

[5] O. Mestek, M. Loula, A. Kaňa, and M. Vosmanská, "Can ultrafast single-particle analysis using ICP-MS affect the detection limit? Case study: silver nanoparticles," *Talanta*, vol. 210, p. 120665, 2020.

[6] S. Wilbur, "A comparison of the relative cost and productivity of traditional metals analysis techniques versus ICP-MS in High Throughput commercial laboratories," *Agilent Technologies Application Note*, 2005.

[7] A. Jang, Z. Zou, K. K. Lee, C. H. Ahn, and P. L. Bishop, "State-of-the-art lab chip sensors for environmental water monitoring," *Meas Sci Technol*, vol. 22, no. 3, p. 032001, 2011.

[8] C. Dincer *et al.*, "Disposable sensors in diagnostics, food, and environmental monitoring," *Advanced Materials*, vol. 31, no. 30, p. 1806739, 2019.

[9] K. R. Rogers and E. N. Koglin, "Biosensors for environmental monitoring: an EPA perspective," in *Biosensors for Direct Monitoring of Environmental Pollutants in Field*, Springer, 1998, pp. 335–349.

[10] O. A. Sadik, A. K. Wanekaya, and S. Andreescu, "Advances in analytical technologies for environmental protection and public safety," *Journal of Environmental Monitoring*, vol. 6, no. 6, pp. 513–522, 2004.

[11] M. P. Bhat, M. Kurkuri, D. Losic, M. Kigga, and T. Altalhi, "New optofluidic based lab-on-a-chip device for the real-time fluoride analysis," *Anal Chim Acta*, vol. 1159, p. 338439, 2021.

[12] K. Pyrzynska, A. Kubiak, and I. Wysocka, "Application of solid phase extraction procedures for rare earth elements determination in environmental samples," *Talanta*, vol. 154, pp. 15–22, 2016.

[13] S. Balasubramanian *et al.*, "Digital colorimetric analysis for estimation of iron in water with smartphone-assisted microfluidic paper-based analytical devices," *Int J Environ Anal Chem*, pp. 1–18, 2021.

[14] C. Camaschella, "Iron deficiency," *Blood, The Journal of the American Society of Hematology*, vol. 133, no. 1, pp. 30–39, 2019.

[15] R. Jahanshahi and M. Zare, "Assessment of heavy metals pollution in groundwater of Golgohar iron ore mine area, Iran," *Environ Earth Sci*, vol. 74, no. 1, pp. 505–520, 2015.

[16] World Health Organization, *Guidelines for drinking-water quality*, vol. 1. world health organization, 2004.

[17] T. Pal, P. K. Mukherjee, and S. Sengupta, "Nature of arsenic pollutants in groundwater of Bengal basin-a case study from Baruipur area, West Bengal, India," *Curr Sci*, vol. 82, no. 5, pp. 554–561, 2002.

[18] M. M. Mentele, J. Cunningham, K. Koehler, J. Volckens, and C. S. Henry, "Microfluidic paper-based analytical device for particulate metals," *Anal Chem*, vol. 84, no. 10, pp. 4474–4480, 2012.

[19] D. M. Cate, P. Nanthasurasak, P. Riwkulkajorn, C. L'Orange, C. S. Henry, and J. Volckens, "Rapid detection of transition metals in welding fumes using paper-based analytical devices," *Annals of occupational hygiene*, vol. 58, no. 4, pp. 413–423, 2014.

[20] B. Giri, *Laboratory methods in microfluidics*. Elsevier, 2017.

[21] P. Rattanarat, W. Dungchai, D. Cate, J. Volckens, O. Chailapakul, and C. S. Henry, "Multilayer paper-based device for colorimetric and electrochemical quantification of metals," *Anal Chem*, vol. 86, no. 7, pp. 3555–3562, 2014.

[22] X.-L. Guo, Y. Chen, H.-L. Jiang, X.-B. Qiu, and D.-L. Yu, "Smartphone-based microfluidic colorimetric sensor for gaseous formaldehyde determination with high sensitivity and selectivity," *Sensors*, vol. 18, no. 9, p. 3141, 2018.

[23] G.-H. Chen, W.-Y. Chen, Y.-C. Yen, C.-W. Wang, H.-T. Chang, and C.-F. Chen, "Detection of mercury (II) ions using colorimetric gold nanoparticles on paper-based analytical devices," *Anal Chem*, vol. 86, no. 14, pp. 6843–6849, 2014.

[24] A. Motalebizadeh, H. Bagheri, S. Asiaei, N. Fekrat, and A. Afkhami, "New portable smartphone-based PDMS microfluidic kit for the simultaneous colorimetric detection of arsenic and mercury," *RSC Adv*, vol. 8, no. 48, pp. 27091–27100, 2018.

[25] A. K. Ellerbee *et al.*, "Quantifying colorimetric assays in paper-based microfluidic devices by measuring the transmission of light through paper," *Anal Chem*, vol. 81, no. 20, pp. 8447–8452, 2009.

[26] Y. Xia *et al.*, "Smartphone-based point-of-care microfluidic platform fabricated with a ZnO nanorod template for colorimetric virus detection," *ACS Sens*, vol. 4, no. 12, pp. 3298–3307, 2019.

[27] S. Shariati and G. Khayatian, "The colorimetric and microfluidic paper-based detection of cysteine and homocysteine using 1, 5-diphenylcarbazide-capped silver nanoparticles," *RSC Adv*, vol. 11, no. 6, pp. 3295–3303, 2021.

ISSN: 2521-2293

[28] M. D. Abràmoff, P. J. Magalhães, and S. J. Ram, "Image processing with ImageJ," *Biophotonics international*, vol. 11, no. 7, pp. 36–42, 2004.
[29] C. A. Schneider, W. S. Rasband, and K. W. Eliceiri, "NIH Image to ImageJ: 25 years of image analysis," *Nat Methods*, vol. 9, no. 7, pp. 671–675, 2012.
[30] I. C. H. H. T. Guideline, "Validation of analytical procedures: text and methodology," *Q2 (R1)*, vol. 1, no. 20, p. 05, 2005.
[31] P. Bruce, P. Minkkinen, and M.-L. Riekkola, "Practical method validation: validation sufficient for an analysis method," *Microchimica Acta*, vol. 128, no. 1, pp. 93–106, 1998.
[32] S. Walfish, "Analytical methods: a statistical perspective on the ICH Q2A and Q2B guidelines for validation of analytical methods," *Biopharm Int*, vol. 19, no. 12, pp. 1–6, 2006.
[33] D. M. Cate, J. A. Adkins, J. Mettakoonpitak, and C. S. Henry, "Recent developments in paper-based microfluidic devices," *Anal Chem*, vol. 87, no. 1, pp. 19–41, 2015.

BIUST Teaching, Research, & Innovation Symposium 2023 (TRDAIS 2023)
Botswana International University of Science and Technology
Palapye, Botswana, 18 - 19 September 2023
ISSN: 2521-2293

Simulation of Energy Consumption in Hybrid Electric Vehicles used in a Semi-Arid Region: A case for Palapye, Botswana

Matthias O. T. Motsomi*, M. Tunde Oladiran
Botswana International University of Science and Technology,
Department of Mechanical, Energy and Industrial Engineering
P/Bag 16, Palapye, Botswana
matthias.motsomi@studentmail.biust.ac.bw

Abstract

Electric vehicles are renowned for their merits such as reduced pollution, no emission and small reliance on non-renewable fossil fuels, yet their adoption is low. The low adoption of electric vehicles is due to their disadvantages such as low range, long charging hours and some potential consumers have the fear of running out of charge while driving. A prediction of the energy consumption of an electric vehicle helps to alleviate such fear. In this work simulation results are presented which compare the energy consumption of a Toyota Prius, a hybrid electric vehicle modeled in ADVISOR simulation package, when used under summer European and Palapye Botswana ambient conditions respectively. The New European Driving Cycle was used and ambient conditions were varied in the input parameters. Results show that the state of charge are respectively 50% and 54% under hotter conditions of Palapye and a European country. The gradient of the state of charge of the battery pack during the simulation period is also steeper for Palapye conditions than for a European country which shows that energy is consumed at a higher rate in the former. Based on the difference in the state of charge for both conditions, results show that there was an 8% higher energy consumption under Palapye's conditions. The results can inform consumers on what to expect when purchasing and operating a hybrid electric vehicle. Results also provide a guide for the design of electric vehicles intended for use in a semi-arid country such as Botswana. It can be concluded that electric vehicles consume more energy under harsher or more hostile environmental conditions owing to the use of auxiliary systems such as air conditioners and other temperature control systems. Future research work needs to develop better battery storage systems and driving cycles that accurately model conditions in hot climate regions.

KEYWORDS: ADVISOR, hybrid electric vehicle, energy consumption, ambient conditions, state of charge

1. Introduction

Transportation plays a pivotal role in the day to day lives of people in society, be it directly, whether they use passenger vehicles to help them to get from one destination to another, or indirectly where vehicles are used to transport goods (Li, 2017). Transportation is important for the economy since it helps to get goods from their places of production to the market and for workers to reach their places of employment (Filip, 2014). Such involvement of transportation in the economy can be taken to imply that, with economic growth comes an increased need for transportation (Filip, 2014). Increased use of transportation is seen through the increase of vehicles on the roads which in turn means that the problems associated with use of internal combustion engine vehicles, such as air pollution and reliance on non-renewable fuel sources, become worse (Kadij, 2016). Table 1 below shows the countries or continent with highest levels of CO_2, it is worth noting also that these are some of the most developed countries and continents in the world. The carbon dioxide is principally from combustion of fossil fuels in transportation vehicles.

ISSN: 2521-2293

Table 1: Regions with highest levels of CO_2 level in unit Metric tonnes.

Country or continent	China	America	Europe
CO_2 (Mt)	11680	4535	1028

Sources: world population review, euro stat

Research and development efforts by governments and automobile companies have been made to mitigate the problems of using internal combustion engine vehicles for transportation, where the results include development of alternative fuel vehicles such as electric vehicles (EVs) (Bjerkan, 2016). EVs are vehicles that use an electric motor for propulsion, instead of an internal combustion engine, and a battery pack as a source of energy instead of a fuel tank (Ding, 2017). EVs come in two main types being pure electric vehicles, which use an electric motor as the sole source of traction force, and hybrid electric vehicles (HEVs) which use both fuel and a battery as energy sources and a motor as well as an engine for traction (Ding, 2017). In line with the high levels of air pollution as shown from table 1, figure 1 shows how EVs are adopted in high numbers in the same countries.

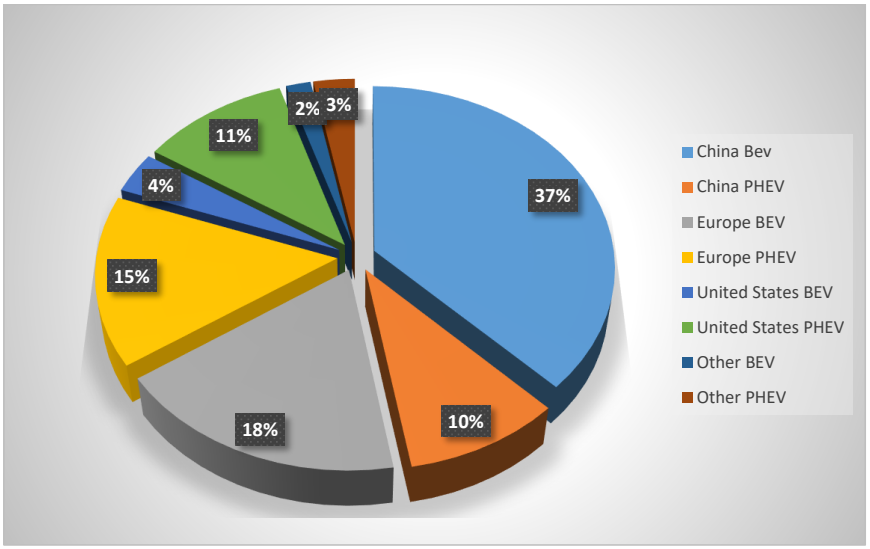

Figure 1: Regions with most EVs worldwide
Source: Global Electric Vehicle Outlook 2022

Most currently available models of electric vehicles use an AC motor for traction, have temperature control technology for both the cabin and the battery pack as well as the features of conventional vehicles including motorized windows, wipers, entertainment features, etc. In a conventional vehicle the 12V battery that runs features using 12V is charged through the alternator while in an electric vehicle the battery is charged through a DC-DC converter which draws power from the traction battery pack that is usually of a higher voltage, to charge it. In this way the traction battery pack is the main energy source for the vehicle.

ISSN: 2521-2293

Common battery chemistry for the traction battery pack is Li-ion (Faraz, 2021). The battery technology has concerns of thermal runaway which is a situation where the battery self-heats and the result is a release of gas, shrapnel or particulates and extreme heat (Liu, 2017). Thermal runaway occurs when heat generated by the battery exceeds heat dissipated to the battery's surrounding (Golubkov, 2014). Cooling systems for the batteries are thus important and electric vehicles have temperature control systems for the battery packs because over cooling the battery cells also affects their performance (Pandya, 2021). The temperature control systems keep the cells at their optimum performance temperature range. Cabin temperature control through air conditioning is another temperature control system in electric vehicles (Piao, 2020). Now that these systems run on the 12V system, which draws energy from the traction pack, they affect the range of an electric vehicles (Badin, 2013). How much energy they require depends on the effect of the external temperature on the temperature control systems, that is, how much energy is required by the compressor in order to compress the refrigerant so that it may reach a temperature higher than that of the environment in order to dissipate heat from the battery pack. Most EV cooling systems run on a refrigeration cycle (Piao, 2020). For cabin cooling or heating, the energy required to overcome the temperature depends on how hot or cold the cabin air is, where the bigger the difference between the set temperature and the cabin air temperature, the more energy is required to achieve the desired temperature (Moran, 2014). Compressor input work is used to account for the energy consumed by the cooling systems and also to model the system. Equations 7 through 10 show how energy consumed is determined from the compressor input work.

The climate where an electric vehicle is used thus impacts the range of the vehicle because of the energy drawn by the temperature control systems (Badin, 2013). Table 2 shows the climate experienced in the regions that have most EVs, where Norway is the sampled European country since it is the leader in European countries adopting the use of electric vehicles.

Table 2: Climate experienced in different developed countries that adopt EVs.

Country	China	America	Norway
Climate	Tropical in the south and subtropical in the north	Tropical, arctic and alpine	maritime

Sources: NCCS report, Gunnar Ketzler (2022)

Botswana is described as a developing country with a semi-arid climate. To promote adoption of electric vehicles in such a country it is important to predict how an electric vehicle would perform in the conditions of a semi-arid climate. Literature review shows that two-wheel electric vehicles and hybrid electric vehicles are the most suited types of electric vehicles for adoption in developing countries. This work thus presents simulation results and analysis of a hybrid electric vehicle under conditions of Botswana.

ISSN: 2521-2293

The total energy available after a trip is the sum of energy required by the traction motor, E_{mot}, energy required by the auxiliary components, E_{aux} and energy recuperated through regenerative braking , E_{reg}, as shown in equation 1. For the scope of this work, regenerated energy will be neglected since it is not affected by ambient conditions as shown in equations 2 and 6. Energy as a function of power and time is illustrated in equations 3 through 5, this is because the power rating of components and how long they are in use is relied on to determine the energy they consume.

$$E_{tot} = E_{mot} + E_{aux} + E_{reg} \quad (1)$$

$$E_{req} = E_{mot} + E_{aux} \quad (2)$$

$$E_{req} = \int P\,dt \quad (3)$$

$$= P\int dt \quad (4)$$

$$= P\Delta t \quad (5)$$

Where P is component rated power, t is time, J is joules of energy and s is seconds.

Therefore $E_{req} = J_{mot} + J_{aux}$ (6)

$$\dot{W}_c = \dot{m}(h_{out} - h_{in}) \quad (7)$$

$$E_{cool} = \int kW\,dt \quad (8)$$

$$= kW\int dt \quad (9)$$

$$= (kW)^* \Delta t \quad (10)$$

Where $\dot{W}_c$ is compressor input work, $\dot{m}$ is refrigerant mass flow rate, h_{out} is the enthalpy of the refrigerant exiting the compressor and h_{in} is enthalpy of the refrigerant entering the compressor

2. Literature review

Numerous studies on the adoption of electric vehicles in developing countries make mention of electric two-wheelers and hybrid electric vehicles being the types most suited for early adoption (PLotz, 2014). Infrastructure for supporting the use of electric vehicles is expensive to develop (Li Y. , 2016) hence electric two-wheelers and plug-in hybrid electric vehicles are easier to operate because they can be re-charged at home using a house power outlet and a dedicated electric vehicle charger to charge the battery pack of the hybrid electric vehicle.

How far one can travel on a single charge, travel range that is, has been determined to be one of the critical decision making factors for consumers hence need to determine the energy consumption of electric vehicles (Hardman, 2016) (Dua, 2019). Energy consumption of electric vehicles impacts the range of the vehicle because the higher it is, the lower the range of the vehicle. It is influenced by the road type, driving style as well as ambient conditions (Badin, 2013). Temperature has an impact on the energy consumption of the traction motor, where higher temperatures reduce the motor efficiency which then leads to higher energy consumption in order to attain the same results (Khalifa, 2010). It is thus important to investigate the influence of temperature on the energy consumption of EVs in different regions because EVs will perform differently in climates with significantly diverse temperatures.

ISSN: 2521-2293

EV energy consumption can be determined through road tests where an EV is driven for a known distance and a recording of the vehicle's state of charge is taken at the beginning and end of the trip (Hu, 2017). The expected energy consumption is a function of time and the power rating of the traction motor as shown in equation 1. Simulations are another way to determine the energy consumption of EVs. EV models can be built and simulations ran to predict the energy consumption of an EV (Genikomsakis, 2017). Simulation may be a difficult task in some instances because of the complexity of having to account for the effect of many varying conditions and also the regeneration of power during vehicle braking (Kavalchuk, 2015). Some simulation packages are available for making simulations easier of which they have inbuilt vehicle models and they can run simulation over established test cycles.

3. Methodology

3.1 Chosen Vehicle Model

In line with literature review, a hybrid electric vehicle is modeled and its energy consumption simulated. One of the inbuilt hybrid electric vehicles available in the Advanced Vehicle Simulator (ADVISOR) simulation package is the Toyota Prius hybrid which was chosen for this work.

ADVISOR makes an approximation of the continuous behaviour of a vehicle as a sequence of steps using basic physics calculations and measured component performance. The vehicle is assumed to be at steady state, whereby the effect of changing voltage, current, RPMs and torque are neglected. The simulator takes driving profile, conditions in which the vehicle is to be driven in and vehicle parameters as inputs. It then works backwards using the desired vehicle speed to determine the required torque and speed of each component including the energy source. The required energy to put the vehicle through the chosen cycle is the vehicle's energy consumption.

3.2 Chosen Driving Cycle

A driving cycle or procedure is a description of the velocity and how long a vehicle is to be driven, so as to assess its performance. For most countries, urban areas usually have the most developed infrastructure that supports use of electric vehicle. Urban areas commonly have inhabitants who earn enough to afford an electric vehicle. For these reasons, the New European Driving Cycle (NEDC) is chosen for testing the proposed vehicle. The cycle is a dynamometer test used for passenger vehicle type approval in Europe. It consists of sub-cycles for simulating city driving. Figure 2 shows the velocity vs time graph for the cycle, it shows how the vehicle is accelerated and decelerated.

ISSN: 2521-2293

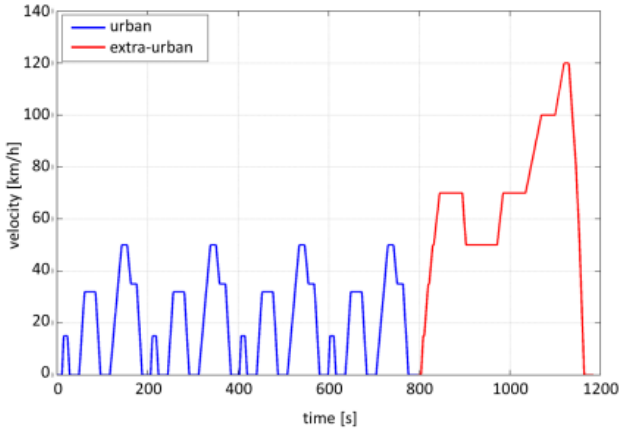

Figure 2: New European Driving Cycle (NEDC)
Source: ResearchGate

3.3 Input parameters

To put the summer temperatures of the Botswana's climate into perspective, a week's temperature recordings for Palapye are shown in table 3. The ambient temperature used as input is the average of the temperature recordings and the inbuilt summer conditions for the vehicle model used are ones used for summer operation of the vehicle under NEDC.

Table 3: Temperature recording taken at 1300 of each day from Saturday October 8th till Friday October 14th 2022.

Day	Mon	Tue	Wed	Thu	Fri	Sat	Sun
Date						08/10	09/10
	10/10	11/10	12/10	13/10	14/10		
Temperature (°C)	35	33	35	35	36	37	34

ISSN: 2521-2293

4. Results

The energy consumption pattern of the simulated vehicle under the inbuilt normal European conditions is shown in figure 3. Figure 4 shows the energy consumption of the same vehicle but with the input temperature increased.

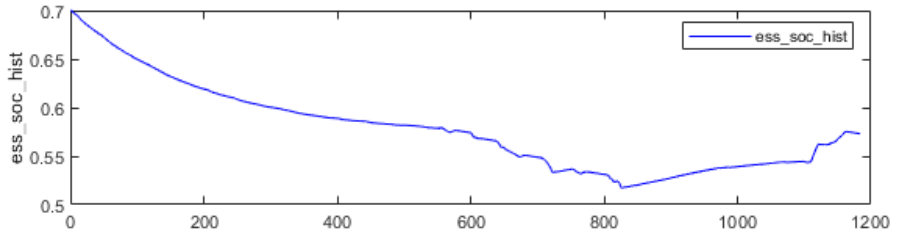

Figure 3. Simulated energy consumption in the hybrid Toyota Prius.

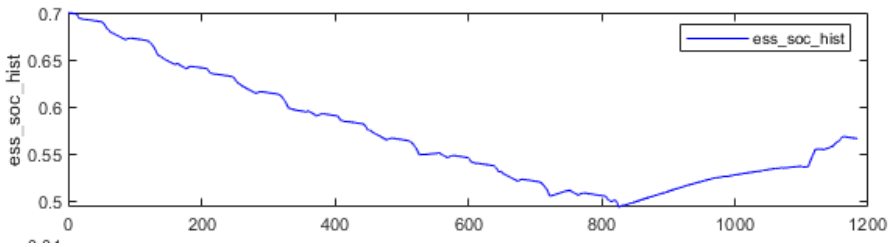

Figure 4. Simulated energy consumption in the hybrid Toyota Prius but under a higher ambient temperature.

It can be observed that just after the 800s mark, the two graphs show approximately 4% difference in state of charge where the graph for normal European use is higher than for use in Palapye's ambient summer conditions. Both graphs rise thereafter which is a representation of the energy recovered by the vehicle during regenerative braking.

5. Conclusion

This work presents the simulation of energy consumption in a hybrid electric vehicle if it were to be used in the conditions of a semi-arid country such as Botswana. The simulation was focused on temperature effects on the energy consumption of an electric vehicle and disregarded difference in humidity among other factors that influence energy consumption of an EV. Potential customers, researchers and automobile developers can expect at least a 4% higher energy consumption from a hybrid EV based on the results presented.

References

Badin, F. (2013). evaluation of ev energy consumption influencing factors. *World electric vehicle journal*, 112-123.

ISSN: 2521-2293

Bjerkan, K. (2016). Incentives for promoting battery electric vehicles (BEVs) in Norway. *Transportation Research part D*, 169-180.

Ding, N. (2017). The electri vehicle: A review. *International journal of electric and hybrid vehicles*, 49-66.

Dua, R. (2019). understanding potential for battery electric vehicle adoption using large-scale consumer profile data. *Energy reports*, 515-524.

Faraz, A. (2021). *Battery electric vehicles.* Research gate.

Filip, N. (2014). The role of transpport in economic development. Constanta: Mircea cel Batran.

Genikomsakis, K. (2017). a computationally efficient simulation model for estimating energy consumption of electric vehicles in the context of route planning applications. *transportation research part D*, 98-118.

Golubkov, A. (2014). themral runaway experiments on consumer Li-ion batteries with metal-oxide and livin-type cathode. *RSC Advances*, 3633-3642.

Hardman, S. (2016). comparing high-end and low-end adopters of battery electric vehicles. *Transportation research part A*, 40-57.

Hu, K. (2017). differences in energy consumption in electric vehicles: an exploratory real-world study in Beijing. *journal of advanced transportation*.

Kadij, G. (2016). *NOx emissions from euro 5 and euro 6diesel passenger cars - test results in the lab and on the road.* TNO Innovation for life.

Kavalchuk, I. (2015). advanced simulation of power consumption of electric vehicles. *international journal of computer and systems engineering*, 53-59.

Khalifa, F. (2010). effect of temperature rise on the performance of induction motors., (pp. 549-552).

Li, W. (2017). A review of factors influencing consumer intentions to adopt battery electric vehicles. *Renewable and sustainable energy reviews*, 318-328.

Li, Y. (2016). infrastructure to facilitate usage of electric vehicles and its impact. *transportation research procedia 14*, 2537-2543.

Liu, J. (2017). experimental study of thermal runaway process of 18650 lithium ion battery. *materials*.

Moran, M. (2014). *fundamental of engineering thermodynamics.* Don Fowley.

Pandya, C. (2021). Adetailed review on cooling system in electric vehicles. *international research journal of engineering and technology*, 377-384.

Piao, C. (2020). research on electric vehicle cooling system based on active and passive liquid cooling. *Journal of physics conference series*.

PLotz, P. (2014). who will buy electric vehicles? identifying early adopters in Germany. *Transportation research part A*, 96-109.

BIUST Teaching, Research, & Innovation Symposium 2023 (TRDAIS 2023)
Botswana International University of Science and Technology
Palapye, Botswana, 18 - 19 September 2023
ISSN: 2521-2293

USSDs vs Apps: Understanding the Adoption and Continuous Use of Mobile Applications in Botswana

Winnie Ramafifi
Dept of Computer Science and Information Systems
Botswana International University of Science and Technology (BIUST)
Palapye, Botswana
rw18000642@studentmail.biust.ac.bw

Kopo M. Ramokapane
Dept of Computer Science
University of Bristol
Bristol, United Kingdom
marvin.ramokapane@bristol.ac.uk

***Abstract*— Mobile applications are not only crucial for service delivery, but they also offer users convenience in completing everyday tasks. Consequently, mobile application development in Botswana has risen significantly in the last few years. However, their adoption and use remain low despite their prevalence and usefulness. Currently, there is no research evidence on why Botswana-developed mobile apps have a low adoption rate or what factors inhibit users from using such applications. To address this gap, we present the findings of a case study (n=79 users) exploring the adoption and use of the Mascom mobile app. Our findings highlight performance and usability as the main impediments to adopting and using mobile applications in Botswana. We also found that the need for the internet to use the app, lack of practical usefulness, and low social influence around the use of the app discourage users from downloading and using the app. Based on these findings, we provide design recommendations for entities (i.e., developers and companies) interested in developing a mobile application for the Botswana market. For example, developers should review the functionality of their application and identify features that are most useful to users. Lastly, our study provides building blocks for developers and designers hoping to build mobile applications for Batswana users.**

Keywords—Mobile apps; Mobile app adoption; usability; user study; survey;

I. Introduction

Mobile applications are not only crucial for service delivery, but they also offer users convenience in completing everyday tasks. In the second quarter of 2022, the number of Apple mobile apps was just over 2.1 million [1]. The global revenue from mobile apps (i.e., for Android and Apple) stood at around 318 billion USD in 2020. Statista states that this number is expected to double by 2025 [2]. Despite this growth and prospects, the adoption and use of mobile apps in Botswana remain low. For instance, while the largest mobile service provider in Botswana boasts over 1.5 million subscribers, their android app has just over 10 000 downloads in the Google Play store.

It is usually assumed that people instinctively integrate mobile app use into their lives. However, the factors that motivate such use, especially in developing countries such as Botswana, still need to be studied. While there are efforts [5,6] to bridge this gap in countries neighboring Botswana countries, the factors influencing the adoption and continuous use of mobile apps by Batswana are missing in the literature. Nonetheless, marketing managers and mobile app developers are usually required to understand how consumers decide what apps to use. When these factors are well-understood, app developers can develop better apps that meet users' needs, and marketers can decide better what product or services should be served to customers. Moreover, this is important not only for marketers and developers but also for users. This means users' preferences are considered.

This paper aims to bridge this gap by investigating the factors that inhibit Batswana users from adopting and using mobile apps designed and developed for them. Using Mascom mobile app as a case study, we ask two fundamental questions: (1) what factors inhibit the adoption and continuous use of the Mascom mobile app, and (2) what considerations should be put in place to improve the adoption and continuous use of the Mascom mobile app.

Our findings show that app performance expectancy, unclear app utility, and poor usability may impede adopting and using mobile applications in Botswana. Reliance on the internet for functionality also discourages use and adoption. In summary, our contributions are as follows:

- An in-depth understanding of the factors that hinder the adoption and continuous use of the mobile app in Botswana. Using a qualitative approach, we provide factors hindering Batswana from adopting mobile apps.
- Practical recommendations to improve the adoption and continuous use of the mobile application. Based on the findings, this paper proposes a set of design and general recommendations for improving mobile app adoption and continuous use. These are factors that designers and developers in Botswana need to consider when developing mobile apps that are attractive to mobile app users.

ISSN: 2521-2293

II. Related Work

A. Mobile App Adoption

Mobile app adoption studies are not new; several researchers worldwide have investigated why users adopt and use various mobile applications. When examining the usage of fitness apps, Herrmann and Kim found that effectiveness or usefulness yielded a more positive attitude to the app [11]. After surveying 1435 participants, Frey et al.[3] found that a person's mobile app adoption pattern is strongly influenced by their current life stage. Others, for example, Lu et al.[4] found that perceived usefulness, perceived ease of use, and compatibility are significant antecedents of the intention to use travel apps. This echoes the results of Humbani et al. study conducted in South Africa to explain the adoption and the intention to use mobile payment apps. Humbani et al.[5] found that "Drivers" were better predictors of adoption than "inhibitors", while satisfaction emerged as the strongest predictor of continuance intentions. Another prior effort, similar to our study, was conducted by Oksiutyc and Lubinga, which aimed at identifying factors affecting the adoption and use of mobile safety apps [6]. Their results show that most young people were unaware of safety apps but would use the ones recommended by their friends. Despite these studies, no research has investigated what inhibits Batswana from adopting and using mobile apps.

B. USSDs

While many mobile apps offer services, some users still prefer USSD technology. The most appealing aspect of USSD transactions is that they do not require an internet connection [3], making them ideal in a relatively emerging country with unreliable data [7]. However, USSDs suffer usability issues, and knowing multiple USSDs for different services can be a hustle. In Botswana, no study has investigated whether the use of USSDs impacts the adoption and use of mobile apps.

C. Technology adoption theories

Prior research [8,9,10] has proposed several frameworks to understand what influences technology adoption and use. One of the most often utilized theories is the Theory of Reasonable Action [11], which focuses on one aspect that defines a person's behavioural purpose and attitudes about that behaviour. Attitudes are intuitive and are formed by a set of ideas about the object of behaviour (e.g., using an application is more convenient than USSD). Another framework is Technology Acceptance Model (TAM). The TAM Model was characterized as an information system theory that analyses users [9] to see if they accept the use of technology in their field of expertise. Other frameworks focus on information flow (i.e., diffusion of innovation (DOI)), or subjective matters as norms and attitudes (e.g., theory of planned behaviour (TPB)). The framework used in this study is the Adoption and continuous use framework; it is based on literature and theoretical models on technology adoption [9]. This framework focuses on various constructs that influence the use of an application. Moreover, it not only focuses on adoption but also on why users continue to use an application.

III. Methodology

To understand what inhibits users from adopting Botswana-developed mobile apps, we conducted a qualitative survey based on the Adoption and Continuous use framework [9] using the Mascom mobile app as a case study. The Adoption and Continuous use framework aims to understand what factors influence mobile app adoption and continuous use. These factors include performance expectancy, ease of use, social influence, enjoyment, incentives, facilitating conditions, aesthetics and trust.

D. Ethical considerations

While the study did not undergo an ethics review process, we did not collect personal information. Participants were made aware of the study's purpose and asked for consent before participation. Participation was entirely voluntary and anonymous.

E. Study Design

Participants. Our study was targeted at students who were active mobile users owning or had previously owned a Mascom Simcard. We also targeted students who had owned and used smartphones for over three years and had installed several Botswana-developed mobile apps. One of the reasons for selecting students as a target group for our research is that students represent the age group of the population that spends the most time using mobile apps. They tend to use mobile apps not only for their private needs but also for their education. Moreover, students are a very social and interconnected segment of the population that actively uses social media and is widely exposed to various social influences.

To understand the deters and the influencers, we were interested in users and non-users of the Mascom mobile app. We defined a user as a respondent who owned Mascom Simcard and was using the Mascom app, while a non-user was any respondent who had never downloaded or used the mobile app or had previously downloaded the app but no longer used or had the app. We hypothesised that users would give us factors behind their adoption and use while non-users would reveal hindering factors.

Over four weeks, we recruited participants through our existing social and professional networks in and outside BIUST using social media and word-of-mouth. Interested participants were given a link that they could use to complete the survey. No compensation was given to participants.

Materials. Using the Adoption and Continuous use framework, we elicited a mixture of Likert and open-ended questions for each of the eight framework constructs. In addition, the survey also included questions on demographic background and experience with using mobile applications. In the end, the survey questionnaire had 17 questions for users and 19 for non-users.

Data analysis. We analyzed the questionnaire results using basic statistics for Likert questions and thematic analysis (for open-ended questions) to build a codebook [5]. First, the two researchers independently analyzed the first three responses to

ISSN: 2521-2293

build the codebook. Then, they met and discussed the codebook, clearing the disagreements to produce the final codebook, which was then used to analyze all the remaining responses. For the mobile app users' questionnaire, saturation was reached after 8 participants and 23 non-users.

IV. FINDINGS

This study investigates what factors inhibit the adoption and continuous use of mobile applications in Botswana. In this section, we discuss the findings of our study. We first begin with discussing the factors that impede the adoption and continuous use of the Mascom app from respondents (i.e., users) who have installed and have the app in their phones, then for non-users in the light of the adoption and continuous model constructs. Fig 1 summarises the findings of our study. We conclude this section by presenting factors that may encourage users to download and use the Mascom mobile app.

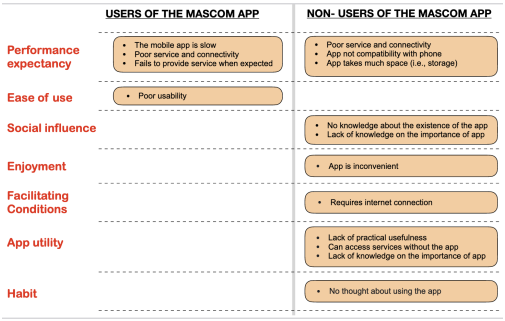

Figure 1. Summary of the results.

F. Participants' Demographics.

Eighty-six (86) respondents completed our survey. However, seven were removed because they either straight-lined or provided responses that did not make sense. In the end, we had 79 respondents, 46 males, 32 who identified as female, and one who did not disclose their gender. Of the 79, 66 were 18 - 23, 2 were older than 30, while the rest were between 24 and 30.

Twenty-six (26) owned just one Simcard, a Mascom Simcard, while 44 owned two simcards, either a Mascom and Orange sim, or Mascom and BeMobile simcards. Only 9 owned all three simcards. Fig x summarises these numbers.

Regarding Mascom app download, sixty-four (64) had never downloaded the app, eleven (11) had used the app, and four (4) downloaded it and then uninstalled it. In summary, 68 respondents were classified as non-users of the app.

G. Users of the Mobile App

In consideration of the adoption and continuous use model, performance expectancy and usability were the topmost cited constructs perceived as the top impediments to continuous use.

Performance expectancy. Most participants revealed that the mobile app was generally slow (e.g., P7 "The app is extremely slow"), and they usually experienced poor connection, particularly in rural areas. P3 explained, "It takes ages to connect… poor network connection in rural areas". Participants reasoned that these performance issues affected their intention to use the app and encouraged them to seek other alternatives to get the same services. Other respondents explained that they did not have a full understanding of how the app could help them achieve their goals, "I Don't really know what it can do apart from showing my balance, be it airtime or data balance." P10

Usability. Other users raised concerns about the usability of the mobile app. They explained that it is sometimes hard to find the services they want to use. For example, P5 highlighted that the app had so many categories: "There are many categories, and it can be hard to find the service I'm looking for, a search option would be nice." Other participants explained that the consistent requirement of login credentials (i.e., effort) sometimes discouraged them from getting the service through the app.

H. Non-users of the Mobile App

Our analysis revealed that the most common factors impeding adoption and continuous use were performance expectancy, social influence, app utility, facilitating conditions, and habit.

Performance Expectancy. Non-users also cited a lack of reliable network connection or poor service for not using the mobile app. Further analysis showed that non-users, particularly those without knowledge of the app, believed there were no benefits. They explained they could still access services without using the app, P23 "I can access most of the services freely without the use of the mobile app."

Social influence. Almost half of the non-users did not know about the existence of the app or its uses. The majority of them did not know or seen anyone use the app. Some respondents further explained that none of their close friends used the app, hence their lack of awareness. P54 reported: "I do not know about it and its uses… no one I know has that app."

App utility. Some participants cited the app's lack of practical use as their main reason for not using it. They reported that they mostly download and use apps because of their functionality. For example, P50 declared, "Not sure what the benefits of using [the app] are… what can I do with it?"

Facilitating conditions. Most non-users reported that they did not use the app because of the cost and the resources needed. They mostly highlighted that the app needed the internet function, a condition they struggled to meet. Participants explained they did not always have an internet connection or afford to subscribe to Mascom data bundles. P23 "The mobile app requires internet connectivity, so I don't have that privilege…" Other respondents further explained that this is defeating because this is the same app they need to buy calling credit (i.e., airtime) or even subscribe to the internet. P61

"it's not convenient for me as it requires internet to use it, so I can't use it to get airtime or maybe subscribe for the internet because I need those two to use the app." We also found that three respondents were not using the app because their mobile phones did not meet the requirement of the app, for example, P25 "my phone is old… I can't update it… I can't have the app"

ISSN: 2521-2293

Habit. Other respondents explained that they did not use the app out of habit; they are used to accessing the Mascom services through other means, for example, USSD codes or quick codes. P7 explained it is easier and more convenient to use codes than the app, "I am just used to using codes, I can check my balance, I can do everything… I am not used to using the app."

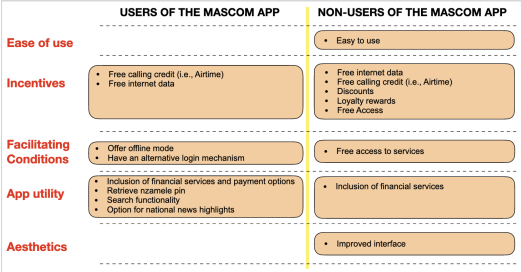

Figure 2: Users' desires for the app

V. Factors that may encourage users to use the app

As part of our survey, we also asked all the respondents what factors would encourage them to use the application. Respondents explained that incentives, app utility, usability and internet-free services would encourage them to use the app. Fig 2 shows the summary of the results.

Incentives. Both users and non-users cited the need to incentive the use of the app. The majority explained that they needed to see the benefits of using the app, P31 "I should be given extra airtime for using the app to buy airtime." Others explained that incentives could be in the form of free internet data and discounts for some services.

Facilitating conditions. Respondents reported that accessing the services through the app should be free. They mentioned that they used to be allowed to access Facebook and Wikipedia for free though those services were internet-based. For example, P47 said, "Why can we just be allowed to use the app without a data subscription? It should be free." Moreover, other app users also suggested that the app should provide an alternative login mechanism and should refrain from repeatedly signing them out from using the app.

App utility. The majority of participants desired improvement in the services provided by the app, and they requested more features. For instance, all the app users asked for search functionality and the inclusion of financial services. P8 said, "More payment options for shopping and utilities," while P5 added, "A search bar to easily find services under different categories."

Usability and aesthetics. Some respondents reported that improvement in the aesthetics and usability could encourage them to use the app. One participant explained that having to provide a username and password all the time to use the app was tiring and annoying. They suggested the app should consider an alternative login mechanism, P9 "biometric log in [would help]."

VI. Discussion

I. Discussion of the results

While the study did not undergo an ethics review process, we did not collect personal information. Participants were made aware of the study's purpose and asked for consent before participation. Participation was entirely voluntary and anonymous.

App utility. Our results show that many non-users needed help understanding the app's purpose or the services offered. This was also alluded to by the app users, who wondered whether the features they had were even useful. For the app to be adopted, the purpose of the app should be clear. Our results suggest that developers or app owners should design apps that have apparent use and functionality. This may also explain why most consumers use USSDs.

Facilitating conditions. Users and non-users of the mobile app explained that they do not always afford the internet service to use the app. Arguably, this may be the reason why most respondents do not use the app to access services. This is also possible since the internet connection in Botswana is still scares, which may affect any use of mobile applications because they mostly rely on the internet. App developers and owners should ensure that their mobile apps can offer services offline where possible.

Usability and aesthetics. Our results suggest that users are not using the app because of its usability and aesthetics issues. Prior studies [12] have cited usability as an important factor in technology adoption. Our results suggest the Mascom app is not an exception; some users stopped using the app because it took more work to use. Developers and app owners should invest in including users in their design process to ensure aesthetics and usability are ensured.

Social influence. Most non-users reported that they were only aware of the existence of the app after the survey. This may be due to a lack of app marketing or user conversations about the app. This finding suggests that app owners should invest in advertising their applications. It is a common practice to advertise mobile apps on social media, particularly the services that users can get through the app.

Based on the findings, to engender adoption and continuous use of the mobile app, mobile app owners in Botswana should:

- Review their apps' functionality and identify features that are most useful to users. Common features and services should be easy to access.
- Offer users alternative ways of accessing the app (e.g., biometric login) to create an easier way into the app, which may eventually create the habit of using the app.
- Invest in advertising services the app offers and offer incentives (i.e., loyalty bonuses) to help raise awareness and value for using the app.

ISSN: 2521-2293

- Offer some services offline. Where possible, users should be able to access services without an internet connection or mobile data subscriptions.
- Improve performance and usability of their apps. Apps should go through proper testing phases with various versions of mobile phones and should have less dependency on third-party libraries to reduce loading and delayed connectivity.

J. *Limtations of the study*

Since this is the first study to explore the adoption and continuous use of mobile apps in Botswana, there was no empirical research to compare and contrast our findings.

Our study investigates the adoption and continuous use of one mobile app; users may have different perceptions about other apps (e.g., apps from other mobile service providers). Nonetheless, our findings provide critical insights into the perception of locally developed apps in Botswana.

Notably, therefore, the thematic analysis of participants' responses does not expose any evidence that the issues they mentioned are as they describe them in the Mascom mobile app; their opinions may have been influenced or be based on what they expected from mobile applications developed in Botswana.

Lastly, our survey was written in English, which could have affected participants who are more confident responding in Setswana. Notwithstanding, our sample is primarily young adults studying at the university level.

VII. CONCLUSION

This is the first study in Botswana to explore what factors inhibit mobile app adoption and continuous use. Using the Mascom app as a case study, our results suggest that app performance expectancy, utility, and usability may be the main impediments to adopting and using mobile applications in Botswana. Reliance on the internet for functionality also impedes use. These findings provide a foundation for what app owners should consider when building future mobile applications. This study focused on the Mascom app; future studies should investigate whether these factors are the same for other mobile applications, particularly those in the same category. Moreover, this study calls for more usability studies around mobile apps.

ACKNOWLEDGMENT

We would like to thank all the participants who took part in our study, and the feedback from colleagues and friends around Botswana International University of Science and Technology.

REFERENCES

[1] Appfigures. (July 22, 2022). Number of available apps in the Apple App Store from 1st quarter 2015 to 2nd quarter 2022 [Graph]. In Statista. Retrieved October 17, 2022, from https://www.statista.com/statistics/779768/number-of-available-apps-in-the-apple-app-store-quarter/

[2] Statista. (September 10, 2021). Revenue of mobile apps worldwide 2017-2025, by segment (in million U.S. dollars) [Graph]. In Statista. Retrieved October 24, 2022, from https://www.statista.com/forecasts/1262892/mobile-app-revenue-worldwide-by-segment

[3] Frey, Remo Manuel, Runhua Xu, and Alexander Ilic. "Mobile app adoption in different life stages: An empirical analysis." Pervasive and Mobile computing 40 (2017): 512-527.

[4] Jiaying Lu, Zhenxing Mao, Mengbin Wang & Liang Hu (2015) Goodbye maps, hello apps? Exploring the influential determinants of travel app adoption, Current Issues in Tourism, 18:11, 1059-1079, DOI: 10.1080/13683500.2015.1043248

[5] Humbani, M. and Wiese, M. (2019), "An integrated framework for the adoption and continuance intention to use mobile payment apps", International Journal of Bank Marketing, Vol. 37 No. 2, pp. 646-664. https://doi.org/10.1108/IJBM-03-2018-0072

[6] Oksiutyc, Anna, and Elizabeth Lubinga. "Factors affecting the adoption of personal safety apps among millennials in Johannesburg, South Africa." South African Journal of Information Management 23.1 (2021): 1-9.

[7] Aisha Salaudeen. Ussd codes may not be as safe as we think. https://www.stearsng.com/article/ussd-codes-may-not-be-as-safe-as-we-think/, 2018 (accessed June 01, 2022).

[8] Martin Fishbein and Icek Ajzen. Belief, attitude, intention, and behavior: An intro duction to theory and research. Philosophy and Rhetoric, 10(2), 1977.

[9] Viswanath Venkatesh, James YL Thong, and Xin Xu. Consumer acceptance and use of information technology: extending the unified theory of acceptance and use of technology. MIS quarterly, pages 157–178, 2012.

[10] Fred D Davis. Perceived usefulness, perceived ease of use, and user acceptance of information technology. MIS quarterly, pages 319–340, 1989.

[11] Lynn Katherine Herrmann and Jinsook Kim. The fitness of apps: a theory-based examination of mobile fitness app usage over 5 months. Mhealth, 3, 2017.

[12] Alicia David and Peyton Glore. The impact of design and aesthetics on usability, credibility, and learning in an online environment. Online Journal of Distance Learn ing Administration, 13(4), 2010.

BIUST Teaching, Research, & Innovation Symposium 2023 (TRDAIS 2023)
Botswana International University of Science and Technology
Palapye, Botswana, 18 - 19 September 2023
ISSN: 2521-2293

The Implementation of Virtual Reality-Building Information Modelling in Botswana Higher Education AEC Programmes

Keoagile Kerileng
Department of Civil and Environmental Engineering
Botswana International University of Science and Technology
Palapye, Botswana
Kerilengk@biust.ac.bw

Abstract— *Botswana as a developing country will see an immense growth in the construction industry. A reflection on the construction history of Botswana and a peek into the future Botswana's construction industry illustrates a country with a sure growth in the construction industry. Therefore this paper will discuss why and how incorporating Building Information Modeling (BIM) and Virtual Reality (VR) Technologies into higher education teaching practices can ease the industry towards transitions in the technology era. As the construction industry transitions, adequately qualified students and specialists will become crucial for the Architectural, Engineering and Construction (AEC) industry. The adoptation and adaptation of Building Information Modeling (BIM) and Virtual Reality (VR) across the world by governments and private industries has made it mandatory to embrace construction technologies in various forms. The introduction of VR and BIM would transform the AEC industry. The use of three-dimensional (3-D) immersive learning can enrich student's ability to identify various building principles, as well as increase engagement and retention which can make the learning experience meaningful. This paper advocates for implementing VR-BIM into the AEC undergraduate program.*

The paper carries out a methodology for implementing the VR-BIM. By reviewing previous literature, making an in-depth analysis of the program and accreditation requirements. This paper illustrates how VR-BIM can be implemented in the curriculum into existing course model. Potential challenges to the VR-BIM implementation are identified and some solutions proposed. From this perspective lab classroom layout suitable for the application is designed and adjusted to various layouts to accommodate different teaching practices, learning styles and objectives. Comparisons between head-mounted displays (HMD) are considered and suitable equipment proposed.

Keywords—BIM;VR; Architectural Engineering and Construction; Higher Education Curriculumn

I. INTRODUCTION

BIM adoption is spreading like a wildfire across the engineering, and constructions industry (Hong et al 2020). Currently to accommodate the need for Building Information Model (BIM) and Virtual Reality (VR) experts the industry outsources expertise, however this is not a sustainable solution longterm [1].As the industry embraces and adopts BIM and VR a demand for professionals competent in the use of BIM and VR will increase [2]. As the industry transitions a more sustainable solution would be the production of BIM and VR qualified graduates ([3], [4]. BIM-VR qualified are a significant need of the future Architectural Engineering and Construction (AEC) industry workforce [5]–[7]. AEC graduates are unprepared for a digital future and research has suggested AEC educators embrace digital technologies to transform the industry [8]–[10] .

A. What is BIM

The National BIM Standard, defined BIM as "a digital representation of physical and functional characteristics of a facility, forming a reliable basis for decisions during its life cycle from inception onward"[11]. [12] define BIM as "a modeling technology and associated set of processes to produce, communicate, and analyze building models." BIM Models are made of smart objects representative a physical element such as doors and columns that hold a set of data. It can virtually build a structure before physically constructing it, allowing the project participants to explore and analyze a project digitally and make changes. Practicing BIM in the Industry has optimized construction, led most contractors' adoption of it in various parts of the world, when compared to architects and engineers (McGraw-Hill, 2012). The outcomes of BIM definitions enlightened AEC users to embrace BIM in construction industry. VR has been implemented into the BIM curriculum as a visualization technology tool which offers interaction of virtual models in virtual environments. It can be applied in teaching architectural visualizations for learners to appreciate the final model. In structural engineering it can be

ISSN: 2521-2293

used to visualize to optimize the structural design of a building or for error checking and collision detection. It is evident that immersive learning experiences are possible Virtual Reality in the AEC curriculum (Bouska & Schneiderova Heralova, 2019). Previous studies in education have found that VR increases student engagement, increases enjoyment, mastery and promotes immersive learning experiences through simulation (Mystakidis, 2022; Suleman, 2019; Edwards, 2018). VR creates replicas of the real environment when well executed it can be an effective tool for higher education (Krajcovic et al. 2022). Instead of using the traditional paper data and 2D layouts learning experiences can be more immersive when students walk through an AEC environment virtually. And the more complex and actual the virtual replica students can see problems and even design accurate or replicate accurate real world scenarios.

The COVID pandemic helped many AEC, universities and their stakeholders to realize and utilize BIM and VR technologies. BIM alone cannot accomplish all needs required in construction industries, the virtual reality (VR) coupled with BIM can improve the accuracy of designs, speed up the construction process, and reduce costs by enhancing efficiency and collaboration of BIM-VR. It brought attention to BIM-VR revolutionizing the construction industry at large. BIM-VR is an interactive multimedia technology that enables users to connect with digital objects, offering users a simulated physical presence in an enhanced virtual world (Biocca & Levy, 1995). Virtual Reality (VR) idea was to simulate BIM and able to define VR in conjunction to AEC industry. Dioniso et al. 2013 defined VR as computer-generated simulations of three-dimensional objects that look real and need physical user interaction. VR technology has a wide range of applications that can help a project with accelerated site training and protection, design progress, and coordination with all parties involved, and lower project costs (Behzadi, 2016). Type of VR, Immersive VR is one of the useful one because it immerses the user into an environment and gives them a sense of presence in a location where they are not physically present.

Various type of VR is used in different important sections of AEC projects, therefore the combination of BIM- VR are the future of the building industry. In the modern construction process, BIM and VR technologies are used to perform worker safety preparation, defect management, quality management, project scheduling, knowledge collection, safety management, logistics management, and project progress assessment (Ahmed, et al., 2017). Adding the virtual interface technologies to BIM will continue to revolutionize the instructional methods used in construction education and enhance students' learning experience (Messner & Horman, 2003). The 3D immersive experience can be a valuable resource for strengthening students' ability to build their sense of space (Paes, et al., 2017).

While BIM has developed into a trending innovative technology, its applications and benefits in the AEC industry have not been maximized primarily due to a lack of trained BIM professionals (Gu & London, 2010; Lee & Hollar, 2013). This demand is followed by a necessity to implement BIM in AEC education. Introducing BIM in learning can indicate the latent potential of BIM in developing learning capacity in a collaborative construction industry. Therefore, many institutions must adjust their program curricula to integrate BIM (Chen & Gehrig, 2011). Several studies have considered BIM in higher education from international perspectives (Babatunde Solomon, 2018; Kim et al. 2017; Ozorhon & Karahan,2017) In Botswana however this remains untouched territory and research has not been adequately discussed the possibility implementing a BIM curriculum in higher education. This gap remains in the prevailing body of knowledge which is the motivation for this paper. BIM-VR technologies should not be treated as an optional division but rather a principal element of AEC curriculum (McPhee, 2016). BIM-VR technologies must be adopted a core and consistent pedagogical practice (Gelic & McLeod 2018).

BIM-VR research in Botswana is limited when compared with the developed nations, so this project contributes to the body of local knowledge. This work will therefore be beneficial to the various industry stakeholders in the private and public sectors such as Special Economic Zones Authority (SEZA), Morupule Coal Mine, DEBSWANA, Association of Consulting Engineers Botswana (ACEB), Botswana Engineer Registration Botswana Engineer Registration Board (B-ERB), Botswana Institute of Engineers (BIE), Botswana Innovation Hub (BIH), Ministry of Infrastructure of and Housing Development (MIHD), and Ministry of Finance and Economic Development (MFED). The focal point of the research is to suggest possible strategies that may be initiated by the Botswana educational administration, government and other regulatory agencies to promote BIM-VR adoption. The project will therefore help public officials and decision makers influence future policy making for supporting BIM digital technology usage in the Botswana architecture engineering and construction industry as well as educational institutions.

A. Global perspectives on BIM digital technologies

BIM digital technologies is an innovation that has spread like a wildfire across the globe, due centralized model which requires all engineers work on the same model, as compared to old times today's models are bringing the entire team in one centralized model which fosters collaboration and distance is no longer a barrier as everything can be done remotely BIM is on the rise worldwide. It is currently required in all governmental projects in the USA Bosch-Sijtsema, Isaksson, Lennartsson, & Linderoth (2017), and gaining wide industry awareness and adoption in European Union Eadie, Browne, Odeyinka, McKeown,&McNiff. (2013) Similarly, BIM implementation is moving rapidly in Hong Kong and Singapore as clients have started to realize its various benefits [13], [14] While BIM adoption is promising in the above countries, it is considered to be relatively lukewarm in developing regions Saka & Chan (2019).

ISSN: 2521-2293

B. SADC perspectives on BIM digital technologies

In the SADC region BIM use remains relatively low. In his study Saka & Chan (2019) found that BIM is still in its germination stage in southern Africa and few studies have considered BIM development in the engineering and construction industry. BIM was only introduced in South Africa around 2004 (Kotze, 2013). In comparison to the aforementioned developed countries, South Africa is less mature in terms of exposure and usage of BIM. Examples of where BIM has been used are for the construction of the Nelson Mandela Bay and Mbombela stadiums for the 2010 FIFA World Cup. Although South Africa is starting to experience an increased uptake in BIM (Kotze, 2013), However South Africa has taken steps towards the implementation of BIM digital technologies. Mutale, Danstan, Tembo, Matipa & N'gandu (2014) in their paper titled Building Information Modelling: an assessment of its viability in cost management in the Zambian construction industry found that limited knowledge regarding BIM resulted in limited use in the Zambian construction industry Zavirima (2022). In Tanzania studies reflected the low awareness and knowledge of BIM led to slow adoption of BIM digital technologies Ally & Makenya (2018).

C. BIM and VR in Higher Education

Academia and the AEC industry are aware of the growing need for BIM-VR ready graduates (Hosseini et al. 2018; Hosseini et al. 2016). BIM-VR cannot simply be a one size fits all. A consensus must be reached on the requirements and curriculum direction (Wu et al. 2015) Effective BIM-VR curriculum must be tailor designed to suit culture and industry-oriented curricular (Best & Langston, 2005). There needs to be a connection between curricula and the industry, graduates must be fully prepared to competently perform BIM and VR related tasks. Another barrier is lack of limited availability of BIM educators and expert support (Mills et al. 2013) BIM and VR is relatively new and few educators are trained to teach BIM and VR content (Hon et al. 2015).

II. Conclusion

The necessity of BIM-VR technology advancement in Botswana's architecture engineering and construction industry, for higher education is a relevant necessity, and a graduate is likely to be absorbed by highly rated companies if BIM digital technologies. is part of their profile, they even become internationally competitive. BIM-VR digital technologies encourages sustainable economic development, environment maintenance, reducing inequality and collaboration in goal achievement. Moreover, should Botswana adopt BIM-VR digital technologies., the nation will be recognized as having standards and this will be a fulfilment of some international standards and agreements. BIM-VR digital technologies implementation has a potential in Botswana as informed by patterns in the developing world and more recently in neighboring South Africa.

References

[1] W. Wu and R. R. A. Issa, "BIM education and recruiting: Survey-based comparative analysis of issues, perceptions, and collaboration opportunities," *J. Prof. Issues Eng. Educ. Pract.*, vol. 140, no. 2, pp. 1–9, 2014, doi: 10.1061/(ASCE)EI.1943-5541.0000186.

[2] B. Hosseini Hashemi and M. A. Jafari, "Experimental evaluation of elastic critical load in batten columns," *J. Constr. Steel Res.*, vol. 65, no. 1, pp. 125–131, 2009, doi: 10.1016/j.jcsr.2008.02.016.

[3] B. Succar, W. Sher, and A. Williams, "Architectural Engineering and Design Measuring BIM performance : Five metrics Measuring BIM performance : Five metrics," *BIM-benefit*, vol. 8, no. 2, pp. 120–142, 2012.

[4] X. Zhao, P. Wu, and X. Wang, "Risk paths in BIM adoption: empirical study of China," *Eng. Constr. Archit. Manag.*, vol. 25, no. 9, pp. 1170–1187, 2018, doi: 10.1108/ECAM-08-2017-0169.

[5] P. M. Bosch-Sijtsema, P. Gluch, and A. A. Sezer, "Professional development of the BIM actor role," *Autom. Constr.*, vol. 97, no. October 2018, pp. 44–51, 2019, doi: 10.1016/j.autcon.2018.10.024.

[6] Y. Hong, A. W. A. Hammad, S. Sepasgozar, and A. Akbarnezhad, "BIM adoption model for small and medium construction organisations in Australia," *Eng. Constr. Archit. Manag.*, vol. 26, no. 2, pp. 154–183, 2019, doi: 10.1108/ECAM-04-2017-0064.

[7] R. Jin, Y. Zou, K. Gidado, P. Ashton, and N. Painting, "Scientometric analysis of BIM-based research in construction engineering and management," *Eng. Constr. Archit. Manag.*, vol. 26, no. 8, pp. 1750–1776, 2019, doi: 10.1108/ECAM-08-2018-0350.

[8] K. Baradi, M. Oraee, M. R. Hosseini, L. Tivendale, and J. Pienaar, "Teaching collaboration in tertiary BIM education: a review and analysis," *AUBEA 2018 Educ. Build. Prof. Futur. Glob. World - Technol. Proc. 42nd Australas. Univ. Build. Educ. Assoc. Conf.*, no. September, pp. 1–10, 2018, [Online]. Available: https://bit.ly/3tMFgPq.

[9] S. O. Babatunde, D. Ekundayo, A. O. Adekunle, and W. Bello, "Comparative analysis of drivers to BIM adoption among AEC firms in developing countries: A case of Nigeria," *J. Eng. Des. Technol.*, vol. 18, no. 6, pp. 1425–1447, 2020, doi: 10.1108/JEDT-08-2019-0217.

[10] T. Puolitaival and P. Forsythe, "Practical challenges of BIM education," *Struct. Surv.*, vol. 34, no. 4–5, pp. 351–366, 2016, doi: 10.1108/SS-12-2015-0053.

[11] NIBS, "2013 Annual Report to the President of the United States," p. 56, 2013.

[12] X. Wang, *BIM Handbook: A guide to Building Information Modeling for owners, managers, designers, engineers and contractors*, vol. 12, no. 3. 2012.

[13] C. T. W. Chan, "Barriers of Implementing BIM in

ISSN: 2521-2293

Construction Industry from the Designers' Perspective: A Hong Kong Experience," *ISSN J. Syst. Manag. Sci. J. Syst. Manag. Sci.*, vol. 4, no. 2, pp. 1816–6075, 2014.

[14] J. Rogers, H. Y. Chong, and C. Preece, "Adoption of Building Information Modelling technology (BIM): Perspectives from Malaysian engineering consulting services firms," *Eng. Constr. Archit. Manag.*, vol. 22, no. 4, pp. 424–445, 2015, doi: 10.1108/ECAM-05-2014-0067.

BIUST Teaching, Research, & Innovation Symposium 2023 (TRDAIS 2023)
Botswana International University of Science and Technology
Palapye, Botswana, 18 - 19 September 2023
ISSN: 2521-2293

Study on bio-inspired multi-phalangeal prosthetic hand as a terminal device

Onalethata I. Maswabi
Dept. of Mechanical, Energy and Industrial Engineering
Botswana International University of Science and Technology
Palapye, Botswana
onalethata.maswabi@studentmail.biust.ac.bw

Rodrigo Jr. Jamisola
Dept. of Mechanical, Energy and Industrial Engineering
Botswana International University of Science and Technology
Palapye, Botswana
jamisolar@biust.ac.bw

***Abstract*— Upper limb amputation may be a result of surgery, trauma, disease, or due to a congenital manifestation. Regardless of its cause, losing hands is the most devastating situation because we use them everyday. Experiencing such long-term disability can affect mental, emotional and social well being of an individual. Upon addressing this issue, millions of money have been poured in developing artificial substitution devices, from simple traditional cosmetic prostheses that are body-powered and cable-driven systems to highly complex electromechanical devices in research laboratories known as bionic arms. The realisation for prosthetic devices was after World War II due to large number of imputed soldiers returning home. The US Navy Bureau of Medicine and Surgery and the US Army Surgeon General initialised a national treatment program of artificial limbs prostheses replacement. In a research article by *Clement, 2011* men are 67% highly probable of loosing their hands. It further states that, this commonly happens during the productive working years at 60% chance between ages of sixteen to fifty-four. Botswana Demographic Survey Report for 2017 illustrates that there are 9, 520 persons with arm impairment. The majority of these impairments mostly occur at industrial workplaces, recreational activities like sports, and day to day automobile accidents. In this study, the clinical importance of existing prosthetic devices is investigated. The prosthetic devices are reviewed in contrast with the unique problems faced by users on the service or product delivery, maintenance and practical implications of the devices are assessed. We found out that users have reported social issues, dissatisfaction, and discomfort more especially in old traditional devices. They Kind them unsuitable for showing affection because of their unusual shape and feel. And they go well with certain clothing styles.**

Keywords—Amputation; Upper limb; Prosthesis

I. INTRODUCTION

A. Background

The human arm is a complex system capable of performing sophisticated movements and gestures that enable us to interact with the environment. Losing hands is the most devastating situation, considering that we use them to manipulate things daily. Before and after surgery patients go through counselling. Henceforth, it is not wrong to say amputation does not only affect persons physically but both physically, emotionally, socially and psychologically [1].

From Botswana Demographic Survey Report for the year 2017, there are 9 520 persons with arm impairment. In a research paper by Clement, Bugler and Oliver, they present that man are the most highly probable group with 67\% chance of loosing their hands [2]. It further states that, this commonly happens during the productive working years at 60\% chance between ages of sixteen to fifty-four. In most cases, the majority of this impairments mostly occur at industrial workplaces if safety is not highly exercised, recreational activities like sports, and day to day automobile accidents.

	Disability															
Age Groups	Sight/Visual Impairment		Hearing Impairment		Speech Impairment		Impairment of Leg(s)		Impairment of arms(s)		Remembering		Self-Care		Total	
	Number	Percentage	Number	Percentage	Number	Percentage	Number	Percentage	Number	Percentage	Number	Percentage	Number	Percentage	Number	Percentage
0-4	94	0.2	136	0.8	583	7.5	720	2.8	339	3.6	-	-	573	8.4	1,374	1.5
5-9	1,226	2.7	710	4.2	1,226	15.8	392	1.5	277	2.9	355	3.9	245	3.9	3,034	3.3
10-14	2,206	4.9	679	4.0	831	10.7	440	1.7	417	4.4	1,082	11.7	803	11.8	4,945	5.4
15-19	1,748	3.9	1,023	6.1	827	10.7	555	2.1	307	3.2	438	4.8	394	4.3	4,224	4.6
20-24	2,045	4.6	878	5.2	675	8.7	739	2.8	431	4.5	192	2.1	347	5.1	4,343	4.8
25-29	1,990	4.4	681	4.0	651	8.4	514	2.0	543	5.7	675	7.4	473	7.0	4,297	4.7
30-34	2,769	6.2	1,132	6.8	887	11.4	1,004	3.8	354	3.7	577	6.3	637	9.4	5,863	6.4
35-39	2,317	5.2	498	3.0	479	6.2	1,233	4.7	879	9.2	243	2.7	389	5.7	4,928	5.4
40-44	2,601	5.8	1,031	6.1	312	4.0	1,317	5.0	757	8.0	353	3.9	-	-	5,430	6.0
45-49	3,330	7.4	848	5.0	443	5.7	824	3.2	437	4.6	507	5.6	71	1.0	5,662	6.2
50-54	3,494	7.8	811	4.8	187	2.4	2,055	7.9	603	6.3	822	9.0	200	2.9	6,634	7.3
55-59	2,000	4.5	1,062	6.3	132	1.7	1,949	7.5	572	6.0	223	2.5	213	3.1	4,561	5.0
60-64	2,721	6.1	552	3.3	234	3.0	1,900	7.3	424	4.5	544	6.0	330	4.9	5,476	6.0
65-69	2,731	6.1	1,199	7.1	78	1.0	1,889	7.2	834	8.8	701	7.7	146	2.1	5,682	6.2
70-74	2,777	6.2	824	4.9	-	-	2,542	9.7	528	5.5	655	7.2	126	1.9	5,647	6.2
75+	10,888	24.2	4,770	28.3	221	2.8	8,044	30.8	1,628	17.1	1,744	19.2	1,928	28.4	18,824	20.7
Total	44,939	100.0	16,864	100.0	7,744	100.0	26,115	100.0	9,520	100.0	9,092	100.0	6,796	100.0	90,965	100.0

Figure 1: Distribution of population with disabilities by age, source - http://www.statsbots.org.bw/sites/default/files/Botswana\%20Demographic\%20Survey\%20Report\%202017.pdf.

Tons of money have been invested in rehabilitation engineering to assist individuals with disabilities and aid physical and psychological recovery of lost limbs and/or have defects in their bodies [3]. The realisation of the need for these artificial limb systems was after World War II. The US Navy Bureau of Medicine and Surgery and the US Army Surgeon General initialised a national treatment program of artificial limbs prostheses replacement [4].

ISSN: 2521-2293

Although many prosthetic hands have been proposed and developed, similar research papers have highlighted that most patients prefer traditional hook devices or other simple mechanism as terminal devices - see [5, 6, 7, 8]. Size, weight, appearance and power requirements and other not stated limitations are still imposing a challenge in methods of actuation and degrees of motion in both Externally powered and Body powered prosthesis [9].

B. Purpose of Study

In this paper, we describe the design of a bio-inspired Body power mechanical hand that requires a single actuator and successfully grasp and pick object. Favourable properties of the device include

- Is 3D printed, which offers opportunity for scalability, simple and quick edits, rapid manufacturing processes and more
- The hand resembles the human arm when under-actuated. its is not stiff nor loose.
- needs a single actuator
- works with no need for sensory feedback

The design of the arm start with research work from literature on understating the arm as a biological system, amputation and the clinical significance of artificial limbs. Their follows the designs of our fingered hand.

II. METHODS

In this chapter we study the biomechanics of the hand from both visual aspect and anatomical viewpoint when grasping. We also look into amputation and the use of prosthesis as a method of replacing the impaired hand.

A. The Human Hand

In this section the authors analyse the hand from an anatomical and functional viewpoint, and graphical simulations of the hand, it is essential to understand the biological system of the hand to coordinate the hand gestures. The hand is a prehensile, multi-fingered appendage extending the forearm [10]. It combines mobility, muscle strength, dexterity, and sensitivity. Capable of being expressed into several grips when grasping an object. These grasping mechanism is made all possible by coordination of several pairs of antagonistic muscles to control the fingers' gestures. To fully appreciate the interplay of this muscles, it is important to appreciate and understand the movements at each joint and, the anatomical relationships, actions of the tendons and muscles acting on those joints.

Each finger has three joints:

- Metacarpophalangeal (MP or knuckle) joint between the metacarpal and proximal interphalanges,
- Proximal interphalangeal (PIP) joint between the proximal and middle phalanges, and
- Distal interphalangeal (DIP) joint between the middle and distalphalanges.

This joints allow the fingers to flex to different gestures when picking and/or grasping an object. The most common are

- **Power grasp** – mainly used for holding objects by wrapping the fingers around the object and pushing it against the inner part of the palm, with counter-pressure from the thumb and the hand position is static. Such grips includes cylindrical grip, spherical grip and lateral prehension (thumb is adducted).
- **Precision grasp** – the object is held between the tip of the index finger and thumb, and usually supported by the first digit of the middle finger. The hand's position is dynamic. Such grips include palmar prehension (pulp to pulp), tip-to-tip, and lateral prehension (pad-to-side; key grip).
- **Hook grasp** – used to suspend or pull objects.

(a) cylindrical grip (b) spherical grip

Figure 2: Power grips [11]

(a) tripod grip (b) tip-to-tip grip

(c) palmar grip

Figure 3: Precision grips [11, 12]

Although the terms grasp and grip can be used interchangeably, it is important to differentiate the two (2) words. The first difference is that, grip is to hold or seize an object in the hand while grasp is the action to grip. As of other

ISSN: 2521-2293

sources of information, there are mainly two (2) types of grasps. The power grasp and precision grasp. In this paper we recognise the hook grasp as the other type as it can have many gripping positions as well as the involvement of other fingers while holding objects.

In the precision grip the thumb is abducted in both the metacarpophalangeal and the carpo-metacarpal joints, whereas in the power grip both joints are adducted [13]. The power grip is the strongest when the hand is held dorsiflexed, the combined fingers form one jaw of the clamp with the palm as the other jaw. The thumb in the adducted position is pressed with the pulp surface against the object to be grasped, and this, according to Napier, introduces an element of precision into the power-grip complex, Landsmeer continues. The thenar muscles are used in all forms of power grip except hook grip [14].

The human hand consists of two types of muscle groups which are, extrinsic muscles and intrinsic muscles. The former extends to the forearm while the latter are within the palm. Extrinsic muscles are made up of the long flexors and extensors that coordinate the index, middle and finger they are the thenar(thumb) and hypothenar(little finger). The movements of the fingers except the thumb are based on interplay of several muscles. Although, the thumb and the thenar and hypothena have intrinsic muscles they also have extra extrinsic muscles to serve other purposes that add more favourable capabilities.

B. Amputation

Amputation is the accidental or surgical removal of a body part. Upper limb amputation as an example, commonly are the result of a traumatic injury but may also be a result of a planned operation to prevent the spread of disease in an infected finger or hand. In the least cases, amputated limbs can be replanted (reattached). However, in most cases, surgical replanting may be impossible and advisable that the patient is denied replanting due to medical reasons and complications such as rejection or a spread of disease. Other reasons include, amputated part could be chronically painful, stiff, and/or the patient having an abnormal or absent feeling.

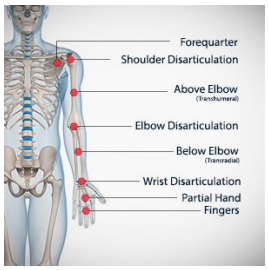

Figure 4: Upper limb extremity amputation levels, source-https://www.prostheticsindia.org/wp-content/uploads/2018/10/amputation-types-upper-limbs.jpg

There are different kinds of arm amputation and people can be amputated due to a number of reasons. The most common include:

- Cancer
- Birth defects
- Cardiovascular diseases, particularly from diabetes or peripheral arterial disease
- Injury (for example, from a motor vehicle crash, work-related accident, or military combat)

Before surgery, the surgeon examines the hand. Often they do imaging like X-rays or others to assess the part. The type of amputation will depend on the part and the amount of tissue being removed based on the extent of the injury and health of the remaining part.

During surgery, the surgeon closes the wound of the amputated area by shortening the bone or tendon so that there's enough soft tissue to cover the bone and rearranging the skin to cover the wound. Recently, in more complicated and sophisticated surgeries, the surgeon may shape the stump to fit a prosthesis later.

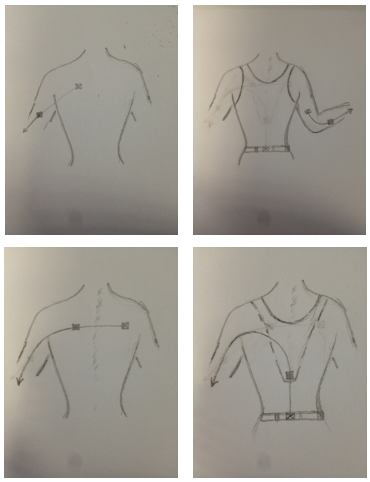

Figure 5. Human force harnessing points and architectures

C. Prosthesis

The evolution of robotic systems has formed highly specialised artificial limb devices to address amputation and save humanity. These bio-inspired technologies are applied in the neuroscience field to design prosthetic implantable limbs that resemble real limbs as in touch, control, and appearance [10]. This device is called a prosthesis. The prosthesis type will depend on the location and length of the stump, functionality, lifestyle needs, and the most notifiable, appearance. They

ISSN: 2521-2293

should enable a person to perform daily activities independently and comfortably. Quite a number of reasons could be drawn from the use of the devices by patients. They restore the length of the partially amputated area, allow the hand amputee to stabilise and hold objects.

At best, a prosthesis may enable the patient to function as well or nearly as well as before the amputation. Successful use of prosthesis depends on a patient's medical conditions, physical & cognitive capabilities, characteristics of the amputation stump, and how well the prosthesis socket fits and connects to the body.

There are two types of modes of controls so far; body-powered (cable transmission) and externally-powered (mainly electric motor driven). These devices are mostly manufactured and used in the western countries and the cost of an externally-powered prosthetic hand ranges from $\$4,000$ to $\$20,000$; depending on the mode of control. [4, 15, and 16] states that 90\% of upper limb impairment is currently using body-powered prostheses due to their simplicity, inexpensiveness, functionality, reliability, and sensory proprioceptive feedback of shoulder motion harnessing and the tension cable transmission. However, chunks of money are invested in externally-powered devices. Thus, this leaves an enormous gap between the two devices.

Quite a number of control mechanisms can be formulated from body motions. As illustrated in Figure 1. However, at higher levels some of the control architectures might be not good enough or absent to control the artificial hand. For instance, elbow movements are absent in above-elbow and shoulder disarticulation, and some of the body motion if not all maybe insufficient to operate the prosthesis. At present, the most common bio-mechanical control source is the shoulder motion [17].

D. Clinical Significance

The final stage after laboratory testing and evaluations is the prescription of the devices in the sense of clinical use to patients. The prescription is in the means that they are purchased by patients, fitted with a training program and maintenance for its use. In short, the fore-mentioned points are clinical significance requirements for a prosthetic device to be legally recommended to patients.

Some difficulties come along with providing prostheses and developing their clinical significance. Artificial upper-limbs, BPs, and EPs have a low record of usage by patients due to several factors. Limbs may be rejected because of stigma and/ or psychological trauma from amputation, too heavy, uncomfortable, and too unreliable to control. Whatever the rationale to the rejection may be, the solution is to emphasise a close interaction between engineers, patients, surgeons, prosthetists, and physical therapists in the design and development of prostheses devices. In other words, success with a prosthesis is most likely to occur when the clinical team involved has many different types of professionals, depending on the person's needs. For more complicated cases, the team may include a psychiatrist, occupational therapist, social worker, psychologist, and family members. A prosthetist's expertise is to evaluate the amputee's(stump) overall functional capabilities and develop a prosthesis treatment plan (covering designing, fitting, fabricating), adjusting the prosthesis, providing lifetime follow-up care to maintain the prosthesis, and provide advice and instruction on care.

Prosthesis fitting requires is a specialised skill. It can be hard for people to make the physical and mental adjustments necessary to function with the prosthesis. Thus, the whole process of selecting and adjusting components and assessing the overall prosthesis function is challenging and takes significant time. Not all patients are candidates for all types of prostheses. Lastly, developing prosthetic devices for clinical use with commercial considerations is also a heavy task to be dealt with. The field for this kind of technology is limited and specialised. For instance, a large scale production means more of the products with higher capital investments that will end up not being utilised. Thus, in the present-day, the method of production and delivery is based on patient requests for the prostheses.

Privacy and legal concerns of the devices are such that the security personnel does not ask people to remove a prosthesis. Otherwise, a special place should be arranged for unfitting the device as some of the clothing has to be removed to unfit a prosthesis. It is recommended that a person writes a letter describing his prosthesis more especially when traveling by air.The evolution of robotic systems has formed highly specialised.

IV. BIO-MECHANICAL HAND DESIGNS

In this section of this research study we describe and formulate the architectures of our bio-mechanical robot as it is designed as a prosthetic device for amputees. Before that, it is the authors intention to highlight that the study will benchmark and improve the transmission, design methods and the aesthetics of the existing researches. Thus, rather than reinventing the wheel, these models will be the base for the designs.

Design objectives

- **Appearance** - should resemble the general form of the human hand
- **Control** - A simple voluntary closing mechanism to control the four fingers with less input force
- **Manufacturability** - Affordable low cost process and scalable for different patients as compared to other prosthesis
- **Weight** - lighter in weight than current prosthetic hands

ISSN: 2521-2293

A. *Fingers*

Understanding the human arm was the starting point for the entire design process. We studied visually the handling and grasping the process of a different object. The human hand was simply sketched to identify different locations of various joints and the possible range of motion. The fingers can be spread apart sideways and rolled slightly culminating in an impressively large amount of total degrees of freedom. Fortunately, to perform the majority of common gripping tasks, only a small amount of motion is required. When grasping, the human finger achieves a con-formal adaptive grip by bending the knuckles to enclose the object in between the fingers and the palm.

The implementation of the movements of the articulations in the arm is based on some mechanisms to flex, extend or fold fingers and other joints like wrist and/or elbow. Basically, the preferred ones are; bar-linkage transmission and/or tension cable transmission. Moreover, the mechanisms can optionally be fitted with spring or elastic rubber string return mechanism added to each articulation.The template is designed so that author affiliations are not repeated each time for multiple authors of the same affiliation. Please keep your affiliations as succinct as possible (for example, do not differentiate among departments of the same organisation). This template was designed for two affiliations.

1) Bar-Linkage Mechanism: If we study the finger anatomy from the fingertip to the last knuckle. That is, the joint between the metacarpals and proximal phalanges joint to the distal phalanges tip, it can be noticed that each finger has three links. Therefore, the first opportunity for simplification comes from treating the distal phalanges and intermediate phalanges as one fixed link as opposed to two separate links joined by the last knuckle.Looking at the hand from the side view, it can be noticed that the human finger rotates approximately 90° from full extension to full closure. Similarly, the second knuckle joint also rotates approximately 90° at this time. It was concluded that the two joints move approximately at the same rate in a $1:1$ ratio. Therefore, that realisation opened up many mechanical possibilities for simple linkages which would allow for the base finger to be rotated actively while at the same time passively linked to the first joint.

2) Cable transmission : The idea of this mechanism is motivated by the human hand actuation mechanism. To achieve the grasping and releasing of objects, two pairs of systems must work together. It can either be tension cables with spring return, tension cables with elastic cord return or bidirectional tension cables for finger flexion and extension. The mechanism consists of force transmission cable inside a stationary hose. This mechanism reduces the weight of the hand and it's easy to implement.

B. *Design Optimisation*

As Childress has pointed out [17], positioning the prosthesis in the world space is the main goal to be achieved in prosthesis control . Designing and manufacturing artificial hand is not to duplicate the human hand but to have a device that enable the user to interact with the environment in the real world.

IV. Results And Discussions

The results of this work have been encouraging. The bio-mechanical hand has satisfactory appearance and control. The movement of the fingers appears realistic and input force are minimised for ease control.

Figure 6: The prototype during experimental testing, grasping an object

IV. Discussion And conclusions

The bio-mechanical hand is modelled from PLA, acrylic and wood that were selected based on weight, aesthetics and toughness. The material are light in weight and impose an aesthetically appealing appearance after finish. Using 3D printing manufacturing technology allows for easy product prototyping and inexpensive mass production for clinical fitting. Although the palm is made of wood, the device can be wholly 3D printed to give realistic appearance with rubberised soft 'skin', improve grip and avoiding the need for cosmetic glove.

The hand is compliant when under actuated and resembling the natural posture of the hand but becomes rigid when actuated. These results in a stiff and stable grip. All the fingers are actuated by a single tension cable (although more may extend their capabilities even further). Consequently, these allows the device to be a modular prosthetic terminal device which can be fitted to either a body- powered or externally-powered prosthesis.

Experiments to evaluate the performance of the body-powered prosthesis are discussed on the previous section. Although the designs closely resemble the human factor form, the designs can further be improved as in design and material selection for prototyping and manufacturing.

Although the design some how are close to resemble the human factor form, the design can be further improved as in design and material selection for manufacturing and

ISSN: 2521-2293

prototyping. The control for the artificial limb has to be smooth with low impedance. This is because the response of BP devices is determined by the mechanical impedance when interacting with objects in the surrounding. When grasping, the middle responds better than other fingers. These is because the tension cable mechanism align with the middles finger. With other fingers, there is slack within the finger tension cable and the fingers. Consequently, reducing performance of the overall prototype.

It further was noticed that the finger as well as the palm lack a firm grim. If the cabling mechanism is no pulled firm enough to grasp the object, it will fall. Comparing this to the human flesh, the PLA plastic used to manufacture the fingers is hard. When the object is held in the hand, the muscles deform and try to take the shape of the object. For this phenomenon to work in our model, the a different filament is proposed. For instance, thermoplastic elastomers (TPE) are a typical materials that the author suggests. They have different range of flexibility, ranging from partially flexible like a car tire but others can be elastic and fully flexible like a rubber band.

Despite the limitations imposed by the hand, we believe that a prosthetic terminal device with design features of the artificial hand in this research paper has the potential to be used as a terminal device in many robotic manipulator system as well as prosthetic devices.

Acknowledgment

Foremost, I would like to express my deepest appreciation to my supervisor Prof. Rodrigo Jr. S. Jamisola, who gave me the golden opportunity to do this wonderful project on the topic "Development of a Mechanically Powered Bionic Arm and Bionic Fingers for Above and Below-Elbow Amputees" as a Final Year Project and and a joined research to publish several papers for the research work and results. It has exposed me to both research and innovation work in mechatronics and robotics. For his patience, motivation, enthusiasm, immense knowledge and guidance helped me to do a functional product and preparing this thesis. I could not imagine having a better advisor and mentor for my undergraduate final year project.

References

1. I. Vujaklija, D. Farina, and O. Aszmann, "New develop- ments in prosthetic arm systems," *Orthopedic Research and Reviews*, vol. 20168, pp. 31–39, 07 2016.
2. R.Clement,K.E.Bugler,andC.W.Oliver,"Bionicpros- thetic hands: A review of present technology and future aspirations," *The surgeon*, vol. 9, no. 6, pp. 336–340, 2011.
3. R. J. Bozeman Jr, "Control system for prosthetic devices," Dec. 27 1994. US Patent 5,376,128.
4. A. L. Muilenburg and M. A. LeBlanc, "Body-powered upper-limb components," in *Comprehensive management of the upper-limb amputee*, pp. 28–38, Springer, 1989.
5. D. G. Shurr, J. W. Michael, and T. M. Cook, *Prosthet- ics and orthotics*. Prentice Hall Upper Saddle River, NJ, 2002.
6. J.W.MichaelandJ.H.Bowker,Atlasofamputationsand limb deficiencies: surgical, prosthetic, and rehabilitation principles. American Academy of Orthopaedic Surgeons Rosemont, IL, 2004.
7. P. E. Klopsteg and P. D. Wilson, Human Limbs and Their Substitutes: Presenting Results of Engineering and Med- ical Studies of the Human Extremities and Application of the Data to the Design and Fitting of Artificial Limbs and to the Care and Training of Amputees. Hafner, 1968.
8. H. H. Sears, J. T. Andrew, and S. C. Jacobsen, "Expe- rience with the utah arm, hand, and terminal device," in *Comprehensive Management of the Upper-Limb Am- putee*, pp. 194–210, Springer, 1989.
9. A. M. Dollar and R. D. Howe, "The sdm hand as a prosthetic terminal device: a feasibility study," in *2007 IEEE 10th International Conference on Rehabilitation Robotics*, pp. 978–983, IEEE, 2007.
10. H. H. Ehrsson, B. Rose´n, A. Stockselius, C. Ragno¨, P. Ko¨hler, and G. Lundborg, "Upper limb amputees can be induced to experience a rubber hand as their own," *Brain*, vol. 131, no. 12, pp. 3443–3452, 2008.
11. Y. D. C. Grandett, N. S. Argote, and R. R. Serrezuela, "Analysis between elm and ann in emg signals obtained for the control of a robotic hand prosthesis," 2006.
12. A. Selin, "Pencil grip: A descriptive model and four em- pirical studies.," 2004.
13. J. Landsmeer, "Power grip and precision handling," *An- nals of the rheumatic diseases*, vol. 21, no. 2, p. 164, 1962.
14. I. Charles Long, P. Conrad, E. Hall, and S. Furler, "Intrinsic-extrinsic muscle control of the hand in power grip and precision handling: an electromyographic study," *JBJS*, vol. 52, no. 5, pp. 853–867, 1970.
15. M. A. LeBlanc, "Innovation and improvement of body- powered arm prostheses: A first step," *Clin Prosthet Or- thot*, vol. 9, no. 1, pp. 13–16, 1985.
16. J. A. Doeringer and N. Hogan, "Performance of above el- bow body-powered prostheses in visually guided uncon- strained motion tasks," *IEEE Transactions on Biomedical Engineering*, vol. 42, no. 6, pp. 621–631, 1995.
17. D. S. Childress, "Powered limb prostheses: their clinical significance," *IEEE transactions on biomedical engineer- ing*, no. 3, pp. 200–207, 1973.

BIUST Teaching, Research, & Innovation Symposium 2023 (TRDAIS 2023)
Botswana International University of Science and Technology
Palapye, Botswana, 18 - 19 September 2023
ISSN: 2521-2293

Paper An Evaluation of the Mining Licensing Regimes in the SADC Region:

The case of Angola, Botswana and Zambia

Munyindei Masialeti
Mining and Geological Engineering Department
Botswana International University of Science and Technology
Palapye, Botswana
masialetim@biust.ac.bw

***Abstract*— Mining is an important strategic sector in the Southern African Development Community region with significant contributions to the gross domestic product, employment, poverty reduction and foreign exchange earnings in many of its member countries. It is also a major producer of rhodium cobalt, chromium, tantalum, manganese, industrial and gem diamonds where some of the member countries are ranked among the top ten global producers.**

The limited mine development in most African countries due to insufficient investment and inadequate exploration for minerals has resulted in most African countries to compete with the rest of the world for risk capital from foreign mining companies who in addition to technical and managerial abilities have the ability to mobilise the high-risk capital needed for such investment. Consequently, most African countries revised their mining codes to cope with the stiffer competition for foreign direct investment and mounting pressure from major donors.

An appropriate mining regulatory framework is one of the four factors for attracting investment and reducing investment risks for private mining companies. The regulatory framework together with mining codes stipulate the allocation, tenure, and operation of mining rights. Therefore, the licensing regimes enshrined in the mining codes are critical factor for analysing the mining regulatory framework.

This paper evaluates licensing regimes for Zambia, Angola and Botswana mining codes to assesses whether they are appropriate for attracting investments and minimising investment risk for private mining companies. A six-point assessment tool was developed based on the characteristics of an appropriate regulatory framework to make the assessment.

It was found that the three countries under review have favourable regulatory frameworks to attract FDI and reduce the investment risk with Botswana meeting 92% (5.5 out of 6) of the requirements, followed by Zambia with 75% (4.5 out of 6). Although the Angolan mining rights could not be explicitly evaluated it was found to meet at least a third of the requirements. In addition, artisanal and small-scale mining that are reserved for citizens in all the three countries are not expected to attract foreign direct investment.

Keywords*— *Mining rights, mining legislation, mining regulatory framework, mining codes, SADC mining

I. INTRODUCTION

Mining is an important strategic sector in Southern African Development Community (SADC) region. It contributes significantly to the gross domestic product (GDP), employment, poverty reduction and foreign exchange earnings in many of its member countries. The latest SADC official compilation from [1] for GDP and Mining's contribution to it for the period 2006 to 2015 is presented in the Table 1.

Table 1: GDP and contribution to GDP from Mining in SADC Countries

Country	Average GDP (US$ Million) (2006 to 2014)			GDP (US$ Million) (2015)		
	GDP (Total)	*Mining*	*Mining (% of GDP)*	*GDP (Total)*	*Mining*	*Mining (% of GDP)*
Angola*	98,097	37,928	39	115,114	25,512	22
Botswana	13,059	2,948	23	14,384	2,625	18
Democratic Republic of Congo (DRC)	24,890	3,913	16	37,587	6,647	18
Lesotho	2,252	141	6	2,280	167	7
Madagascar	8,956	16	0.18	8,920	20	0.22
Malawi	5,824	52	1	6,430	n.a	n.a
Mauritius	10,374	32	0.31	11,681	25	0.21
Mozambique	12,843	349	3	15,466	772	5
Namibia	10,611	1,281	12	11,545	1, 428	12
Seychelles	1,096	0	0	1,380	0	0
South Africa (RSA)	337,846	26,854	8	314,792	22,431	7
Eswatini	4,077	12	0.3	3,946	6	0.15
Tanzania	33,904	1,338	4	45,772	1,821	4
Zambia	20,575	2,736	13	21,274	2,697	13
Zimbabwe	10,357	767	7	14,419	1,098	8
SADC Total	594,761	78,367	13.18	624,990	65,249	10.44
*Includes Petroleum						

Source: Compiled from [1]

For the period under review, South Africa generated the highest income from mining at more than US$22 billion in 2015 accounting for about 7% of its GDP. The most significant percentage contributions to GDP from mining was 22% (Angola), 18% (DRC and Botswana), 13% (Zambia) and 12% (Namibia). The strategic position of Mining in SADC including its contribution to the gross domestic product

ISSN: 2521-2293

(GDP), employment and poverty reduction and as a source for earning foreign exchange has also been highlighted by [2]

Table 2: Status of Mineral Production in SADC in 2020

Country	Mineral	Percentage of Global Production	Ranking in Production	
			Global 2020 (2019)	***SADC 2020 (2019)***
Angola	Gem Diamond	11.22	4(4)	2 (2)
	Industrial Diamond	1.68	7(7)	5 (5)
Botswana	Gem Diamond	19.04	3(3)	1 (1)
	Industrial Diamond	10.96	5(4)	3 (2)
Congo D R	Cobalt	67.07	1(1)	1 (1)
	Tantalum	35,67	1(1)	1(1)
	Copper	8.24	4(4)	1(1)
	Tin	5.29	7(7)	1(1)
	Gem Diamond	4.17	6(6)	4 (4)
	Industrial Diamond	22.43	3(3)	1(1)
Madagascar	Graphite	5.11	3(4)	1 (2)
	Cobalt	0.75	12 (8)	2 (2)
	Titanium	2.62	10(9)	3 (2)
	Beryllium	0.50	4(3)	2 (2)
Mozambique	Graphite	1.93	6(2)	2 (1)
	Zircon	8.42	4(4)	2 (2)
	Tantalum	5.59	6(7)	2(2)
	Titanium	10.57	3(3)	2(2)
	Beryllium	1.32	3(*)	1 (1)
Namibia	Uranium	11.34	3(4)	1(1)
	Gem Diamond	2.30	7(7)	5(5)
	Industrial Diamond	0.16	10(10)	6 (6)
South Africa	Fluorspar	2.77	5(5)	1 (1)
	Vermiculite	28.38	1(1)	1 (1)
	Zircon	25.23	2(2)	1 (1)
	Steam Coal	4.25	6(7)	1 (1)
	Iron	2.38	7(7)	1 (1)
	Chromium	45.49	1(1)	1 (1)
	Manganese	31.04	1(1)	1 (1)
	Titanium	11,28	2(2)	1 (1)
	Vanadium	8.12	3(3)	1 (1)
	Palladium	33.15	2(2)	1 (1)
	Platinum	67.62	1(1)	1 (1)
	Rhodium	80.93	1(1)	1 (1)
	Gem Diamond	5.48	5(5)	3 (3)
	Industrial Diamond	11.05	4(5)	2
Zambia	Beryllium	0.03	7(6)	3
	Copper	4.24	7(8)	2
Zimbabwe	Vermiculite	6.33	6(6)	2
	Chromium	4.78	5(5)	2
	Lithium	0.46	7(5)	1
	Palladium	6.47	5(5)	2
	Platinum	9.06	3(3)	2
	Rhodium	6.52	3(3)	2
	Gem Diamond	0.86	8(10)	6
	Industrial Diamond	4.63	6(6)	4

Compiled from [3]

In addition, SADC region is endowed with vast mineral resources that are of global significance. Table 2 below shows the minerals mined in each country as well as their ranking and contribution to the global mineral production among the top ten for 2019 and 2020. The region contributes significantly to global mineral production of Rhodium (RSA (80.93%)), Cobalt (DRC (67%)), Chromium (RSA (45%)), Tantalum (DRC (36%)), Manganese (RSA (315)), Industrial diamonds (DRC (22%), RSA (11.5), Botswana (11%))and Gem Diamond (Botswana (19%), Angola (11%)).

However, there is limited mining development in most African countries due to insufficient investment and inadequate exploration for minerals. As indicated by [4], investment in the mining sector in the developing world (Africa inclusive) has relied on aid and soft loans during independence era (1960 to 1990) and predominantly on Direct Foreign Investment (DFI) before and after that era. As such, African countries must compete with the rest of the world for risk capital from foreign mining companies who in addition to technical and managerial abilities have the ability to mobilise the high-risk capital needed to invest for locating and developing new mineral deposits [5,6]

On the other hand, mobilising financial, technical and managerial resources for mine development entails a mining policy that fosters predominantly private sector participation in the operation and development of mines while the government focusses on regulating and promoting the mineral [5]. To cater for this, most African countries revised their mining codes [4] to cope with the stiffer competition for foreign direct investment and mounting pressure from major donors [7]. Moreover, large-scale mineral exploration and development often leads to the development of improved legal frameworks that foster foreign investment in mineral extraction [8]. Likewise, SADC countries have revised and enacted mining codes to create a conducive investment environment for foreign mining companies, to attract foreign investment and ultimately boost mineral production [9].

A survey of 80 international companies that invest in developing countries revealed that after the mineral potential and existing infrastructure, stable legal and fiscal framework, including a mining code are among the other criteria used for making such investments [6]. The same study recommended appropriate regulatory frameworks, economic and fiscal policy, institutional reforms and infrastructure, as well as environmental effects as the four main strategic areas for attracting investments and reducing investment risk for private mining companies. The concept of the regulatory framework as used in the survey to denote both “the mining code and the issue of mineral rights and licenses” has been adopted in the study.

This paper evaluates licensing regimes in mining codes for Zambia, Angola and Botswana to assesses whether they are appropriate for attracting investments and minimising investment risk for private mining companies. The three countries selected represent a major base metal producer (Zambia), a diamond producer (Botswana) and a country where mining is not the main stay but second after petroleum (Angola).

ISSN: 2521-2293

II. METHODOLOGY

To assess the mining codes against attractiveness and low risk to investment the research was divided into two phases. The first phase involved reviewing literature to identify the characteristics of a mining regulatory framework that make it attractive for and reduce risk for investment for the development of an assessment tool. Phase two involved applying the tools developed to the licensing regimes in the mining codes.

A. The mining regulatory framework factors for attracting and reducing risk for investment

As reported by [6], mining code was defined by the world bank as "the combination of statute law, regulations and agreements which governs the allocation, tenure and operation of mining rights". In addition, the mining code together with the issuance of mineral rights constitute the regulatory framework. Therefore, the licensing regime in a mining code is critical factor for analysing the mining regulatory framework.

An appropriate regulatory framework reduces the investment risks in two ways; firstly, by having stable policies and reducing the uncertainty factor; and secondly by providing protection against foregoing mining rights. To be appropriate, a regulatory framework must have following six characteristics;

- It must be clear and stable, with minimal ministerial discretion, and coordination with other legislation.
- It must be impartial (equally applied) to all investors irrespective of their category (private or public) or their origin.
- The mining rights must be transferable.
- It should provide long-term security of tenure
- The provisions for conditions of termination should be clearly stated
- The conversion from exploration and exploitation licenses should be easy.

B. Development of an Assessment tool

Based on the factors above, a mining licence regimes Assessment tool has been developed in table 3 below.

Table 3: Tool for assessing the attractive to and minimizing risks to mining investment

Criterion	Description
1	Clarity and stability of the framework
2	Impartiality of the framework
3	Transferability of mining right
4	Security of tenure of mining right
5	Clarity of conditions for terminating a mining right
6	Ease of conversion of mining right from exploration and exploitation

III. ASSESSMENT OF LICENSING REGIMES

In this section the tool developed above is applied to assess the mining licence regimes for the three countries.

Assessment of mining rights for Botswana

The mining rights in Botswana are prospecting licence, retention licence and mineral permit [10]. Table 4 presents the assessment of Botswana licensing regime.

Table 4: Assessment of Botswana licensing framework

#	Criterion	*Exploration licence*	*Retention Licence*	*Mining licence*	*Mineral Permit*
1	Clarity	Application requirements including obligations and rights of holder as well as types of minerals are clearly stated			
	Stability	Not Stable Although the licence is offered by the minister, the government can acquire mining rights over an area			
2	Impartiality	No specific Preference Except for Government Investment			reserved for citizens or citizen owned companies as small-scale mining operations
3	Transferability of mining right	Possible upon approval by the minister		Not transferable	Possible upon approval by the minister
4	Security of tenure of mining right	adequate for the stage of mining (3 years and renewable)	adequate for the stage of mining (3 years)	Adequate for the stage of mining (25 years; renewable)	Adequate for the type of mining operation (5 years; renewable)
5	Clarity of conditions for terminating a mining right	Conditions for refusal, suspension or closure are clearly stated for both individuals and companies			
6	Ease of conversion of mining right from exploration and exploitation	Not Applicable New Minerals can be included Can apply for a mining licence upon expiry of licence	Can apply for a mining licence upon expiry of licence	Cannot be converted to any other licence	

Assessment of mining rights for Angola

According to [11] the characteristics of the 2011 Mining Code (approved by Law 31/11 of 23 September 2011) are as follows:

- The Angolan legal system does not impose any restrictions on mineral rights that can be acquired and exercised by foreign entities
- Mineral rights for exploration or mining of minerals for civil construction or mining of mineral-medicinal waters may only be granted to Angolan citizens, or to companies co-owned with Angolan citizens,
- Artisanal mining is reserved for Angolan citizens only.
- The mineral rights for exploration are granted for an initial period of up to five years, with possible two one-year extensions

ISSN: 2521-2293

- Mining rights are granted for a period of up to 35 years with possible extension of one or more 10-year periods.
- Mineral rights are granted, from the outset, for the whole of the mineral process under a single-contract model.

Although the mining rights for Angola could not be explicitly evaluated due to unavailability of the English version of the mining codes, the following could de deduced from the mining law reviews.

- The mining codes meets the impartiality, security of tenure and conditions for termination or refusal of a mining right.
- The contract model adopted in the mining code is unique.

Assessment of mining rights for Zambia

The mining rights in Zambia are the exploration and mining licence [12]. Table 5 presents the assessment of Zambian licensing regime.

Table 5: Assessment of Zambian licensing framework

#	Criterion	Exploration licence	Mining licence
1	Clarity	Application requirements including obligations and rights of holder as well as types of mining operations are clearly stated	
	Stability	Not Stable Although the licence is offered by a committee chaired by the director of mining cadastre, the minister may close an area and the government can acquire mining rights over an area	
2	Impartiality	No specific Preference Except for Government Investment	Artisanal and Small-scale mining operations are reserved for citizens or citizen owned or empowered companies
3	Transferability of mining right	Not mentioned	Not mentioned. However, operations may be differed upon written approval
4	Security of tenure of mining right	adequate for the stage of mining (4 years and renewable)	Adequate for each scale of mining 2 years for artisanal mining 10 years for small scale mining 25 years for large scale mining All are renewable
5	Clarity of conditions for terminating a mining right	Conditions for refusal, suspension or closure are clearly stated for both individuals and companies	
6	Ease of conversion of mining right from exploration and exploitation	application for a mining licence within 6 months before expiry of prospecting licence	Conversion is not catered for

IV. Discussion and Conclusions

The mining Acts for Botswana and Zambia have been used to assess the mining rights using the six-criteria tool developed from the literature review. However, the mining rights for Angola could not be explicitly evaluated due to unavailability of the English version of the mining code in public domain.

It has been found that:

- All the mining rights meet the criteria of security of tenure for both the various stages of mine life cycle and the scales of mining operations
- The Application requirements including obligations and rights of holder as well as types of minerals are clearly stated in the mining Acts of Botswana and Zambia
    - Except for the retention licence, all mining rights in Botswana are transferable upon approval by the minister. The Zambian act is silent on the matter.
    - Only artisanal and small-scale mining operations are reserved for citizens. However, large scale mining operations are generally not subject to any restrictions.
    - The conditions for termination and conversion of one mining right to the other are clearly stated

It can therefore be concluded that the three countries under review have favourable regulatory framework to attract FDI with Botswana meeting 92% (5.5 out of 6), followed by Zambia with 75% (4.5 out of 6).

Although the Angolan mining rights could not be explicitly evaluated it meets at least a third of the requirements. Artisanal and small-scale mining that are reserved for citizens are not expected to attract DFI.

References

[1] Southern Africa Development Conference, “SADC Statistical Yearbook 2015,” 2016.

[2] O. O. Awolusi, “Mining Sector and Economic Growth in Southern African Economies: A Panel Data Analysis 14-15 June 2016,” Annual Forum 2016: Industrialisation and the Mining Economy, Trade and Industrial Policy Technology, Johannesburg, 2016.

[3] C. Reichl and M. Schatz, “World Mining Data,” Minerals Production, vol. 37, 2022.

[4] C. Frick, “Direct Foreign Investment and the Environment: African Mining Sector,” in Conference on Foreign Direct Investment and the Environment Lessons to be learnt from the Mining Sector, Paris, France, 2002.

[5] The World Bank, “Strategy for African Mining. World Bank Technical Paper Number 181, Africa Technical Department Series, Mining Unit, Industry and Energy Division,” Washington, DC, 1992.

[6] B. Campbell, “Revisiting the Reform Process of African Mining Regimes,” Canadian Journal of Development Studies, vol. 30, no. 1-2, pp. 197-217, 2010.

[7] H. Besada and P. Martin, “Mining Codes in Africa: Emergence of a "Fourth" Genearatio?,” The North-South Institute (NSI), 2013.

[8] Holman Fenwick William, “A guide to Investing in a Mining Project: An overview of Four of Asia Pacific's Key Mining Areas: Indonesia, Mongolia, Vietnam and Australia,” Holman Fenwick Willan Singapore LLP, 2012.

[9] Economic Commission for Africa, “Africa Review Report on Mining (Summary),” United Nations Economic and Social Council, Addis Ababa, Ethiopia, 2009.

[10] Republic of Botswana, Mines and Minerals Act, 1999.

[11] I. Sousa and H. Moreira, “Chapter 1: Angola,” The Mining Law Review, pp. 1-10, 2016.

[12] Republic of Zambia, Mines and Minerals Development Act, 2015.

ISSN: 2521-2293

BIUST Teaching, Research, & Innovation Symposium 2023 (TRDAIS 2023)
Botswana International University of Science and Technology
Palapye, Botswana, 18 - 19 September 2023
ISSN: 2521-2293

Submission Type: Paper

Track: Infrastructures and Mining

The Pros and Cons of Ban on Coal Energy: Way Out for Africa

Oniyide G. O.

Botswana International University of Science and Technology,

Department of Mining and Geological Engineering

Corresponding Email: oniyideg@biust.ac.bw

Abstract

Coal usage has contributed immensely to evolution of general manufacturing, iron and steel production, power generation, railways and other industries. Apart from its usage in the industries, coal mining is also an important source of income for many countries. The call for world transition from coal to renewable energy has been on for some times in the past. This is because coal is considered one of the most green-house-gas intensive sources of electricity. This paper, therefore, investigates the pros and cons of banning coal as a source of energy generation. The data used in this study were mostly sourced from the literature. The study reveals that China, the United States, India, Russia, Japan, Germany, South Africa, South Korea, Indonesia and Poland are the top ten top countries in the world using coal energy. The findings also show that the cons outweigh the pros. It is recommended that African countries whose main source of energy generation is from coal should endeavour to reduce its environmental impact through coal liquefaction and gradual phase-out of coal fired plants.

Keywords: Ban, coal, energy.

ISSN: 2521-2293

I. INTRODUCTION

The human-caused (anthropogenic) changes to the climate have been attributed to Greenhouse gas (GHG) emissions. Global GHG emissions sources are usually attributed to five broad sectors, characterised by the Intergovernmental Panel on Climate Change (IPCC) Working Group III (WG3) as energy systems, industry, buildings, transport, and AFOLU (agriculture, forestry and other land uses). Most of the emissions are from carbon dioxide from burning fossil fuels: coal, oil, and natural gas. Electricity generation and transport are major emitters, the largest single source being coal-fired power stations with 20% of GHG. Deforestation and other changes in land use also emit carbon dioxide and methane [1],[2].

The United Nations Framework Convention on Climate Change (UNFCCC) established an international environmental treaty to combat "dangerous human interference" with the climate system, by 2022 the UNFCCC had 198 parties. Its supreme decision-making body, the Conference of the Parties (COP), meets annually to assess progress in dealing with climate change [3].

The treaty established different responsibilities for three categories of signatory states, which are developed countries, developed countries with special financial responsibilities, and developing countries. The developed countries, who are members of Organisation for Economic Co-operation and Development (OECD) also called Annex 1 countries, originally consisted of 38 states, 13 of which were Eastern European states in transition to democracy and market economies, and the European Union [1].

It was recognized that Annex I nations had produced most of the GHG emissions, and therefore were responsible for taking the first steps in reducing emissions. Annex 1 countries are called upon to adopt national policies and take corresponding measures on the mitigation of climate change by limiting their anthropogenic emissions of GHG as well as to report on steps adopted with the aim of returning individually or jointly to their 1990 emissions levels. The developed countries with special financial responsibilities are also called Annex II countries. They include all the Annex I countries with the exception of those in transition to democracy and market economies. Annex II countries are called upon to provide new and additional financial resources to meet the costs incurred by developing countries in complying with their obligation to produce national inventories of their emissions by sources and their removals by sinks for all greenhouse gases not controlled by the Montreal Protocol. The developing countries are then required to submit their inventories to the UNFCCC Secretariat [4].

Because key signatory states are not adhering to their individual commitments, the UNFCCC has been criticized as being unsuccessful in reducing the emission of carbon dioxide since its adoption [5]. For example, in 2009, the Chinese government maintained that coal would remain its major energy source despite the impact on global warming [4].

Coal is carbon-rich mineral that has been used to generate electricity in the US and other developed nations since the 1800s [6]. Coal being a major industrial and residential fuel in some countries, currently produces roughly 27% of the world's energy, second only to crude oil, and is the largest single source of electricity (~41%). Globally, enough reserves are available to last more than a century, with nearly half the known reserves in the US, China and India. These countries have large projected increases in energy demand over coming decades. Coal-fired power plants are currently among the least expensive power source in cost to generators per kWh of electricity. Hence there are enormous economic and socio-political incentives to expanded construction of coal-fired power plants. However, emissions from coal-fired plants have substantial impacts on both air quality and climate change. The potential risks associated with Coal-fired power plants are emission of carbon dioxide (CO2), sulphur dioxide (SO2), a precursor of fine particulate and acid rain, nitrogen oxides (NOx, which is NO+NO2), gases influencing tropospheric ozone and methane as well as particulate, in addition to producing other pollutants such as mercury and solid waste [4] [7] [8] [9].

Figure 1 shows the world population forecast between 2022 and 2100. It is projected that Africa will witness a tremendous population growth which implies that there will be increase in energy consumption. The continent, therefore, needs to strategise on ways of increasing electricity generation and distribution. This, however, must be achieved with serious consideration for environmental sustainability.

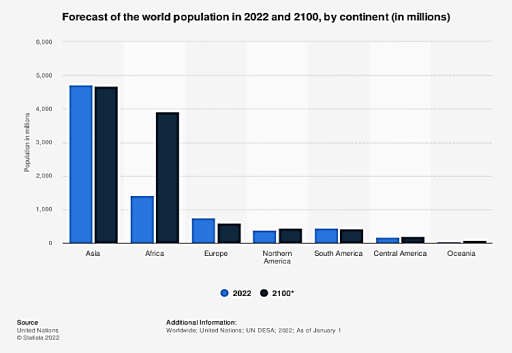

Figure 1: Forecast of the world population in 2022 and 2100 by continent (in millions)

ISSN: 2521-2293

Figure 2 shows electricity consumption by country for the year 2022. It is obvious that African continent is far behind in terms of electricity consumption. The reason can be attributed to inadequate power supply and low level of industrialization.

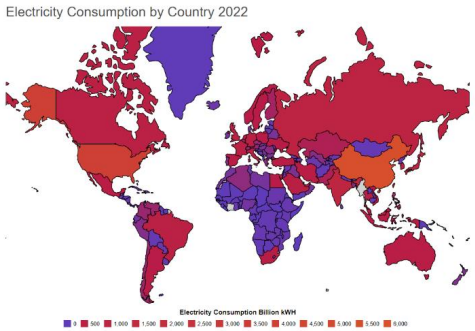

Figure 2: Electricity consumption by country for the year 2022

II. METHODOLGY

The data used in this research were sourced from online data repositories such as ourworldindata, Statistica, worldometers, worldpopulationreview and published articles. The first set of data is on global CO_2 emission from industries and fossil fuel. The second set of data captures global CO_2 emission from coal. The dataset on coal consumption by country is from worldometers.

III. RESULTS

Global CO_2 emission from industries and fossil fuel

Figure 3 shows the global CO_2 emission from the seven continents: Africa, Antarctica, Asia, Australia, Europe, North America and South America between 1750 and 2020. The figure revealed that Asia, Europe and North America have the highest CO_2 emission with peak values of 20608,592 million tonnes, 8015,589 million tonnes, and 7376,088 million tonnes respectively. Africa, Antarctica, Australia, and South America have peak CO_2 emission of 1408,479 million tonnes, 1230,511 million tonnes, 416,001 and 0,015 million tonnes respectively. It is worth noting that the emission from Antarctica is negligible when compared with other continents. This is reason is that it is the only continent with no permanent human habitation.

Figure 4 shows countries with highest CO_2 Emission from fossil fuels and industry. It is evident from the figure that China, United States, European Union, India and Russia are on top, while Brazil, South Africa and United Kingdom follow.

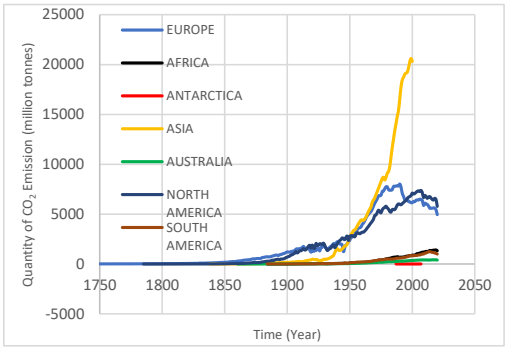

Figure 3: Global CO_2 emission by continents from industry and fossil fuel

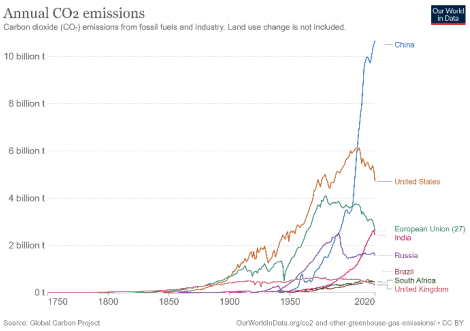

Figure 4: Global CO_2 emission by counties with highest emission

Figure 5 shows the comparison in level of CO_2 emission per person in the year 2005 and 2020. It is observed from the figure that there is reduction in the CO_2 emission across the continent except for Asia.

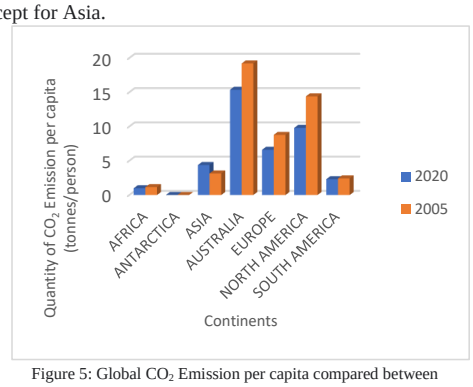

Figure 5: Global CO_2 Emission per capita compared between 2005 and 2020

Figure 6 presents the global CO_2 emission per capita for all the continents. As may be observed from Figure 6, it seems obvious

ISSN: 2521-2293

that the world's most populous countries and highest overall energy consumers would also use the largest amount of coal. However, when broken down into per capita usage (Figure 6), which divides the total usage by the number of people living in the country, the list of most coal-dependent countries changes significantly. Figure 6 revealed that Australia, Europe and North America have the highest CO_2 emission with peak values per capita.

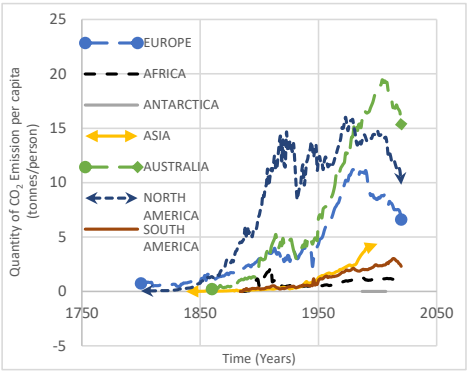

Figure 6: Global CO_2 Emission Per Capita

Global CO_2 emission from coal

Out of the fifty countries with the highest electricity consumption, only three African countries are on the list, with South Africa 21 (207.10 Billion kWH), Egypt 23 (159.70 Billion kWH) and Algeria (55.96 Billion kWH) having 21st, 23rd and 46th positions respectively. Table 1 shows the ten countries with the highest coal consumption. Numbers are expressed in Million cubic feet (MMcf). Not all these countries depend on coal for electricity generation.

Table 1: Ten countries with the highest coal consumption

S/N	Countries	Coal Consumption (MMcf)	Countries	Per Capita Coal Consumption (MMcf)
1	China	4,320	Australia	5,343
2	India	966	Bulgaria	4,927
3	United States	731	Serbia	4,878
4	Germany	257	Kazakhstan	4,858
5	Russia	230	Czech Republic	4,654
6	Japan	210	New Caledonia	4,213
7	South Africa	202	Poland	3,917
8	South Korea	157	South Africa	3,599
9	Poland	149	Greece	3,587
10	Australia	130	Germany	3,133

Figure 7 presents countries, indicating their coal utilization for electricity generation. It is obvious from the figure that China, United States and India are in the forefront. Following them are Japan, Germany, Russia, South Africa and so on.

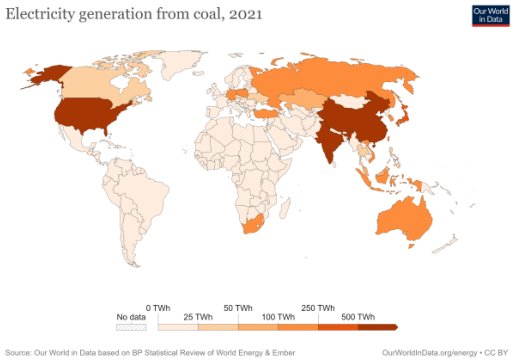

Figure 7: Electricity generation from coal

Aside using coal for generation of electricity, coal has been used for centuries to cook food, heat homes and businesses, fuel furnaces and forges, power the steam engines of locomotives and ships, and more. Figure 8 shows coal consumption by counties.

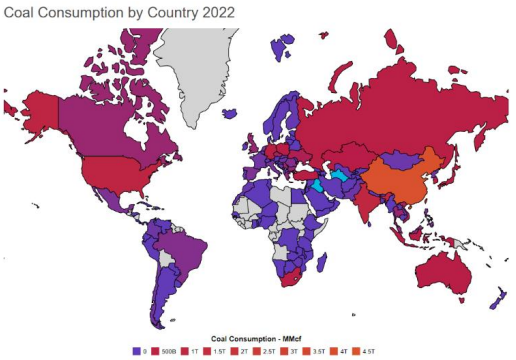

Figure 8: Coal consumption by counties.[10]

Coal has been termed "dirtiest" of the fossil fuels, known to release significant amounts of greenhouse gases and other air pollutants when burned. Figure 9 shows the global CO_2 emission from coal by continent while Figure 10 shows emission by country. This trend is not different from the one described for global CO_2 emission from industry and fossil fuel

ISSN: 2521-2293

Also, the trend of the global CO_2 emission from coal per capita (Figure11) is like the one observed for global CO_2 emission from industry and fossil fuel.

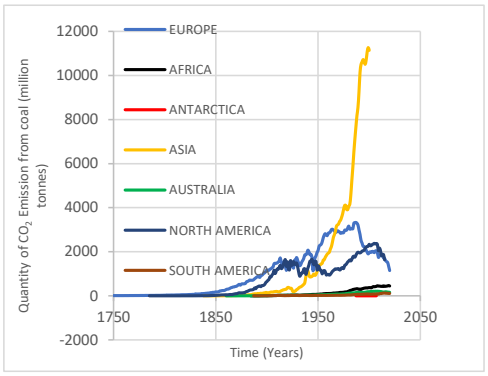

Figure 9: Global CO_2 Emission from coal by continent

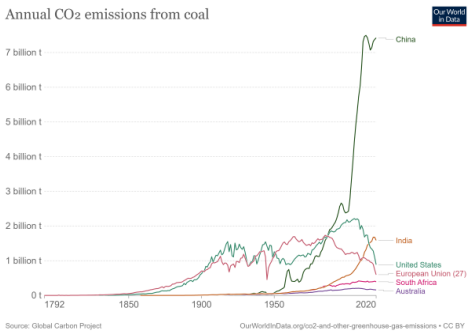

Figure 10: Global CO_2 Emission from coal by countries

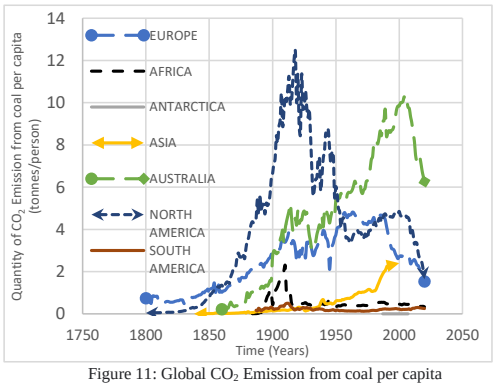

Figure 11: Global CO_2 Emission from coal per capita

When will countries phase out coal power?

Based on the significant contribution of coal power to greenhouse gases and other air pollutants, the question that comes to mind is "When will countries phase out coal power?"

Climate experts calculate that the use of coal, primarily in power plants generating electricity, is responsible for 30% of all global warming. Data such as this has prompted the majority of the world's countries to attend international meetings such as the 2021 COP26 climate summit in Glasgow, Scotland, and pledge to reduce their coal use as part of a global shift toward cleaner energy. Figure12 presents the map of countries that have pledged to phase out coal power at specified dates, while Figure 13 shows the distribution of existing, closing, planned and under construction power plant across the globe.

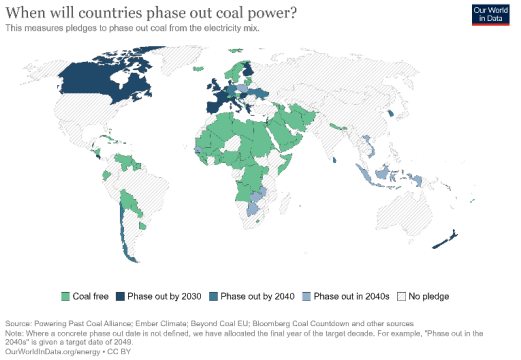

Figure 12 Plan to phase out power plant across the globe.

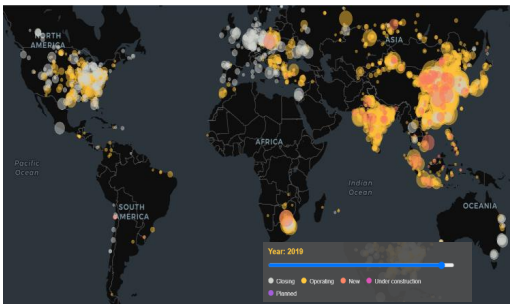

Figure 13 Distribution of power plant across the globe

Source: IndexMundi.com: Electricity - Consumption - Country Comparison

ISSN: 2521-2293

IV. CONCLUSION

The human-caused (anthropogenic) changes to the climate have been attributed to Greenhouse gas emissions. It is important to limit generation of Greenhouse gas emissions in order to counter its side effect such as extreme weather, food supply disruptions, and increased wildfires, global warming and so on. It is important for the African countries to have a strategic plan to achieve alternative renewable energy as replacement for the coal energy utilization.

REFERENCE

[1] Heede, Richard. (2014). Tracing anthropogenic carbon dioxide and methane emissions to fossil fuel and cement producers, 1854–2010. Climatic Change. 122. 10.1007/s10584-013-0986-y.

[2] Lamb, William & Wiedmann, Thomas & Pongratz, Julia & Andrew, Robbie & Crippa, Monica & Olivier, Jos & Wiedenhofer, Dominik & Mattioli, Giulio & Al Khourdajie, Alaa & House, Jo & Pachauri, Shonali & Figueroa, Maria & Saheb, Yamina & Slade, Raphael & Klaus, Hubacek & Sun, Laixiang & Ribeiro, Suzana & Khennas, Smail & Can, Stephane & Minx, Jan. (2021). A review of trends and drivers of greenhouse gas emissions by sector from 1990 to 2018. Environmental Research Letters. 16. 10.1088/1748-9326/abee4e.

[3] R. Stavins, J. Zou, et al., "International Cooperation: Agreements and Instruments." Archived 29 September 2014 at the Wayback Machine Chapter 13 in: Climate Change 2014: Mitigation of Climate Change. Contribution of Working Group III to the Fifth Assessment Report of the Intergovernmental Panel on Climate Change. Cambridge University Press, 2014.

[4] Shindell, D. & G, Faluvegi. (2009). The net climate impact of coal-fired power plant emissions. Atmospheric Chemistry and Physics Discussions. 10. 10.5194/acp-10-3247-2010.)

[5] Schiermeier, Quirin (2012). "The Kyoto Protocol: Hot air". Nature. 491 (7426): 656–658. Bibcode:2012 Natur.491..656S. doi:10.1038/491656a. PMID 23192127. S2CID 4401151]

[6] National Research Council of the National Academies 2010 Hidden Cost of Energy Unpriced consequences of energy production and use Washington DC USA the national academies press.

[7] Mittal, M. L., Sharma, C., & Singh, R. (2012,August). Estimates of emissions from coal fired thermal power plants in India. In 2012 International emission inventory conference (pp.13-16).2.

[8] Giuliano, S., Buck, R., & Eguiguren, S. (2011). Analysis of solar-thermal power plants with thermal energy storage and solar-hybrid operation strategy. Journal of Solar Energy Engineering, 133(3).3.

[9] Nazari, S., Shahhoseini, O., Sohrabi-Kashani, A.,Davari, S., Paydar, R., & Delavar-Moghadam, Z.(2010). Experimental determination and analysisof CO2, SO2 and NOx emission factors in Iran'sthermal power plants. Energy, 35(7), 2992-2998

[10] Hannah Ritchie, Max Roser and Pablo Rosado (2020) - "CO_2 and Greenhouse Gas Emissions". Published online at OurWorldInData.org. Retrieved from: 'https://ourworldindata.org/co2-and-other-greenhouse-gas-emissions' [Online Resource]

BIUST Teaching, Research, & Innovation Symposium 2023 (TRDAIS 2023)
Botswana International University of Science and Technology
Palapye, Botswana, 18 - 19 September 2023
ISSN: 2521-2293

Are Biofuels a real alternative for fuel supply in the developing world or just a perception?

Gift Bakumbi*, Moses Tunde Oladiran

Faculty of Engineering and Technology, Botswana International University of Science and Technology, Palapye, Botswana

*Contact author: Email: bakumbi.gift@gmail.com/gift.bakumbi@bera.co.bw

ABSTRACT

Most countries in the Southern African subcontinent do not produce oil except Angola, South Africa and the Democratic Republic of Congo (DRC). However, oil is a huge socio-economic growth driver in these countries for industrialisation and transportation. These countries operate on high import bills, growing environmental impacts from greenhouse gas (GHG) emissions and global warming leading to climate change. Studies have revealed that one way of addressing these challenges is through the inclusion of Biofuels in the energy supply mix. However, there are competing and conflicting needs which these developing countries are still grappling with such as sustainable food production and food security. This paper considers the real potential of biofuels in developing countries vis-a-vis food production and security challenges. It estimates the pragmatic biofuel production levels that can be achieved without creating food production conflict.

Keywords: *Biofuels, SADC Countries, Feedstock, Food Security, Production Capacity*

1. Introduction

Southern African Development Community (SADC) countries require energy for development and economic growth. Central to their energy supply are fossil-based petroleum fuels imported from markets such as The Middle East, Asia, and Europe (https://wits.worldbank.org/). SADC countries are *price takers.* They grapple with ever-changing fuel prices and shortages amidst economic hardships and challenges. These, and environmental pollution caused by emissions from fuel combustion, make petroleum fuels undesirable and compel the world to remove or reduce their use. In response, SADC, accepted international protocols on climate change and global warming. SADC domesticated these protocols through policies and action plans (SADC, 2010) (SADC, 2012). Some outcomes of 2021 United Nations Climate Change Conference (COP26) are reducing 2030 emissions and limiting global warming to 1.5°C (2.7°F) and end international financing for fossil fuels (UN, 2021). These challenge SADC to rethink its energy self-sustenance which should be met through clean production responding to Sustainable Development Goal number seven (SDG 7).

Albeit energy challenges, SADC is endowed with vast coal resources (Cairncross, 2001). South Africa has been producing fuel from coal since mid-1930's (United States Environmental Protection Agency, 1980) (Yiming Li, 2019) whilst Botswana plans to do so by 2025 (https://www.spglobal.com/, 2020). However, the process should be *green* and resultant fuels emit less GHGs. Biofuels can help

ISSN: 2521-2293

developing countries reach self-sustenance and clean energy (Oladiran , et al., 2011), due to their advantages e.g. low carbon emissions and renewability. Biofuel production requires feedstocks, which are often food production sources. SADC struggles with food security and has numerous droughts and high malnutrition levels. Food unsecured population was 51.3million (15%) of SADC's population in 2020/21 (Centre for Coordination of Agricultural Research and Development for Southern Africa, 2021). Availability of farmland and adequate rainfall are other challenges (Mega Trends in the Southern African Region, 2020). This challenge remains valid whether biofuels are produced from edible or non-edible sources. Even in cases where agro-wastes are feedstocks, agro-production must precede biofuel production. Using waste as feedstock could achieve energy security, GHG emission reduction, pollution control and waste management, thus achieving other environmental and public health goals. Improved waste management could release land required for feedstock farming.

This paper considers realistic biofuel production capacity in selected SADC countries, feedstock availability, energy-food conflict, land availability, food production and policies for biofuel production and use.

Fuel Consumption in SADC

The world's oil demand is 97,103,871barrels/day (Worldometers (https://www.worldometers.info/oil/oil-consumption-by-country/), 2022) of which 48.6% is road transport (Statistica (https://www.statista.com/), 2020). See figure 1 below.

Figure 1: World Oil Demand by Sector, 2020

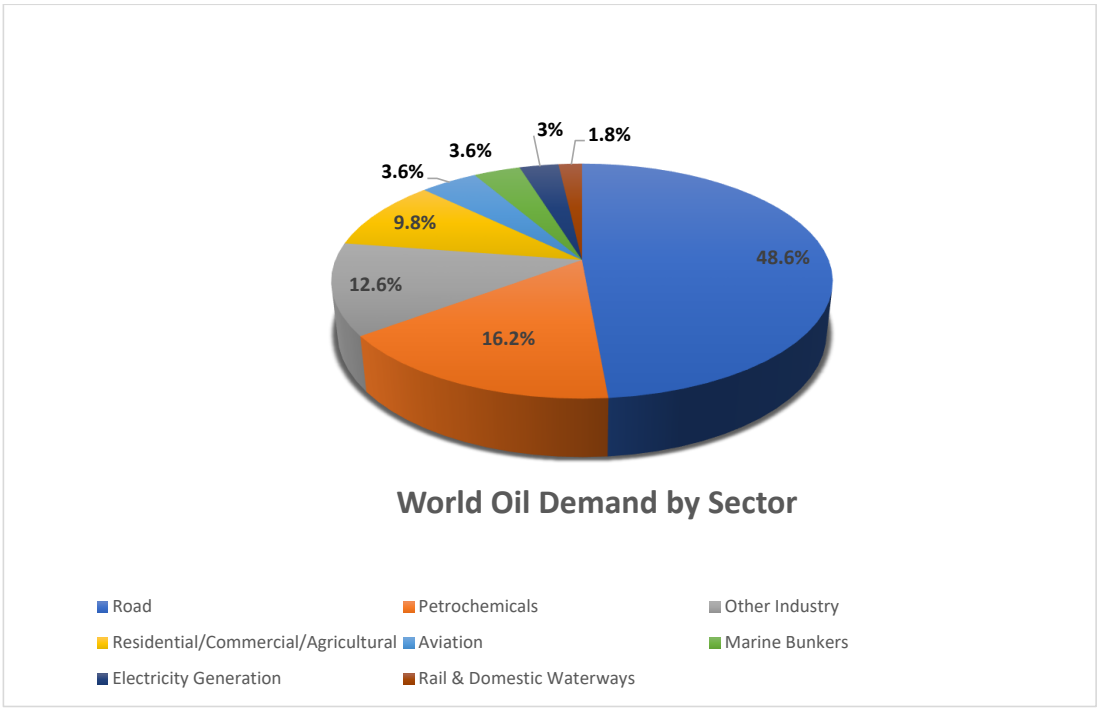

Source: (Statistica (https://www.statista.com/), 2020)

ISSN: 2521-2293

SADC has 8,618,000,000barrels or 0.98% of world's 1,650,585,140,000 barrels proven oil reserves. Angola makes up 98% of SADC's oil reserves at 8,423,000,000barrels. SADC's oil reserves are an insignificant contributor to global oil production. SADC is a net importer of oil with 950,300barrels/day demand and 285,146barrels/day deficit.

Table 1: SADC Countries Oil Statistics

Country	**Daily Oil Consumption (barrels)**	**World share %**	**Production barrels/ day**	**Exports/ day**	**Imports/ day**	**Daily Surplus or Deficit (incl. exports & imports)**	**Oil Reserves (barrels)**
South Africa	640,000	0.70%	136,517	9,018	416,531	-95,970	15,000,000
Angola	133,000	0.10%	1,796,743	1,681,354	0	-17,611	8,423,000,000
Tanzania	71,999	0.074%	0	0	0	-71,999	0
Mauritius	28,000	0.029%	517	0	0	-27,483	0
Zimbabwe	24,000	0.025%	189	0	0	-23,811	0
Botswana	21,000	0.022%	0	1	1	-21,000	0
DRC	21,000	0.022%	20,000	16,263	0	-17,263	180,000,000
Malawi	6,001	0.0062%	517	0	0	-5,484	0
Eswatini	5,300	0.0055%	775	0	0	-4,525	0
Total	**950,300**	**0.98%**	**1,955,258**	**1,706,635**	**416,531**	**-285,146**	**8,618,000,000**

Source: (Worldometers (https://www.worldometers.info/oil/oil-consumption-by-country/), 2022)

ISSN: 2521-2293

2. Biofuel Policies in SADC

Biofuel refers to matter derived from organic material, that is burned to produce energy. Common biofuels are; bio-alcohols (ethanol and methanol), bio-gas, bio-diesel or solid bio-mass. Bio-alcohols and biodiesel can be used in vehicles and machinery, bio-gas for heating, cooking and lighting whilst bio-mass for heating, cooking or electricity generation.

South Africa was first in SADC to use biofuels from 1920's to 1960's (GP Von Maltitz, 2008), other countries followed forty years ago: Zimbabwe (1980) and Malawi (1982) (Johnson, 2019). Real interest and commitment to biofuel production started a decade ago when SADC countries established biofuel policies; South Africa (2007), Mozambique (2009) and Angola (2010). Zambia, Malawi and Tanzania followed (United Nations University, 2012). These countries blend fuels depending on availability of biofuels.

South Africa

The South African Biofuels Industrial Strategy targeted 2% biofuel penetration of road transportation fuels (E. Gnansounou, 2007). South Africa set new targets in the Biofuels Regulatory Framework 2019 whose purpose is implementation of the Biofuel Industrial Strategy (Department of Energy, 2019) and has five aspects:

a. Feedstock protocol: mitigates food security risk and prioritises rainwater fed crops.
b. Mandatory blending: minimum 2% bioethanol and 5% biodiesel.
c. Cost recovery: provides and allows cost neutrality of blenders, infrastructure and equipment.
d. Subsidy: provides subsidy to farmers and manufacturers for first generation biofuels only.
e. Selection criteria: objective selection method for projects requiring subsidy considering the socioeconomic benefits.

Tanzania

A task force was set up to develop a National Biofuel Policy, however, due to the time required for policy development, it established guidelines (Jacqueline Cleaver, 2010). Guidelines address; institutional framework, application procedures for investors, land acquisition and use, contract farming and sustainability of biofuel production.

a. Institutional framework: ease of entry into biofuel industry and reducing unnecessary red tapes and institutional bottlenecks whilst creating alignment in the setting up and licensing of biofuel producers.
b. Land acquisition: Tanzania categorises land into two types; village land administered by local councils and general land controlled by Central Government. Village land is not available to investors unless it has been converted to the general land use and the process is lengthy (3years).

Botswana

Renewable Energy Strategy set a target of 20% of total electricity consumption by 2030 (Economic Consulting Associates Limited, 2017), however, it had no specific target for biofuels. The recently promulgated Biofuel Guidelines are to; create a conducive environment, guide investors and stakeholders, provide policy and regulatory frameworks, facilitate development new and innovative

ISSN: 2521-2293

technologies for biofuel production and ensure significant accounting to set standards and requirements. The guidelines are split into technical, economic and policy formulation.

a. Technical: environmental and social impacts, sustainability, project appraisal, feedstock, distribution, and blending.
b. Economic viability: estimated cost of production.
c. Policy formulation: institutional framework, permitting and licensing procedures, incentives, land acquisition and use, contract farming, quality and blending.

Zimbabwe

Zimbabwe Biofuels Policy targets 2% and 20% blending for biodiesel and bioethanol respectively by 2030 (Ministry of Energy and Power Development, 2015). Its objectives are to:

a. Improve viability, long-term growth and sustainability;
b. Ensure maintenance of bio-fuel product quality and standards;
c. Improve productivity and economic viability of bio-fuel feedstock;
d. Implement development trajectories balancing bio-fuel investments with biodiversity maintenance, water and air pollution;
e. Implement production models that increase community benefits and foster institutional cooperation and coordination.

Between the 1980's and 1990's Zimbabwe produced ethanol from molasses with blending of up to 15%. Production continually suffered setbacks of droughts. Recently mandatory blending of 10% was introduced, however its implementation depends on availability of feedstock.

Eswatini

In 2009, the Government established National Biofuels Development Strategy and Action Plan. The strategy provides guidance for the development and nurturing of the biofuels industry (Ministry of Natural Resources and Energy, Swaziland, 2009). The strategy recognises that development of biofuels is challenging making it uneconomic when international oil prices are favourable. It recommends a phased implementation plan considering the inadequate resources and calls for a biofuel regulator.

Eswatini has produced bioethanol in the past from its sugarcane production, however delayed biodiesel production for inadequate feedstock research.

Malawi

Malawi used biofuels from 1980's and blended up to 20% for bioethanol and 9% for biodiesel. Biofuels contribute 4% of Malawi's transport energy consumption (Ministry of Natural Resource, Energy and Mining, Malawi, 2018). The Energy Policy prioritises biomass and biofuels and targets to reduce over-reliance on biomass by rolling out efficient cooking stoves. It promotes biofuels production without compromising food security and aims to provide fiscal and pricing incentives to encourage biofuels production and use. It considers large projects for biofuels production, flex vehicles and introduction of biofuels compatible infrastructure e.g. pumps.

Angola

Angola's Atlas and National Strategy for the New Renewable Energies recognises that biomass could generate more than 3GW energy. Depending on technology used sugarcane potential ranges between 1.1 and 2.9kW whilst 120MW has been mapped for municipal waste around major urban

ISSN: 2521-2293

areas (Ministry of Energy and Water, Angola). Biomass resource is suitable for mini grids, small engines and biodigesters. It determines the costs for biomass energy projects as high as US$1,880/kW – US$6,800/kW, identifies the levelised cost of energy (LCOE) range (US$0.06/kWh – US$0.2/kWh) and sets renewable technology targets though not specifying biofuels outside the earmarked biomass power projects.

Mauritius

Mauritius established a Long-Term Energy Strategy, 2009 – 2025 which recognises the abundance and role of biomass from sugar cane for electricity generation. It aims to diversify diesel supply with biodiesel manufacturing and proposes biodiesel importation considering inadequate feedstock for local production. It proposes 10% ethanol blending increasing to 20% later based on available 150,000tonnes of molasses, estimating 120,000tonnes for producing 25 million litres ethanol.

3. Biofuel Production Trends

In 2020 global ethanol production was 26.06billion gallons dropping from 29.03billion gallons in 2019 (US Department of Energy: Energy Efficiency Renewable Energy, 2021). United States of America (USA) and Brazil makes 84% whilst 16% is shared between European Union, China, Canada and the rest of the world. Africa produced 400barrels/day ethanol in 2012 (Index mundi, 2012). 50% being Malawi and the rest from South Africa and Ethiopia. European Union produces 32.3% of the world's biodiesel followed by USA: 18.1%, Indonesia: 15%, Brazil: 12.2% and 13.63% shared between China, India, Canada, Argentina, Thailand, Colombia and Paraguay (FAO, 2021). Despite its potential, Africa does not feature in the world biodiesel statistics.

4. Research and Education

Scholars continue to publish work on biofuels ranging from feedstock analysis to production and analysis of biofuels and engine performance including technologies used to produce biofuels. (Gnansounou, et al., 2007) (Jonas, et al., 2020) (Oladiran , et al., 2011) Governments support research, e.g. in Botswana, Department of Energy supports Biogas and Biodiesel researches and previously partnered with the Japanese Government for the jatropha research.

Evolution of biofuels and their success should follow thorough research and well-established policies and strategies.

5. Quality Standards

Biofuel quality is important in determining performance of vehicle or equipment. Ideally biofuel properties should be like those of conventional fuels for seamless interchangeable use and mixing. Quality standards set limits for the critical parameters within which biofuels should be produced. They specify test methods and procedures for ascertaining product quality.

Some SADC countries have developed standards to address quality of biofuels. Table 2 indicates the various standards applied in SADC. However, all SADC countries have functioning Standards Organizations (e.g. BOBS, SABS, SAZ for Botswana, South Africa and Zimbabwe respectively) which can create quality standards for biofuels.

Table 2: Technical & Quality Biofuel Standards in SADC Countries

ISSN: 2521-2293

Country	Standard (s)
Botswana	BOS626 Automotive Biodiesel
Eswatini	SZNSSANS 1935 Automotive biodiesel SZNS019 Standard specification for denatured fuel ethanol - blending SZNS054 Standard Specification for 10 volume % Ethanol Gasoline Blend
Malawi	MS805 BIODIESEL FUEL – SPECIFICATION MS845 Biodiesel flue-Specification MS573 ETHANOL – SPECIFICATION
Mauritius	MSEN15376 Automotive fuels - Ethanol as a blending
South Africa	SANS833 Biodiesel production - Quality management system SANS1935 Automotive biodiesel SANS465 Automotive fuels - Requirements and specifications for fuel ethanol - blending SANS1462 Automotive fuel ethanol - Quality management system
Tanzania	TZS1104 Ethanol Gel for domestic Heating TZS1099 Automotive biodiesel fuel
Zimbabwe	ZWS719 Biodiesel fuel blend stock (B100) ZWS968 Diesel fuel oil, biodiesel blend (B5 to B20) ZWS962 Denatured fuel ethanol - blending ZWS964 Ethanol (Parts 1 – 15) ZWS1020 Part 2 Biogas Systems

6. Feedstocks

SADC countries could each produce biofuels depending on feedstocks capacity to complement each other. Land scarcity and food security challenges should be well taken care of.

Angola

Angola considered four feedstocks: forestry residues and energy crops, agro-food industry residues (sugarcane), farming activity residues and solid waste. Forestry resource potential is 50MW by estimating annual increases of biomass/ha. The sugarcane potential areas were determined from large areas with at least 10,000ha and without environmental restrictions but with high irrigation potential. Agricultural and livestock waste was also considered. Solid waste was considered by using population statistics quantifying waste/capita and its energy potential.

Botswana

Jathropha has been studied for biodiesel production whilst other studies considered non-food indigenous plants for food security concerns and climatic conditions. Recent studies are focusing on production of biodiesel from animal tallow considering the country's beef industry. Recently through the support of the United Nations Development Programme (UNDP) biogas digesters were constructed for farmers. Waste from landfills can be explored, however, it includes other forms that are not biodegradable. This reason and the amount of waste per landfill makes it unattractive for investors. Efforts to produce 106,000tons sugar/annum from 100,000ha with sugarcane were thwarted by an Environmental Impact Assessment (EIA) for forest reserve conservation concerns.

Eswatini

ISSN: 2521-2293

Eswatini is third largest producer of sugarcane in Africa and produces at least 60million litres ethanol (International Renewable Energy Agency, 2014) and plans to increase production to meet E10 blending. Biodiesel from jatropha was attempted with plans to cultivate 10,000ha in 10 years and supply 13million litres biodiesel. It was aborted due to lack of investment when the initial company ceased operations (Ministry of Natural Resources and Energy, Swaziland, 2009).

Malawi

Malawi reached 20% and 9% blending levels for ethanol and biodiesel respectively. Sugarcane is used for ethanol while jatropha for biodiesel. Malawi's Energy Policy prohibits the use of food crops for biofuels. Due to deforestation, it is not advisable to consider forestry biomass.

South Africa

Maize, sorghum, sugarcane, canola, soybean and sunflower were considered. Due to food security maize is excluded because it is a staple food for both humans and cattle. Sorghum production has been declining due to reduced demand. Sugarcane is considered better and has potential to produce ethanol, sugar, electricity, and other by-products. Canola is not well understood and was abandoned whilst sunflower had to be modelled for water use and yield. Soybean is selected.

Tanzania

Sugarcane, sorghum, cassava and sisal are potential feedstock for ethanol (German Technical Cooperation (GTZ), 2005). Ethanol can be produced from sugar or molasses. Sugarcane bagasse can also generate electricity thereby increasing the overall efficiency. Sisal production trails to the 1950's for fibre twine production. However, useful fibre constitutes only 2% of the plant and the rest waste and bole. Sisal waste could be used for biogas production. Bole is rich in pulp and liquid juice which has been studied for ethanol production. Sunflower, palm, various nuts, coconut, avocado have been studied as biodiesel feedstocks and have good yields. Jatropha has been identified since it is non-food and is widely spread and adapted to the climatic conditions.

Zimbabwe

Biofuels Policy identifies sugarcane, cassava and sweet-sorghum as feedstocks for ethanol whilst jatropha for biodiesel (Ministry of Energy and Power Development, 2015). The 10% blending could be achieved through jatropha production (Raphael M. Jingura, 2011). The situational analysis conducted by the Worldwide Fund for Nature (Enos Shumba, 2009) affirmed sugarcane and jatropha as suitable feedstocks for biofuels.

Table 3: Summary of selected feedstocks for SADC countries

Country	Biodiesel	Ethanol
Angola	Jatropha	Sugarcane
Botswana	Jatropha, animal tallow, waste oil	Sweet-sorghum
Democratic Republic of Congo	Palm Oil	Cassava
Eswatini	Jatropha	Sugarcane
Malawi	Jatropha	Sugarcane
Mauritius		Sugarcane
South Africa	Soybean	Sugarcane, sweet-sorghum
Tanzania	Jatropha	Sugarcane, sorghum, and sisal
Zimbabwe	Jatropha	Sugarcane

ISSN: 2521-2293

Sugarcane leads followed by sweet-sorghum as ethanol feedstocks whilst jatropha is for biodiesel in SADC. These are selected based on low or no competition with food, ease of cultivation, climatic conditions, and adaptability to a particular country. Therefore, determining the overall potential of biofuel production for a particular country should be based on the condition that current production and uses of feedstock are not disturbed.

7. Land Availability

Feedstock production requires land which is also used for other purposes e.g. residential, wildlife, food production, forest sanctuaries etc. Land is amongst the world's most scarce resources and under pressure as human population grows, human needs change e.g. rapid urbanisation and mining, and world's consciousness towards conservation (wildlife and forests). This affects SADC which is endowed with natural resources ranging from minerals, wildlife and world heritage sites and is dependent on farming activities.

Angola

Angola has 57million hectares agricultural land or 45.6% of total land area. 61.4% (35million hectares) is arable land whilst only 16% (5.6million hectares) is cultivated (The World Bank, 2021). 29.4million hectares of arable land remain uncultivated and available for food and energy production.

Botswana

Statistics Botswana, 2019 reported total arable land as 117,416ha. 75.2% (88,288ha) were cultivated (Statistics Botswana, 2020). However, this excludes the commercial sector. The African Development Bank reported 155,699ha planted in 2019 (African Development Bank, 2021) against 259,562.34ha arable land (The World Bank, 2022) for both commercial and traditional sectors.

Democratic Republic of Congo

DRC has 226,705,000ha land area. 31,500,000ha (13.9%) is agricultural land (Food and Agriculture Organisation of the United Nations, 2022). Arable land is 5.205% of land area (11,800,000ha) (The World Bank, 2022). AfDB recorded 13,380,657.80ha harvested area in 2018 (African Development Bank, 2021).

South Africa

South Africa's land area is 121,309,000ha. Agricultural land is 96,341,000ha (79.4%) (Food and Agriculture Organisation of the United Nations, 2022). Arable land is 9.892% (11,999,886.28ha) (The World Bank, 2022). In 2020, 6,557,050ha (54.6% arable land) were cultivated with summer crops whilst 1,986,940ha were winter crops (Department of Agriculture, Land Reform and Rural Development: South Africa, 2021).

Tanzania

Tanzania's land cover is 88,580,000ha and 39,650,000ha (44.8%) is agricultural land (Food and Agriculture Organisation of the United Nations, 2022). 15.24% (13,499,592ha) land area is arable (The World Bank, 2022). In 2018, 11,043,509.67ha (81.8% arable land) was cultivated (African Development Bank, 2021).

ISSN: 2521-2293

Zimbabwe

41.9% (16,200,000ha) of Zimbabwe's 38,685,000ha land area is agricultural (Food and Agriculture Organisation of the United Nations, 2022). Arable land is 10.34% (4,000,029ha) land area (The World Bank, 2022) whilst 1,740,085.177ha was cultivated in 2018 (African Development Bank, 2021).

8. Feedstock Yields

Feedstock yield is crucial in determination of biofuel potential. The yields are determined firstly as the fuel content per tonne (L * 1000kg $^{-1}$) e.g. litres ethanol/tonne of sugarcane, then agricultural yields (1000kg * ha^{-1}) e.g. tonnes of sugarcane/hectare and finally fuel content/hectare (L * ha^{-1}) e.g. litres of ethanol/hectare.

Sugarcane

The industrial yield of anhydrous ethanol is 85litres/tonne of sugarcane for standard distillery (Marina Oliveirade Souza Dias, 2015). When optimised it is 88L/ton. The agricultural yield is 71 tonnes/hectare (Marina Oliveirade Souza Dias, 2015). The calculated fuel content/hectare is 6,035litres/hectare, below the GTZ's 7,561L/ha (German Technical Cooperation (GTZ), 2005).

Sweet-sorghum

Sweet-sorghum's yield can reach 8,000L/ha, i.e. 30% higher than sugarcane yield (Daniel E. Ekefre, 2017). Ekefre et al. 2017 calculated the lowest yield for Dale as 5,077L/ha and the highest for Theis as 7,619L/ha (Daniel E. Ekefre, 2017).

Cassava

Ademiluyi and Mepba 2013, determined the ethanol yields for cassava as 150L/ton for fresh tubers and 333L/ton for dry chips (Mepba, 2013). GTZ 2005, determined ethanol yield for cassava as 1,702L/ha (German Technical Cooperation (GTZ), 2005).

Sorghum

Ramirez et al. 2016 concluded that for lower solid to liquid ratios i.e. 1:5 & 1:4, ethanol yield ranged between 355L/ton and 368L/ton. Increasing ratio to 1:3 dropped yield to 305 – 325L/ton (2016). GTZ 2005, determined ethanol yield for sorghum as 325L/ha (German Technical Cooperation (GTZ), 2005).

Jatropha

Demafelis and Angeles 2009**,** estimated the jatropha yields in Thailand as 3 – 4 ton/ha, agricultural yield and 30 – 35% oil yield (Angeles, 2009). M. Jonas et al. 2020, determined the oil yield for jatropha to be 38.7 – 45.8% (Jonas, et al., 2020). GTZ 2005, stated the oil yield for jatropha as 1,892L/ha (German Technical Cooperation (GTZ), 2005).

Palm Oil

Palm oil yield is 5,950L/ha (German Technical Cooperation (GTZ), 2005).

SoyBean

Soybean oil yield is 446L/ha (German Technical Cooperation (GTZ), 2005). In South Africa the agricultural yield for soybean was reported to be 2.5 – 3ton/ha (Department of Agriculture, Forestry

ISSN: 2521-2293

and Fisheries, South Africa, 2010) whilst the biodiesel yield is 171.4L/ton (Sparks, et al., 2010). Combining the two, 428.5L/ha is obtained, close to 446L/ha reported by GTZ 2005.

9. Estimated Biofuel Potential

In estimating biofuel potential fuel consumption, food requirements, land required for food production and biofuel production were considered. Fuel consumption was split between petrol and diesel assuming they are equal for ethanol and biodiesel production respectively Arable land was divided by subtracting the land required for a country to be food secure and land already used for crop production. Then, land required for biofuel production was subtracted. Where the resultant was a negative number or very close to zero it was concluded that land is unavailable for biofuel production. For countries where available land is more than enough to produce biofuels then consideration was made for additional production to supply the region. Land required for biofuel production was determined by dividing the biofuel demand by the biofuel yield/hectare.

$$\text{Land required for biofuel production} = {}^{biofuel\ demand}/_{biofuel\ yield\ per\ hectare}$$

Potential biofuel production for SADC was determined for countries which have adequate arable land. These countries: Angola, Madagascar, Mozambique, South Africa, Tanzania, Zambia and Zimbabwe could produce SADC's fuel requirements by releasing 4.5% of their unused arable land additionally to land required for them to be fuel and food secure. 33.55billion litres biofuels/year could be produced from 34.25million hectares. Additional 4.5% (1.8million ha) of land, would increase production by 4.8billion litres resulting in 38.3billion litres against SADC's 37.95billion litres fuel demand (Index mundi, 2012). Food farming would not be a problem because the balance of arable land under this scenario would be 38.6million hectares. Other SADC countries are considered not to have sufficient land for both food and biofuels. See Table 4.

ISSN: 2521-2293

Table 4: Biofuel Potential in SADC Countries

Country	**A. Total food production** (Oxford Martin School, 2020) **Tons**	**B. Annual food required (1.5kg/person** (Bloomberg, 2020) *** population*365) Tons**	**C. Deficit/surplus food (A – B) Tons**	**D. Additional Land required for food production (C/(A/cultivated land** (African Development Bank, 2021))*** Ha**	**E. Annual Fuel demand** (Index mundi, 2012) **Litres**		**F. Biofuel land requirement (E / Yield** (German Technical Cooperation (GTZ), 2005)**) Ha**		
					E1. Gasoline	**E2. Gasoil**	**F1. Ethanol**	**F2. Biodiesel**	**F3. Total**
Angola	19,991,124	17,994,282	1,996,842	-	1,450,756,375	3,191,664,025	191,874	1,686,926	1,878,800
Botswana	56,907	1,287,515	-1,230,608	3,366,974	475,848,091	475,848,091	93,726	251,505	345,232
DRC	39,724,899	49,034,648	-9,309,749	3,135,831	348,181,530	533,878,346	204,572	89,727	294,299
Eswatini	5,854,566	635,190	5,219,376	-	121,863,536	127,666,561	16,117	67,477	83,594
Malawi	22,656,841	10,473,650	12,183,191	-	104,454,459	168,287,740	13,815	88,947	102,762
Mauritius	3,187,379	692,993	2,494,386	-	168,287,740	377,196,658	22,257	-	-
South Africa	59,740,922	32,643,045	27,097,877	-	11,489,990,490	12,940,746,865	1,519,639	29,015,128	30,534,767
Tanzania	39,657,501	32,704,482	6,953,019	-	429,423,887	1,044,544,590	56,795	552,085	608,879
Zimbabwe	6,084,093	8,137,453	-2,053,360	587,272	237,924,046	533,878,346	31,467	282,177	313,644
Total	**196,954,232**	**153,603,258**	**43,350,974**	**7,090,077**	**14,826,730,154**	**19,393,711,222**	**2,150,262**	**32,033,972**	**34,161,977**

ISSN: 2521-2293

Table 5: Additional Biofuel Potential in SADC Countries

Country	G. Available land (Arable land (The World Bank, 2022) – F3) Ha	H. Biofuel Potential Litres	I. Additional Land (4.5%*G) Ha	J. Additional Fuel from additional land Litres		K. Total Biofuel Potential Litres	L. Balance Land (G -I) Ha
				J1. Ethanol (15%*I*H1)	J3. Biodiesel (85%*I*H2)		
Angola	29,400,000	4,642,420,400	1,323,000	1,500,480,450	2,127,648,600	3,628,129,050	28,077,000
Botswana	No land	-		-	-	-	-
DRC	No land	-		-	-	-	-
Eswatini	No land	-		-	-	-	-
Malawi	No land	-	-	-	-	-	-
Mauritius	31,615	-	-	-	-	-	-
South Africa	3,454,896	24,430,737,355	155,470	176,326,678	58,938,803	235,265,481	3,299,426
Tanzania	2,456,082	1,473,968,477	110,524	125,350,460	177,744,222	303,094,682	2,345,559
Zimbabwe	1,672,671	771,802,392	75,270	85,367,708	121,049,551	206,417,260	1,597,401
Total	**37,015,264**	**31,318,928,624**	**1,664,264**	**1,887,525,296**	**2,485,381,176**	**4,372,906,473**	**35,319,386**

ISSN: 2521-2293

10. Development

International Renewable Energy Agency (IRENA) and SADC Centre for Renewable Energy and Energy Efficiency (SACREEE) in 2017 launched SADC Entrepreneurship Support Facility, aimed at supporting renewable energy market development through training, mentorship, and linkage to financial institutions (IRENA, 2021). Financial institutions such as commercial banks, multilateral development banks and non-banking financial institutions should setup facilities for funding biofuels development. Governments and energy regulators should introduce incentives for biofuel development. Such incentives should be administered by independent regulators for fair distribution.

Capacity building initiatives will be required to develop human resource capital in the field of biofuels. Policies studied at section 2 indicate that some governments have put in place incentive mechanisms to help develop the biofuel market in SADC. Governments should provide adequate resources such as infrastructure, blending mandates and standards to increase the uptake of biofuels.

11. Conclusions

SADC has potential for both sufficient food and biofuel production considering arable land available and feedstock yields. Four countries (Angola, South Africa, Tanzania and Zimbabwe) could produce 35.7billion litres/annum from (35million hectares) 54% of their total arable land. However, rainfall patterns, irrigation possibilities, production technologies and costs were not assessed.

Countries with inadequate land could produce second generation biofuels. Though not analysed, Botswana and Namibia could use waste tallow for biodiesel production. Agro-waste and algae were not assessed but have potential to increase biofuel production capacity.

Analysis of naturally occurring feedstock was not done. For example, in Botswana some indigenous plants can be used for biofuel production, their potential production capacity could be assessed.

Malawi has successfully blended conventional fuels with biofuels for four decades, this is an indication that biofuels are not just a perception. If well developed and sustainably produced biofuels could gradually replace petroleum fuels.

ISSN: 2521-2293

References

African Development Bank Africa Information Highway Portal [Online]. - African Development Bank, August 21, 2021. - https://dataportal.opendataforafrica.org/harltl/minimum-set-of-core-agricultural-data-2021.

African Development Bank African Energy Portal [Report]. - [s.l.] : https://africa-energy-portal.org/country/congo-democratic-republic.

African Development Bank Comoros Country Strategy Paper 2021 - 2025 [Report]. - 2021.

Andrea Sonnleitner Josef Rathbauer, Josoa Ramarolanonana Randriamalala, Léa Irène Benjamin Raoliarivelo, Julien Honoré Andrianarisoa , Radobarimanjaka Rabeniala & Albrecht Ehrensperger Jatropha mahafalensis oil from Madagascar: Properties and suitability as liquid biofuel [Journal] // Energy for sustainable development. - 2013. - Vol. 17. - pp. 326 - 330.

Angeles Rex Demafelis & Domingo Samoa Biofuel Study Report [Report]. - 2009.

Bloomberg Bloomberg [Online]. - Bloomberg, December 14, 2020. - https://www.bloomberg.com/news/features/2020-12-15/no-more-hunger-how-to-feed-everyone-on-earth-with-just-the-land-we-have.

Cairncross B. An overview of the Permian (Karoo) coal deposits of southern Africa [Journal] // African Earth Sciences. - 2001. - Vol. 33. - pp. 529-562.

Centre for Coordination of Agricultural Research and Development for Southern Africa Food Security Challenges in the SADC Region [Report]. - 2021.

Daniel E. Ekefre Ajit K. Mahapatra, Mark Latimore Jr., Danielle D. Bellmer, Umakanta Jena, Gerald J. Whitehead, Archie L. Williams Evaluation of three cultivars of sweet sorghum as feedstocks for ethanol production in the Southeast United States [Journal] // Heliyon. - 2017. - Vol. 3.

Department of Agriculture, Forestry and Fisheries, South Africa Soya Beans Production Guidelines. - 2010.

Department of Agriculture, Land Reform and Rural Development: South Africa Crops and Markets First Quarter 2021 [Report]. - 2021.

Department of Energy South African Biofuels Regulatory Framework [Report]. - 2019.

E. Gnansounou . Panichelli & J. D. Villegas Sustainable Liquid Biofuels for Transport [Report]. - 2007.

Econergy International Corporation, Alf International, Blueprint Cape Pty, SICS and Efficientia Mozambique Biofuels Assessment [Report]. - 2008.

Economic Consulting Associates Limited Renewable Energy Strategy for Botswana [Report]. - 2017.

Economic Development Board of Madagascar Madagascar, The Boundless Energy Island [Report]. - 2018.

Enos Shumba Allan Carlson, Harrison Kojwang, Mxolisi Sibanda and Mufaro Masuka BIO-FUEL INVESTMENTS IN SOUTHERN AFRICA: A SITUATION ANALYSIS IN BOTSWANA, MALAWI, MOZAMBIQUE, ZAMBIA AND ZIMBABWE [Report]. - [s.l.] : World Wide Fund for Nature (WWF), 2009.

FAO OECD - FAO Agricultural Outlook 2021 - 2030 [Report]. - 2021.

Food and Agriculture Organisation of the United Nations FAOSTAT [Online]. - March 2022. - https://www.fao.org/countryprofiles/index/en/?iso3=COM.

ISSN: 2521-2293

Fuel ethanol production from commercial grain sorghum cultivars with different tannin content [Journal] // Journal of Cereal Science. - 2016. - Vol. 69. - pp. 125 - 131.

German Technical Cooperation (GTZ) Liquid Biofuels for Transportation in Tanzania [Report]. - 2005.

Gnansounou Edgard, Panichelli Luis and Villegas David Juan Sustainable Liquid Biofuels for Transport: The context of Southern African Development Community. - Lausanne : [s.n.], 2007.

GP Von Maltitz A Brent Assessing the biofuel options for Southern Africa [Report]. - 2008.

https://wits.worldbank.org/ https://wits.worldbank.org/ [Report].

https://www.spglobal.com/ Botswana to fast-track US$4B coal-to-liquid plant, coal-bed methane project [Report]. - [s.l.] : https://www.spglobal.com/, 2020.

Index mundi index mundi [Online]. - index mundi, 2012. - https://www.indexmundi.com/energy/?product=gasoline&graph=consumption.

International Renewable Energy Agency Swaziland Renewable Energy Readiness Assessment [Report]. - 2014.

IRENA Renewable Energy Assessment Botswana [Report]. - 2021.

Jacqueline Cleaver Rommert Schram and Godwil Wanga Bioenergy in Tanzania: The Country Context [Report]. - 2010.

Jan Van Vreden Marcus Wigan, Arvid Kruze, Kirsten Dyhr-Mikkelsen & Hans Henrik Lindboe Proposal for Energy Policy of the Republic of Seychelles, 2010 - 2030 [Report]. - 2010.

Jean-Philippe Praene Ali Hamada Fakra, Fiona Bénard-Sora, Leslie Ayagapin Comoros's energy review for promoting renewable energy sources [Journal] // Renewable Energy, Elsevier. - 2021. - Vol. 169. - pp. 885 - 893.

Johnson Batidzirai and Energy security, agroindustrial development,and international trade: The case of sugarcane [Report]. - 2019.

Jonas Mbako , Ketlogetswe Clever and Gandure Jerekias Variation of Jatropha curcas seed oil content and fatty acid composition with fruity maturity stage [Journal] // Heliyon. - 2020. - Vol. 6.

Keshini Beetul Shamimtaz Sadally, Ranjeet Bhagooli & Daneshwar Puchooa An investigation of biodiesel production from microalgae found in Mauritian waters [Journal] // Biofuel Research Journal . - 2014. - Vol. 2. - pp. 58 - 64.

Law Daniel Allen AN ENERGY ANALYSIS AND CHARACTERIZATION OF SAFOU (DACRYODES EDULIS) AS BIOFUEL FEEDSTOCK [Report]. - 2010.

Marina Oliveirade Souza Dias Rubens Maciel Filho, Paulo Eduardo Mantelatto, Otávio Cavalett, Carlos Eduardo Vaz Rossell, Antonio Bonomi & Manoel Regis Lima Verde Leal Sugarcane processing for ethanol and sugar in Brazil [Journal] // Environmental Development. - 2015. - Vol. 15. - pp. 35 - 51.

Mauritius Research Council Jatropha Cultivation for Biofuel Production in Mauritius [Report]. - 2006.

Mepba F. T. Ademiluyi and H. D. Yield and Properties of Ethanol Biofuel Produced from Different Whole Cassava Flours [Article] // Hindawi Publishing Corporation. - 2013.

Michael Brüntrup Raoul Herrmann Bioenergy Value Chains in Namibia: Opportunities and Challenges for Rural Development and Food Security [Conference].

ISSN: 2521-2293

Ministry of Energy and Power Development Biofuels Policy of Zimbabwe [Report]. - 2015.

Ministry of Energy and Water, Angola Atlas and National Strategy for the Renewable Energies [Report].

Ministry of Energy, Zambia National Energy Policy [Report]. - 2019.

Ministry of Natural Resource, Energy and Mining, Malawi National Energy Policy [Report]. - 2018.

Ministry of Natural Resources and Energy, Swaziland National Biofuels Development Strategy and Action Plan [Report]. - 2009.

Nhantumbo I. and Salomão, A. Biofuels, land access and rural livelihoods in Mozambique [Report]. - 2010.

Oladiran Moses Tunde and Gandure Jerekias Biodiesel for Sustainable Energy Provision in Developing Countries [Journal] // Low Carbon Economy. - 2011. - Vol. 2. - pp. 138-143.

Oxford Martin School Our World in Data [Online]. - Ocford University, March 2020. - https://ourworldindata.org/agricultural-production.

Raphael M. Jingura Rutendo Matengaifa, Downmore Musademba and Kumbirai Musiyiwa Characterisation of land types and agro-ecological conditions for production of Jatropha as a feedstock for biofuels in Zimbabwe [Journal] // Biomass and Bioenergy. - 2011. - Vol. 35. - pp. 2080 - 2086.

Romeela Mohee Sumayya Mauthoor, Zumar M.A. Bundhoo, Geeta Somaroo, Nuhaa Soobhany & Sanjana Gunasee Current status of solid waste management in small island developing states: A review [Journal] // Waste Management, Elsevier. - 2015. - Vol. 43. - pp. 539 - 549.

SADC SADC Policy Paper on Climate Change: Assessing the Policy Options for SADC Member States [Report]. - Gaborone : [s.n.], 2012.

SADC Southern Africa Sub-Regional Framework of Climate Change Programmes [Report]. - 2010.

Sparks GD, Ortmann GF and and Lagrange L An Economic Evaluation of Soybean-Based Biodiesel Production on Commercial Farms in the Soybean-Producing Regions of KwaZulu-Natal [Conference] // Joint 3rd African Association of Agricultural Economists (AAAE) and 48th Agricultural Economists Association of South Africa (AEASA) Conference. - Cape Town : [s.n.], 2010.

Statista Statista [Online]. - statista, 2022. - https://www.statista.com/statistics/1155675/agricultural-production-in-angola-by-type-of-farming/#:~:text=The%20agricultural%20production%20in%20Angola,roughly%2012%20million%20metric%20tons..

Statistica (https://www.statista.com/) Distribution of oil demand in the OECD in 2020, by sector [Report]. - 2020.

Statistics Botswana Annual Agricutural Survey Report 2019: Traditional Sector [Report]. - 2020.

TG Lipper L. and Benton Mega Trends in the Southern African Region. [Report]. - 2020.

The World Bank Angola Agriculture Support Policy Review: Realigning Agriculture Support Policies and Programs [Report]. - 2021.

The World Bank The World Bank Data Catalog [Online]. - The World Bank, 2022. - https://data.worldbank.org/indicator/AG.LND.ARBL.ZS?end=2018&locations=BW&start=1961&view=chart.

ISSN: 2521-2293

TheGlobalEconomy.com TheGlobalEconomy.com [Online]. - https://www.theglobaleconomy.com/rankings/gasoline_consumption/.

UN https://unfccc.int/ [Report]. - 2021.

UNDP and UNCDF Madagascar, Energy and the poor [Report]. - 2020.

United Nations University Biofuels in Africa Impacts on Ecosystem Services, Biodiversity and Human Well-being [Report]. - 2012.

United Nations University World Institute for Development Economics Research Potential biofuel feedstocks and production in Zambia [Report]. - 2017.

United States Environmental Protection Agency SASOL: South Africa's Oil from Coal Story - Background for Environmental Assessment [Report]. - 1980.

US Department of Energy: Energy Efficiency Renewable Energy Alternative Fuels Data Center [Online]. - June 2021. - https://afdc.energy.gov/data/10331.

Wikipedia Wikipedia [Online]. - 2022. - https://en.wikipedia.org/wiki/Table_of_biofuel_crop_yields.

Worldometers (https://www.worldometers.info/oil/oil-consumption-by-country/) Oil Consumption by Country [Report]. - 2022.

Yiming Li Changqing Li A Comparative Study for the Development of Coal-to-Liquids Industries in China, South Africa and United States [Journal] // Green and Sustainable Chemistry. - 2019. - Vol. 9. - pp. 85-93.

BIUST Teaching, Research, & Innovation Symposium 2023 (TRDAIS 2023)
Botswana International University of Science and Technology
Palapye, Botswana, 18 - 19 September 2023
ISSN: 2521-2293

Book of Abstracts

BIUST Teaching, Research, & Innovation Symposium 2023 (TRDAIS 2023)
Botswana International University of Science and Technology
Palapye, Botswana, 18 - 19 September 2023
ISSN: 2521-2293

EVALUATION OF THE GREULICH AND PYLE ATLAS FOR AGE ESTIMATION PURPOSES AMONGST THE BOTSWANA POPULATION USING X-RAY IMAGES OF THE HAND AND WRIST

Baraedi Olaotse,[a;] Panzirah-Mabaka Kaone,[b] ; Mokgadi Janes,[c] ; Mosothwane Morongwa,[d] and Phokedi Gothatamang Norma,[a*]

[a]Department of Chemical and Forensic Sciences, Botswana International University of Science and Technology, Plot 10071, Boseja Ward, Private Mail Bag 016, Palapye, Botswana, [b]Department of Forensic Pathology, Botswana Police Service, P.O Box 1082 Gaborone, Botswana, [c]Chemical, Biological Nuclear and Radiological Weapons Management Authority, Ministry of Defence, Justice and Security, Private Bag 00384 Gaborone, Botswana, [d]Archaeology Unit, University of Botswana
Plot 4775, Notwane Road, Gaborone, Botswana

ABSTRACT

The applicability of Greulich and Pyle atlas for estimating age for court cases that require age estimation amongst the Botswana population is often questioned because the atlas has been adopted without being evaluated for Botswana. It has long been established that accuracies of such age estimation methods are dependent on different factors such as the general health and nutrition of the population. This study aimed to determine the level of accuracy of the Greulich and Pyle atlas in estimating age for the Botswana population or confirm if there is need to develop Botswana age estimation specific standards. The seventy-eight (78) x-ray image samples used in this study were collected from the three locations of Gaborone, Palapye and Serowe for patients aged between five and sixteen years, who visited the hospital between March and September 2021. The images were compared with the Greulich and Pyle age estimation standards. Based on the results obtained, the mean skeletal age difference for females was found to be 0.524 years, indicating that age was underestimated by up to 0.524 years (about 6 months) for females while the mean skeletal age difference was found to be 0.129 years for males. Overall, the Greulich and Pyle atlas under-estimated the male age by 0.129 years (1.5 months). Based on these findings, we can conclude that the Greulich and Pyle atlas can be used to estimate age but with caution as there is a possibility of errors. There is need for this atlas to be revised to reduce errors in age estimation for the Botswana context.

Key words: Age Eestimation, Greulich and Pyle atlas, mean skeletal age, chronological age, Botswana population, standard error of estimate

[*]***To whom correspondence should be addressed.***
Email: ***phokedig@biust.ac.bw***

BIUST Teaching, Research, & Innovation Symposium 2023 (TRDAIS 2023)
Botswana International University of Science and Technology
Palapye, Botswana, 18 - 19 September 2023
ISSN: 2521-2293

THE ABUNDANCE OF DIATOM SPECIES IN FRESHWATER SOURCES OF BOTSWANA FOR THE CONFIRMATION OF DEATH BY DROWNING AND SITE OF DROWNING

Kemiso Kabo[a], Baraedi Olaotse[a], and Phokedi Gothatamang Norma[a]*

[a]Department of Chemical and Forensic Sciences, Botswana International University of Science and Technology, Plot 10071, Boseja Ward, Private Mail Bag 016, Palapye, Botswana

ABSTRACT

The diagnosis of drowning is one of the most difficult tasks in forensic medicine, especially when dealing with decomposed bodies, which do not possess autopsy findings specific to death by drowning when compared to fresh ones. Diatoms are important under these circumstances as they can resist putrefaction and allow for the determination of the cause of death even at the decomposition stage. The diatom test is therefore often used as the most reliable test to assess the diagnosis of drowning in both fresh and decomposed bodies. The test can also be used to mark specific freshwater areas as sites for drowning. The use of diatoms in forensic death investigations is only possible with the availability of existing detailed diatom databases. Studies leading to the creation of databases about the various species of diatoms have already been performed in many parts of the world. However, there are no established diatom databases in Botswana. Forensic pathologists in the country only look for evidence of cerebral anoxia and hypoxemia during the investigation of deaths due to drowning. However, these methods do not include tests which reflect the ecologic properties of the environment in which the death took place and, cannot be used to locate drowning site(s). This challenge needs to be addressed because the death of a victim found in water is not always necessarily related to drowning and should be thoroughly investigated. We present the findings of a study carried out to establish the existence of diatom species in freshwater sources in the Central District of Botswana. The samples were digested using the cold hydrogen peroxide method and visualised using the Scanning Electron Microscopy (SEM) technique. Alterations were made during the sample digestion stage by including the use of the suction pump filtration technique and employing the use of aluminum foil and carbon tape when preparing the samples for SEM examination instead of coating. The results revealed that samples from Ramokgonami river were dominantly the *Pinnularia, Stephanodiscus* and *Thalassiosira* genera while those collected at Lecheng dam were mostly the *Nitzschia* and *Thalassiosira* genera. The identified species were used as starting point towards the creation of a new national database for Botswana and will be updated from time to time. It will benefit forensic pathologists in the investigation of deaths by drowning.

Key words: Diatoms, death by drowning, forensic investigation, drowning site, freshwater sources, Botswana

****To whom correspondence should be addressed.***
***Email:** phokedig@biust.ac.bw*

BIUST Teaching, Research, & Innovation Symposium 2023 (TRDAIS 2023)
Botswana International University of Science and Technology
Palapye, Botswana, 18 - 19 September 2023
ISSN: 2521-2293

Poster
Life Sciences and Environment

Branchiopods studies in Botswana: Taking over from Pioneers

Murphy Tladi[a,b]
[a]*Okavango Research Institute, University of Botswana, Maun, Botswana*
[b]*Department of Biological Sciences and Biotechnology;*
Botswana International University of Science and Technology
Palapye, Botswana
murphy.tladi@studentmail.biust.ac.bw / murphytladi@ymail.com

Abstract

Branchiopods are crustaceans found across the globe in wetlands including temporary wetlands. In Southern Africa, most of the studies were made by pioneer explorers who visited the continent in the 19th and early 20th centuries. These explorers were crucial in identifying and recording the distribution of these taxa. Studies in Botswana extended into the 21st century and were important for extending the distribution of already known species and some introduced new methods for studying these taxa. Here we highlight gaps identified by an MSc thesis that have been recommended for further investigation by new researchers in the field and used a sample of published papers to support the recommendations. Coordinates of locations from select studies that identified branchiopods in Botswana were plotted on a map to show the land covered when sampling for branchiopods and their wetlands in Botswana. The number of branchiopods listed in sampled studies was combined to form a pie chart diagram of the proportion of branchiopods in Botswana. Study gaps recommended by the MSc study were used to make a schematic diagram showing how the gaps can flow from fieldwork through lab work to exploring the commercialization of this natural resource. Furthermore, the Tswana names of these taxa were searched for online to see if we have a record. The results showed that pioneer explorers identified temporary wetlands that are mostly located closer to major roads, and settlements or by locating major known temporary wetlands. From the selected studies, 29 branchiopods species were identified but only 4 species were studied to explore the thermal physiology and only one species was studied to see the effects of light and temperature on the hatching success of the eggs. Anostraca seems to be the most sampled branchiopods followed by Cyclestherida, Laevicaudata and Spinicaudata combined (7), and Anomopoda (5). Only one species of Notostraca was identified in the sampled studies. Fourteen study gaps were highlighted with 4 gaps recommended for field work, 6 for lab work and 4 more for exploration of potentially commercializing this natural resource. Pioneer studies have left most of the country unexplored for branchiopods which could be the starting point for new researchers in the field. There is a need to search for cryptic wetlands that are not close to roads or settlements and duplicate bio-ecology studies on the other branchiopods species to increase the resolution of conclusions drawn from the MSc study. Fieldwork needs to be updated and lab work must be intensified to investigate further the remaining questions on the biology of these taxa then explore ways of commercializing this natural resource so that the community may benefit. Indigenous knowledge of these taxa such as Tswana names must be explored and recorded so that the information can be achieved. In conclusion, pioneer studies on branchiopods in Botswana left some gaps that can be explored by new researchers in this field. There is a need to explore wetlands in previously unreached areas and update fieldwork studies, carry out intensive lab work and explore ways of commercializing this natural resource. Indigenous knowledge of these taxa must be recorded while the older generation is still available to assist.

Keywords: Branchiopods, Botswana, bio-ecology, genomics, aquaculture, indigenous knowledge

BIUST Teaching, Research, & Innovation Symposium 2023 (TRDAIS 2023)
Botswana International University of Science and Technology
Palapye, Botswana, 18 - 19 September 2023
ISSN: 2521-2293

Submission Type: Poster
Track: Life Sciences and Environment

Evolutionary Dynamics of Hepatitis B Virus Sub-genotype A1 in Botswana

Doreen Ditshwanelo, Kebaneilwe Lebani
Department of Biological sciences and Biotechnology
Botswana International University of science and Technology
Palapye, Botswana
doreen.ditshwanelo@studentmail.biust.ac.bw, lebanik@biust.ac.bw

Abstract

Background: Botswana has an intermediate HBV prevalence of 2-7 %. The predominant genotypes are A, D and E with a prevalence of 80%, 18.6% and 1.4% respectively. No studies have investigated the origins and evolutionary history of the HBV genotypes in Botswana.

Objectives: We sought to investigate the Time to Most Common Recent Ancestor (tMRCA) of the predominant HBV sub-genotype, A1 (HBV/A1) in the population of Botswana. We also aimed to determine the diversity of HBV/A1 open reading frames (ORFs) in Botswana HBV sequences.

Methodology: A retrospective study utilizing the available online, 24 near-full length HBV sequences from Botswana.Additional 130 near full-length sequences were included as references. Bayesian coalescent analyses were used to study the population dynamics of the 154 HBV/A1 sequences. The temporal signal was estimated through the root-to-tip method using node density in tempEST. Correlation coefficient was used to indicate the amount of variation in genetic distance explained by sampling time and used as a measure of the clockliness of the data. Skyline plots were used to estimate the effective HBV infections in Botswana population over time. Botswana sequences were partitioned into 7 HBV ORFs and used to calculate nucleotide diversity based on pairwise distances analysis implemented in MEGA.

Results: he estimated tMRCA of HBV/A1 dated back to 1939 with 95% Highest Posterior Density (HPD) range of 1939–1995. Skyline plot analysis showed an increase in the size of the HBV/A1 infected population around the years 1999-2000. Pre-core region had highest median diversity of 1 (IQR, 0.0115–1) and the surface region was relatively conserved with median diversity of 0.0075 (IQR, 0.0029–0.0135).

Conclusion: Study provides baseline subgenotype-based phylodynamic information by predicting the tMRCA of HBV/A1 sequences revealing the evolutionary dynamics of HBV/A1 thus aiding in theoretical, clinical prevention and treatment of HBV/A1 in Botswana. Study also confirmed that the surface region is the most conserved region hence an ideal target for effective HBV vaccine designs.

Keywords: HBV genotype A1, full-genome sequences, Botswana, tMRCA, diversity

BIUST Teaching, Research, & Innovation Symposium 2023 (TRDAIS 2023)
Botswana International University of Science and Technology
Palapye, Botswana, 18 - 19 September 2023
ISSN: 2521-2293

Submission Type: Poster
Choose Track: Life Sciences and Environment

Potential of Native Plant Species for Rhizofiltration Technology of Cu and Ni in the Acid Mine Drainage from BCL Mine

Gorata Ishmael, Ofentse Arnold Keitshweditse, Venecio U. Ultra, Jr.
Department of Earth and Environmental Sciences
Botswana International University of Science and Technology
Palapye, Botswana
gorata.diboko@studentmail.biust.ac.bw

Abstract

Mining introduces countless contaminants into the environment as well as heavy metals that accumulate at toxic levels in the soils and water of an ecosystem including the food chain. These heavy metals must be removed from the environment to prevent the harm that they cause and the use of plants for environmental remediation is a cost-effective method of removing contamination caused by mining activities. Different plant species take up heavy metals differently due to their unique characteristics. Identification of plants for use in heavy metal removal was based on the concentration of Cu and Ni that they have up taken over time. Plants that are native to the BCL mine were sampled and analyzed for Cu and Ni contents in different plant tissues of each species. The plants were *Cyperus Papyrus [Ornamental grass]*, *Phragmites austrilis [Perennial reed]*, *Carex Paniculate [Perennial grass]* and *Baumea Rubiginosa [Coastal grass]*. The highest Cu and Ni contents in the plant tissues revealed that *C. Papyrus* and *C. Paniculate* has the greatest potential for bioaccumulation of Cu and Ni. The *C. papyrus* can accumulate Cu up to 312.37mg/kg (BAF= 142.86; TF=0.72), and Ni up to 399.21mg/kg (BAF= 486.35; TF= 2.84) when present at substrate with low HM concentrations, and can accumulate Cu of 1288.62mg/kg (BAF= 81.41; TF=0.67) and Ni up to 457.76mg/kg (BAF= 8.38; TF= 0.84) at high HM substrate. The *C. Paniculate* accumulated Cu up to 206.75mg/kg (BAF=8.70; TF=0.07) and Ni about 954.20mg/kg (BAF= 31.53; TF=0.38) at low HM substrate, and Cu up to 317.83mg/kg (BAF= 39.24; TF=0.46), and Ni up to 179.45mg/kg (BAF=24.76; TF= 0.64) at high HM substrate. *Phragmites austrilis and Baumea Rubiginosa also* accumulated Cu and Ni above the normal concentration and had BAF>1 and TF> 1 but at lower magnitude compared to other two species. Overall, all the plant species growing in the waterways at the base of the mine tailings in BCL mines are Cu and Ni hyperaccumulators and have great potential the HM load in the acid mine drainage.

Keywords: Bioaccumulation . Acid mine drainage . Rhizofiltration . Heavy Metals

BIUST Teaching, Research, & Innovation Symposium 2023 (TRDAIS 2023)
Botswana International University of Science and Technology
Palapye, Botswana, 18 - 19 September 2023
ISSN: 2521-2293

Submission Type: Poster
Choose Track: Life Sciences and Environment

Influence of chelating agents on the heavy metal accumulation in plants (*Eucalpytus globolus,* and *Schinus mole*

Trust Manyiwa, Venecio U. Ultra, Jr.
Department of Earth and Environmental Sciences
Botswana International University of Science and Technology
Palapye, Botswana
manyiwat@biust.ac.bw

Abstract

The enhancement of phytoextraction potential of *eucalyptus* and *schinus mole* as affected by chelating agents Ethylenediaminetetraacetic acid (EDTA), citric acid was assessed utilizing a pot culture experiment in Monarch Gold mine and Cu-NI mine tailings. Chelates were applied on 18-months-old plants periodically within 16 days from chelate application at 4-day interval. Results showed that plants treated with EDTA and citric acid have higher toxicity score and low photosynthetic rate, evapotranspiration and stomatal conductance compared to the control. The bioavailability of heavy metals following chelate application in soil was also determined 16 days after treatment application. The results showed that the application of chelating agents increased the accumulation of heavy metals(As, Cu, Cr, Ni, Mn) in the roots, stem and leaves of both *eucalyptus* and *schinus mole* wherein the concentrations of heavy metals were higher in plants treated with EDTA indicating the effectiveness of EDTA as a chelating agent. Citric acid also enhanced the uptake of the heavy metals only that it occurred in a much slower process and for some metals, the uptake enhancement was less compared to those with EDTA. The concentration of available heavy metals was also highest in soil of plants treated with EDTA while citric acid treated plants had the lowest concentration of available heavy metals in the soil. Considering the toxicity of EDTA on *eucalyptus* and *schinus mole*, EDTA application will deter the regeneration and successive re-growth and ratooning of the shoots. Based on the results, the use of citric acid is more promising as a chelating agent for enhancing the phytoextraction potential of *eucalyptus* and *schinus mole* in a continuous cropping and ratooning because it has low toxicity on plants and that the plants can fully recover after chelate treatments and harvest of shoots

Keywords: *Phytoextraction, Eucalyptus and schinus mole, chelating agent, heavy metals*

BIUST Teaching, Research, & Innovation Symposium 2023 (TRDAIS 2023)
Botswana International University of Science and Technology
Palapye, Botswana, 18 - 19 September 2023
ISSN: 2521-2293

Submission Type: Poster
Choose Track: Life Sciences and Environment

Assessment of the Heavy Metal Contaminations in Soils and Plant Shoots in the Vicinity of the Kgwakgwe Manganese Mine in Kanye, Botswana

Kevin Tumelo Molefi, Trust Manyiwa, Venecio U. Ultra, Jr.
Department of Earth and Environmental Sciences
Botswana International University of Science and Technology
Palapye, Botswana
manyiwat@biust.ac.bw

Abstract

The quantity of heavy metals (HM) in soils and plants around the Kgwakgwe Manganese mine in Kanye Botswana was examined in this study. The concentration of Cr, Mn, Cu, Zn, As, and Pb were measured in soils from 11 locations within the vicinity of the mine as well as on the plants present in a ten-meter transect line in each site. Results showed that *Bridellia mollis* Hutch is appropriate for Cr phytoextraction with a bioaccumulation factor (BF) greater 1.00, whereas others plant species such as *Ziziphus mucronata* with Mn-BF of 0.53, *Portulaca olecera* and *Oxycuryum cubesense* with Cr-BF and Cu-BF of 0.42, respectively, and *Asparagus africanus* with Cr-BF of 0.44 can be considered as tolerant to HM and they can be used for phytostabilization to prevent spread of pollutants or withstand high levels of contamination. Acidification, a high contamination factor, and a pollution index ranging from 1.22 to 2.08 were all indicators of current levels of HM contamination in the surface soils. The concentration of heavy metals determined were in this sequence Mn (1143.00 - 7978.00) > Zn (77.80 - 1009.00) > Cr (10.00 - 268.00) > Pb (15.60 - 549.80) > Cu (0.00 - 193.80) > As (0.00 - 87.30) with manganese having the highest concentration and the least concentration being Arsenic in soil samples. In plants, the average sequence in heavy metal concentration in plants shoots was as follows Mn (2103.39) > Zn (41.02) > Pb (9.63) > Cr (5.97) > As (4.41) > Cu (3.97) for trees and Mn (1655.15) > Zn (82.41) > Pb (32.00) >Cr (30.66) >Cu (13.96) > As (5.31) for grasses. The food crops had an average heavy metal concentration in the following sequence Mn (459) > Cu (111.08) > Cr (18.96) Zn (7.68) > Pb (6.55) > As (0.00) and the herbs had the following sequence Mn (1252.17) > Cu (89.85) > Pb (19.02) > Cr (17.00) As (2.57). The heavy metals concentration sequence identified in shrubs were as follows Mn (2704.00) > Zn (31.95) > Cr (16.00) > Pb (8.20) > Cu (3.50) > As (0.00) and for ferns Mn (250) > Cu (10.00) > As and PB (2.00) > Cr (1.30) > Zn (0.60). Overall, these results had indicated that the surface soils are highly contaminated with different HM but several plant species or combinations of these plants that could be used for phytoremediation to restore the study area and possible species for phytostabilization for revegetation and prevent the spread of pollutants to vulnerable environment.

Key words: *Bridellia mollis; Heavy metals in food crops; manganese contamination; phytoremediation*

BIUST Teaching, Research, & Innovation Symposium 2023 (TRDAIS 2023)
Botswana International University of Science and Technology
Palapye, Botswana, 18 - 19 September 2023
ISSN: 2521-2293

Submission Type: Poster
Choose Track: Life Sciences and Environment

Enhancement of phytoremediation potential of Eucalyptus in Fly Ash using Biodegradable Chelating Agents

Leatile Victoria Aminah Phiri, Trust Manyiwa, Venecio U. Ultra, Jr.
Department of Earth and Environmental Sciences
Botswana International University of Science and Technology
Palapye, Botswana
manyiwat@biust.ac.bw

Abstract

There is a great need for soil remediation from various pollutants and contaminants including heavy metals arising from wastes coming from industrial and mining activities. Such brings the need for soil remediation techniques to be extensively assessed including phytoremediation which is highly effective and cost friendly. The phytoremediation ability of eucalyptus plants was assessed in Morupule B fly ash and in fly ash amended with compost and sewage sludge. Ethylenediaminetetraacetic acid (EDTA) and citric acid applied at a rate of 5 mmol kg^{-1} were used in the study as chelating agents to improve the phytoremediation potential of eucalyptus plants. Plant leaves from two-year-old plants were taken every four days after chelate application to assess the heavy metal content in them while photosynthetic parameters such as photosynthetic rate, transpiration rate, and stomatal conductance were measured before the addition of chelating agents, eight days and on the sixteenth day after addition of chelating agents. Total heavy metal content was measured in the soil after plant culture. Results showed that chelating agents' addition enhanced the uptake of heavy metals by plant leaves, e.g. arsenic values increased on the fourth day but it decreased by close to 50%, which suggested toxicity stress. Nickel content plummeted four days after the addition of EDTA in the fly ash amended plant unlike the one with citric acid which had dropped. However, Ni decreased by about 34 % on the eighth day on plants treated with EDTA compared to 10% on plants treated with citric acid, indicating that EDTA was effective on the uptake of heavy metals compared to citric acid. However, EDTA was found to be toxic to plants as it reduced the photosynthetic rate and chlorophyll contents in plants. In contrast, citric acid interaction with compost and sewage sludge positively influenced these parameters. Overall, the results showed that citric acid could be used as an alternative chelating agent that will enhance heavy metal uptake of eucalyptus in fly ash especially when fly ash were amended with sewage sludge and compost.

Key words: *phytoremediation, eucalyptus, EDTA, citric acid, fly ash, compost, sewage sludge, heavy metals*

BIUST Teaching, Research, & Innovation Symposium 2023 (TRDAIS 2023)
Botswana International University of Science and Technology
Palapye, Botswana, 18 - 19 September 2023
ISSN: 2521-2293

Choose Submission Type:Poster
Choose Track: Pure and Applied Sciences

FTIR Characterization of Biochar for Potential application as Fertilizers

Tshepo Pheko-Ofitlhile[1] and Lucia Lepodise[2]
[1]Department of Chemical and Forensic Sciences, [2]Department of Physics and Astronomy
Botswana International University of Science and Technology
Palapye, Botswana
phekot@biust.ac.bw, lepodisel@biust.ac.bw

Abstract

Biochars are materials formed by pyrolysis of various types of organic matter (green waste, plant offcuts etc.). Studies have shown that the existence of these materials in soil can help to improve soil fertility. Biochars have been used as a key ingredient for artificial fertilizers in an attempt to replicate human made dark soils from the Amazon also known as terra preta. The fertility of terra preta soils is attributed to the content of aromatic hydrocarbons. Therefore, establishing the presence of aromatic hydrocarbons in biochars will contribute towards the manufacture of fertilizers with similar properties as terra preta. In this present study we report the infrared spectra of cow dung biochar (CB) and biochar from a mixture of coal and cow dung (CCB). CCB has peaks at 550 cm-1, 799 cm-1, 874 cm-1, 919 cm-1, 1066 cm-1, 1415 cm-1 and 1575 cm-1 which corresponds to peaks at 549 cm-1, 795 cm-1, 874 cm-1, 920 cm-1, 1046 cm-1, 1403 cm-1 and 1564 cm-1 for CB. Despite the similarities, there is a profound difference in the spectra of these two materials. A peak at 1040 cm-1 appeared for CCB but did not have a corresponding peak for CB. Three peaks at 1891 cm-1, 2106 cm-1 and 2388 cm-1 appeared for CB and did not have any corresponding peaks in the spectrum of CCB. These results display the capability of this technique in distinguishing closely related materials. Furthermore, a comparison was made between the spectra of biochars and hydroquinone which is an aromatic hydrocarbon. The results hint that aromatic hydrocarbons exist in the biochars under study. The spectrum of hydroquinone exhibited peaks at 760 cm-1 and 920 cm-1 which were observed in the spectra of CBB and CB. Corresponding peaks at 792 cm-1 and 917 cm-1 were also found in the spectrum of terra preta. This shows that biochars have a potential to be used in the manufacture of fertilizers that mimic terra preta soils.

Keywords: Biochar, cow dung, aromatic hydrocarbons, FTIR, spectroscopy

BIUST Teaching, Research, & Innovation Symposium 2023 (TRDAIS 2023)
Botswana International University of Science and Technology
Palapye, Botswana, 18 - 19 September 2023
ISSN: 2521-2293

Submission Type: Poster
Choose Track: Life Sciences and Environment

Impact of *Lippia Javanica*, *Artemisia Afra* and *Sutherlandia Frutescens* on Oxidative Stress and Lipids Profile in Rats Fed High-Fat Diet

Naumie GASEMODIMO, Keagile BATI, Laone KEALOTSWE, Dagmai H. MEHRETEAB, Goabaone GAOBOTSE, Tebogo E. KWAPE and Kabo MASISI
Department of Biological Sciences and Biotechnology
Botswana International University of Science and Technology
Palapye, Botswana
masisik@biust.ac.bw

Abstract
Oxidative stress is a health problem linked with several illnesses such as diabetes, obesity and many other cardiovascular diseases. However, the exact mechanisms of oxidative stress are not clearly understood. In this study, we hypothesized that medicinal plants such as *Lippia javanica*, *Artemisia afra* and *Sutherlandia frutescens* can improve lipid profiles and hence improve oxidative stress in animal models. The main aim of the study was to assess antioxidative and lipid metabolism properties of *Lippia javanica*, *Artemisia afra* and *Sutherlandia frutescens* grown in Botswana in rats through a number of biomarkers including lipid profiles, antioxidant enzymes and lipid peroxidation. Four groups of female Sprague Dawley rats were fed high fat diets (60% beef tallow) with one of the following administered orally for 5-weeks (a) distilled water as a control, (b) *Lippia javanica* extract (50 g/kg), (c) *Artemisia afra* extract (50 g/kg) and (d) *Sutherlandia frutescens* extract (50 g/kg). *Sutherlandia frutescens* and *Artemisia afra* extracts showed significantly higher antioxidant activity (P<0.05) as measured by 2,2-diphenyl-1-picryl-hydrazyl (DPPH) and 2,2′-azinobis-(3-ethylbenzothiazoline-6-sulfonic acid) (ABTS) assays. Compared to the control group, *Sutherlandia frutescens* and *Artemisia afra extracts* reduced plasma low density lipoprotein cholesterol (P<0.05). The *Sutherlandia frutescens* group showed reduced fecal total cholesterol (TC) and liver triglycerides (P<0.05). All extracts reduced liver TC as compared to the control group (P<0.05). Furthermore, *Sutherlandia frutescens* extracts showed increased in antioxidant enzyme activity with superoxide dismutase significantly increased (P<0.05). Current data suggest that the intake of *Sutherlandia frutescens* and *Artemisia afra* may assist attenuate oxidative stress by reducing lipid profile and improving antioxidant enzymes. However, further studies are necessary to understand other mechanisms of action.

Keywords: Oxidative stress, antioxidant, lipid profile, *Lippia javanica*, *Artemisia afra* and *Sutherlandia frutescens*

BIUST Teaching, Research, & Innovation Symposium 2023 (TRDAIS 2023)
Botswana International University of Science and Technology
Palapye, Botswana, 18 - 19 September 2023
ISSN: 2521-2293

Submission Type: Poster
Track: Life Sciences and Environment

Baobab (*Adansonia digitata*) seed as a source of biodiesel and protein hydrolysates: Optimization of production processes and characterization of the products

Keletso Masisi, Amare Gessesse and Gaolathe Rantong
Department of Biological Sciences and Biotechnology
Botswana International University of Science and Technology
Palapye, Botswana
mk18100061@studentmail.biust.ac.bw & gessessea@biust.ac.bw & rantongg@biust.ac.bw

Abstract

Increase in global population has placed a demand on fuel and protein sources therefore putting a strain on their supply and production. The increasing demand for fuel products is currently met by increased usage of fossil fuel, a nonrenewable energy source. However, burning of fossil fuel poses several challenges such as the massive release of greenhouse gasses that are associated with health problems and environmental impacts. To overcome these challenges, in recent years attention has been given to renewable energy sources. One of the renewable energy sources that attracted the attention is biodiesel, a liquid biofuel that has very good potential to replace diesel used in the transport sector. Despite such an attractive potential, to date the production of biodiesel is hindered by limited supply of feedstocks. Therefore, identification of hitherto unexploited natural resources, such as oil bearing plants, could allow sustainable production of biodiesel. *Adansonia digitata* is one of the underused plants that can be exploited and can be used as a source of oil for biodiesel production. In this study *A. digitata* seed oil was used to produce biodiesel. The resulting biodiesel showed a density of 878 kg/m3, a viscosity of 4.276 mm 2 /s, a cloud point of 5°C, pour point of -11°C and an iodine number of 57.9. All these values fall within the international standards indicating its usefulness for fuel application. The oil meal was used for the isolation of protein. The functional properties of the seed protein were tested and exhibited properties that make it suitable for application in the food industry. The protein had a water holding capacity of 1.29 g/g, a water solubility index of 3.25 %, oil holding capacity of 1.14%, foam capacity of 41% and foam stability of 67%. This indicates the potential usefulness of *A. digitata* seed protein in food production. The protein was then enzymatically hydrolyzed and used for microbiological growth as a peptone. In general the peptone prepared from the seed protein was able to support the growth of the test microorganisms the same as or better than the commercial peptone. Utilization of the protein for food and nonfood application could on the one hand help to lower the production cost of the biodiesel and on the other hand

BIUST Teaching, Research, & Innovation Symposium 2023 (TRDAIS 2023)
Botswana International University of Science and Technology
Palapye, Botswana, 18 - 19 September 2023
ISSN: 2521-2293

Submission Type: Poster
Choose Track: Life Sciences and Environment

Antioxidant and Antibacterial Evaluation of Essential Oil Obtained from *Lagerra Decurrens*

Tamia Lone MOTSUMI[1], Eniah SERAME[2], Kabo MASISI[1], Tshepo PHEKO-OFITLHILE[2] and Abdullah MAKHZOUM[1]
[1]*Department of Biological Sciences and Biotechnology*
[2]*Department of Chemical and Forensic Sciences*
Botswana International University of Science and Technology
Palapye, Botswana
phekot@biust.ac.bw
makhzouma@biust.ac.bw

Abstract
The essential oils represent a good source of aromatic and pharmaceutical compounds. *Lagerra decurrens* is a plant species which belong to the Asteraceae family and is found in Subharan Africa including Botswana. In this work, antioxidant and antibacterial activity of *Lagerra decurrens* essential oils were evaluated. Essential oils were extracted from the leaves of *Lagerra decurrens* using Clevenger apparatus. Antioxidant activity measured by 2,2-diphenyl-1-picryl-hydrazyl (DPPH), and total phenolic content (TPC) showed DPPH radical scavenging activity to be 101.3±6.94 and TPC of 842.6±42.1 of the leaf essential oils. Furthermore, antimicrobial activity of the essential oils was determined against bacterial colonies of *Escherichia coli*, *Pseudomonas aeruginosa* and *Staphylococcus aureus* using agar disc diffusion assay. Our results showed inhibition against *Staphylococcus aureus* as compared to a commercial broad-spectrum antibiotic (Ampicillin), with no antibiotic activity observed against the *Escherichia coli*, and *Pseudomonas aeruginosa*. Suggestions for future work include conducting minimum inhibitory concentration (MIC) and minimum bactericidal concentration (MBC) measurements to determine the potency of these essential oils' antimicrobial effects, as well as research into their potential applications in medicine and pharmaceutical industry.

Keywords: Antioxidant, antibacterial, essential oil, *Lagerra decurrens*

BIUST Teaching, Research, & Innovation Symposium 2023 (TRDAIS 2023)
Botswana International University of Science and Technology
Palapye, Botswana, 18 - 19 September 2023
ISSN: 2521-2293

Adaptation of mouse embryonic fibroblasts in culture to different embryonic stem cell media formulations

Monica M. Mazebedi, Malebogo C. Moseki, Keagile Bati and Goabaone Gaobotse
Department of Biological Sciences and Biotechnology
Botswana International University of Science and Technology
Palapye, Botswana
gaobotseg@biust.ac.bw

Abstract

Mouse Embryonic Stem Cells (mESCs) have been useful in the creation of knockout mice and the study of early mammalian development. Because human and mouse ESCs share similar properties of pluripotency and self-renewal, results of studies undertaken in mESCs are directly applicable to hESCs. Human ESCs can be utilized to alleviate different disorders and for testing the toxicity of novel medications. Mouse Embryonic Fibroblasts (MEFs) serve to sustain the proliferation and pluripotency of ESCs in culture by supplying important substrates/nutrients and preventing spontaneous differentiation. This study was aimed at evaluating the effects of 5 different ESC media formulations on the proliferation of MEFs. We hypothesized that different mESC media formulations may improve the proliferation of MEFs. MEFS were derived from E13.5 Murphy Roths Large (MRL) pregnant mice in the BIUST animal house and cultured in MEF media (88.5% DMEM, 1% Glutamine, 10% FBS, 0.5% PenStrep). The MEFs were cultured for 7 days without passaging in 5 media formulations containing varying concentrations of DMEM, PenStrep, Glutamine, NEAAs, β-mercaptoethanol and Recombinant LIF. Cell morphology and proliferation were then observed. Cell viability was determined using MTT assay. Media 1 (400µl PenStrep, 2ml Glu, 1ml NEAA, 200µl β-met, 100µl LIF), 2 (360µl PenStrep, 1.8ml Glu, 0.9ml NEAA, 180µl β-met, 90µl LIF), and 3 (320µl PenStrep, 1.6ml Glu, 0.8ml NEAA, 160µl β-met, 80µl LIF), were found to promote short term proliferation of MEFs while media 4 (440µl PenStrep, 2.2ml Glu, 1.1ml NEAA, 220µl β-met, 110µl LIF), and 5 (480µl PenStrep, 2.4ml Glu, 1.2ml NEAA, 240µl β-met, 120µl LIF), with the highest NEAA concentration, were found to be more appropriate for long term culturing of MEFs. Cells cultured in media 1 and 5 displayed 99% and 95% viability respectively. Cells in media 3, with the second lowest NEAA concentration, displayed the lowest viability of 84%. These findings may contribute to studies aimed at optimizing MEF culture protocols. MEFs are crucial for culturing ESCs used in the alleviation of diseases such as HIV/AIDS and cancer. Further studies aimed at optimizing MEF and, by extension, ESC culture protocols are requisite.

Keywords: Stem cells, viability, pluripotency, morphology, proliferation, and feeder layers

BIUST Teaching, Research, & Innovation Symposium 2023 (TRDAIS 2023)
Botswana International University of Science and Technology
Palapye, Botswana, 18 - 19 September 2023
ISSN: 2521-2293

Submission Type: Poster
Choose Track: Life Sciences and Environment

Anthocyanins, Phenolic Content and Antioxidant Potential of the Selected Edible Wild Fruits of Botswana

Yengemadzo Tapiwa HEADLON, Emmanuel SEKOPO, Keletso LASHANI, Goabaone GAOBOTSE, Kabo MASISI

Department of Biological Sciences and Biotechnology
Botswana International University of Science and Technology
Palapye, Botswana
masisik@biust.ac.bw

Abstract

Edible wild fruits are good sources of bioactive compounds such as anthocyanins and phenolic acids. Accumulating evidence shows that edible wild fruits have various bioactivities including, antioxidant and free radical scavenging activities. However, there are limited studies on the bioactive compounds and bioactivities of the edible wild fruits of Botswana. Therefore, in this study, we hypothesized that edible wild fruits of plants such as *Ximenia americana*, *Vangueria infausta, Grewia flava* and Moleshampe are sources of bioactive compounds and have bioactivities. The main aim of the study was to assess anthocyanins and phenolic content and antioxidant potential in four selected edible wild fruits that are used as food and treatment for various diseases by the people of the Tswapong region of Botswana. Total phenolic content (TPC), total anthocyanin content (TAC) and antioxidant activity were evaluated using standard protocols. TAC was significantly higher ($P<0.05$) in Moleshampe fruits when compared to the other three plants. The antioxidant potential assessed by TPC, 2,2-diphenyl-1-picrylhydrazyl (DPPH) and 2, 2'-Azino-Bis-3-Ethylbenzothiazoline-6-Sulfonic Acid (ABTS) assays showed significantly higher ($P<0.05$) activities of *Ximenia americana* fruits when compared to the other three fruits. Using 3-(4,5-dimethylthiazolyl-2)-2,5-diphenyltetrazolium bromide (MTT) assay, hydrogen peroxide (H_2O_2)-induced cell loss was significantly reduced ($P<0.05$) by preincubating HeLa cells with *Ximenia americana* when compared to the other three plants. Moreover, *Ximenia americana* fruits-treated HeLa cells showed differentiation during morphological assay when compared to with the other wild fruits. Our data suggest that *Ximenia americana* fruits are a source of phenolic acids and have antioxidant potential, therefore, can be considered for mitigation of oxidative stress.

Keywords: Antioxidant, edible wild fruits, anthocyanins and phenolic acids

BIUST Teaching, Research, & Innovation Symposium 2023 (TRDAIS 2023)
Botswana International University of Science and Technology
Palapye, Botswana, 18 - 19 September 2023
ISSN: 2521-2293

Submission: / Poster /
Track: / Computing and Industries /

Using Smartphone Gyroscope Crowdsourced Data To Profile Botswana Roads

Billy Lebogang, Dimane Mpoeleng
Department of all Computer Science and Information System
Botswana International University of Science and Technology
Palapye, Botswana
lb19000961@studentmail.biust.ac.bw, mpoelengd@biust.ac.bw

In Botswana, roads play a fundamental role in economic development and bring about vital social benefits. Road users will include motorists who transport goods and people to pedestrians who use them for their health needs and socio economic benefits. Road surface texture is a significant road attribute that is closely aligned with ride comfort, driving safety, road management, and other factors [2]. Road quality has become a significant concern due to the increase in the use of roads country wide. Botswana recorded a total of 17 341 from the year 2018 accidents from 16 642 in 2014 [3]. Road roughness is undoubtedly one of the most significant road quality measures.

In every mode of transport being used, bad roads are challenging as they can result in causing health issues to the user, threaten their safety while using them, and even cost them time and money for using them and even reduce the lifespan of the motor [1]. As for a user that is concerned about these issues they will by all means avoid such kinds of roads, but the problem remains that these roads are usually obscure unless in the case of a regular user. In this study, we present a solution to this issue using the sensor technology and included into our cellphones and crowdsourced data. Our smartphones' advanced technological capabilities must be used to address our daily issues. This sensor technology includes a gyroscope, accelerometer, and GPS.

Keywords: *Gyroscope, accelerometer, GPS, crowdsourcing, mapping*

BIUST Teaching, Research, & Innovation Symposium 2023 (TRDAIS 2023)
Botswana International University of Science and Technology
Palapye, Botswana, 18 - 19 September 2023
ISSN: 2521-2293

Submission Type: Poster
Track: Life Sciences and Environment

Complete whole genome characterization of multi-drug resistant *Proteus mirabilis*-MN029, a bacterial strain for evaluation of antibacterial activity of *Kigelia africana* bark extract

Motlatsi Nketsang, Abdullah Makhzoum, Gaolathe Rantong, Teddie Rahube*
Department of Biological sciences and Biotechnology
Botswana International University of Science & Technology
Palapye, Botswana
** nm20100097@studentmail.biust.ac.bw*

Abstract

Proteus mirabilis is a Gram-negative, rod-shaped bacteria that belongs to the order Enterobacterales in the family of Morganellaceae. *P. mirabilis* contribute to urinary tract infections (UTIs) and frequently recovered from many clinical samples. The emergence and spread of multi-drug resistant *P.mirabilis* isolates are increasing at a high rate, presenting a big problem in modern healthcare. Many of the modern drugs are currently ineffective against multi-drug resistant strains, hence the need for discovery of alternative drugs especially from indigenous plants. There are many reports on the antimicrobial activity of plants against resistant bacteria.

Whole genome sequencing (WGS) has emerged as an essential tool in the analysis of microorganisms of public health concern, including surveillance of antimicrobial resistance which can lead to more understanding of the resistance mechanisms evolving in bacteria. Our study employed WGS using HiFi long-read PacBio technology for identification and genome characterization of a multi drug resistant *P. mirabilis* MN029 strain. *Kigelia africana, an* indigenous plant originating from the sub-Saharan Africa was collected from Shakawe and near Tsodilo Hills. The plant was subjected to *in-vitro* assays to test its antimicrobial properties against the *P. mirabilis* MN029 which is resistant to eight clinically important antibiotics; amoxicillin/clavulanic acid, ampicillin, cefuroxime, chloramphenicol, fosfomycin, penicillin, trimethoprim/sulfamethoxazole, and ceftriaxone. The complete genome sequence of *P. mirabilis* MN029 is 3,989,563 bp with an average G+C content of 38.49%. The genome has 3,636 protein

BIUST Teaching, Research, & Innovation Symposium 2023 (TRDAIS 2023)
Botswana International University of Science and Technology
Palapye, Botswana, 18 - 19 September 2023
ISSN: 2521-2293

Submission: Poster

Track: Life Sciences and Environment

Screening and characterization of biosurfactant producing microbes from the environment

Kaone Mokwena, Aobakwe Letus, and Lemme P. Kebaabetswe

Department of Biological Sciences and Biotechnology

Botswana International University of Science and Technology

Palapye, Botswana

mk22100002@studentmail.biust.ac.bw

Abstract

Biosurfactants are secondary metabolites produced by bacteria, fungus, yeast and have the most potential uses in the medical and food sectors as antibacterial agents and surfactants. In this study, bacterial isolates from different environments (Palapye wastewater treatment plant, farm treated with pesticides, oil contaminated scrap yard soil and Palapye dumping sites), were screened for the production of biosurfactants. The following screening assays were performed; hemolytic activity, oil spreading, drop collapse and emulsification test. The results showed that two (2) isolates from the Palapye wastewater treatment plant produced biosurfactants. Both isolates were identified to be *Pseudomonas*, a gram-negative bacterium. Molecular analysis showed that the strains were the *Pseudomonas aeruginosa* LESlike4 and *Pseudomonas sp.* WTB11-2, with accession numbers CP006985.1 and KY327832.1, respectively. The antimicrobial activity of the biosurfactant extracts produced by each isolate were assessed using agar disk diffusion method against two pathogenic bacteria (*E. coli* and *S. aureus*). The extracts showed antimicrobial activity against the pathogenic bacteria.

Keywords: Biosurfactants, *Pseudomonas aeruginosa*, , *Pseudomonas aeruginosa* LESlike4, *Pseudomonas sp*. WTB11-2 and pathogenic bacteria.

BIUST Teaching, Research, & Innovation Symposium 2023 (TRDAIS 2023)
Botswana International University of Science and Technology
Palapye, Botswana, 18 - 19 September 2023
ISSN: 2521-2293

Choose Submission Type: Poster
Choose Track: Computing and Industries

A Biorobotics Approach on the Methodology to Study the Mechanisms of a Bionic Arm

Laone Ronaldo Pilane and Rodrigo Jamisola Jr
Department of Mechanical, Energy and Industrial Engineering
Botswana University of Science and Technology
Palapye, Botswana
pl20001350@studentmail.biust.ac.bw

Abstract

We present a methodology for the study of the mechanisms of a bionic arm using a biorobotics approach, where we simulate our design in the computer and verify the emergent behaviour in nature. This is important because the resulting design is guaranteed to work just like the real biological arm. The design of the mechanisms is inspired by nature and drawn using Solidworks. The Solidworks design is imported into Gazebo and robot operating system (ROS) as the simulation platform where the design is subjected to random and explicitly designed complex movements in order to induce emergent behaviours. These types of behaviours are results of the bioinspired design which can be unknown to the human designer. The simulation will enable such emergent behaviours that will allow the designer to verify them with nature. The methodology presented specifies how these can be achieved.

Keywords: Bionic arm, mechanism design, biorobotics, Gazebo, robot operating system (ROS)

BIUST Teaching, Research, & Innovation Symposium 2023 (TRDAIS 2023)
Botswana International University of Science and Technology
Palapye, Botswana, 18 - 19 September 2023
ISSN: 2521-2293

Choose Submission Type: **Poster**
Choose Track: C**omputing and Industries**

Green and Intelligent SDN Routing: Trends Of Energy Efficient Technologies

Dimakatso Setso, Thabo Semong
Department of Computer Science and Information Systems
Botswana International
University of Science and Technology (BIUST)
Palapye, Botswana
sd19100154@studentmail.biust.ac.bw, semongt@biust.ac.bw

Abstract
The amount of energy consumed by network infrastructures has seen a significant increase due to the continuous growth of internet applications, content and services. Reducing this power consumption is one of the major challenges in computer networks because of high energy cost and environmental issues. Several methods have been deployed for introducing energy efficiency in ICT networks, which we generally define as green networking. This study discusses the concept of an emerging technology Software Defined Network (SDN) with intention to drive the attention toward environment friendly adoption and implementation of SDN that could deal with the growing number of users and network equipment. SDN is a technology that splits the data plane from the control plane, and the architecture allows for traffic engineering, programmability and ease of various network management functions. If network control and management is obtained flexibly, we can devise methods to reduce the energy consumption of networks consequently. We aim to highlight the key features of SDN and their effect on intelligent green technology. The study will also provide a review of literature works on green SDN, in relation to existing energy saving protocols, algorithms, techniques and the various energy efficiency capabilities categorized in accordance with the scope in which they are applied generally and in different network types. We review the different capabilities and extensions required to build Green SDN and outline the performance metrics and parameters used to evaluate these various technologies and techniques. The goal is a network infrastructure that optimizes both energy consumption and performance, hence the need for intelligent energy efficient technologies that consequently maintain Quality of Service.

Keywords: Software Defined Networking, Green SDN, Green Technology, Energy Saving, Routing

BIUST Teaching, Research, & Innovation Symposium 2023 (TRDAIS 2023)
Botswana International University of Science and Technology
Palapye, Botswana, 18 - 19 September 2023
ISSN: 2521-2293

Molecular dynamics study of the decarboxylation of methyl palmitate using Nickle Molybdate catalyst.

Maipelo Nyepetsi[1*], Oyetunji Olayinka[2], Foster Mbaiwa[1]

1.Department of Chemical and Forensics Sciences, Botswana International University of Science and Technology, Palapye, Botswana

2. Department of Chemistry, University of Botswana, Gaborone, Botswana

**nyepetsim@buist.ac.bw*

Abstract

The world is currently experiencing energy crises, which is mainly due to the rapidly depleting fossil-based fuels and is made worse by rapidly increasing population and *geo-political tensions*. The increase in fossil-based fuel prices and green-house gas emissions from these fuels has motivated a search towards alternative sources of energy and biodiesel is a promising alternative. Its attractiveness is since it can be used in the current diesel engines with little or no modification to the engine. It is produced by reacting plant derived oils or animal fats with short chain alcohols like methanol in the presence of a catalyst. Biodiesel has several limitations including high viscosity, high pour point and cloud points and high acid values. These properties are connected to high composition of unsaturated and saturated methyl esters. One of the ways of improving these poor flow properties is by converting fatty acid methyl esters (FAMEs) to hydrocarbons (HC). In this study Molecular Dynamics coupled to Reactive Force Field (Reaxff) was used to model the decarboxylation of FAMEs on Nickel Molybdate ($NiMoO_4$) catalyst. We studied effect of changing temperatures and changing surfaces on the decarboxylation of methyl palmitate. The results shows that the α- $NiMoO_4$ performed better in terms of selectivity towards the desired $C_{15}H_{30}$ and in the conversion of methyl palmitate than the β-$NiMoO_4$. All the reactions were found to follow first order kinetics, from which the Activation Energy (Ea) was determined. The α-$NiMoO_4$ surface (110) had the lowest activation energy of 14.13kcal/mol which was also the closest to what was observed in literature of 10.11kcal/mol[1]. It was also found that increase in temperature increased the formation of smaller molecules like CO_2 and C_2H_4, however there was no activity observed at temperatures below 1000K.

Keywords: BIODIESEL, Reaxff , Methyl Palmitate, Decarboxylation , Nickel Molyddate

[1] S. V Sancheti, G.D. Yadav, P.K. Ghosh, Synthesis and Application of Novel NiMoK / TS - 1 for Selective Conversion of Fatty Acid Methyl Esters / Triglycerides to Ole fi ns, (2020). https://doi.org/10.1021/acsomega.9b03993.

BIUST Teaching, Research, & Innovation Symposium 2023 (TRDAIS 2023)
Botswana International University of Science and Technology
Palapye, Botswana, 18 - 19 September 2023
ISSN: 2521-2293

Choose Submission Type: Poster
Choose Track: Life Sciences and Environment

Antioxidant and antimicrobial activities of *grewia flava* herbal extracts

Gofaone Coin, Ofentse Mazimba, Kabo Masisi and Disang Lekutlane
Department of Chemical and forensic science
Botswana University of Science and Technology (BIUST)
Palapye Botswana
Gofaone.coin@studentmail.biust.ac.bw, mazimbao@biust.ac.bw, masisik@biust.ac.bw, lekutlaned@biust.ac.bw

Abstract

Grewia flava (family: *Malvaceae*) is relatively understudied although plants species in the same genus are known to have a wide range of medicinal properties such as diabetes, diarrhoea, cough, digestive problems, ulcerative colitis, heat stroke and sore throat. The current study was aimed at determining the antioxidant and antimicrobial properties of *Grewia flava* twig and root extracts. Antioxidant assay of the crude extracts were performed using 2, 2′-diphenyl-1-picrylhydrazyl (DPPH) scavenging activity and the *in-vitro* antimicrobial activity was investigated by the Agar well diffusion method. All the extracts under study exhibited free radical scavenging activity against DPPH, which is regarded as an indication of antioxidant properties, methanol twig extract showed strongest activity with IC_{50} value (concentration needed to inhibit 50% of the radical) of 15 µg/mL, compared to 23 µg/mL for the standard ascorbic acid. Methanol extracts exhibited better antioxidant activity when compared to other solvents (*n*-hexane, acetone and distilled water), hence antimicrobial activity was only investigated for the methanol extracts. Growth inhibition was observed against four bacterial strains: *Escherichia coli*, *Bacillus subtilis*, *Staphylococcus aureus* and *Pseudomonas aeruginosa* and two fungal strains (*Aspergillus Niger* and *Rhizopus Oryzae*) for both twig and root extracts. The current study revealed important antioxidant and antimicrobial properties of *Grewia flava* twig and root extracts which support the plant parts usage in Folklore medicine.

Keywords: *Grewia flava*, Antioxidant, antimicrobial, Folklore medicine

BIUST Teaching, Research, & Innovation Symposium 2023 (TRDAIS 2023)
Botswana International University of Science and Technology
Palapye, Botswana, 18 - 19 September 2023
ISSN: 2521-2293

Choose Submission Type: Poster
Choose Track: Life Sciences and Environment

Preliminary Screening of Traditional Herbal Concortions Sold by Street Vendors at Dibete (Central District) in Botswana

Ontlametse Phiri[1], Lucia M. Lepodise[2], Tshepo Pheko-Ofitlhile[1]
[1]Department of Chemical and Forensic Sciences, [2]Department of Physics and Astronomy
Botswana International University of Science and Technology
Palapye, Botswana
ontlametse.phiri@studentmail.biust.ac.bw

Abstract

From the ancient times, different medicinal plants have been used to treat different health ailments and discomfort in people. Approximately 80% of the people's population in the world, depend on herbal medicines as their principal source of health care needs.The application and the use of medicines primarily produced from medicinal plants is noticeably surging.Documentation is needed for different plant use as they differ in space and time to avoid loss of precious knowledge from one generation to the next. This study aims to investigate the properties, quality as well as the authenticity of the herbal concoctions which are prepared to ease different body ailments. These herbal medicines have been used without any further scientific knowledge to back up their use. It is essential to know the properties of these medicines which allow for the commercialization and proper use of these concoctions.The Fourier Transform Infrared (FTIR) technique was employed to characterize samples from four (4) different vendors. The samples that were studied were intended for the same purpose of easing body pains. Preliminary results hinted similarities between the studied materials. There is evidence of common absorption peaks between the 4 samples which suggests that they contain similar compounds which vibrate at the same energies. The corresponding absorption peaks between the different herbal concoctions appeared between 3750-3200 cm^{-1}, 2934-2920 cm^{-1}, 1595-1390 cm^{-1} and 840-468 cm^{-1}. Despite the similarities in the spectra of these materials, there are slight differences in their spectra. These results are quite interesting in that, although the herbal concoctions were prepared by different people they have very close similarities in their FTIR spectra. Further work will be done to explore the properties of these materials in order to gain insight on their efficacy.

Keywords: Herbal medicine, Efficacy, Traditional herbal concoction, Medicinal Plant, Fourier Transform Infrared Spectroscopy (FTIR)

BIUST Teaching, Research, & Innovation Symposium 2023 (TRDAIS 2023)
Botswana International University of Science and Technology
Palapye, Botswana, 18 - 19 September 2023
ISSN: 2521-2293

Submission Type: Poster
Choose Track: Life Sciences and Environment

Impact of Morupule Fly Ash Dumpsite on Surface Water and Groundwater Quality in Palapye, Botswana.

Katumelo Gajaje, Koziba Gaotlhobogwe, and Venecio U. Ultra, Jr.
Department of Earth and Environmental Sciences
Botswana International University of Science and Technology
Palapye, Botswana
gk19100097@studentmail.biust.ac.bw

Abstract

Fly ash, a mineral residue produced by coal-fired power plants, is a major environmental concern due to its adverse effects on air, water, soil, and plants, especially if it is physically contained in a dumpsite. Fly ash dumpsite have an adverse effect on the local environment, particularly the quality of the groundwater and surface water. This study was conducted to assess the impact of the Morupule fly ash dumpsite on the physicochemical characteristics of surface water and groundwater the surrounding areas. Surface water and groundwater samples were collected at specific intervals along a 40-kilometer transect line running northeast and southwest from the Morupule fly-ash dumpsite in relation to the prevailing winds of the Morupule Power Station which are Northeastly winds. Analyses revealed that surface water and groundwater sampled near (5km radius) the Morupule fly ash dumpsite on the southwest generally had higher average of pH (11.47), total dissolved solids (12.73 mg/l), alkalinity (98.00 mg/l). The average heavy metal content was higher in areas far away (southwest direction) from the fly ash dumpsite, particularly in surface water (As = 0.03 mg/kg, Fe= 18.17 mg/kg, Mn= 4.25 mg/kg, and Pb= 0.02 mg/kg), whereas in ground water the highest concentrations (Fe= 7.65 mg/kg and Pb= 0.02 mg/kg) were found in areas nearer to the dumpsite (1 to 5 km, southwest direction) and these elements exceeded the BOB's 2015 standards, as compared to areas far away from the dumpsite(20 to 40km, southwest and northeast direction). The study shows that the surface and ground water are affected by the dumpsite which could have emanated from fly ash deposition and subsequent leaching of contaminates into groundwater especially in areas with proximity to the fly ash dumpsite. Consequently, surface water and ground water extracted from these sites needs to be treated to meet the standards of drinking water.

Keywords: *Heavy metals, fly ash dumpsite, surface water, groundwater, leaching*

BIUST Teaching, Research, & Innovation Symposium 2023 (TRDAIS 2023)
Botswana International University of Science and Technology
Palapye, Botswana, 18 - 19 September 2023
ISSN: 2521-2293

Submission Type: Poster
Track: Life Sciences and Environment

Nutrient Supplementation and Potential Health Risk Assessment of Geophagic Soils of Botswana

Tsholofelo Leah K. Molale, Peter N. Eze
Department of Earth and Environmental Sciences
Botswana International University of Science and Technology
Palapye, Botswana
Mt20100120@studentmail.biust.ac.bw

Abstract

Geophagy, the deliberate consumption of earth materials including soils, has been widely reported across the globe at different periods of human history. In Botswana, geophagic practice is a well-rooted practice among different demographic groups. Soil consumption has been a part of many Batswana's lives, mostly prevalent in women (especially during pregnancy) and young children. Although widely practised in Botswana, geophagy's nature and potential human health risks are grossly under-researched. This study sought to determine the concentration of potentially toxic and essential and trace essential elements and compute the extent of potential harm to consumers. A total of 30 geophagic soil samples, that were shown to me by locals, were collected from six places namely; Gaborone, Mochudi, Molapowabojang, Palapye, Tonota and Francistown. ICP-MS and ICP-EOS were used for the determination of potentially toxic elements (PTEs); (As, Cd, Pb, and Hg) and essential and trace essential elements (Fe, Ca, Zn, Cu, K, Mg, Mn, Ni, Cr) contents in the soils. All the above-mentioned essential elements were detected in the geophagic soils therefore, there is a possibility of nutrient supplementation to consumers. Ratios such as hazard quotient (non-carcinogenic risk) (HQ), hazard Index (HI), chronic daily intake (CDI) and Carcinogenic risk (R) were computed and Permitted Maximum Tolerable Daily Intake (PMTDI) recommended by the World Health Organisation (WHO) will be compared to the concentration of elements in the soil samples. HQ and HI values for all the PTEs were found to be <1, meaning consumption of these geophagic is less likely to cause adverse non-carcinogenic health effects. Carcinogenic Risk values for all carcinogenic metals (As, Cd, Ni and Cd) were lower than the acceptable limit of $1*10^{-6}$; meaning consumption of the geophagic soils is less likely to cause cancer. A study of this nature is important as it provides insights into the health outcome of this under-studied behaviour among Batswana.

Keywords: Soil ingestion, potentially toxic elements, essential elements, carcinogenic, Batswana

BIUST Teaching, Research, & Innovation Symposium 2023 (TRDAIS 2023)
Botswana International University of Science and Technology
Palapye, Botswana, 18 - 19 September 2023
ISSN: 2521-2293

Submission Type: Poster
Track: Pure and Applied Sciences

Fabrication and thermoelectric properties of copper oxide polymer composite (CuO/PANI)

Atlang G. Mpolokang
Department of Physics and Astronomy
Botswana International University of Science and Technology
Palapye, Botswana
ma19100109@studentmail.biust.ac.bw

Abstract

The ultimate success in the drive towards a greener and sustainable global environment can only be achieved if a significant portion of the 70 % of waste energy that is lost as heat from various industrial and commercial devices is recovered and is converted into useful applications. This ambitious goal requires more efficient and affordable thermoelectric devices that operate in the lower midrange (150 – 300^{o}C) temperatures. In this work we report the synthesis of non-toxic semiconductor (Copper oxide) and conducting polymer (polyaniline) composite thermoelectric material to meet the desired goal. Through morphology manipulation at nanoscale which lowered the lattice thermal conductivity and semiconductor doping the figure of merit of copper oxide (CuO) was improved by 10^2 to produce a better performing thermoelectric material (copper oxide – polyaniline composite) that operates in the lower midrange temperature where most of the current commercial devices are operated.

Keywords: *Metal oxide – polymer composite, Power factor, Figure of merit, Nanomaterials*

BIUST Teaching, Research, & Innovation Symposium 2023 (TRDAIS 2023)
Botswana International University of Science and Technology
Palapye, Botswana, 18 - 19 September 2023
ISSN: 2521-2293

Submission Type: Poster
Track: Pure and Applied Sciences

Development of a mercury (II) ion sensor based on peroxidase-like activity of Fe_3O_4@C@AuNPs

Boikanyo Motlhaedi, Melisew Tadele Alula, Joy Mokone
Department of Chemical and Forensic Science
Botswana International University of Science and Technology (BIUST)
Palapye, Botswana
mb19100129@studentmail.biust.ac.bw; alulam@biust.ac.bw; mokonej@biust.ac.bw

Abstract

Mercury is a toxic heavy metal that has a range of adverse effects on human health. As a consequence, the development of some feasible, practical, and highly sensitive platforms for the determination of Hg^{2+} would be necessary in order to achieve enhanced pollution control and environmental monitoring. In this work, magnetic composites, Fe_3O_4@C@AuNPs with a peroxidase-like activity was produced and employed for the colorimetric detection of mercury ions. A simple solvothermal process was used to synthesize Fe_3O_4@C nanocomposites. To immobilize gold nanoparticles (AuNPs) on Fe_3O_4@C support, a simple heat induced AuNPs synthesis method was employed. The composites were characterized using different techniques including, X-ray powder diffraction (XRD), scanning electron microscopy (SEM), and Fourier translation infrared spectroscopy (FT-IR). In the presence of hydrogen peroxide and Hg^{2+}, Fe_3O_4@C@AuNPs composites enhance the oxidation of colorless 3,3,5,5'-tetramethylbenzidine (TMB) solutions into a blue-colored 3,3,5,5'-tetramethylbenzidine diamine (oxTMB) that enables to determine quantification of Hg^{2+} colorimetrically. The method displayed remarkable selectivity and sensitivity for Hg^{2+} detection. Despite the fact that the developed method has a detection limit of 187 nm, which is more than the WHO limit of 30 nm, it is nevertheless effective. With percentage recoveries ranging from 82.7% to 105%, the suggested approach proved practicality and reliability for real sample analysis using tap water. The results showed that the suggested approach provided simple and low-cost sensing for Hg^{2+} detection.

Keywords: Colorimetric; magnetic composites; mercury (II); peroxidase-like activity

BIUST Teaching, Research, & Innovation Symposium 2023 (TRDAIS 2023)
Botswana International University of Science and Technology
Palapye, Botswana, 18 - 19 September 2023
ISSN: 2521-2293

Choose Submission Type: Poster
Choose Track: Life Sciences and Environment

PRODUCTION OF SYNTHETIC GAS AS FUEL FOR ELECTRICITY GENERATION IN THE GAS ENGINE

Thabang Obuseng, Mmoloki Makoba, Khumiso Malebeswa, Paul Serban Agachi
Department of Chemical, Materials and Metallurgical Engineering
Botswana International University of Science and Technology (BIUST)
Palapye, Botswana
thabang.obuseng@studentmail.biust.ac.bw

Abstract

Botswana has over 212 Btons of coal resources, over the years experts have come up with different technologies that convert this coal into useful products, one of them being coal gasification. Syngas (H_2, CO, CO_2 & CH_4) produced through coal gasification can be used to generate electricity. This project is focused on the production of synthetic gas from Botswana coal using a small- scale fixed-bed gasifier. The gasification experiments were carried out in a pilot plant using coal from Mabesekwa (composite). The process was carried out at different operating conditions: temperature (800 - 900 ^oC), coal particle size (1 to 10 mm) and a residence time of 60 and 120 minutes. This was done to assess the quality and quantity of gas produced under these conditions for optimization purposes. The better quality syngas was achieved at 850 ^oC at a residence time of 120 minutes. It contained 6.38% of H_2, 10.76% of CO, 82.60% of CO_2 and 0.26% of CH_4. However this a lower quality compared to the standard composition of syngas, which contains 25-30 % H_2,30-60% CO,5-15% CO_2 and 0-5% CH_4 .This was achieved using a feeding rate of 108 g/min.

Keywords: Fixed-bed reactor, coal-gasification, syngas

BIUST Teaching, Research, & Innovation Symposium 2023 (TRDAIS 2023)
Botswana International University of Science and Technology
Palapye, Botswana, 18 - 19 September 2023
ISSN: 2521-2293

Choose Submission Type: Poster
Choose Track: Computing and Industries

On the CO_2 Storage in Botswana

Boikanyo Mokgweetsi, Leungo Kelebopile
Department of Mechanical and Energy Engineering
Botswana International University of Science and Technology
Palapye, Botswana
boikanyo.mokgweetsi@studentmail.biust.ac.bw

Abstract

Carbon dioxide Capture and Storage (CCS) is hardly considered for developing countries because it is considered costly, and less important than other economic goals. Like many countries, Botswana's energy needs are heavily dependent on fossil fuels. The country's electricity supply is reliant on the 132 MW Morupule A and 600 MW Morupule B coal power plants that are estimated to generate about 5 Mt CO_2 annually at full capacity. However, there has not been CCS activity in the country to incorporate into the plants. The purpose of this study is to share insights on the potential of CCS in Botswana.

This study was based on data from previous reports on the potential geological storage capacity available in Botswana. The reports were based on a basin-scale assessment that worked with insufficient data but were able to draw reasonable conclusions on the locations of potential storage sites and their potential storage capacities with the help of simulations. In this study, existing literature was also used to identify potential CO_2 transportation options and possible ways to offset costs in the CCS system.

It was found out that there are three potential storage sites that can provide sufficient geological storage capacity for CO_2 in Botswana; Passarge Basin, Mmashoro Low and Lephephe Graben. They were identified on the basis of geological distribution and structural controls on overall Karoo thickness. Data from previous reports suggest that CO_2 from power plants can be stored for the next 57 to 191 years. The three identified storage sites are found to be within a 450 km radius from the power plants. Mmashoro Low and Lephephe Graben have a potential conflict with coal-bed methane exploration in their localities.

It was also found out that, compared to trucks, pipelines were the more attractive choice of transportation considering the high CO_2 generation volumes of the power plant. Storage and transportation cost might be high ($4 to $45/t$CO_2$) but there are potential options to offset them. They are based on Carbon dioxide Capture and Utilization, (CCU) pathways which include, selling some of the captured CO_2 to industries like construction, chemical, and enhanced oil recovery.

Overall there is potential for CCS in Botswana. And there are possible ways to reduce the running and/ implementation costs. Such pathways can even lead to greater economic goals through creation of new markets.

Keywords: Carbon capture and storage, carbon capture and utilization, developing countries

BIUST Teaching, Research, & Innovation Symposium 2023 (TRDAIS 2023)
Botswana International University of Science and Technology
Palapye, Botswana, 18 - 19 September 2023
ISSN: 2521-2293

Choose Submission Type: Poster
Choose Track: Life Sciences and Environment

Investigating Coal Syngas as a Fuel for the Turbocharged-Gas Engine

Khumiso Malebeswa, Mmoloki Makoba, Pradeep Kumar Sahoo, Thabang Obuseng
Department of Mechanical and Industrial Engineering, Botswana International University of Science and Technology, P/bag 16, Palapye, Botswana

Khumiso.malebeswa@studentmail.biust.ac.bw

Abstract

The search for clean and efficient energy using alternative fuels has generated great interest to alleviate shortage, high emissions and inefficient power production. In this study performance and emission analysis is carried out in a 30kW turbocharged spark ignition engine. This is a 4 cylinder and a 4-stroke fuelled engine powered by with coal synthetic gas (syngas). The syngas is produced from Botswana coal through the process of gasification, and has a calorific value of 28 MJ/kg. Coal gasification is conversion of coal into combustible gases (carbon monoxide, hydrogen, carbon monoxide and methane) at high temperatures of around 1000 °C. Syngas is produced, collected, and used as a fuel using a in the gas engine. Gas engine (genset) produces electricity by a combination of a gas engine with an electric generator (alternator). Genset covert the chemical energy in the syngas to mechanical energy through combustion. The mechanical energy then rotates a shaft coupled alternator to produce 30 kW of electricity Based on the calorific value and composition of the syngas, the syngas flow is 0.0286kg/s, airflow is 0.0372 kg/s with the air-fuel ratio being 1.3.

Keywords: Gas engine, emission, syngas, gasification, performance, turbocharged

BIUST Teaching, Research, & Innovation Symposium 2023 (TRDAIS 2023)
Botswana International University of Science and Technology
Palapye, Botswana, 18 - 19 September 2023
ISSN: 2521-2293

Submission Type: Poster
Track: Computing and Industries

Ethics, Regulation and Governance of Critical Systems Running on Artificial Intelligence: Auditing and Policy Implications

Kebakaone Marumo
Department of Mathematics and Statistical Sciences
Botswana International University of Science and Technology
Palapye, Botswana
mk22100159@studentmail.biust.ac.bw

Abstract

Artificial Intelligence (AI) has been gaining popularity, especially in critical systems like autonomous driving vehicles and medical diagnostics among others. Critical systems by definition are systems that should always be efficient and whose failure can cause damage, and loss of life and are linked to the survival of the user. These systems, if they run on AI, should be audited to make sure they are accountable, fair, and transparent to increase users' trust.

This study aims to address ethical concerns in applications of artificial intelligence to address societal problems (those with solutions based on critical systems) and formulate a way to audit, regulate and govern the use of AI in critical systems. This was done by reviewing literature and analyzing current policy implications and interventions specific to critical systems whether (mission, safety, or business critical). The end game was to produce a framework to audit and regulate AI use across human social systems.

Keywords:
Critical systems, artificial intelligence, AI ethics, regulation and governance

BIUST Teaching, Research, & Innovation Symposium 2023 (TRDAIS 2023)
Botswana International University of Science and Technology
Palapye, Botswana, 18 - 19 September 2023
ISSN: 2521-2293

Impact of separation on complementation in the lattice of topologies

Tsie Ramodimo [♭] and Zechariah Mushaandja [♯]

September 23, 2022

Abstract

The family of all topologies on a set X is a complete lattice. Its structure has been studied by several authors and complementation has received considerable attention (see [1], [2], [3] and [4]), with positive and interesting results emerging when X is finite. Anderson and Stewart ([4]) show that if X is infinite then things are different. For instance, there is no infinite Hausdorff first countable space with a Hausdorff first countable T1- complement. In this paper, we investigate how the T1 separation and countability impact on complementation in the lattice of topologies.

Keywords: Complete lattice, complement, $T1$ separation, first countable

[♭] Email: tsie.ramodimo@studentmail.biust.ac.bw (*presenter*)
Department of Mathematics and Statistical Sciences, Botswana International University of Science and Technology (BIUST), Private Bag 16, Palapye, BOTSWANA

[♯] Email: mushaandjaz@biust.ac.bw (*corresponding author*)
Department of Mathematics and Statistical Sciences, Botswana International University of Science and Technology (BIUST), Private Bag 16, Palapye, BOTSWANA

References

[1] H. Gaifman. On complementation in the lattice of all topologies. Canad. J. Math, 1966.

[2] G. Birkhoff. On the Combination of topologies. Fund. Math, 1936, 156-166.

[3] A. K. Steiner. The lattice of topologies: structure and complementation. Trans. Amer. Math. Sot., 122 (1966) 379-398.

[4] B. A. Anderson and D.G Stewart. T1-complements of T1 topologies. Proc. Amer. Math. Sot., 23(1969) 77-81.

BIUST Teaching, Research, & Innovation Symposium 2023 (TRDAIS 2023)
Botswana International University of Science and Technology
Palapye, Botswana, 18 - 19 September 2023
ISSN: 2521-2293

HOUSE PRICE PREDICTION USING MACHINE LEARNING IN BOTSWANA

Mogolodi Ndlovu, Dr Tshiamo Sigwele
Department of Computer Science and Information Systems
Botswana International University of Science and Technology
Palapye, Botswana
nm19000756@studentmail.biust.ac.bw, sigwelet@biust.ac.bw

The residential property market has great growth potential in Botswana. According to the Monetary Policy report from the Bank of Botswana, the average price of residential property rose by 11.4%. High population growth and rapid urbanization have created high demand and shortage of residential facilities in Botswana. Therefore, property prices are rising rapidly yearly as the demand increases with population growth and urbanization. The problem arises during the valuation of the residential facilities as different factors such as location of property, area of property and their physical condition must be considered to determine the selling price of a house. Currently in Botswana valuation of property is done manually which means this system of valuation is prone to human errors which may yield inaccurate and delayed predictions. Thus, it is not efficient in terms of predictions. More expenses may be incurred as some resources have to be used e.g., transport fees for the agent who will be carrying out the valuation process. It also requires necessary skills to carry out the price prediction while on the other hand there is a limited number of knowledgeable people and companies that do house price prediction in Botswana which makes the service not easily accessible to all parts of the country. The research proposes a machine learning framework based on multiple linear regression of high precision for valuation of house properties by accurate predictions of prices based on the factors that affect house prices. This will be of benefit to Botswana, both agent and buyers, as less resources will be used, and the model will provide accurate predictions.

Keywords: house Price Prediction, Machine Learning, Regression Algorithm

BIUST Teaching, Research, & Innovation Symposium 2023 (TRDAIS 2023)
Botswana International University of Science and Technology
Palapye, Botswana, 18 - 19 September 2023
ISSN: 2521-2293

Submission Type: Poster

Track: Computing and Industries

BUILDING A CIVIL UNREST PREDICTION MODEL BY MOBILITY DATA AND SENTIMENTAL BIG DATA ANALYTICS

Tebogo Regoeng and Dimane Mpoeleng

Department of Computer Science and Information Systems

Botswana International University Of Science and Technology (BIUST)

rt22100115@studentmail.biust.ac.bw

mpoelengd@biust.ac.bw

ABSTRACT

Anonymized mobility data is information that is private and can be protected via encryption or erasing the connection between an individual and stored data. The data is anonymized in a sense that it does not reveal people's privacy such as name. device's location, browser history, etc. Prominent cyber platforms such as facebook, twitter, instagram, blogs, google, news and many more capture anonymised data. Such data can be used to aid the prediction of civil unrest, riots, civil wars, military wars, social unrest, protest etc. The use of mobility data will help us analyze the current conflicts and predict civil unrest that are ongoing and those to come, for example in North Mozambique, Ukraine, Mexico etc. Our investigation on the models will help us predict civil unrests and enable us to prepare for upcoming ones. Mobility data can help us reveal patterns that can be used to predict conflict, however it has been sparsely used in predicting civil unrest such as civil wars, protests, riots and social unrest. The aim of the work is to develop and build on a model that is diverse as well as efficient to help detect civil unrest and help make futuristic decisions that will help prevent any form of danger and conflict from occurring. This proposal is part of the prerequisite for the Computer Science MSc programs as stipulated in the post graduate guide.

Keywords: Civil Unrest Predictions, Mobility Data, Spatial Analysis, Neural Networks, Big Data

.

BIUST Teaching, Research, & Innovation Symposium 2023 (TRDAIS 2023)
Botswana International University of Science and Technology
Palapye, Botswana, 18 - 19 September 2023
ISSN: 2521-2293

Choose Submission Type: Exhibit
Choose Track: Computing and Industries

A PLANT DISEASE, TYPE, AND SOIL CATEGORY RECOGNITION APPLICATION/SOFTWARE THAT USES IMAGES, WEBCAM

Bakang Kgopolo
Department of Mechanical Energy and Industrial
Botswana International University of Science and Technology
Palapye, Botswana
kb19000882@studentmail.biust.ac.bw

Abstract

The threat to global food security has increased because of numerous plant disease problems and the type of soil used for plant growth. Various methods of detecting plant disease or soil type have been developed to maintain food security by identifying plant diseases, plant type, and soil characteristics. Some people, however, continue to rely on their knowledge and information to carry out these activities, even though human error is prone to plant disease detection via leaf inspection. Deep learning and machine vision will be used in this project to create software or an application that uses real-time images, webcams, and/or video files to recognize plant disease and plant type by comparing the real object to the data uploaded to the system. The system's deep learning algorithms have been trained to predict whether a plant has a disease and to retrieve all relevant data on that plant. Android Studio (Kotlin language) and Machine Learning will be used to create an augmented reality system that uses computer vision for the system. This will be designed for both smart phones and mobile applications and if possible, UAV (Self Driving SmartCam Drones). The system will also be able to identify the type of soil in a particular environment and retrieve relevant data which will allow people to assess important rangeland and pasture variables that are critical to proper management and choose the best soil for improved plant growth. When it comes to this application, people, mostly farmers will not need to go and hire plant specialists and or scientists because the application will tell the plant type and name, health status, diseases detected, causes, prevention, and treatment for the disease. The application is also bound to recognize the type of soil in any environment, it's characteristics and plant growth succession rate.

Keywords: Android Studio, Kotlin, deep learning, machine vision, plant disease

BIUST Teaching, Research, & Innovation Symposium 2023 (TRDAIS 2023)
Botswana International University of Science and Technology
Palapye, Botswana, 18 - 19 September 2023
ISSN: 2521-2293

Choose Submission Type: Exhibit
Choose Track: Pure and Applied Sciences

Design fabrication and characterization of a solar food dryer for Palapye, Botswana

Paida Muengwa
Davison Munyaradzi Murape
Department of Physics and Astronomy
Botswana International University of Science and Technology, Botswana
mp18000745@studentmail.biust.ac.bw

Abstract

Dehydration is a way to preserve food that may spoil. Drying removes water and thus prevents fermentation or the growth of molds. It also slows the chemical changes that take place naturally in foods as when fruit ripens. People in Botswana and the rest of the world have been drying food for thousands of years by placing the food on mats in the sun. This simple method, however, allows the food to be affected or ruined by dust, airborne molds and fungi, insects, rodents, and other animals. Furthermore, open air drying is often not possible in humid conditions. Solar food dryers represent a major improvement upon this ancient method of dehydrating foods.

This study profiles the design, fabrication and performance evaluation of an indirect cabinet solar dryer. The dryer consists of a separate solar collector that heats up ambient air entering the collector and creates a convectional current that drives warm air into a coupled drying chamber. Food samples comprising tomatoes and apples were used for the performance evaluation of the dryer. The comparison experiment sought to differentiate the performance of the dryer from the largely uncontrolled natural drying i.e., direct sun drying. The results from the experiment showed that the temperature inside the drying chamber was consistently higher than the ambient air temperature. The drying rate of the dryer and percentage moisture loss content were 0.18 kg/hr and 91 % respectively. For natural drying the drying rate and percentage moisture loss were found to be 0.14 kg/hr and 71 % respectively. The dryer revealed its ability to dry products without them losing most of their original color as compared to direct sun drying as well as protecting products from birds, insects, strong winds and being soiled. Some of the open-air dry samples were eaten up by birds.

Keywords: Solar dryer, design, fabrication, drying chamber, food dryer

BIUST Teaching, Research, & Innovation Symposium 2023 (TRDAIS 2023)
Botswana International University of Science and Technology
Palapye, Botswana, 18 - 19 September 2023
ISSN: 2521-2293

Submission type: Exhibit
Track: Pure and Applied Sciences

THE RELATION BETWEEN FLUID PRESSURE AND ENERGY

Tsikoane B.E Mabaleha
Department of Chemical, Materials and Materials Engineering
Botswana International University of Science and Technology
Palapye, Botswana
53988608tsix@gmail.com

Abstract

Fluid pressure is a measurement of the force per unit area on an object in the fluid or on the surface of a closed container. And this pressure evenly applies in all directions of the container due to the arrangement of particles in fluids. The particles of a liquid have enough energy to break free of some of the forces of attraction between the particles. So particles in liquids can move around and also move over each other, allowing liquids to flow whilst for gases, the particles have enough energy to overcome the forces of attraction between the particles, so are free to move in any direction. They move quickly in straight lines, colliding with each other and the walls of their container.

In addition, conservation of energy and other motion theorems such as the Brownian motion of particles (which is explained as the random motion/thermal motion of the molecules caused by collisions within that medium) were used to establish the relationship between fluid pressure and energy. One of the experiments that is of interest in this topic is the experiment of deep-sea diving. Deep sea divers have certain limitations when it comes to how deep they can go without being at risk of pressure imbalance. This pressure imbalance comes forth due to changes in the surrounding, mostly due to the change in the average kinetic energy of the water particles as the depth increases of which affects the physical properties of the water, such as density. *More information about this experiment is present in the main document*.

In conclusion, the main objectives of establishing the relationship between pressure and energy were met. Hence, new inventions to improve working conditions of marine biologists could be implemented, which may lead to the discovery of valuable organic plants. Moreover, the same topic is of great relevance in space exploration as countries around the globe are embarking on a race of discovering life beyond earth and understanding the universe at large.

Keywords: Fluid pressure, energy

ISSN: 2521-2293

Programme of Activities

ISSN: 2521-2293

Opening Programme

Tuesday, 19 September 2023

TEACHING, RESEARCH, & INNOVATION SYMPOSIUM 2023 (TRDAIS 2023)

BIUST Auditorium
0900 - 1025 Hrs

Director of Ceremonies: Dr. Lemme Kebaabetswe, Virology and Applied Microbiology

09:00 - 09:05	Introductions Ms. Itumeleng Mangole Acting Director, Communications and Public Affairs
09:05 - 09:15	Welcome Remarks Professor Elisha M. Shemang Deputy Vice-Chancellor for Academic Affairs
09:15 - 09:25	Official Opening of TRDAIS 2023 Professor Otlogetswe Totolo BIUST Vice Chancellor
09:25 - 09:35	Inspirational Message Professor Abraham A. Ogwu Deputy Vice-Chancellor for Research, Development, and Innovation
09:35 - 09:40	Singing Intermission Professor Venecio U. Ultra Jr. Agro-environmental Chemistry and Bioremediation
09:40 - 09:45	Introduction of the Guest Speaker Professor Rodrigo S. Jamisola Jr. Overall and Program Chair, TRDAIS 2023
09:45 - 10:15	Plenary Session: Micro/Nano Robotics Surgery at the MSRL in ETH-Zurich Professor Bradley Nelson ETH Zurich, Switzerland
10:15 - 10:25	Guest Speaker Appreciation Professor Goitseone Malumbela Overall Chairman, BIUST 10th Anniversary Committee

ISSN: 2521-2293

Closing Programme

Tuesday, 19 September 2023

TEACHING, RESEARCH & INNOVATION SYMPOSIUM 2023 (TRDAIS 2023)

BIUST Auditorium
1530-1650 Hrs

Director of Ceremonies: Dr. Lemme Kebaabetswe, Virology and Applied Microbiology

15:30 - 15:40	Vote of Thanks Professor Wellington Masamba Dean, Faculty of Science
15:40 - 15:50	Parting Message Professor Joseph Chuma Dean, Faculty of Engineering and Technology
15:50 - 16:00	Poem Reading Intermission Ms. Kediemetse K. Kgakole Admissions and Enrollment, Postgraduate School
16:00 - 16:30	Awarding Ceremonies To announce the awards: Professor Rodrigo S. Jamisola Jr. Overall and Program Chair, TRDAIS 2023 To give the awards: Professor Goitseone Malumbela Overall Chairman, BIUST 10th Anniversary Committee
16:30 - 16:40	Congratulatory Message Professor Patricia Makepe Director, Centre for Business Management, Entrepreneurship and General Education
16:40 - 16:50	Official Closing of TRDAIS 2023 Symposium Professor Boikanyo Makubate Dean, Postgraduate School

ISSN: 2521-2293

Appendices

ISSN: 2521-2293

Reviewers for Life Sciences and Environment

Name	Reviews
Biological & Biotechnological Sciences	
Gessesse Amare	2
Nyamukondiwa Casper	2
Makhzoum Abdullah	2
Kebaabetswe Lemme	4
Rahube Teddie	4
Kwape Tebogo Elvis	3
Zhou Nerve	2
Masisi Kabo	2
Nkwe David	3
Gaobotse Goabaone	3
Rantong Gaolatlhe	4
Mazebedi Richard	1

Name	Reviews
Earth & Environmental Sciences	
Loago Molwalefhe	1
Alexander Proyer	2
Venecio Ultra Jr	10
Peter Eze	3
Fulvio Franchi	2
Sithabile Tirivarombo	4
Kasuyazu Shindo	1
Esther Mosase	2
Kebonyethata Dintwe	1
Mpho Keeditse	1

Reviewers for Infrastructures and Mining

Name	Reviews
Mining & Geological Engineering	
Raymond Suglo	3
Beheemalingeswara Konka	3
Asfawossen Kassaye	2
Thierry Bineli-Betsi	3
Rahul Verma	3
Jerome Yendaw	3
Munyindei Masialeti	3
Gafar Oniyide	5

Name	Reviews
Civil & Environmental Engineering	
Moatlhodi Wise Letshwenyo	1
Goitseone Malumbela	3
Bhagabat Parida	1
Gabatsoswe Lebitsa	3
Elijah Chaparanganda	2
Gofetamang Ditalelo	1
Salessie Mayunga	1
Ezekiel Kholoma	1
Zahid Sultan	1
Wada Patella	2

ISSN: 2521-2293

Reviewers for Pure and Applied Sciences

Name	Reviews
Physics & Astronomy	
Conrad Bertrand Tabi	1
Mario Einax	2
Cosmas Muiva	3
Roberto De Propris	2
Lucia Malebogo Lepodise	2
Chamunorwa Oscar Kureba	7
Davison Munyaradzi Murape	3
Jacobus Diener	1
George Chimowa	1
Henry Vasco	2
Chemical & Forensic Sciences	
Wellington Masamba	3
Cecil Kingondu	4
Foster Mbaiwa	2
Ofentse Mazimba	4
Pogisego Dinake	4
Tshepo Pheko Ofitlhile	2
Sebusi Odisitse	3
Stephen Majoni	3
Bernard Baituti	3
Melisew Alula	4
Gothatamang Phokedi	1
Tiroyamodimo Tau	4
Joy Mokone	3
Disah Mpadi	4

Name	Reviews
Mathematics & Statistical Sciences	
Gatsinzi Jean-Baptiste	2
Boikanyo Oganeditse	2
Lungu Edward	1
Hailu Habtu Zegeye	3
Kassa Semu Mitiku	2
Shaw Sachin	3
Rao Subash	1
Gabaitiri Lesego	1
Akindeinde Saheed	2
Mushaandja Zechariah	1
Pako Ramasu	1
John Njagarah	1
Ndwapi Nkumbuludzi	2
Doctor Obonye	1
Zidana Chipo	2
Kagiso Dintle	2
Chipepa Fastel	1
Gidey Hagos Hailu	2
Otlaadisa Masego	1

Reviewers for Teaching

Name	Reviews
Center for Management & Entrepreneurship	
Masego Makepe	3
Tsaone Mokgwathi	3
Gladys Gamariel	3
Lyken Dawn Segosebe	3

BIUST Teaching, Research, & Innovation Symposium 2023 (TRDAIS 2023)
Botswana International University of Science and Technology
Palapye, Botswana, 18 - 19 September 2023
ISSN: 2521-2293

Reviewers for Computing and Industries

Name	Reviews
Mechanical, Energy, & Industrial Engineering	
Zeundjua Tjiparuro	2
Pradeep Sahoo	3
Rodrigo Jamisola	10
Albert Ude	7
Norman Gwangwava	5
Oduetse Matsebe	4
Vivekanandhan Chinnasamy	5
Leungo Kelebopile	4
Mosalagae Mosalagae	3
Keletso Orapeleng	2
Badziili Nthubu	4
Computer & Information Systems	
Venu Kuthadi	3
Irina Zlotnikova	3
Ralalakshmi Selvaraj	4
Nedev Zhi	2
Hlomani Hlomani	3
Semong Thabo	3
Maupong Thabiso	4
Dinakenyane Othapie	4
Sigwele Tshiamo	3
Mphago Banyatsang	2

Name	Reviews
Electrical, Computer, & Telecommunications Engineering	
Joseph Chuma	1
Murtala Adamu Zungeru	1
Abid Yahya	8
Nonofo Ditshego	3
Mmolokii Mangwala	2
Modisa Mosalaosi	1
Bokani Mtengi	1
Boyce Sigweni	4
Lilian Livutse Amuhaya	2
Ravi Samikannu	5
Chemical, Materials, & Metallurgical Engineering	
Edison Muzenda	2
Paul Agachi	1
Enoch Ogunmuyiwa	1
Phillip Oladijo	7
Gwiranai Danha	2
Tirivaviri Mamvura	2
Babatunde Obadele	1
Prasad Raghupatruni	1

ISSN: 2521-2293

Judges for Poster and Paper Presentations

Kebaabetswe Lemme
Venecio Ultra
Sachin Shaw
Cecil Kingondu
Mario Einax
Jerome Yendaw
Goitseone Malumbela
Rajalakshmi Selvaraj
Norman Gwangwava
Abid Yahya
Tirivaviri Mamvura
James Juana
Gaolathe Rantong
Sithabile Tirivarombo
Habtu Zegeye Hailu
Jens Andersen
Conrad Tabi
Raymond Suglo
Elijah Chaparanganda
Thabiso Maupong
Vivekanandhan Chinnasamy
Ravi Samikannu
Gwiranai Danha
Adane Abraham

Session Chairs

Ame Selepeng
Gregory Hillhouse
Raymond Suglo
Abid Yahya
Venecio Ultra
Habtu Zegeye Hailu
Rajalakshmi Selvaraj
Albert Ude

ISSN: 2521-2293

TRDAIS 2023 Symposium Committee

Overall and Program Chair:	Prof. Rodrigo S. Jamisola Jr.
Overall and Program Co-Chair:	Dr. Chamunorwa Oscar Kureba
Overall Chair:	Prof. Jens E.T. Andersen

Program Committee Members

Life Sciences and Environment:	Refilwe Setso
Pure and Applied Sciences:	Mello Tumisang
Infrastructures and Mining:	Sebinanyane Babedi
Computing and Industries:	Thabang Matabana
Teaching:	Dineo Sebuso
Symposium Preparations:	Kediemetse Kgakole
	Hendrick Ontlafetse

ISSN: 2521-2293

Author Index

ISSN: 2521-2293

PROCEEDINGS OF THE BIUST TEACHING, RESEARCH & INNOVATION SYMPOSIUM 2023 (TRDAIS 2023)

PALAPYE, BOTSWANA

18-19 SEPTEMBER 2023

TEACHING RESEARCH & INNOVATION SYMPOSIUM 2023

BIUST

BOTSWANA INTERNATIONAL UNIVERSITY OF SCIENCE & TECHNOLOGY